

**DESIGN OF A PIEZOELECTRIC GENERATOR FOR
VIBRATION ENERGY HARVESTING USING
NON-FERROELECTRIC PZnT-NT**

ZAINAB SHAKIR RADEEF

**FACULTY OF ENGINEERING
UNIVERSITY OF MALAYA
KUALA LUMPUR**

2018

**DESIGN OF A PIEZOELECTRIC GENERATOR FOR
VIBRATION ENERGY HARVESTING
USING NON-FERROELECTRIC PZnT-NT**

ZAINAB SHAKIR RADEEF

**THESIS SUBMITTED IN FULFILLMENT OF THE
REQUIREMENTS FOR THE DEGREE OF DOCTOR OF
PHILOSOPHY**

**FACULTY OF ENGINEERING
UNIVERSITY OF MALAYA
KUALA LUMPUR**

2018

UNIVERSITY OF MALAYA
ORIGINAL LITERARY WORK DECLARATION

Name of Candidate: Zainab Shakir Radeef

Registration/Matric No: KHA120140

Name of Degree: Doctor of Philosophy

Title of Project Paper/Research Report/Dissertation/Thesis (“this Work”):

Design of a piezoelectric generator for vibration energy harvesting using non-ferroelectric PZnT-NT

Field of Study: Engineering Design

I do solemnly and sincerely declare that:

- (1) I am the sole author/writer of this Work;
- (2) This Work is original;
- (3) Any use of any work in which copyright exists was done by way of fair dealing and for permitted purposes and any excerpt or extract from, or reference to or reproduction of any copyright work has been disclosed expressly and sufficiently and the title of the Work and its authorship have been acknowledged in this Work;
- (4) I do not have any actual knowledge nor do I ought reasonably to know that the making of this work constitutes an infringement of any copyright work;
- (5) I hereby assign all and every rights in the copyright to this Work to the University of Malaya (“UM”), who henceforth shall be owner of the copyright in this Work and that any reproduction or use in any form or by any means whatsoever is prohibited without the written consent of UM having been first had and obtained;
- (6) I am fully aware that if in the course of making this Work I have infringed any copyright whether intentionally or otherwise, I may be subject to legal action or any other action as may be determined by UM.

Candidate’s Signature:

Date:

Subscribed and solemnly declared before,

Witness’s Signature

Date:

Name:

Designation:

DESIGN OF A PIEZOELECTRIC GENERATOR FOR VIBRATION ENERGY HARVESTING USING NON-FERROELECTRIC PZnT-NT

ABSTRACT

Over the past years, there are a considerable knowledge and continuous striving toward scavenging a sustainable power from piezoelectric harvesters, which convert the waste mechanical energy to useful electrical energy. Among the piezoelectric materials, non-ferroelectric materials are more cost-effective and ease to build using the wet chemical method. In this study, a novel non-ferroelectric was manufactured from $0.7\text{PbZn}_{0.3}\text{Ti}_{0.7}\text{O}_3-0.3\text{Na}_2\text{TiO}_3$ (PZnT-NT) through *p-n* junction construction. It was demonstrated that the increment of conductivity via adding the Na_2TiO_3 plays an essential role in increasing the permittivity of the non-ferroelectric harvester and hence improved the generated power density. The performance of the device was studied experimentally over a cantilever test rig; the vibrating cantilever (0.4 m/s^2) was excited by a motor operated at 30 Hz. The generated power successfully illuminated a light emitting diode (LED). The PZnT-NT generator produced a volume power density of $0.106 \pm 0.011 \mu\text{W}/\text{mm}^3$ and a surface power density of $10.6 \pm 1.1 \mu\text{W}/\text{cm}^2$. The performance of the proposed device with a size of $(20 \times 15 \times 1 \text{ mm}^3)$ was higher in terms of power output than that of the commercial piezoelectric PbZrTiO_3 (PZT) $(63.5 \times 31.8 \times 0.51 \text{ mm}^3)$, microfiber composite (MFC) $(80 \times 57 \times 0.335 \text{ mm}^3)$ and piezoelectric bimorph device $(70 \times 50 \times 0.7 \text{ mm}^3)$. Compared to other existing ferroelectric and non-ferroelectric generators, the proposed device demonstrated exceptional performance in harvesting the energy at low acceleration and in a low-frequency environment. Moreover, the performance of the proposed PZnT-NT as well as the commercial MFC and PZT bimorph was studied systematically over the Vertical Axis Wind Turbine (VAWT) beam, which was located above an exhaust air outlet of the cooling tower system. For successful implementation of the harvester on an operating VAWT beam, good harvester location

which is rich in vibration energy must be known in a priori to avoid poor power generation at a bad location. Thus, an optimal location selection scheme using two non-destructive vibration techniques, i.e., the Experimental Modal Analysis (EMA) and Operating Deflection Shape (ODS) analysis techniques were adopted to measure the dynamic characteristics and visualise the operating vibration shape of the system. The results showed that the highest displacement was located at the free end (near the rotor part of the VAWT). Furthermore, higher vibration was observed in the horizontal movement compared to the vertical movement of the VAWT beam. As a result, the PZnT-NT generator produced the highest volume power density (i.e. $0.107 \pm 0.008 \mu\text{W}/\text{mm}^3$) compared to the PZT (i.e. $0.036 \pm 0.005 \mu\text{W}/\text{mm}^3$), MFC (i.e. $0.007 \pm 0.001 \mu\text{W}/\text{mm}^3$) and PZT bimorphs (i.e. $0.006 \pm 0.001 \mu\text{W}/\text{mm}^3$). The power density was improved by 66%, 93.8% and 94% using the proposed PZnT-NT over the PZT, MFC and the PZT bimorph respectively. Furthermore, PZnT-NT was the most cost-effective solution in term of the highest power generated per dollar, $(\frac{\mu\text{W}/\text{mm}^3}{\$}) \times 10^5$ (i.e. 7066.7 ± 733.3), compared to PZT (i.e. 22.1 ± 1.4), MFC (i.e. 4.3 ± 0.4) and PZT bimorph (i.e. 35.0 ± 5.0). This has verified the great potential of PZnT-NT materials in harvesting useful energy from the VAWT beam.

Keywords: Piezoelectric; Non-ferroelectric; energy harvesting; Electromechanical properties; wind turbine.

DESIGN OF A PIEZOELECTRIC GENERATOR FOR VIBRATION ENERGY HARVESTING USING NON-FERROELECTRIC PZnT-NT

ABSTRAK

Kebelakangan ini, telah banyak ilmu pengetahuan dan usaha berterusan disalurkan untuk menjana tenaga mampan dari penuai piezo-elektrik yang mampu menjana tenaga peranti pengesan wayarles secara sendiri dengan menukarkan tenaga mekanikal sisa kepada tenaga elektrik yang berguna. Antara bahan-bahan piezo-elektrik, bahan yang bukan feroelektrik (atau penuai yang mempunyai baki pengutuban) ialah bahan yang paling jimat kos dan mudah dibina menggunakan teknik kimia lembab kaedah kimia basah. Dalam kajian ini, sebuah penjanakuasa bukan feroelektrik baharu telah dihasilkan daripada $0.7\text{PbZn}_{0.3}\text{Ti}_{0.7}\text{O}_3-0.3\text{Na}_2\text{TiO}_3$ (PZnT-NT) melalui pembinaan p-n junction. Kajian ini telah membuktikan bahawa kenaikan keberaliran dengan menambah Na_2TiO_3 memainkan peranan dalam menaikkan ketelusan penjanakuasa nano dan seterusnya meningkatkan ketumpatan kuasa yang dijana. Prestasi peranti ini telah dikaji secara ujikaji melalui rig ujian julur. Julur bergetar (0.4 m/s^2) telah diuja oleh motor yang beroperasi pada 30 Hz. Kuasa yang terjana telah berjaya menyalakan diod pemancar cahaya (LED). Penjanakuasa PZnT-NT menghasilkan ketumpatan kuasa per isipadu sebanyak $0.106 \pm 0.011 \mu\text{W}/\text{mm}^3$ dan ketumpatan kuasa per luas sebanyak $10.60 \pm 1.1 \mu\text{W}/\text{cm}^2$. Dari segi output kuasa, prestasi peranti yang dicadangkan bersaiz ($20 \times 15 \times 1 \text{ mm}^3$) adalah lebih tinggi daripada piezo-elektrik PbZrTiO_3 (PZT) ($63.5 \times 31.8 \times 0.51 \text{ mm}^3$), komposit mikrofiber komersial (MFC) ($80 \times 57 \times 0.335 \text{ mm}^3$) dan peranti dwimorf piezo-elektrik ($70 \times 50 \times 0.7 \text{ mm}^3$). Peranti yang dicadangkan menunjukkan prestasi hebat dalam menuai tenaga pada pecutan rendah dan persekitaran yang rendah frekuensi, jika dibandingkan dengan penjanakuasa dari bahan feroelektrik dan bukan feroelektrik yang sedia ada. Tambahan lagi, prestasi PZnT-NT yang dicadangkan dan juga MFC komersial dan dwimorf PZT telah dikaji secara sistematik di atas turbin angin paksi

menegak (VAWT) yang terletak di atas alur keluar angin ekzos pada sistem menara penyejuk. Untuk menggunakan penuai di atas alang VAWT dengan berkesan, lokasi yang bagus untuk penuai yang tinggi tenaga getaran mestilah diketahui dahulu untuk mengelakkan penjana kuasa yang rendah pada lokasi yang tidak bagus untuk penuai. Maka, pemilihan lokasi yang optimum dilakukan menggunakan teknik getaran tanpa musnah, iaitu analisis ragaman eksperimental (EMA) dan analisis bentuk pesongan beroperasi (ODS). Kedua-dua teknik ini telah diambil untuk mengukur ciri-ciri dinamik dan menggambarkan bentuk getaran beroperasi pada sistem. Hasil menunjukkan sesaran tertinggi terletak pada penghujung yang bebas (dekat bahagian rotor VAWT). Tambahan pula, getaran yang lebih tinggi diukur dalam pergerakan melintang berbanding pergerakan menegak pada alang VAWT. Maka, penjanakuasa PZnT-NT dapat menghasilkan ketumpatan kuasa per isipadu tertinggi, iaitu pada $0.107 \pm 0.008 \mu\text{W}/\text{mm}^3$, berbanding PZT (i.e. $0.036 \pm 0.005 \mu\text{W}/\text{mm}^3$), MFC ($0.007 \pm 0.001 \mu\text{W}/\text{mm}^3$) dan dwimorf PZT ($0.006 \pm 0.001 \mu\text{W}/\text{mm}^3$). Ini membuktikan kebolehan hebat bahan PZnT-NT dalam menuai tenaga berguna dari alang VAWT. Ketumpatan tenaga dipertingkatkan sehingga 66%, 93.8% dan 94% menggunakan PZaT-NT ke atas PZT, MFC dan PZT dua bentuk (bimorph). Tambahan lagi, PZaT-NT ialah penyelesaian paling jimat kos dari segi tenaga tertinggi dihasilkan setiap dollar ($(\frac{\mu\text{W}/\text{mm}^3}{\$}) \times 10^5$ (i.e. 7066.7 ± 733.3)) berbanding PZT (i.e. 22.1 ± 1.4), MFC (i.e. 4.3 ± 0.4) dan PZT dua bentuk (bimorph) (i.e. 35.0 ± 5.0). Ini membuktikan potensi bahan PZaT-NT dalam menuai tenaga berguna daripada VAWT.

Kata kunci: Bahan yang bukan feroelektrik; Ciri elektromekanik; Penuaian tenaga; Piezoelektrik; Turbin angin.

ACKNOWLEDGEMENTS

In The Name of Allah SWT, the Sustainer of the world's Most Gracious and Most Merciful.

First of all, I would like to express my sincere thanks to my venerable supervisor, Assoc. Prof. Dr. Chong Wen Tong, for his patience, advice and encouragement. He always played essential key role of managing the research path. Hence, without his wise treatment, it was impossible to me to get a successful achievement. I will always be proud due to I was one of his students.

I pay my deep sense gratitude to my creative supervisor Dr. Khoo Shin Yee, for his extraordinary effort of making the work rich of knowledge. It would have unattainable to achieve any development and novelty without his bright ideas, his smart and warm dealing. Always, he kept his care of me among all the hard and crucial times that restrict my progress.

I would like to seize this opportunity and express my thanks and gratitude to Dr. Ong Zhi Chao, his suggestion and his valuable comments was paved the way in front me. He provides me by incredible support, his assistance is immensely appreciated.

I would like to thank my collogues dr. Ahmad Fazlizan, Mr. Wong Kok Hoe, Mr. Chu Yung Jeh and Mrs. Izdihar for them kindness and continuous support. All the thanks to UM staff members and especially I would like to thanks Mr. Saad in ceramic lab and Mr. Isa in material Lab.

Finally, I want to dedicate this work to my faithful husband Makky W.H, without his immeasurable love, care and support, I cannot pursue my dream. All the thanks to my lovely kids Sarah, Muhamad and Yeser. Always, they are the candles that illuminate my way in this dark life.

TABLE OF CONTENTS

Abstract	iii
Abstrak	v
Acknowledgements	vii
Table of Contents	viii
List of Figures	xii
List of Tables.....	xviii
List of Symbols and Abbreviations.....	xx
List of Abbreviations.....	xxiii
List of Appendices	xxv
CHAPTER 1: INTRODUCTION	1
1.1 Overview	1
1.1.1 Fabrication of a New Piezoelectric and Its Cost Impact.....	4
1.1.1.1 Motivation of Using PZnT-NT Material as Vibration Harvester.....	6
1.1.2 Prior Studies of Vibration Harvesting Technique	7
1.1.3 Energy Harvesting of Wind Turbine	8
1.2 Problem Statement	10
1.3 Objectives of the Research.....	11
1.4 Thesis Outline	11
1.5 Research Flow and Scope	13

CHAPTER 2: LITERATURE REVIEW	15
2.1 The Piezoelectric Material	15
2.2 Electromechanical Properties of the Piezoelectric Harvesters.....	20
2.3 Piezoelectric Configuration and Application Type.....	23
2.4 Enhancement of Piezoelectric Properties by Improving Conductivity	27
2.5 Comparison of the Electromechanical Properties for Various Piezoelectric Harvesters	28
2.5.1 Soft and Hard Piezoelectric Material.....	32
2.6 Polarity of Ferroelectric and Non-Ferroelectric.....	34
2.6.1 Ferroelectric and Non-ferroelectric Piezoelectric Harvesters.....	36
2.6.2 Ferroelectric Brittle Piezoelectric Polycrystalline Harvesters.....	51
2.7 Piezoelectric Cantilever for Energy Harvesting.....	55
2.7.1 Theory of Vibration	56
2.7.1.1 Factors Affecting the Structural Response.....	59
2.7.1.2 Frequency Response Function	60
2.7.1.3 Coherence (COH).....	61
2.7.1.4 Experimental Modal Analysis (EMA)	61
2.7.2 The Vibration Technique of Energy Harvesting	63
2.8 Piezoelectric Energy Harvesting of Windmills.....	68
2.8.1 VAWT Exhaust Air System	69
2.9 Alternative Energy Harvester Circuit.....	70
2.10 Fabrication Cost of Piezoelectric Harvesters	73
2.11 Summary	77

CHAPTER 3: RESEARCH METHODOLOGY	78
3.1 Introduction	78
3.2 Preparation of $0.7\text{PbZn}_{0.3}\text{Ti}_{0.7}\text{O}_3 - 0.3\text{Na}_2\text{TiO}_3$ Harvester	80
3.2.1 Dielectric Measurement and Conductivity of PZnT-NT	83
3.2.2 Energy Harvesting of PZnT-NT over the Test Rig	85
3.2.3 Recharging Lithium Ion Battery using the Piezoelectric Harvesters.....	88
3.3 Shaker Test to Evaluate the Resonance of the PZnT-NT	90
3.4 Location Selection Scheme for Piezoelectric Energy Harvesting.....	90
3.4.1 Experimental Modal Analysis of Cantilever Test Rig.....	91
3.4.2 ODS Analysis	92
3.4.3 Voltage Measurement Verification Test.....	94
3.5 Vertical Axis Wind Turbine VAWT Exhaust Air System.....	95
3.5.1 Experimental Set-up of Wind Turbine VAWT Exhaust Air Recovery System	98
3.5.2 Experimental Modal Analysis and Operation Deflection Shape of VAWT. 100	
3.5.1.2 Voltage Measurement of VAWT based on PZnT-NT	100
3.5.1.2 Voltage Measurement of VAWT based on PZnT-NT	102
3.5.1.3 EMA of the VAWT.....	103
3.5.3 Implementing the PZnT-NT and DC Energy Harvesting over the VAWT..	105
3.6 Cost Analysis	106
CHAPTER 4: RESULTS AND DISCUSSIONS	107

4.1 Introduction	107
4.2 Characterisation of PZnT-NT Harvester	108
4.3 The Performance of PZnT-NT Device	118
4.4 Recharging Battery from PZnT-NT Device	128
4.5 The Alternating Generated Voltage of PZnT-NT	129
4.6 Voltage Measurement Baseline Test	131
4.6.1 Experimental Modal Analysis of Cantilever	132
4.7 Location Selection Scheme of Cantilever	135
4.7.1 Structural Dynamics Effects on the Harvesting Performance	141
4.8 Selection of an Optimal Location of VAWT Beam	144
4.8.1 ODS Spectrum of VAWT	145
4.8.2 EMA Analysis of the VAWT	149
4.8.3 The AC Voltage of the PZnT-NT in the VAWT	156
4.9 The DC Energy Harvesting of VAWT	159
4.10 Cost Analysis of the Piezoelectric Harvesters	162
CHAPTER 5: CONCLUSIONS AND RECOMMENDATIONS	163
5.1 Conclusion	163
5.2 Recommendations	165
References	167
List of Publications and Papers Presented	188
Appendix	189

LIST OF FIGURES

Figure 1.1: Research Flow Chart	14
Figure 2.2: Perovskite Structure, ABO_3 (Mindtouch, 2018).....	16
Figure 2.3: Various Categories of Piezoelectric Material.....	17
Figure 2.4: The Sorting of The Structural Crystalline of Material Based on Crystal Symmetry (Defay, 2011).....	19
Figure 2.5: Orientation of Crystal dipoles (A) Before, (B) During, and (C) After Polarisation (Jan Tichý et al., 2010a).....	20
Figure 2.6: Classification of The Piezoelectric Application Based on Its Piezo-Effects (Jan et al., 2010 b).....	26
Figure 2.7: Mechanical Depolarisation of Hard And Soft Materials.....	33
(Thomas, 2008).....	33
Figure 2.8: Output Rates of Numerous Types of Piezoelectric Material (A. M. Daniels, Zhu;Tiwari, A., 2013)	34
Figure 2.9: The Typical P-E Nonlinear Hysteresis Loop (a) Ferroelectric (b) Anti ferroelectric	35
Figure 2.10: Illuminating of 600 Light-Emitting by Triboelectric and Piezoelectric Hyper Effect (Jung et al., 2015).....	38
Figure 2.11: Synthesised a Flexible Nanocomposite Generator NCG Device (a) Schematic of Formatting Process, (b) Voltage Generation Using Open Circuit of the Polarised NCG, (c) Short Circuit- current Measurement (Park et al., 2013).....	40
Figure 2.12: Poling Affect at the Generation Voltage Rate (Park et al., 2013)	41
Figure 2.13: High Voltage and Instantaneous Generation of Zinc Oxide Nanowires ZnO Nws for Stimulating a Sciatic Nerve of a Frog (Zhu et al., 2012)	42

Figure 2.14: Zinc Oxide Nanogenerator Self-power Sensor for Detecting the Vehicle Speed and Vehicle Weigh (Lin et al., 2013)	42
Figure 2.15: The ZnO-Nano Rod/Poly(Methyl Methacrylate) (PMMA) and ZnO/Poly (3,4-Ethylenedioxythiophene) Poly(Styrene Sulfonate) (PEDOT:PSS) Devices (Briscoe et al., 2013)	44
Figure 2.16: Discrete Cantilever Beam System	57
Figure 2.17: (a) Schematic Diagram of a Cantilever Beam and (b) the Effects of PVEH Patch Location on the Displacement, Strain and Power Results as Given by (Eggborn, 2003) and (Alper Erturk et al., 2009).....	67
Figure 2.18: Energy Harvesting Circuit (Gretarsson, 2007).....	71
Figure 2.19: Typical Rectifier Bridge Circuit with Voltage Regulator	71
Figure 3.1: The Fabrication Process Flow Chart of the PZnT-NT	81
Figure 3.2: The Piezoelectric Harvester Made of $0.7\text{PbZn}_{0.3}\text{Ti}_{0.7}\text{O}_3-0.3\text{Na}_2\text{TiO}_3$	82
Figure 3.3: (a) Agilent 4294A Analyser, (b) PZnT-NT Coupled to the Input Terminal.	83
Figure 3.4: (a) X-ray Diffraction System (PANalytical X'Pert ₃ X-ray Diffractometer), (b) Field Emission Scanning Electron Microscope (ZEISS Sdn. Bhd)	84
Figure 3.5 : Energy Harvesting Experimental Setup	85
Figure 3.6: Schematic Diagram for the Full Wave Rectification Circuit and the Load Resistance.....	86
Figure 3.7: Experimental Set up (a) Cantilever Beam Excited by DC Motor (b) Rectified Circuite with Ion Battery and three LEDs Diodes	89
Figure 3.8: Baseline Test.....	90
Figure 3.9: Experimental Set-up (a) EMA, (b) ODS Analysis and Voltage Measurement	93

Figure 3.10: Voltage Measurement Test (a) Cantilever Test Rig, (b) Multi-Channel Data Acquisition (DAQ) Devices Integrated with the Compact DAQ Chassis, (c) Signal Generate and Power Amplifier	95
Figure 3.11: Assembly of VAWTs System (Tong et al., 2011) (a) Schematic Drawing of VAWT (b) The Boundary Condition of the VAWT and Tower.....	96
Figure 3.12 : Exhaust Air Cooling Tower (Tong et al., 2011).....	97
Figure 3.13: The Optimal Position of the VAWT Over the Exhaust Tower	98
Figure 3.14: Experimental Set-up of Exhaust Wind Turbine Recovery System Integrated with Diffuser Plates	99
Figure 3.15: (a) EMA, and (b) ODS Analyses of the VAWT.....	101
Figure 3.16: EMA Analysis of VAWT: (a) The FRFs Matrix, (b) Hammer Test.....	104
Figure 3.17 : Energy Harvesting of the VAWT: (a) PZnT-NT, (b) PZT, (c) MFC, (d) PZT Bimorph.....	105
Figure 4.1: XRD Patterns of $0.7\text{PbZn}_{0.3}\text{Ti}_{0.7}\text{O}_3-0.3\text{Na}_2\text{TiO}_3$: (a) $\text{PbZn}_{0.3}\text{Ti}_{0.7}\text{O}_3$, (b) Na_2TiO_3	109
Figure 4.2: Surface Characteristics of: (a) Sodium Titanate (Na_2TiO_3) Sheets, (b) $\text{PbZn}_{0.3}\text{Ti}_{0.7}\text{O}_3$ Particles.....	110
Figure 4.3: FESEM PZnT-NT Layouts.....	111
Figure 4.4: PZnT-NT Layouts during (a) Pressing & (b) Releasing Movements, and Its (c) Generated Voltage under Pressing & (d) Generated Voltage after Releasing	112
Figure 4.5: (a)The Dielectric Properties, (b) Loss Tangent of PZnT-NT	114
Figure 4.6: Conductivity of the PZnT-NT & Pure PZnT at Room Temperature.....	115
Figure 4.7: Hysteresis Loop of: (a) Pure $\text{PbZn}_{0.3}\text{Ti}_{0.7}\text{O}_3$, (b) $0.9\text{PbZn}_{0.3}\text{Ti}_{0.7}\text{O}_3-0.1\text{Na}_2\text{TiO}_3$ Versus Various Applied Electric Fields	116
Figure 4.8: Flashing up LED (5mm).....	118

Figure 4.9: The Generated Voltage at Frequency 30 Hz of Various Harvesters	119
Figure 4.10: The Optimal Power Output of Various Harvesters	121
Figure 4.11: (a) Current Density and, (b) Power Density of Piezoelectric Devices versus Resistance.....	123
Figure 4.12: The Storage Battery Circuit with Three LEDs	128
Figure 4.13: Energy Harvesting based on PZnT-NT and Charging Time of Rechargeable Ion-Battery	129
Figure 4.14: Voltage Generated Signal of PZnT-NT Mounted over Cantilever and Excited at Frequency of 90 Hz	130
Figure 4.15: AC Voltage using Shaker Excitation at 90 Hz	130
Figure 4.16: The AC Voltage of PZnT-NT under Finger Pressing.....	131
Figure 4.17: The Maximum Voltage Generation of PZnT-NT based on Frequencies in Range of (10-300 Hz).....	132
Figure 4.18: FRF of Cantilever Beam using Impact Testing	133
Figure 4.19: (a) Harvested Voltage, (b) Magnitude Ranking at 95.2 Hz.....	135
Figure 4.20: EMA Magnitude Ranking at 95.2Hz.....	136
Figure 4.21: ODS Analysis at Frequency 95.2 Hz (a) Vibration Pattern (b) The Displacement versus Time	137
Figure 4.22: (a) Magnitude Ranking, (b) ODS Spectrum at 95.2 Hz	138
Figure 4.23: (a) Harvested Voltage, (b) Magnitude Ranking at 23.1 Hz.....	139
Figure 4.24: EMA Magnitude Ranking 23.1 Hz.....	140
Figure 4.25: (a) ODS Vibration Pattern, (b) ODS Magnitude Ranking at 23.1 Hz.....	141
Figure 4.26: Harvested Voltage at 90 Hz Excitation for Various Measurement Points in Comparison to Baseline Voltage.....	143
Figure 4.27: Harvested Voltage at 95.2 Hz Excitation for Various Measurement Points in Comparison to Baseline Voltage.....	143

Figure 4.28: ODS Spectrum of VAWT Beam at Three Directions	145
Figure 4.29: The Overall Deflection Shape based on ODS Analysis at Frequency in the Range of (0.5–300 Hz)	146
Figure 4.30: ODS Spectrum of the Free End (Point 1) (Label is Red) and the Clamped End (point 9) of VAWT Beam (Label is Blue): (a) Response Compared in x-axis (b) Response Compared in y-axis, (c) Response Compared in z-axis)	147
Figure 4.31: Diffuser and the Wind Effect of the VAWT	148
Figure 4.32: The Set of FRFs based on the EMA Analysis of VAWT in Three Orthogonal Directions when the Excited Force Acts in Y- direction	149
Figure 4.33: The FRF Raw Data and Coherence Set based on the EMA Analysis of VAWT when the Force Excitation Act in Y-direction	150
Figure 4.34: The Overall Dynamic Respond of the VAWT based on EMA Analysis at Frequency in Range of (0.5-300 Hz) when the Force Act in Y-axis	151
Figure 4.35: The FRF Set on the EMA Analysis of VAWT in Three Orthogonal Directions when the Impact Forces Act in Z-direction.....	152
Figure 4.36: The FRF Raw Data and Coherence Set based on the EMA Analysis of VAWT when the Force Excitation Act in Z-direction.....	153
Figure 4.37: The Overall Mode Shape based on EMA Analysis at Frequency in Range of (0.5-300 Hz) Z-axis Direction.....	154
Figure 4.38: The Overall Mode Shape based on EMA Analysis at Frequency in Range of (0.5-300 Hz) Y-axis and Z-axis Direction	155
Figure 4.39: (a) Recorded AC Voltage, (b) The Instantaneous Acceleration (i.e. x,y, and z) at Point 1 of VAWT Beam.....	157
Figure 4.40: (a) The AC Voltage, (b) The Instantaneous Acceleration (i.e. x,y, and z) at Point 9 of VAWT Beam.....	158

Figure 4.41: DC Voltage of PZnT-NT across Different Loads	159
Figure 4.42: The Generated Power of the Piezoelectric Harvesters Compact to VAWT Structure	160
Figure 4.43: Optimal Power Density of PZnT-NT Comparing with Others Commercial Harvesters.....	161

University of Malaya

LIST OF TABLES

Table 2.1: Piezoelectric Applications with Different Configurations.....	25
Table 2.2: Comparative Properties between Different Types of Piezoelectric Materials	31
Table 2.3: Comparison of Characteristics between Soft Ceramics and Hard Ceramics (APC International, 2014).....	32
Table 2.4. Power and Current Density of the Flexible Ferroelectric Nanogenerator Material	46
Table 2.5: Power and Current Density of the Flexible Non-polarised Nanogenerator Piezoelectric Material.....	48
Table 2.6: The Power Density of Brittle Piezoelectric Films	54
Table 2.7: The Cost Analysis of Ferroelectric and Non-ferroelectric Harvesters-(GmbH, 2017).....	75
Table 2.8: The Power Consumption for the Polarisation Process.....	76
(Mems-pie, 2017b).....	76
Table 2.9: The Power Consumption for the Sintering Process Using Furnace (Keith, 2017; Sante, 2017).....	76
Table 3.1: The Microfiber and Piezoelectric Bimorph Properties	87
Table 3.2: Wind Turbine Characteristics (a)Performance (b)Physical Parameter (Tong et al., 2011; Abdullah, 2016).....	97
Table 3.3: Piezoelectric Harvesters' Prices Excluding the Tax and Shipping.....	106
Table 4.1: Comparison of Volume Power Density Based on Low Acceleration and Frequency	126
Table 4.2: Comparison of Surface Power Density for Numerous Nanogenerators	127
Table 4.3: Natural Frequencies, Damping and Mode Shapes of Cantilever Beam.....	134

Table 4.4: The Dynamic Characteristics of the VAWT Beam when the Force Act in y-direction.....	150
Table 4.5: List of the Utilized Harvesters and Performance and Prices	162

University of Malaya

LIST OF SYMBOLS AND ABBREVIATIONS

List of Symbols

D_i	Charge Density Displacement (C/m ²)
d_{ijk}	Third –Rank Tensor of Piezoelectric Coefficient (10 ⁻¹² C/N)
X_{ik}	The Applied Stress (N/m ²)
E_k	Electrical Field (N/C)
K_3^T	Dielectric Constant or Permittivity Constant
ϵ_0	Permittivity in Vacuum =8.854 × 10 ⁻¹² F/m
ϵ_T	Permittivity of Material (F/m)
ϵ'	Real Dielectric Part
ϵ''	Imaginary Dielectric Part
i	Imaginary Part; $i = \sqrt{-1}$
$\tan (\delta)$	The Dielectric Loss Tangent
σ_e	The Effective Conductivity (S/m)
w	The Angular Frequency (Hz)
E_C	The Storing Energy (mJ)
C_C	The External Capacitor (µf)
U_t	The Voltage at Steady Stead (V)
P	Dissipated Power of The Load (µw/cm ³)
R_L	The Load Resistance (Ω)
m	Excited Mass (kg)
P_r	Remnant Polarisation (µC/cm ²)
$\left[\begin{matrix} H \\ n \times n \end{matrix} (f) \right]$	Raw FRF Transferred Matrix
$\left[\begin{matrix} Q \\ n \times 1 \end{matrix} (f) \right]$	Excited Force Matrix

$\left[\ddot{\mathbf{X}}(f) \right]_{n \times 1}$	Response of The System
$n \times 1$	Column Factor, Matrix with One Column
x	Displacement Element (m)
\ddot{x}	Acceleration Element (m/s ²)
\dot{x}	Represent the Velocity (m/s)
C	Damping Ration
k	The Stiffness
$f(t)$	Denote the Harmonic Force Function of Time
$\{P\}$	Principle Coordinators
$[\Phi]^T$	Invers Eigenvectors Mode Shape
$[\Phi]$	Eigenvectors or Mode Shape
$[m]$	Excited Mass Matrix
r^{th}	Number of Mode
σ_r	Decay Rate
ζ_r	Damping Ratio
$\omega_{0,r}$	Natural Frequency
$q_{p,r}$	The r^{th} Mode Forcing Function in Principal Coordinate.
β_r	Magnification Factor
ω	The Excitation Frequency of The Forcing Function (Rad/s)
θ_r	Phase Angle
$\phi_{i,r}$	The r^{th} Mode Normalized Mode Shape at i^{th} DOF
$q_{p,r}$	Generalized Force
$H_{i,j}(\omega)$	Transfer Function due to i^{th} DOF and j^{th} DOF of Response
$\phi_{i,r} \& \phi_{j,r}$	Mode Shapes due to i^{th} DOF and j^{th} DOF
$\gamma_{i,j}^2(\omega)$	Coherence (COH)

$CS_{I:J}(\omega)$	Cross-Spectral Density
$AS_{J:J}(\omega)$	Auto-Spectrum Function
$B_I(\omega)$	Output Response
$A_J^*(\omega)$	Complex Value in the Frequency Domain
$ CS_{I:J}(\omega) ^2$	The Square of the Cross-Spectrum

University of Malaya

LIST OF ABBREVIATIONS

ABO ₃	Perovskite Structure Formula
COH	Coherence
DAQ	Data Acquisition
DOF	Degree of Freedom
EMA	Experimental Modal Analysis
ESPI	Electronic Speckle Pattern Interferometry
FEM	Finite Element Method
FFT	Fast Fourier Transform
FRF	Frequency Response Function
GO	Graphene Oxide
LCD	Liquid –Crystal Display
LED	Light Emitting Diode
MDOF	Multi Degree of Freedom
MEMS	Micromechanical System
MFC	Micro-Fiber Composite
MPB	Morphotropic Phase Boundary
MSS	Molten Salt Synthesis
MWCNT	Multi-Walled Carbon Nanotube
NCG	Nanocomposite Generator
NG	Nanogenerator
ODS	Operation Deflection Shape
p(VDF-TrFE)	Fluoride and Poly[(Vinylidene fluoride-Co-Trifluoroethylene)]
PCBM/P3HT	Phenyl-c61-butyric acid methyl ester/Poly(3-hexylthiophene)
PDMS	Dimethylsiloxane

PEDOT: PSS	Poly(3,4-Ethylenedioxythiophene) Poly (Styrene Sulfonate)
PET	Polyethylene Terephthalate
PFM	Piezo-Response Force Microscopy
PLD	Pulsed Laser Deposition
PMMA	Poly (Methyl Methacrylate)
PMN-PT	Lead Magnesium Niobate-Lead Titanate
PVDF	Polyvinylidene Fluoride
PVEH	Piezoelectric Vibration Energy Harvesting
PZT	Lead Zirconate Titanate
PZT-NT	Lead Zincate Titanate Sodium Titanate
SDOF	Single Degree of Freedom
SIMO	Single Input Multiple Approach
Sol-Gel	Solution Gel
VAWT	Vertical Axis Wind Turbine
ZnO/PEDOT: PSS	Zinc Oxide-Poly Polystyrene sulfonate
ZnO-PC100	Zinc Oxide-Polycarbonate Membrane

LIST OF APPENDICES

APPENDIX A	189
Appendix A.1: Instruments and Equipment's	189
Appendix A.2: The Installation of the PZT	190
Appendix A.3: The Installation of the MFC	190
Appendix A.4: The Installation of the PZT Bimorph	190
APPENDIX B	191
Appendix B.1: Fabrication Processes of PZnT-NT	191
Appendix B.2: Weights and Molars Percentage of the PbZnTiO_3	194
Appendix B.3: Weights and Molars Percentage of the Na_2TiO_3	194
APPENDIX C	195
Appendix C.1. Surface Characteristics of Sodium Titanate (Na_2TiO_3) Sheets and its Size Distribution.....	195
Appendix C.2. Surface Characteristics of $\text{PbZn}_{0.3}\text{Ti}_{0.7}\text{O}_3$ and its Size Distribution	195
APPENDIX D	196
Appendix D.1: Energy Harvesting of Cantilever Beam.....	196
Appendix D.2: The Standard Deviation of the Voltage, Power, and Power Density Using the Cantilver Beam.....	197
Appendix D.3: DC-Current and Standard Deviation of Harvesters Using Cantilever Beam	198
Appendix D.4: Energy Harvesting of VAWT	199
Appendix D.5: The Standard Deviation of the Voltage, Power, and Power Density Using the VAWT	200
Appendix D.6: Current Measurement (Short Circuit).....	201
Appendix D.7: Voltage Measurement (Open Circuit)	201
APPENDIX E	202

Appendix E.1: AC-Voltage at Point 1 over VAWT (Three DOF Directions, PZnT-NT Mounted to the Y-Axis)	202
Appendix E.2: The Acceleration at Point 1 of the VAWT (Three DOF Directions, PZnT-NT Mounted to the Y-axis)	205
Appendix E.3: AC-Voltage at Point 9 over VAWT (Three DOF Directions, PZnT-NT Mounted to the Y-axis)	208
Appendix E.4: The Acceleration at Point 9 of the VAWT (Three DOF Directions, PZnT-NT Mounted to the Y-axis)	211
APPENDIX F	213
Appendix F.1: Powder Cost Including the Shipping, Tax and Handling.....	213
Appendix F.2: Electrode Material Cost Including the Shipping and Tax.....	213
Appendix F.3: PZT Prices from Supplier: Prodigy Integration	214
Appendix F.4: MFC Prices from Supplier	215

CHAPTER 1: INTRODUCTION

1.1 Overview

Piezoelectric materials have a promising avenue that possesses a high sensitivity to the surrounding vibrational energy, enabling the generation of electrical energy and storing it for later use. The basic strategy of developing such materials comes from the need to sustain clean energy and reduce carbon emissions from fossil fuels and thus, this form of sustainable energy system is highly demanded for a greener future. The energy can be harvested from numerous sources such as the wasted vibration of machinery, the wind, tides, rivers, and rain (Woo et al.,2014), the excitation of runways and train railway (Song et al.,2012), from human body activities by investing the biomechanical energy generated from heartbeats (Lu et al., 2015), and from breathing and walking. In this regard, NASA harnesses energy from astronauts' bodies and this energy is activated for powering electronic devices where the piezoelectric harvester represents an ageless electrical energy source (Space, 2016). Basically, the attractive matter of piezoelectric harvesters is the long lifetime term-service (Bosotti,2004) for which this aspect represents one of the salient characteristics of piezoelectric materials.

There are three main transduction mechanisms to convert wasted vibration energy to useful electric energy: piezoelectric, electromagnetic, and electrostatic mechanisms. The harvesting performance has been compared based on the transduction mechanisms whereby piezoelectric mechanisms have been recognized by researchers to be able to generate higher power density and it is easily integrated into the system (Beeby et al., 2006; Kim et al., 2009; Naifar et al.,2016). The piezoelectric utilised mostly for powering wireless sensor nodes thus the required harvested energy was analysed and investigated by numerous researchers (Anton & Sodano, 2007; Roundy et al., 2005a). Most of the prior research studies have been interested in developing new piezoelectric harvester materials or enhancing the harvested energy of vibrated structures based on improving its

dynamic characteristics. Thus, both the piezoelectric harvesting products and the vibration technique will be the focal points that shall be presented in detail in this study.

Conventional piezoelectric material is synthesised from lead zirconate titanate (PZT) which exhibits ferroelectric properties. The manufacturing process of such harvesters imposes high industrial costs. Numerous studies have been carried out embedding an evaluation of harvested energy of piezoelectric material based on the morphological features (i.e. single crystal, microgenerator, and nanogenerator, etc.) of piezoelectric composite materials and their electromechanical properties. Also, the dynamic characteristics of the vibrated system (i.e. natural frequency, damping ratio, and mode shape) have been studied excessively. Recently, considerable advances have been made in the use of non-ferroelectric materials in the energy harvesting field where such products have desirable cost-impact. The energy was harvested using ferroelectric materials (Lebrun et al., 2004), anti-ferroelectric materials (i.e. the remnant polarisation is close to zero and the material has more ability to store the energy compared with the loss of energy) (Patel, Chauhan, & Vaish, 2014), and non-ferroelectric materials (Qin et al., 2016). ZnO-NG is an example of a non-ferroelectric film that has spontaneous polarisation when subjected to a mechanical load (Pazde-Araujo, Ramesh, & Taylor, 2001). Thus, the harvested energy based on the ferroelectricity phase of piezoelectric material should be compared and evaluated.

In terms of studying the dynamic characteristics of the harvesting system, there are numerous studies ongoing that look toward enhancing the harvested power from piezoelectric materials, where the piezoelectric film is integrated to a cantilever beam to realise its practical usage. Important limitation factors that are affecting the generation of electrical power can be listed as follows: frequency matching, properties of piezoelectric material, proof mass, harvesting circuit, strain distribution, and location of the harvester. Inappropriate design without considering these limitation factors may cause high power

loss in the form of mechanical loss (i.e., mismatching of mechanical) impedance measured by the damping factor and reflection ratio, mechanical-electrical transduction loss (i.e. coupling factor of the piezoelectric), and electrical loss from mismatching of the electric impedance (Kim et al., 2007). In terms of the dynamic characteristics of the system, matching of the excited frequency and the natural frequency are the results of an increase in the harvesting performance.

However, the harvested energy or power decreases extensively when the excitation frequency slightly shifts from the resonant point. Another enhancement of the voltage output can be achieved by increasing the frequency bandwidth (Liu et al., 2008) where the voltage improves in percentage by up to 70% within a frequency bandwidth of ± 2 -3Hz. Liu et al. (2008) maintained the overlapping of three examined cantilever type piezoelectric generators with closely spaced natural frequencies, which were connected in a series circuit, and the cantilever configuration was in an array arrangement. It found that this array arrangement enhanced the overlapping effect, which was effective to obtain a wider bandwidth. Moreover, the obtained power output was increased (i.e. a 26% increment) by using an electrical connection after AC-DC rectification, as compared to the direct serial connection from all AC outputs. Optimal harvesting performance can also be achieved through integrating the piezoelectric on the optimal position over a cantilever where this issue has been analysed mathematically and come under several assumptions and conditions such as the using of piezoelectric type d_{31} with assuming a curvature deflection of a beam (Erturk et al., 2008; Liao & Sodano, 2012a). In fact, in real operating system, the system is subjected MDOF excitation and thus there is a specific deflection pattern that will be configured, and it will affect the harvesting performance. In this case, visualising the vibration pattern of a cantilever and measuring the natural frequency and damping ratio can solve such problems. Generally, piezoelectric harvesters are widely utilised for powering wireless sensors particularly in the wind turbine application.

In fact, the construction of smart harvesting system requires a practical design and optimal installation where high excitations of the piezoelectric harvester's films should be avoided; where the strain distribution of piezoelectric cantilever is non-uniform; and the damage could occur at the root of the cantilever (clamped side); and thus, it is necessary to study crack propagation and fatigue on the long operation (Avvari, Yang, & Soh, 2016). Another principal issue to mention is that the amount of harvested energy in the real environment should be evaluated on whether it will be sufficient to power up the wireless node sensors.

1.1.1 Fabrication of a New Piezoelectric and Its Cost Impact

Recently, the piezoelectric has been attractive to most researchers due to the need for manufacturing portable batteries and developing self-power devices with a long lifespan. Extensive developments on piezoelectric materials have been achieved for decades where the ferroelectric lead zirconium titanate ($\text{Pb}(\text{Zr}_x\text{Ti}_{1-x})\text{O}_3$ –PZT) is the most attractive material due to its distinct excellent electromechanical properties (i.e., high remnant polarisation, high coercive field, high piezoelectric coefficient, high piezoelectric voltage coefficient, and high dielectric property). Typically, a brittle piezoelectric harvester can be synthesised by solid state methods (Nabunmee et al., 2011 ; Islam & Priya, 2006). In general, the piezoelectric ferroelectrics films have directional electromechanical properties (i.e. d_{33} , d_{31} , d_{15} , g_{33} , g_{31} , etc.); thus, piezoelectric harvesting energy products have been designed with various architectures according to the type of applied excitation (such as pressing, bending, and extension) (Piezo System, 2013). The conventional fabrication of the sold state method involves milling processes, PZT powder calcination, sintering under high temperature, and polarisation. The sintering temperature has effects on increasing the grain size, the remnant polarisation, and the coercive field. In this regard, Kong (2002) fabricated PZT ceramic under sintering temperature of 1100 °C, and

the formed ceramic possessed remnant polarisation of $22 \mu\text{C}/\text{cm}^2$ and a coercive field of $12.6 \text{ kV}/\text{cm}$ whereby this result reflects well with most findings from prior studies.

Also, Yongqiang (2015) affirmed that the optimal grain size was $1 \mu\text{m}$ where increasing of piezoelectric coefficient d_{33} and remnant polarisation P_r was realised. Also, studying of the composition ratio of the starting raw powder and its effects of ferroelectricity were considered where plenty of determinations confirmed that PZT composite has excellent ferroelectricity phase near the Morphotropic Phase Boundary (MPB) (Kakegawa et al., 1995; Kumari et al., 2013). Piezoelectric is classified to pyroelectric and ferroelectric or in other words, it is classified based on its ferroelectricity phase. In terms of using the piezoelectric materials as energy harvester, there is ability to harvest the energy based on employing the ferroelectric, anti-ferroelectric (Patel et al., 2014), and non-ferroelectric materials (Qin et al., 2016).

The recent advancement of piezoelectric generators has adopted the wet chemical process that distinctly eases fabrication, is cost-effective, and with high power density. Most the non-ferroelectric harvesters have been synthesised based on this method. A ZnO-NG is an example of a nanogenerator film that has a spontaneous polarisation when subjected to a mechanical load. Such a material has high power density, comparable current density, and is cost-effective to manufacture relative to ferroelectric materials. Recently, nanogenerator (NG) piezoelectric devices have attracted the attention of many researchers, because of the multiplicity of their applications. Nanogenerator harvesters can be synthesised as thin/thick piezoelectric patches with high sensitivity to surrounding mechanical vibrations. Recent advances have demonstrated the high-energy density of ferroelectric and non-ferroelectric harvesters. Non-ferroelectric material (e.g. ZnO-NGs) films can be prepared easily without sintering and polarisation processes, making them cost-effective in the industry.

1.1.1.1 Motivation of Using PZnT-NT Material as Vibration Harvester

Permanent power sources for implementing self-power long lifetime devices is a recent challenge, especially in health monitoring applications such as powering wireless devices for the structural health monitoring of wind turbine blades. The pros and cons of adopting piezoelectric harvesters are; harvesting permanent power and the associated high cost of what limits the implication of such harvesters. The motivation was created to fabricate an economical piezoelectric harvester consisting of abundant materials (i.e. zinc, copper, sodium and titanium). The abundance rank of the selected materials is within 25 of the most abundant materials in the Earth's crust. In details, the ranks of titanium, sodium, and zinc are 6, 9, and 25 out of 78 materials (Michael, 2018). Additionally, copper and zinc were selected instead of gold and silver by considering the potential difference and cost (e.g. copper and zinc are more attractive due to good potential difference and low cost). On the other hand, PbZnTiO_3 is one of the piezoelectric materials that has not been investigated sufficiently. There is no prior information about its electromechanical properties or dielectric properties. Also, it has not been utilized as an energy harvester despite its ferroelectricity behaviour, where it was utilized as a memory device in previous study (limited et al., 2008).

On the other hand, the selection of sodium titanate (Na_2TiO_3) as the carrier material to PbZnTiO_3 is very attractive due to the possibility of being used as an anode in the long-life rechargeable lithium-ion battery. In general, supplement conductive fillers such as nanocarbon, nanocarbon black (Banerjee & Cook-Chennault, 2012; Tian & Wang, 2008) and nano-graphite (Hu et al., 2010; Park et al., 2012) were utilized widely to reduce the piezoelectric potential screening effect by increasing the conductivity and mobility of the electrons. Considering low cost solution, sodium titanate is a potential conductive filler that could provide a good alternative to improve the conductivity. Its performance in enhancing the electron mobility will be investigated in this study.

Moreover, sodium titanate is a *p*-type material (alkaline media) and the $\text{PbZnTiO}_3 - \text{Na}_2\text{TiO}_3$ fabrication is based on the low cost wet chemical methods, where it is expected to show chemical interaction with its zinc electrode (Joo et al.,2011). Based on the wet chemical fabrication, the crystallization of material will be grown under a potential difference, where the *n*-type layer will precipitate above the cathode and similarly the *p*-type layer shall be set nearby the anode (This is known as *p-n* junction approach). In this way, the *p-n* approach can further improve the conductivity and hence it is expected to enhance the harvesting performance. Based on the discussions made above, this study's aim is to develop a new harvester with $\text{PbZnTiO}_3 - \text{Na}_2\text{TiO}_3$, which is ease of manufacture, cost effective and comparative advantage in term of harvesting power.

1.1.2 Prior Studies of Vibration Harvesting Technique

Plenty of studies have affirmed that the maximum power density is achieved when the excited frequency matches with harvester natural frequency. It is worth to mention that the enhancement of power generation can be achieved when the PZT harvester was tuned at its natural frequencies by adding tip mass over the free end of the PZT harvester or cantilever (Lumentut & Howard, 2014; Shen, 2009), using a scavenger with appropriate resonance characteristics, different geometries (Ayed et al.,2009, Sang, Dayou, & Liew, 2013), and utilising a multi-degree of freedom system for harvesting the energy efficiently over wider bandwidths (Roundy et al., 2005b).

Basically, at a frequency, all the parts or distributed masses of the structure will be oscillated to configure a potential motion pattern. All the elements of oscillator will be moved harmonically in particular displacement and thus, the nodes (i.e. places with zero displacement) and anti-node (i.e. highest displacement) will be configured in specific mode shape. Accordingly, there is a need for recognizing the optimal location where the

selection of optimal location over the host structure plays an essential role in harvesting the optimal power. In fact, there are inadequate prior studies that have been involved in selecting the optimal harvesting location over the cantilever system on a Multi- Degree of Freedom (MDOF) system. Eggborn (2003) detected the optimal location close to the location of maximum bending moment when the cantilever (i.e. flexible beam) was subject to high deflection in its free end and the force act was near to the clamped end.

Liao and Sodano (2012a) have been examined the effect of piezoelectric placement on damping of vibration modes and the effect of patch size on optimal placement. Khoo (2017) investigated the effect of structural dynamics on voltage generation from a novel dual coupled cantilever based Piezoelectric Vibration Energy Harvester (PVEH) system. Two non-destructive vibration techniques have been adopted using the using Experimental Modal Analysis (EMA) and Operating Deflection Shape (ODS) analysis techniques, where these technical tools have been integrated into the location selection scheme for enhancing the vibration energy harvesting purpose. The location selection scheme was based on a measurement procedure on both the harvester and its host structure to identify the optimal location. The results showed that the proposed cantilever PVEH could harvest high voltages in the high displacement region. An optimal location, (i.e. maximum vibration points / anti-nodal points) determined by the location selection scheme could yield a 33.3% improvement in harvested voltage, as compared to the baseline voltage. Meanwhile, if the piezoelectric plate was placed at any minimal vibration points or nodal point on the structure as determined by the location selection scheme, a significant reduction (>70%) in harvested voltage was observed.

1.1.3 Energy Harvesting of Wind Turbine

Wind power is one of the most economical sources of the large-scale alternative energy. Wind turbines are an indispensable source to generate the clean energy and reduce

the dependence on pollution-causing power plants. Recently, most attention directed toward harvesting the wasted energy of windmills (Bressers et al., 2011; Rezaei et al., 2015), the generated power was evaluated based on employing the piezoelectric materials. The piezoelectric was utilised for generating a small-scale of energy by converting the waste vibration energy of the traditional wind turbine. However, the generated power was sufficient for powering wireless sensor nodes or for conducting real-time health monitoring of the wind turbine (e.g. health monitoring of wind blades (Song et al., 2013G. Song et al., 2013) or wireless self-powered diagnosis systems (Davidson & Mo, 2014). Priya (2005a) designed a small-scale windmill model that consisted of 10 piezoelectric bimorph transducers and operated at wind speeds of 10 mph. The generated power was 7.5 mW ($1.04 \mu\text{W}/\text{mm}^3$) at a resistance of 6.7 k Ω . At the same the wind speed, Myers et al. (2007) utilised eighteen piezoelectric patches, and the reported power was 5 mW at a resistance of 20 k Ω . The piezoelectric films were integrated with the portable windmill that was excited mechanically such as by using a camshaft, crankshaft (Chih-Ta Chen, 2006) or by using the magnetic resonance of contactless windmill, where the maximum output power was 0.6 mW at wind speed 10 mph (Bressers et al., 2011). The harvested power using 12 piezoelectric patches and wind speed of 12 mph was 1.2 mW (Chih-Ta Chen, 2006). Numerous studies have explored the power amount that is sufficient for operating wireless node sensors (e.g. flow sensor, powering RF transmitted circuit) whilst considering the effect of wind speed. In several windmill prototype designs, the researchers harvested power densities ranging between $0.0147 \mu\text{W}/\text{mm}^3$ and $1.933 \mu\text{W}/\text{mm}^3$ when the windmills were operated at air speed variants of between 6.7 m/s to 16.3 m/s (He et al., 2013; Li et al., 2011; Liu et al., 2011; Tan & Panda ,2007). Furthermore, Zhang (2015) harvested a high-power density of $17.2 \mu\text{W}/\text{mm}^3$ under a wind speed of 11 m/s. In fact, most of the studies above are interested in harvesting the energy under high vibration and high deflection rates where this issue will be the cause

of structural damage to the harvester. Thus, harvesting useful energy under low excitation level will be the most practical method of providing useful energy whilst maintaining a negligible influence on the harvester structure at the same time.

1.2 Problem Statement

The basic strategy of developing renewable energy sources comes from the need to sustain clean energy and reduce carbon emission from fossil fuels. Piezoelectric materials open a new horizon of eco-green energy fields. Recently, fierce competition has resulted in the fabrication of a piezoelectric nanogenerator harvester (i.e., ZnO to numerous non-ferroelectric material), where the challenge is to fabricate such material that distinctly eases its manufacture (i.e., does not impose polarisation processes and sintering under high-temperature process), cost-effective, and yield comparable performance. When the piezoelectric is integrated into the host cantilever, the selected location will influence its performance. Thus, the location is a crucial factor that cannot be neglected for a successful integration of the harvester to a vibrating system. Previously, the piezoelectric was integrated to the cantilever at the region of highest strain, and therefore the optimal harvesting and damping location using a small patch could be realised here. The patches generated poor power at the free end as it had the lowest strain (i.e. strain node) (Liao and Sodano,2012a).

The limitation of the piezoelectric patch has been aforementioned (Eggborn, 2003), where it was not possible for the harvester to be placed at the clamped end of the beam in some applications and it was possible to be placed at the strain node where the real excitation occurs with MDOF thus, the beam motion in such cases was complex. Therefore, there is a need to find a new detecting method to solve this issue. Detecting the dynamic characteristics of the cantilever and visualising its vibration patterns can be achieved by using EMA and ODS.

To the best of our knowledge, there is no study in selecting an optimum harvesting location based on ODS and EMA tools. EMA could provide a solution for overcoming this problem by visualising the mode shape of the tuned beam. The ODS visualises the vibration patterns where the system is excited by unknown operating forces.

1.3 Objectives of the Research

The objectives of this research include:

- i. To develop an enhanced Lead zirconate titanate (PZT) material based on Lead Zinc Titanate-Sodium Titanate (PZnT-NT) as a vibration energy harvester.
- ii. To compare the performance of the PZnT-NT with other commercial harvesters such as PZT, Micro-Fiber Composite (MFC), and PZT bimorph.
- iii. To develop an experimental procedure of selecting the optimum location over the Vertical Axis Wind Turbine (VAWT) for enhancing the energy generation, where vibration techniques (i.e. ODS analysis and EMA) will be employed for this purpose.

1.4 Thesis Outline

This research is targeted to harvest the waste vibration energy from VAWT beams and convert it to useful electric power. A novel piezoelectric material has been fabricated and tested over the host beam on its optimal location. The optimal location has been detected experimentally. The thesis is divided into five chapters: Introduction, Literature Review, Research Methodology (the experiment setup), Results and Discussions, and finally, the Conclusion and Recommendations. Explanations of the thesis organization are given in the following details:

Chapter 1 presents the introduction with a brief overview of the research problem and the aims to be achieved.

Chapter 2 presents the literature review of the studies relating to piezoelectric harvesters. The commercial types and configuration of the piezoelectric harvester are highlighted. The recent advances of nanogenerator (i.e. ferroelectric and non-ferroelectric) have been compared. A part of the literature review covers the subject of harvesting application (i.e. VAWT). This section also presents the most recent studies of vibration energy harvesting.

Chapter 3 presents the preparation method of the piezoelectric non-ferroelectric material, as well as the description of the experimental procedure and detection methods in selecting the optimal location. Additionally, this chapter involves the installation of VAWT for implementing the PZnT-NT on its optimal location and harvesting the energy.

Chapter 4 presents the physical characterisation (i.e., permittivity, loss tangent, conductivity, and polarisation phase) of the PZnT-NT harvester. Also, the optimal location of the host structure has been selected based on the EMA and ODS tools. The harvested energy and the power density of piezoelectric harvester have been recorded and compared with other commercial piezoelectric harvesters (i.e. PZT bimorph, PZT, MFC). The results have been discussed and compared. This chapter also presents the modal analysis results of the VAWT and the harvested energy from the PZnT-NT have been tested and compared.

Chapter 5 presents the conclusion of the determined results based on the energy harvesting and selection of the optimal location. Additionally, the recommendation for future work has been made.

1.5 Research Flow and Scope

The study aims to fabricate a non-ferroelectric material, and the material performance will be compared with commercial piezoelectric products. In general, a considerable understanding will be directed towards studying the properties of such material. Next, the fabrication of the enhanced $0.7\text{Pb}(\text{Zn}_{0.3}\text{Ti}_{0.7})\text{O}_3 - 0.3\text{Na}_2\text{TiO}_3 - \text{PZnT-NT}$ will be accomplished where the generated signal requires the design of a rectifier circuit. The harvester will be tested, and the performance will be compared with other products. Detecting an optimal harvesting location over a cantilever is an important aim in this study, where the EMA analysis will assist in visualising the mode shape and determine the dynamic characteristics of the test rig at the obtained resonance mode. ODS analysis represents the operational deflection shape (vibration pattern) of the operating system. Finally, the harvesters will be tested in a real operation environment (i.e. VAWT) for evaluating the power density of the PZnT-NT. Details are given in Figure 1.1.

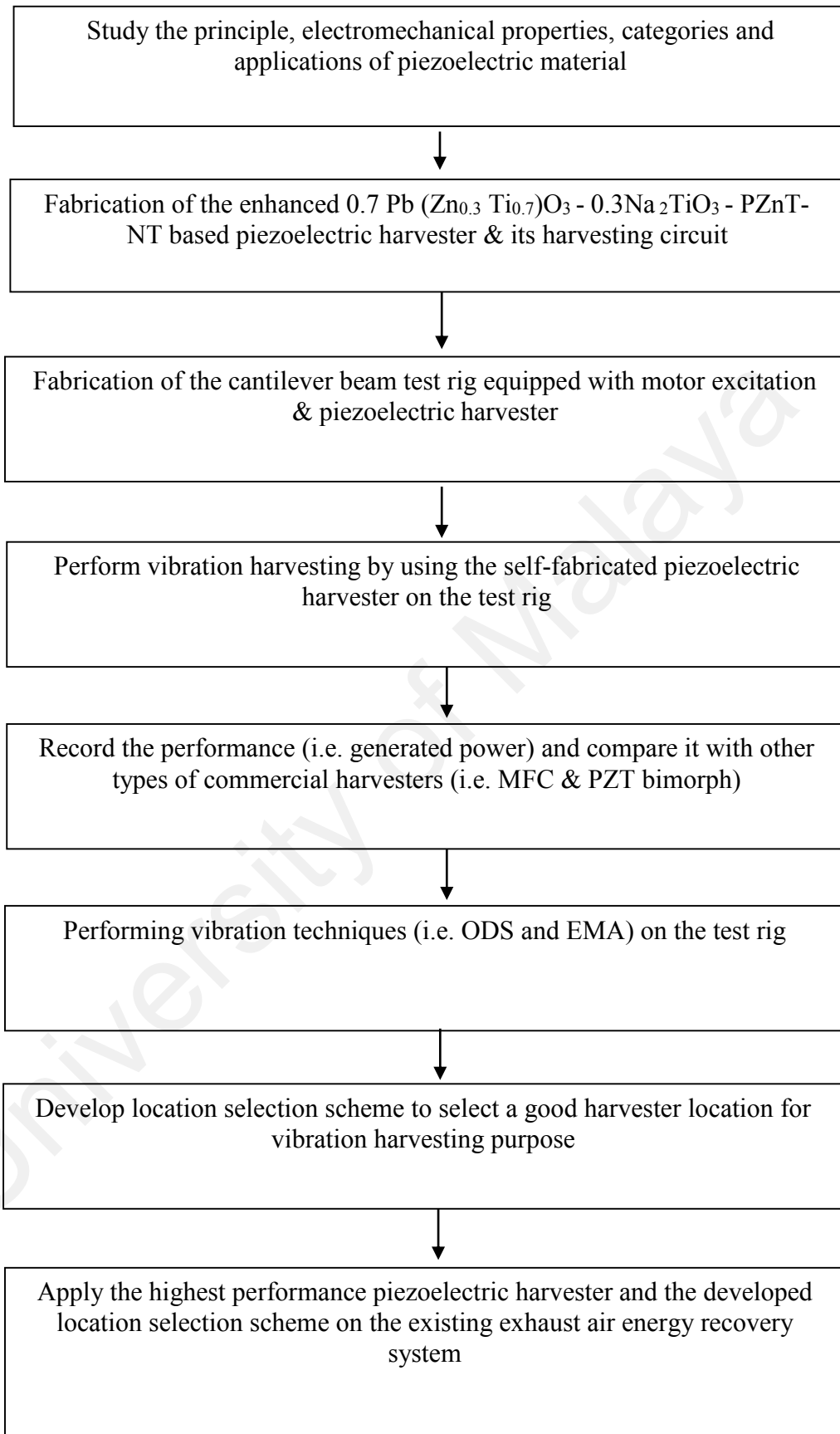


Figure 1.1: Research Flow Chart

CHAPTER 2: LITERATURE REVIEW

2.1 The Piezoelectric Material

The piezoelectric material effect was discovered in 1880 by the Jacques and Pierre Curie brothers. The word “piezo” is derived from the Greek language where “piezin” refers to “pressing” and defines a dipole material that possesses semiconductor behaviour. The piezoelectric materials can be classified as pyroelectric and ferroelectric materials. Note that the prefix “pyro” is the Greek word for “fire”. Pyroelectric materials refer to the material that has spontaneous polarisation resulting from the change of temperature; whereas ferroelectric material is a special portion of pyroelectric materials, and it has a spontaneous polarisation under the Curie point that can reverse the direction of electrical dipoles by applying a high electric field (Jan et al.,2010). Furthermore, ferroelectric materials possess permanent polarisation of the dipoles. A sketch classifying the piezoelectric material is shown in Figure 2.1.

The piezoelectric is one of the semiconductors materials, and certain piezoelectric have perovskite structure (e.g. PbTiO_3 , PbZrTiO_3 , etc.) where the unit cell configuration in cubic cell consists of ABO_3 formula unit per unit cell, and the space group is $O_h\text{-Pm}3m$ (Roth, 1957). The perovskite structure is characterised by its spontaneous polarisation and can be configured to different transition phases such as tetragonal, rhombohedral, orthorhombic, or monoclinic structures.

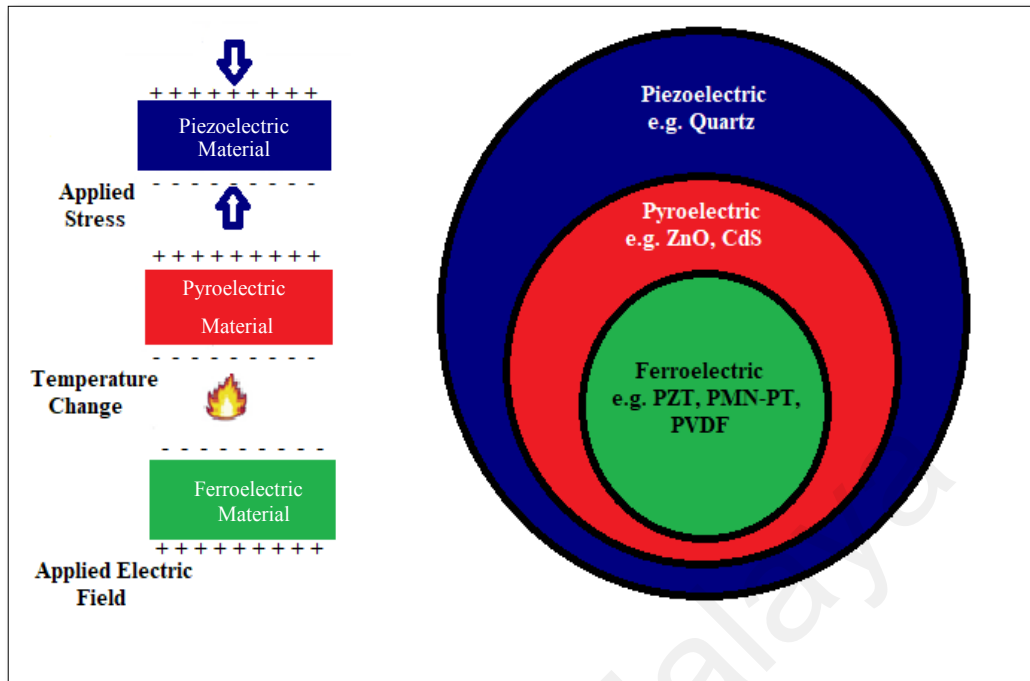


Figure 2.1: Categorization Schematic of Piezoelectric Materials (Keppens, 2016)

The general chemical formula is ABO_3 , where “B” is named the cation and occupies the body centre and “A” unites the electrons that occupy the cubic corners. Three units from oxygen octahedron structure (anion) are distributed at the centre faces of the cubic structure as shown in Figure 2.2.

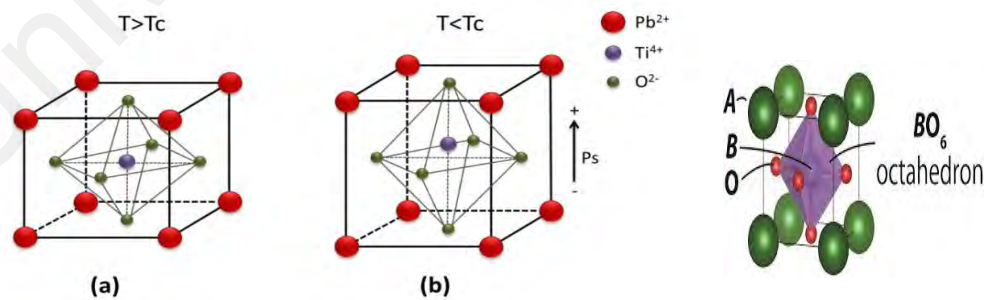


Figure 2.2: Perovskite Structure, ABO_3 (Mindtouch, 2018)

In general, piezoelectric materials could be branched into various categories: Amorphous, Single crystal, Polycrystalline materials and composites or composite-polymer substrate as shown in Figure 2.3.

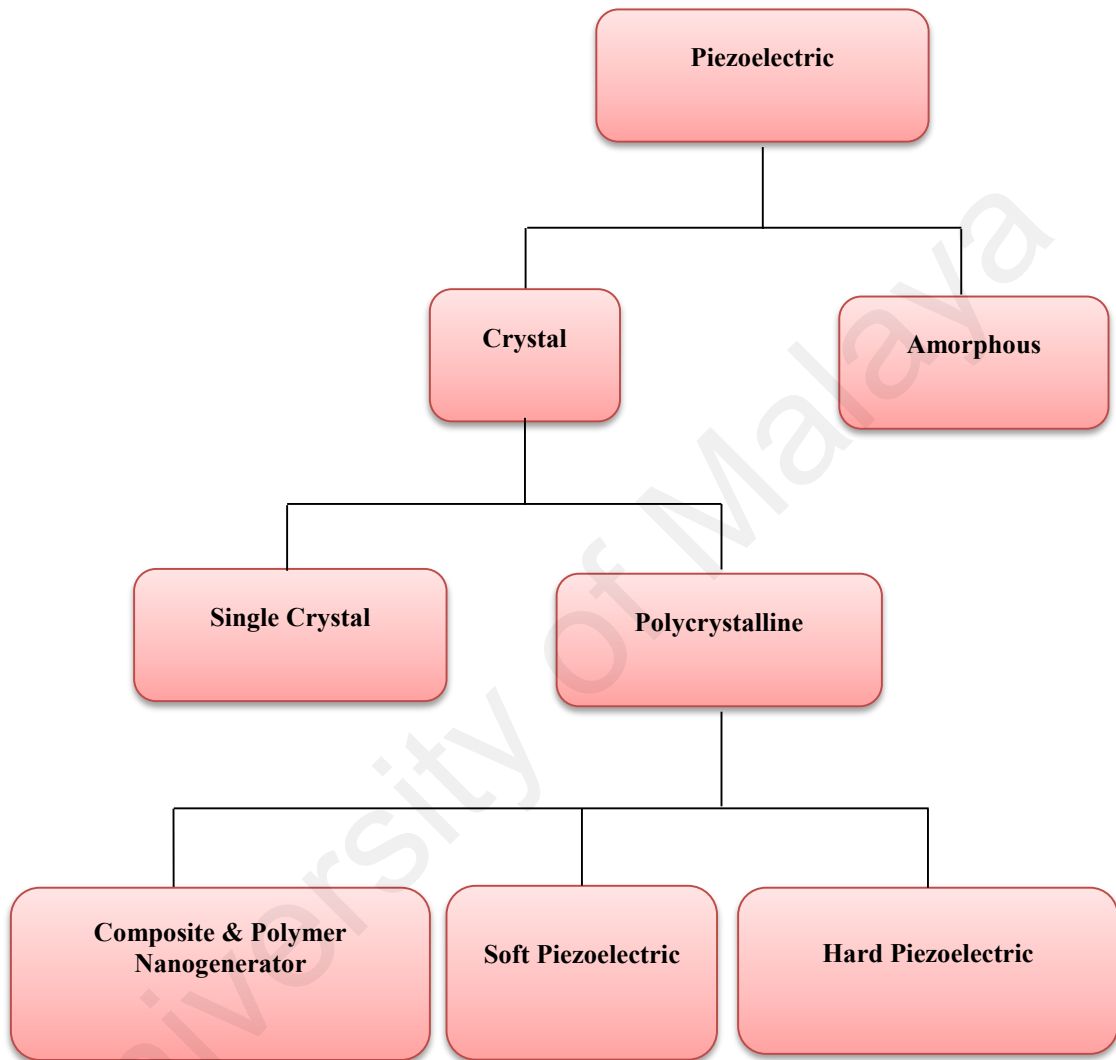


Figure 2.3: Various Categories of Piezoelectric Material

A wide range of sensing applications can be made from Silica Dioxide (SiO_2), Rochelle Salt Potassium Sodium Tartrate ($\text{NaKC}_2\text{H}_4\text{O}_6 \cdot 4\text{H}_2\text{O}$), Lead Zirconate Titanate ($\text{Pb}(\text{Zr}, \text{Ti})\text{O}_3$) ceramic, Zinc Oxide (ZnO), Aluminum Nitrate $\text{Al}(\text{NO}_3)_3$, and Barium Titanate (BaTiO_3). Lead Zirconate Titanate (PZT) is one of the smart materials that can format as a single crystal, bulk, thin/thick multilayer, microfiber patch.

Most of the piezoelectric crystals have a perovskite structure (ABO_3). The conventional methods of ceramic preparation are the solid-state method, hydrothermal synthesis method, solution gel (Sol-Gel) method, and molten salt synthesis (MSS). Recently, the remarkable growth of thin/thick film applications has attributed to the advance of deposition technique of thin/thick films such as the sputtering technology. Thin/thick layers can be deposited onto a substrate layer in order to coat it with a few nano-meters to 100 μm . The thin, thick, and bulk films have been employed in the energy harvesting field. Generally, the thickness of thin film is less than 10 μm and the bulk PZT thickness can be higher than 100 μm (Kok & Swee, 2011). In fact, the thickness is one of the most affected parameters of dielectric property. Previous studies recorded increase of the relative dielectric, loss factor, remnant polarisation with the increase of film thickness with respect to the thickness threshold (Haccart et al,2002; Iijima et al.,2004). These films were manufactured in one of the chemical deposition techniques, Sol-Gel (Nogas-Ćwikiel, 2011), tape casting (Jantunen et al., 2004), pulsed laser deposition (PLD) (Craciun et al., 1999), sputtering (Shibata et al.,2008), spinning (Lund et al., 2012), screen-printing (Baudry, 1987) and to numerous other sophisticated manufacturing methods (Hau et al.,1995). There is also the piezoelectric wafer synthesis by cutting thin slices from the single crystal at a specific orientation.

Fundamentally, the crystal structure can be classified into 32 classes (space group) based on the material crystallography (the dimensional space of the crystal lattice parameter) as illustrated in Figure 2.4. Twenty-one of the 32 classes are non-centrosymmetric. In the non-centrosymmetric category, there are 20 piezoelectric crystal classes.

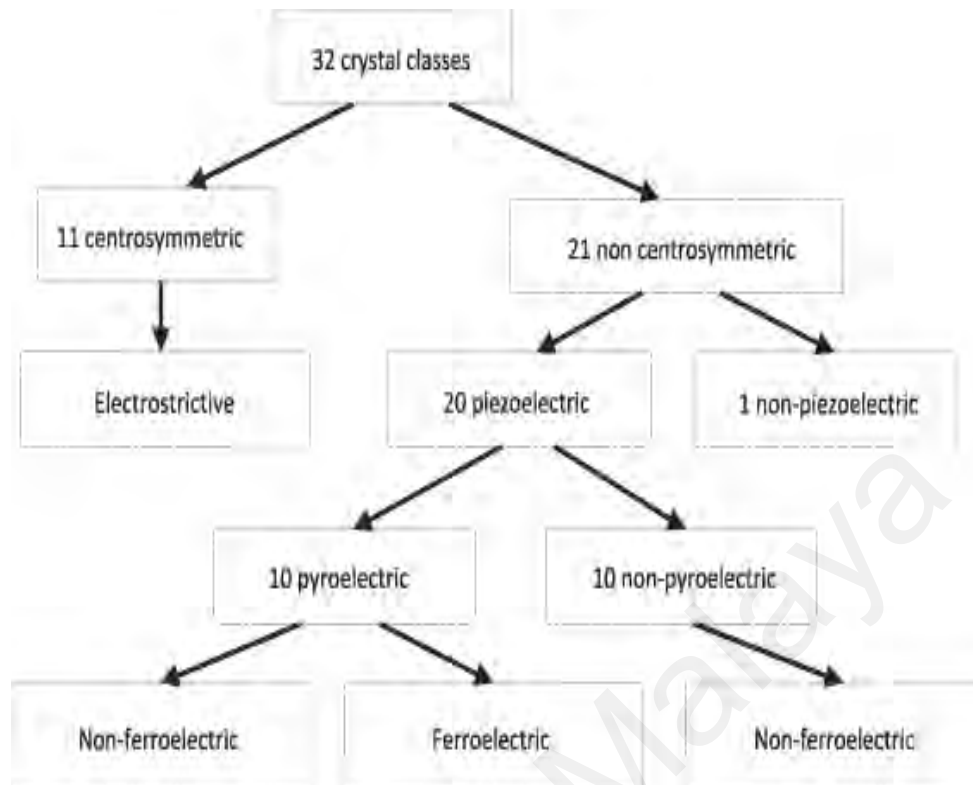


Figure 2.4: The Sorting of The Structural Crystalline of Material Based on Crystal Symmetry (Defay, 2011)

Then, the piezoelectric crystal can be separated into 10 pyroelectric classes and 10 non-pyroelectric crystal classes. Herein, pyroelectric material can be classified into ferroelectric and non-ferroelectric materials, whereas non-pyroelectric material is distinct of non-ferroelectric property. Ferroelectric material exhibits reversal spontaneous polarisation when subject to an external electric field and vice versa. The piezoelectric films (i.e. especially the soft piezoelectric utilised for the harvesting purpose) should be polarised under high external electric fields in order to gain a permanent polarisation where the electromechanical will be improved markedly, where such material has high remnant polarisation. Figure 2.5 shows the polarisation effect on the dipole orientation.

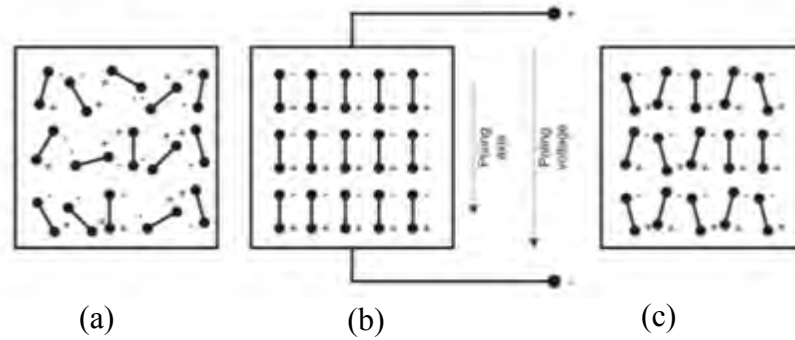


Figure 2.5: Orientation of Crystal dipoles (A) Before, (B) During, and (C) After Polarisation (Jan Tichý et al., 2010a)

The PZT is a ferroelectric material that has a spontaneous polarisation below the Curie point. Prior study has affirmed that the crystal phase in this case was ferroelectric tetragonal (Jan Tichý et al., 2010a). On the other hand, non-ferroelectric has a very low remnant polarisation and hence polarisation is not needed throughout the manufacturing process. Across the remarkable growth of piezoelectric applications, the zinc oxide nanostructure harvester has become one of the promising energy harvesting applications for long terms self-generation devices (Yang et al., 2012). The zinc oxide nanogenerator (ZnO-NG) was fabricated in different morphological structures such as the flexible piezo-nanotubes, piezo-flexible film, piezo-nanofiber, piezo-nanoparticle, piezo-nano rods (Kang et al., 2016) and piezo-nanowires. The zinc nanowires arrays revealed sufficient harvested energy for recharging AA battery and powering micro-devices (Suyitno et al., 2014; Xu et al., 2010).

2.2 Electromechanical Properties of the Piezoelectric Harvesters

Piezoelectric material has reversal effects; in other word, it has direct and converses piezoelectric effects. The direct piezoelectric effect represents the generated electric field upon applying stress (Player, 2016), and it can be expressed as follows:

$$D_i = d_{ijk}X_{ik} \quad (2.1)$$

where D_i is the charge density, d_{ijk} is the third rank tensor of piezoelectric coefficient and X_{ik} is the applied stress, the unit of direct piezoelectric coefficient (i.e. d_{33}) is (CN⁻¹). The converse piezoelectric effect is the strain generated from piezoelectric as a result of applying an electrical field, the unit of converse piezoelectric coefficient is (mV⁻¹). The converse piezoelectric effect is expressed as follows.

$$S_{ij} = d_{ijk}^t E_k \quad (2.2)$$

where S_{ij} is the strain, E_k is the electrical field, and d_{ijk}^t is the piezoelectric strain coefficient. Furthermore, piezoelectric harvesters have long-term lifetime, the flexible microfiber composite has lifetime of around 20 years (Material, 2016). Piezoelectric consists of semiconductor materials that have spontaneous polarisation under exposure to the mechanical stresses or an external electric field. The commonly measured parameters of piezoelectric energy harvesters are the thickness, area, density, capacitance, natural frequency, deflection rate, maximum voltage (open circuit), current and output power rate or power density (Piezo systems, 2016). In particular, the electromechanical properties also play an important role, where the energy density magnitude can be evaluated by the value of piezoelectric strain coefficient (d_{ij}) and piezoelectric voltage coefficient (g_{ij}) (Islam & Priyaa, 2006).

Piezoelectric charge constant, d_{33} is defined as the electrical polarisation generated, D_3 per applied stress, X . The first and second subscripts refer to the direction of electric field and field strength respectively. Alternatively, the d_{33} can express by the strain, S per applied electrical field, E .

$$d_{33} = \frac{D_3}{X_3} = \frac{S_3}{E_3} \quad (2.3)$$

Piezoelectric voltage constant, g_{33} represents the strain developed per applied charge density or field developed per mechanical stress, or the generated electric field per the unit of periodic stress that is applied to the sample.

$$g_{33} = \frac{S_3}{Q_3} = \frac{d_{33}}{K_3^T \epsilon_0} \quad (2.4)$$

where the K_3^T and ϵ_0 are the relative dielectric constant and permittivity in a vacuum (i.e., 8.854×10^{-12} F/m) respectively. Elastic compliances represent the strain magnitude per stress, where the upper subscript E refers to the measurement that is conducted under a closed circuit.

$$S_{33}^E = \frac{S_3}{X_3} \quad (2.5)$$

Additionally, the dielectric constant or permittivity constant is denoted by K_3^T and it can be expressed by the permittivity of material (ϵ_T) per permittivity in a vacuum. Also, It can calculate the relative permittivity from the real dielectric part (ϵ') and the imaginary part (ϵ'') as shown in Eq. (2.6).

$$K^T = \frac{\epsilon^T}{\epsilon_0} = \epsilon' - j\epsilon'' \quad (2.6)$$

The dielectric loss tangent, $\tan(\delta)$, is defined as the ratio between the loss energy to the stored energy in the medium, where there is a portion of electromagnetic energy that will be dissipated as heat under an alternating electric field.

$$\tan(\delta) = \frac{\epsilon''}{\epsilon'} \quad (2.7)$$

The AC conductivity σ can be computed as follows.

$$\sigma = \omega \epsilon' \epsilon_0 \tan(\delta) \quad (2.8)$$

where ω is known as the angular frequency ($2\pi f$). Finally, the storing energy E_C is computed by multiplying the capacitance of the external capacitor of the accumulated voltage, as expressed in Eq. (2.9).

$$E_C = \frac{1}{2} C_C V_t^2 \quad (2.9)$$

where C_C is the external capacitor and V_t is the voltage in the steady state, the power generation or the dissipated power of the load, P across the applied resistances, is computed as follows.

$$P = \frac{V^2}{R_L} \quad (2.10)$$

where V is the voltage at the steady state and R_L is the load resistance of the rectifier circuit. The challenge in energy harvesting is the harvesting of energy under low frequencies, low acceleration and strain. This requires using a soft doped piezoelectric material or by using thin films. This research aims to fabricate a sustainable piezo-harvester with lower cost and higher performance.

2.3 Piezoelectric Configuration and Application Type

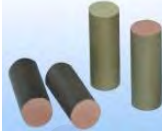
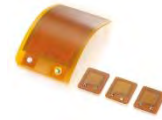
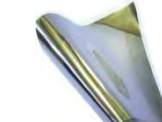
Piezoelectricity is a property of crystalline material hence; the harvested films can be manufactured from single crystal or polycrystalline structures. Basically, the piezoelectric polycrystalline layer deposit (e.g. Sol-Gel) on metal or conductive substrate then anneals under a specific temperature for crystallization of the film. Polycrystalline piezoelectric materials can be classified into soft and hard materials, where soft materials are distinct of their high domain mobility (Ceramic, 2013) and are suitable for energy harvesting applications. It is well known that the piezoelectric has anisotropic properties due to the crystallographic nature of the single-crystal structure, or the morphological alignment of the polycrystalline structure (Du et al.,1999). Thus, the random orientation of dipoles

requires an external electric field for reorienting the domain wall directions and inducing the dipole permanently. Commercial polycrystalline piezoelectric harvesters are fabricated from soft piezoelectric materials (KG, 2013). Most piezoelectric harvesting films are synthesised from PZT, which softens because of *n*-type donor dopant additives (e.g. phosphorus (P), arsenic (As), antimony (Sb), bismuth (Bi), lithium (Li), silicon (Si), tungsten (W^{6+}) and niobium (Nb_{5+}), whereas cation vacancies are considered to facilitate domain wall motion.

The electromechanical properties depend on the crystalline structure hence single crystal (e.g. $PbMg_{1/3}Nb_{2/3}O_3-PbTiO_3$ (PMN-PT)) demonstrate excellent electromechanical properties and normally utilised for sensing (e.g. ultrasonic transducers application) (Zhou et al., 2014), harvesting (Patel et al., 2015) and actuating (Uršič et al., 2011). Other harvesting applications have been fabricated from the soft piezoelectric polycrystalline structure such as $PbTiO_3$, PZT, and $BaTiO_3$. A piezoelectric ignitor is a tool that hits strongly to generate spark; and it is type of single crystal (i.e. PZT or quartz). Amorphous and semi crystalline phases could be realised of PVDF films. Finally, the nanogenerators have been developed and demonstrated to have competitive harvesting performance especially in the wearable harvesting application such as ZnO (i.e. known as a pyroelectric material (Yang et al., 2012)). Generally, Table 2.1 provides a brief detail of some of the piezoelectric configurations.

A schematic of piezoelectric application has been presented in Figure 2.6 for classifying the piezoelectric application according to its required functionality. The piezoelectric harvester is preferred to work in a wider frequency bandwidth due to the need to capture the frequencies of the impedance. It is well known that the tuned harvester can provide higher energy. On the other hand, the tuned application could be subject to damage and reduction of its lifetime.

Table 2.1: Piezoelectric Applications with Different Configurations

Materials Types	Applications and Aspects	Configurations
Single crystal	<p>Applications: Sensing, Harvesting, Transducers & actuators.</p> <p>Aspects: Outstanding electromechanically properties such as high output power rates and high piezoelectric charge constant.</p>	
Bulk material (Eyraud et al., 2008)	<p>Applications: Igniter</p> <p>Aspects: Several thousand volts make a spark from squeezing a crystal and have high g_{33}, high ϵ_{33}^T constant, and high static leakage resistance.</p>	
Multilayer (Noliac, 2013)	<p>Applications: Actuators, flexural piezo-elements like cell phone camera, motors, pumps, sensors, prism positioning, manipulators, printer, etc.</p> <p>Aspects: Convert the electrical energy to mechanical energy and have salient features such as high relative permittivity, high charge constant and high density.</p>	
Monolithic Patch (physikinstrument e, 2013)	<p>Applications: Patch transducer, energy harvester, actuator, and sensor.</p> <p>Aspects: Transform electrical to mechanical energy and vice versa. High formable ceramics can be applied to curved surfaces. It is cost effective and suitable for low energy harvesting purpose</p>	
Microfiber (MFC) (Material, 2015)	<p>Applications: Energy harvester</p> <p>Aspects: Piezo-ceramic ribbon fibers in a tough and flexible polymer matrix. It requires injection molding techniques.</p>	
Piezoelectric Benders (Nolica, 2015)	<p>Applications: Acoustic applications such as buzzers.</p> <p>Aspects: Characterise of higher Q factor and lower mechanical loss. Typical product has performance ranged up to +/- 1500μm stroke and up to 10N blocking force. Unique shaped product has performance ranged up to +/- 150μm and up to 100N blocking force.</p>	
Piezo/polymer (i.e. Polyvinyliden Fluoride Film) (Celina et al., 2005; Porex, 2015).	<p>Applications: Motion sensors, active and passive vibration, marine fouling prevention membranes, Magneto-electric sensors, touchscreen, hand-phone membrane and speakers (Celina et al., 2005; E. S. Materials, 2016).</p> <p>Aspects: High sensitivity to strain, high flexibility, wrap-able, high bandwidth, very low power, eases to manufacture. Low curie temperature, low piezoelectric strain constant, low quality factor and low dielectric constant and high piezoelectric voltage charge.</p>	
Hybrid-stretchable piezoelectric (Institute, 2016)	<p>Applications: Hybrid-stretchable elastic-composite energy harvester.</p> <p>Aspects: High flexibility, wearable and durability, ease to manufacture. Low curie temperature, low piezoelectric strain constant, low quality factor and low dielectric constant.</p>	

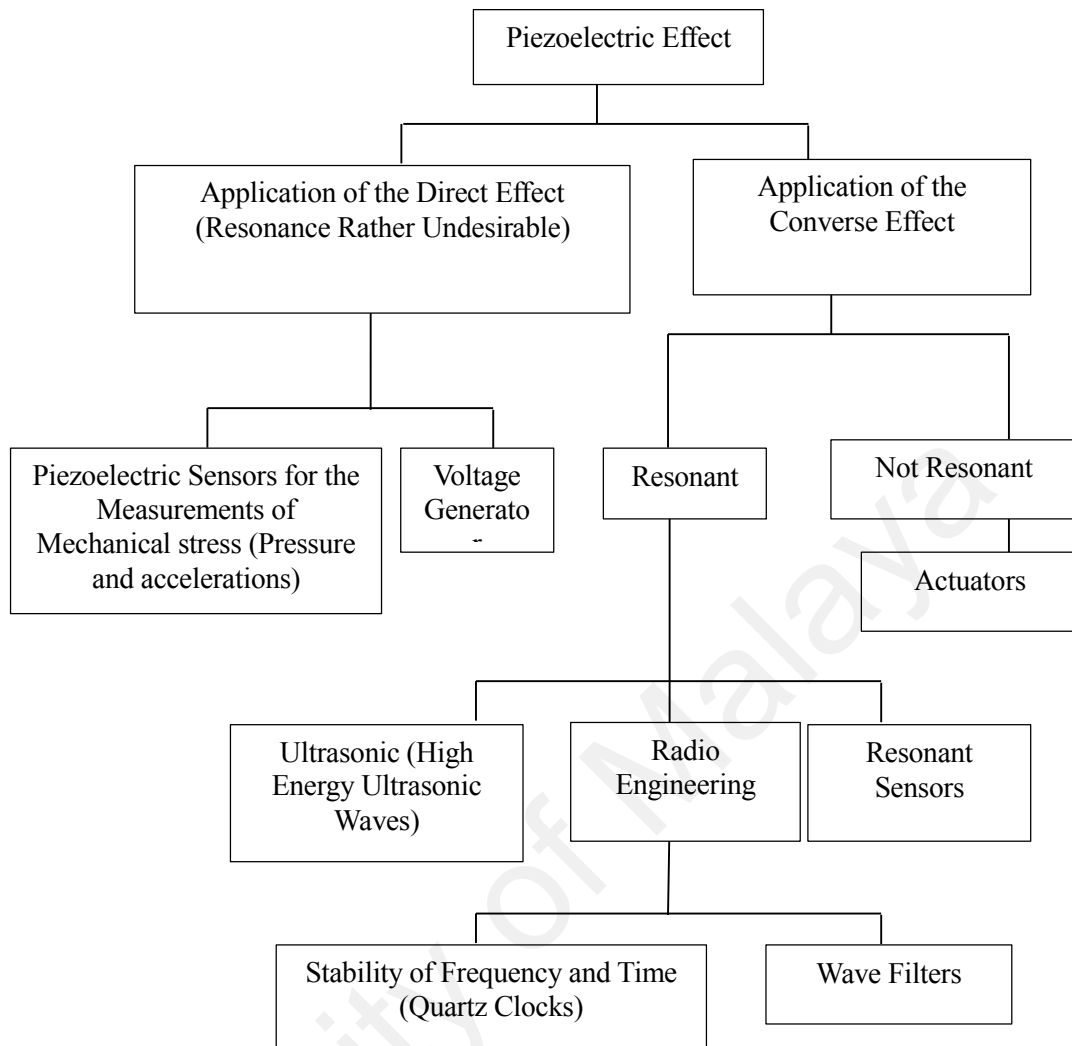


Figure 2.6: Classification of The Piezoelectric Application Based on Its Piezo-Effects (Jan et al., 2010 b)

The most recent advances in the fabrication of zinc oxide nanogenerator (ZnO-NG) harvesters have shifted towards the development of flexible piezo-nanotubes, piezo-flexible films, piezo-nanofibers, piezo-nanoparticles, piezo-nanorods (Kang et al., 2016), and piezo-nanowires. Zinc nanowire arrays have voltage sufficient for recharging AA batteries and powering micro-devices (Suyitno et al., 2014; Sheng Xu et al., 2010). The energy harvested from most flexible NGs is produced by bending, pressing, and stretching the films in the absence of an interference structure. In contrast, common methods of harvesting energy using brittle polycrystalline films employ a classical beam model. The cantilever beam system consists of a piezoelectric element and hosts flexible beam.

Normally, the piezo-transducer is bonded over the clamped side (away from the excitation source) (Daniel et al.,2011; Kumar et al,2014; Nechibvute et al,2011) and optimal performance is achieved only when the impedance matches the applied load of the closed circuit. For flexible NGs, there is inadequate research regarding the estimation of harvester lifetime and the potential tearing that could occur from long-term stress.

2.4 Enhancement of Piezoelectric Properties by Improving Conductivity

The conventional piezoelectric materials such as PZT suffer fatigue problem which leads to poor harvesting power. In this way, the lifetime of the piezoelectric material is short in a harsh working environment. This is because the piezoelectric strain and permittivity of these conventional piezoelectric materials are low and therefore needs improvement. Recently, the enhancement of the piezoelectric strain and permittivity had been achieved by adding supplement conductive fillers such as nanocarbon, nanocarbon black (Banerjee & Cook-Chennault, 2012; Tian & Wang, 2008) and nano-graphite (Hu et al.,2010; Park et al.,2012), sufficient volume fractions from such conductive fillers caused a considerable enhancement of the poling efficiency of the ferroelectric materials (Babu & de With, 2014). Excessive increasing of the conductive filler ratio will result in the yield reduction of ferroelectric phase (Zhou, 2006).

There is no data that has been presented in the previous literature to evaluate the conductivity of the PbZnTiO_3 in the harvesting application. In fact, the PbZnTiO_3 is a ferroelectric material (Taira et al., 2008a). It was utilised mainly for sensing or as memory storage device (Johnson ,1997; Taira et al.,2008a). By choosing a proper conductive filler or the carrier material such as sodium titanate (Na_2TiO_3), *n-p* approach of $\text{PbZnTiO}_3 - \text{Na}_2\text{TiO}_3$ fabrication can be realised using wet chemical method, where the crystallization of the compound was grown under the potential difference of the electrodes (i.e zinc and copper). By this method, it expected two and separated regions will be constructed nearby

the electrodes: n-type region above the zinc electrode and p-type region below the copper electrode. In this way, it is expected that the proposed $\text{PbZnTiO}_3 - \text{Na}_2\text{TiO}_3$ material can improve its power harvesting performance by enhancing its conductivity. In the early stage of the research, the weight ratio of Na_2TiO_3 was fixed at 0.3 wt.%. This is because the early investigation shows that the weight ratio exceeding 0.3 wt.% will cause the proposed harvester to lose the piezoelectricity property. In short, a novel $0.7\text{PbZn}_{0.3}\text{Ti}_{0.7}\text{O}_3 - 0.3\text{Na}_2\text{TiO}_3$ (PZnT-NT) piezoelectric material will be manufactured throughout this study and the effect of conductivity towards the harvesting performance will be measured and evaluated next. This study will focus on investigating the conductivity effect on the ferroelectricity property of the PbZnTiO_3 and its usage in vibration harvesting application.

2.5 Comparison of the Electromechanical Properties for Various Piezoelectric

Harvesters

Evolution of the performance and properties of piezoelectric harvesters have been studied excessively where some researchers have compared the electromechanical properties (i.e. d_{33} , g_{33} , etc.) and numerous others have adopted the comparisons that reflect the real performance in piezoelectric harvesters. In terms of studying the performance, the standardized evaluation parameters of piezoelectric energy harvester are the thickness, area, density, stiffness, capacitance, natural frequency, deflection rate, maximum voltage (open circuit), current and output power rate or power density (short circuit) (Piezo systems, 2016).

Polycrystalline piezoelectric materials can be classified into two types: soft and hard materials where soft material is distinct of high mobility of domains (Ceramic, 2013) and is appropriate for energy harvesting applications. It is well known that piezoelectric material has anisotropic properties due to the crystallographic nature of the single crystal or the morphological alignment of the polycrystalline structure (Du et al., 1999). Thus,

the random orientation of the dipoles requires external electric field to assist in reorienting the electrical domains or in inducing the domain walls motion of the crystalline structure. The negative and positive carriers or dipoles (i.e. electrons and holes) will be separated and shall move inversely across the piezoelectric film surfaces. In doing so, the material gains permanent polarisation. In this regard, a comparative study has established a standardized base for recognizing the electromechanical properties of different piezo-configurations; where Daniels (2013) analysed 25 different piezoelectric materials, which included single crystal, a PVDF, 12 soft PZTs, and 11 hard PZTs.

It was found that the highest output power can be generated by exciting a single crystal, whereas the output power of the hard materials was a lower rate than those of soft materials. In addition, Daniels had compared the relative dielectric constant and the average power generation (P_{avg}) for numerous piezoelectric material configurations, and the results demonstrated the direct relationship with the P_{avg} , the PVDF produced high average power and lower relative dielectric constant.

Results for Thomas demonstrated that the generation of soft PZT materials was 2 times higher than that of hard materials (Thomas, Kunzmann & Schönecker, 2008). In general, the soft piezoelectric material application can be suited with acoustic devices (i.e. the low-power ultrasonic transducers and low-frequency sound transducers) and taped as energy harvesters whereas hard material can be used in actuators, transducers, and other acoustic applications. Soft ceramic products are characterised by a high piezoelectric constant (d_{33}), high permittivity (ϵ), high dielectric losses, and low mechanical quality factor (Daniels et al., 2013; Jan Tichý et al., 2010a; Thomas, 2008) In general, soft piezoelectric materials distinct of excellent figures of merit (e.g. piezoelectric strain constant d , piezoelectric voltage constant g , coupling factor k , quality factor Q_m , and acoustic impedance Z , (Islam & Priya, 2006). Soft materials have a high charge output and dielectric constant, but lower thermal stability, because the Curie temperatures of

most soft materials are lower than those of hard materials. In terms of single crystals or oscillators, single crystals can be employed for energy harvesting (Islam & Priya, 2006), or used in other classic applications such as sonar applications, frequency stabilizers, ultrasonic transducers, microphones, accelerometers, sensitive hydrophones, and ceramic phone cartridges.

Quartz is the best example of a resonator that can be created either by cutting a slab from natural gemstone or by manufacturing the mineral from raw materials. Quartz has outstanding features such as rigidity, high elastic compliance, a high natural frequency, compact design, high quality factors, and lower damping (which reduce energy dissipation). The quartz oscillated 12 million times per second, and this was done by connecting the crystal to a periodic voltage source. As a result, the piezo-crystal will vibrate at a frequency equivalent to the supplied voltage. A comparison between different piezoelectric configurations provides a clear assessment for researchers interested in fabricating a specific piezoelectric device, whether it is a single crystal, soft piezoelectric material, or hard piezoelectric material. The mechanical and electromechanical properties are presented in Table 2.2 based on the results of prior studies (Bowen et al., 2014; Dakua et al., 2013; Daniels et al., 2013; Esterly, 2002; Gusarov, 2015; Kumar et al., 2011; Lee et al., 2006; Materials, 2016; Zhang et al., 2001). Many sensing application syntheses from doped piezoelectric (soften piezoelectric) due to the soft piezoelectric material exhibit high strain constant, high dielectric constant, large coupling factor, low mechanical quality factor and high loss tangent, $\tan(\delta)$. The soft piezoelectric material characterises the high-quality factor, higher coercive field, and low mechanical loss.

Eyraud (2008) conducted an experimental investigation of ignitable material performance versus applied stress where the study measured the generated current and electric charge value when the hard and soft piezoelectric was subjected to a high squeezing force. The research finding affirmed that the only hard piezoelectric can create

an electric spark. In fact, the ignitors generate high voltage that ionizes the air molecules within micro tiny parts of second and has high current value (APC International, 2013; Audigier, 1994). The measured parameters are the generated current and output charge, where applied mechanical stress was 60 MPa during 0.5 s. In case of shock, a hard PZT, and the maximum current was 80 A whereas the mathematically computed current was 60 A.

Table 2.2: Comparative Properties between Different Types of Piezoelectric Materials

Properties	Single Crystal PMN-PT (Lee et al., 2006)	Ferroelectric Soft PZT (Materials,2016)	Ferroelectric PZT (Materials,2016)	Ferroelectric PVDF (Daniels et al.,2013)	Non-ferroelectric ZnO
Ferroelectric	√√√	√	√	√	×
Mechanical Quality Factor	43.00-2800	60.00-1200	575.0-1200	13.00	1770 (Bowen et al., 2014)
Elastic Compliance, S_{33} (10^{-12} m ² /N)	66.60 (Daniels et al.,2013) 119.60 (Zhang et al., 2001)	10.00-15.00 (Daniels et al.,2013)	14-16.1 (Daniels et al.,2013)	472.0 (Esterly, 2002)	6.940 (Bowen et al., 2014)
Charge Constant, d_{33} ($\times 10^{-12}$ CN ⁻¹)	> 2200	250.0-926.0	280.0-307.0	-33.00 (Esterly, 2002)	12.00- 26.70 (Dakua et al., 2013)
Coupling Factor, K_{33}	93.00	0.540-0.770	0.550-0.580	0.150	0.480 (Bowen et al., 2014)
Piezoelectric Voltage constant, g_{33} ($\times 10^{-3}$ Vm/N)	44.00	21.90-45.70	26.30-26.80	-339.0 (Esterly, 2002)	135.0 (Kumar et al., 2011)
Dielectric Losses, $\tan\delta$ (%)	< 0.500	1.350-2.900	0.200-0.350	N/A	N/A
Curie Temperature Range, °C	150.0	150.0-374.0	300.0-350.0	100.0	N/A
Relative Dielectric Constant	> 5000	1800-7066	1105-1650	10.70 (Gusarov, 2015)	8.75 (Dakua et al., 2013)

1 √√√ A very high polarisation (Cao, 2005)

Additionally, the results affirmed that the spark could be generated under squeezed stress only in hard materials. The igniters were utilised by energy harvesting applications such the self- powering FR sensor (Tan et al., 2006).

2.5.1 Soft and Hard Piezoelectric Material

Piezoceramic can be divided into two sorts (soft and hard) according to the BS EN50324-3:2002 European standard. The excellent properties of PZT are realised by adding specific additives to the pure PZT for meeting the application requirements. High mobility of dipolar attributes to the donor dopant (cation) creates vacancies in the crystal structure. Soft ceramic products are characterised by a high charge constant, high permittivity, large dielectric constant, high dielectric losses, and low mechanical quality factor. Also, the hard-ceramic exhibits greater coercive field through polarisation compared with the soft ceramic. A comparison between soft and hard piezoelectric ceramic based on the electromechanical properties are shown in Table 2.3.

Table 2.3: Comparison of Characteristics between Soft Ceramics and Hard Ceramics (APC International, 2014)

Characteristic	Soft PZT	Hard PZT
Piezoelectric Charge Constants (i.e. d_{33} , d_{31})	High	Low
Permittivity	High	Low
Dielectric Constants (i.e. relative)	High	Low
Dielectric Losses	High	Low
Electromechanical Coupling Factors	High	Low
Electrical Resistance	High	Low
Mechanical Quality Factors	Low	High
Coercive Field	Low	High
Polarisation / Depolarisation	Low	High

In terms of energy harvesting, the hard material exhibits low piezoelectric charge constant and lower permittivity than soft ceramic, but the large quality factor property is suitable with the application that requires high frequency generation such as silicon dioxide (SiO₂).

The formatted piezoelectric bulk structure has an electrical effect toward 3-axis (d_{33}). Multilayers of piezoelectric materials are used for harvesting the energy at a lower vibration rate than that of bulk materials. In addition, piezoelectric bulk materials are distinguished by the easy manufacturing process and low capacity, where the multi-components can be customized with complex electrode design. Furthermore, it can be operated under higher electric field with more resistance to humidity (Noliac, 2013).

The soft PZT materials result in a higher charge output 2 times that of hard materials under half-applied mechanical loads as shown in Figure 2.7.

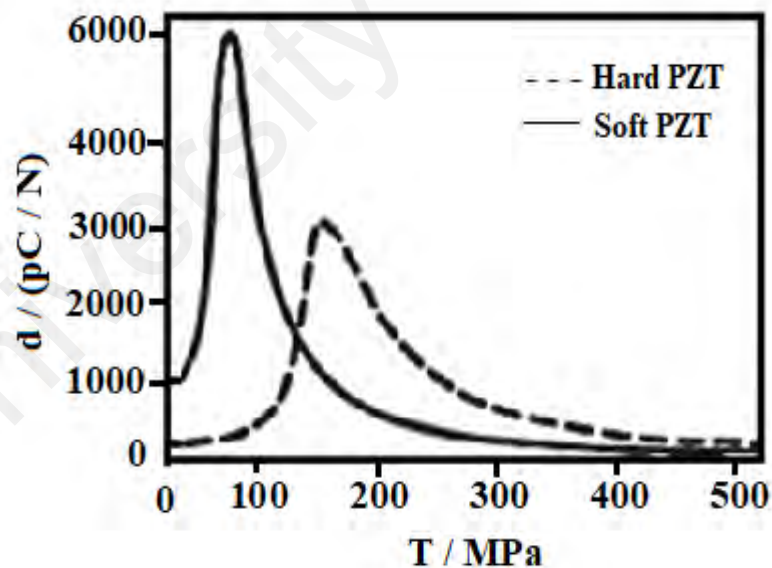


Figure 2.7: Mechanical Depolarisation of Hard And Soft Materials (Thomas, 2008)

The Finite Element Method (FEM) was used to analyse the output power rates for 25 different piezoelectric materials, which included single crystal, a PVDF, 12 soft PZTs,

and 11 hard PZTs (Daniels et al., 2013). This study recorded the highest output power for the single crystal whereas the output power of the hard materials was recorded as being of a lower rate than those of soft materials. In addition, Daniels had compared the relative dielectric constant and strain constant for numerous piezoelectric materials configurations as shown in Figure 2.8.

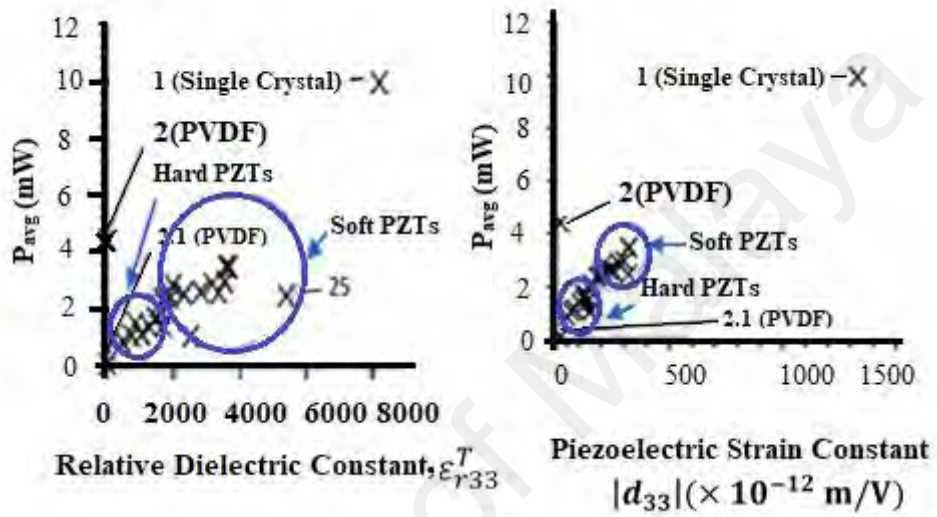


Figure 2.8: Output Rates of Numerous Types of Piezoelectric Material (A. M. Daniels, Zhu;Tiwari, A., 2013)

2.6 Polarity of Ferroelectric and Non-Ferroelectric

The ferroelectric material is recognized by its spontaneous polarisation where the ferroelectric crystals exhibit spontaneous reversing or reorientation of the electrical dipoles below Curie temperature. Increasing the temperature above the curie limit will cause of dramatically reducing of polarity. In this case, this phase of polarity is known as paraelectric phase.

Inherently, the hysteresis loop is phenomena occur in the ferroelectric material that exhibits large piezoelectric response (Xue et al., 2011). Hysteresis loop is detected by applying a strong electric field for switching the domain, accordingly the non-linear variation between the electric field and the polarisation will be drawn during applying

and removing the electric field. The typical nonlinear behaviour of ferroelectric materials illustrated in Figure 2.9.

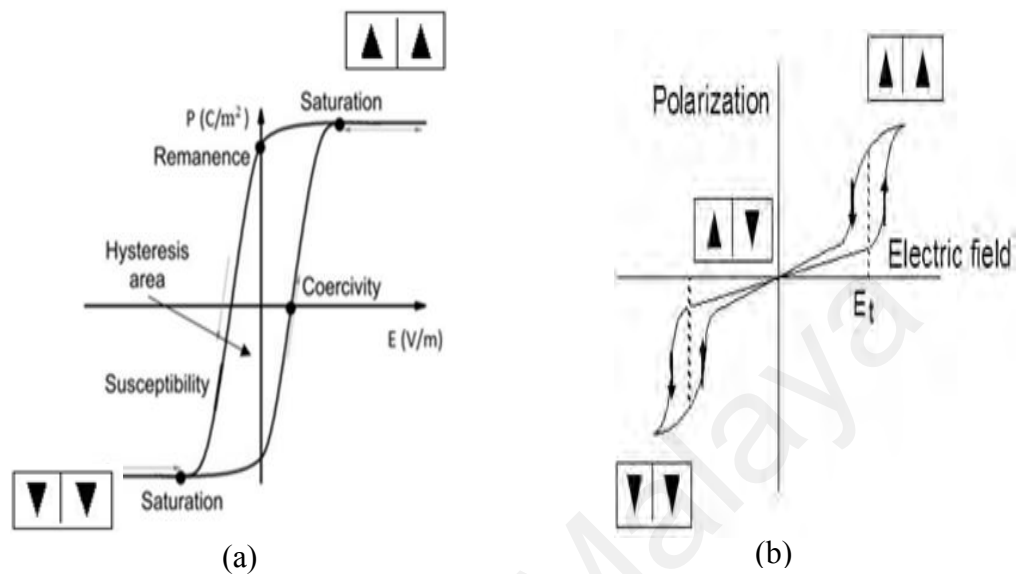


Figure 2.9: The Typical P-E Nonlinear Hysteresis Loop (a) Ferroelectric (b) Anti ferroelectric

Coercivity is the electric field limit that able to polarise the material without damage. Piezoelectric harvesters can fabricate from both ferroelectric and non-ferroelectric materials. The high remnant polarisation is an indication to the superiority of electromechanical properties, where the piezoelectric with high remnant polarisation was reported high piezoelectric strain constant, high permittivity and lower coercive field (Liu & Ren, 2009). Antiferroelectric phase is the phase that has zero remnant polarisation where the dipoles move in parallel anti-direction lines (Kittel, 1951). Recently there are advance scanning microscopic probes such as piezo-response force microscopy (PFM) and time-voltage spectroscopy that utilised for exploring the dynamic phase of the ionic dipoles (Vasudevan et al., 2017).

2.6.1 Ferroelectric and Non-ferroelectric Piezoelectric Harvesters

Commercial piezoelectric materials can be classified into single crystal, soft piezoelectric, hard piezoelectric (Physik Instrumente, 2013), piezoelectric polymer composite groups and nanogenerator. The common conventional methods of piezoelectric material preparation were the solid-state method (Nesbitt et al., 2000; Islam & Priya, 2006; Nabunmee et al., 2011) and the wet chemical methods such as the hydrothermal method, spray drying, aerosol spray, cytochemical, solution gel (Sol–Gel) method (Nogas-Ćwikiel, 2011), etc.

Recently, the nanogenerator has been achieving a rapidly progressive and become an aggressive competitor to the brittle piezoceramic ferroelectric in the energy harvesting field (Qin et al.,2016; Stassi et al., 2015; Zhu et al.,2010). Flexible harvesters can be synthesised as thin/thick piezoelectric patches with high sensitivity to surrounding mechanical vibrations. Recent advances have been demonstrated the high energy density of ferroelectric and non-ferroelectric harvesters. Non-ferroelectric materials (e.g. ZnO-NGs) distinct of low electromechanical properties, such films can be prepared without a polarisation process, making them cost effective in industry. The wet chemical method is carried out at the lower temperatures and hence it becomes more attractive especially for the nanogenerator harvesters. The nanogenerator could be classified into ferroelectric and non-ferroelectric materials. Recent researches have demonstrated that high power density could be harvested from vibration energies using both ferroelectric and non-ferroelectric nanogenerators (Fan et al., 2012; Kang et al., 2016; Liu et al.,2015; Suyitno et al., 2014; Wu et al.,2012; Sheng Xu et al., 2010). Silicon nanowires (SiNWs) is an example of ferroelectric nanogenerator that normally covered by thin flexible polymer, and the importance of preventing the short current leakage in SiNWs was highlighted in (Liu et al, 2015). Another enhancement of nanogenerator can be achieved by using pre-treatment processes, such as reducing oxygen vacancies, air annealing, applying Schottky contact

techniques, and increasing the conductivity. Recent advances have demonstrated the high-energy density of both of the ferroelectric and non-ferroelectric harvesters. In general, the power density of such films is determined by multiplying the maximum voltage values (open circuit) and the current density values (short circuit).

It is well known that pyroelectric materials (e.g. ZnO) are a subgroup of piezoelectric materials, and that ferroelectric materials (e.g. PZT, BaTiO₃ and PMN-PT) are a subset of pyroelectric materials. Ferroelectric materials require high electric field for permanently aligning dipoles, thus the material needs to be polarised in a high electric field. In contrast, ZnO can be classified as non-ferroelectric because of the weakness of its polarisation phase (Pazde-Araujo et al.,2001). It's well known that the ZnO have low electromechanical properties thus the researchers aim to enhance its performance by reducing the screening influence in the ZnO. Yin (2015) fabricated NiO-ZnO nanogenerator based on the n-p junction approach, the current density of this material was increased 13 times larger than the current density in the original ZnO. Based this research the DC current could be generated from NiO-ZnO under vertical compressive force.

In this part, the power generation rates are evaluated for both ferroelectric and non-ferroelectric films. Before making a comparison, it's proper to highlight the ability of NGs to generate power. Three effects have been discovered for flexible NGs: piezoelectric effects, triboelectric effects, and pyroelectric effects. In terms of triboelectric and piezoelectric effects, a group of researchers achieved high generation power using a hybrid piezoelectric-triboelectric system, triboelectric system consists of two friction layers separated by small gap. Normally, the generated signal of the triboelectric and p(VDF-TrFE) nanofiber-PDMS/MWCNT micro structure rectified using two rectified bridge circuits that connected to the oscilloscope (Agilent 2000X), the increasing of the frequency was caused by the increased in voltage peak.

The power and power density of the triboelectric were 98.56 mW and 1.98 mW/cm³ under matched load of 5 MΩ where the generated power and power density of p (VDF-TrFE) were 9.74 μW and 0.689 mW/cm³ under matching load of 30 MΩ (Wang et al., 2016). Similar experimental procedure was conducted using piezoelectric-triboelectric microscale. The triboelectric component produced high voltage, while the PVDF supplied a high current. The maximum peak output was 370 V, current of 12 μA.cm⁻² and power density of 4.44 mW.cm⁻². Recurrent finger tapping (an approximate force of 0.250 N) illuminated 600 light-emitting diodes (Jung et al., 2015), as shown in Figure 2.10.

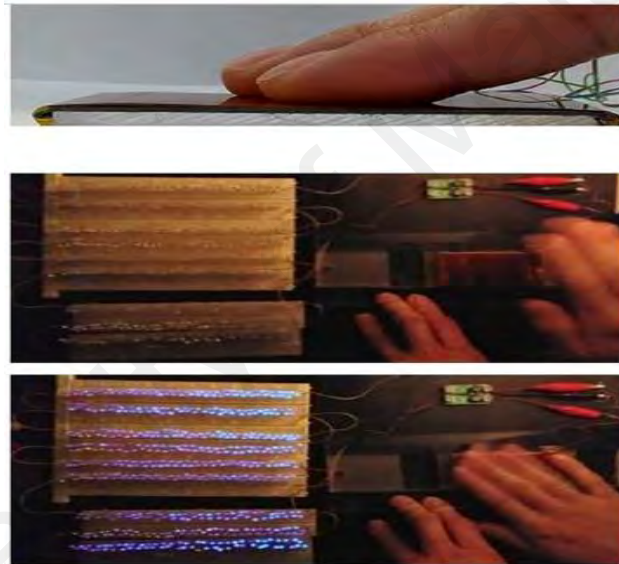


Figure 2.10: Illuminating of 600 Light-Emitting by Triboelectric and Piezoelectric Hyper Effect (Jung et al., 2015)

Herein numerous techniques associated with the synthesis of flexible piezoelectric NG, where some researchers have shifted towards synthesizing NG using ZnO-PEDOT: PSS *p*-type bi-layers (Jalali et al., 2013). The enhancement of NG electro-mechanical properties is achieved by reducing oxygen vacancies; this technique causes significant increases in voltage output and induced current. In general, many pre-treatment processes are used to improve the performance of piezoelectric harvesters, such as oxygen service cleaning, NG air annealing, *p-n* junction and Schottky contact techniques (contact

between metal and semiconductor). Other improvements were achieved by using hybrid devices containing graphene oxide (GO) (Bhavanasi et al.,2015) or by pairing photovoltaic and piezoelectric devices. Improvements in ferroelectric properties were realised using doped GO or reduced GO (RGO) (Karan et al.,2015). In fact, the presence of GO could be altered the hysteresis loop, and in transforming the non-ferroelectric phase to a ferroelectric phase. This leads to considerable increasing in generated voltage and power density (Bhavanasi et al., 2015).

Graphitic carbons were used with BaTiO₃ nanoparticles to reduce the resistance of NG, where the device exhibits ferroelectric behaviour and poled at a temperature of 150 °C and 1 kV for 20 hr. This leads to a voltage increase from 0.2 to 3 V, the amplitudes of the current peaks also increase. The researchers highlighted the importance of testing lifetime and durability. A lifetime test was carried out at 200 cycles per minute for over three days and the results showed outstanding voltage generation stability (Park et al.,2012). The same experimental procedure had been followed for synthesizing PZT-multiwall carbon nanotubes (PZT-MWCs). The recorded voltage and current amplitudes for these were higher than the harvested values for BaTiO₃ nanoparticles (Park et al.,2013) (See Figure 2.11). Additionally, the polarisation of PZT-MWC NGs is given in Figure 2.12.

Gupta (2016) fabricated a flexible ferroelectric microgenerator from lead-free piezoelectric film Na_{0.47}K_{0.47}Li_{0.06}NbO₃ (NKLN) mixed with dimethylsiloxane (PDMS) at a volume fraction of 40:60. The polarisation process was carried out at 50 kV/cm for 24 hr at room temperature. The material had a high d_{33} reached to 460 pC/N, and high induced voltage was achieved, with the voltage peak and a current density of 48 V, 0.43 $\mu\text{A}/\text{cm}^2$ respectively. Hence, the harvester was compressed by a vertical force of 2 kgf at a frequency of 3 Hz (Gupta et al., 2016). In same horizon, flexible BaTiO₃ nanotubes had a voltage of 5.5 V and current density of 350 nA/cm² (Lin et al.,2012).

Polyvinylidene fluoride (PVDF) film is an example of a flexible piezoelectric composite used in numerous sensing applications and employed for energy harvesting. PVDF film could be used in the soles of shoes for harvesting energy from walking. Starner harvested walking energy by using a PVDF film fixed in the soles of shoes (Starner, 1996). Furthermore, PVDF has been used in the straps of bags, as results to the feet pressing the energy could generate and store for later use.

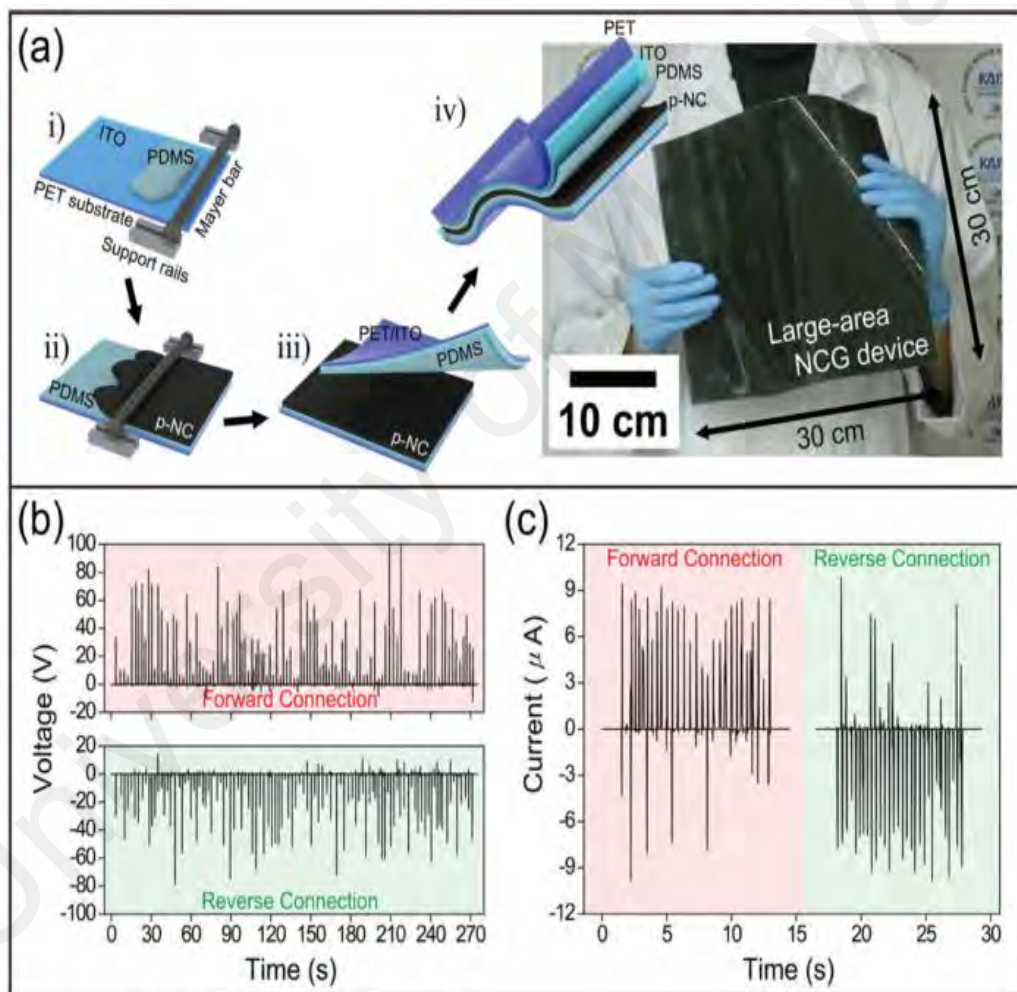


Figure 2.11: Synthesised a Flexible Nanocomposite Generator NCG Device (a) Schematic of Formatting Process, (b) Voltage Generation Using Open Circuit of the Polarised NCG, (c) Short Circuit- current Measurement (Park et al., 2013)

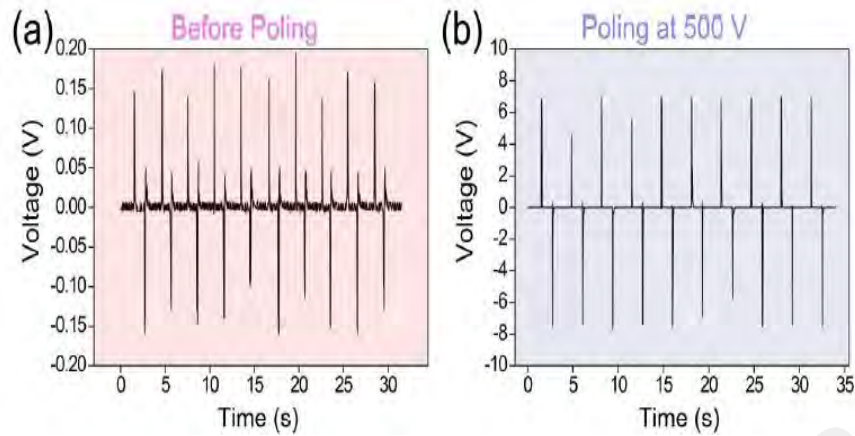


Figure 2.12: Poling Affect at the Generation Voltage Rate (Park et al., 2013)

In terms of non-ferroelectric materials, material science researchers have developed vertical alignment ZnO NWs that are integrated into an insulating layer; the formatted ZnO-NWs have spontaneous electric dipole polarisation. Thus, the developed ZnO NWs provided a high response when tapped with a human palm, and the sciatic nerve of frog directly stimulated under an electric potential of 60 mV to 80 mV as illustrated in Figure 2.13. The maximum voltage (open-circuit) reached 58 V and the current (short circuit) was 134 μA . The maximum power density was 0.78 mW/mm^3 , where the AC voltage was rectified by a bridge rectifier circuit. A ZnO NW seed layer was deposited by RF sputtering, and the NWs were grown densely by using the hydrothermal method.

A polymethylmethacrylate (PMMA) coating layer was employed to cover the ZnO NWs. Nine layers from ZnO NW produced voltage peak (open circuit) and current (short circuit) of 58 V and 134 μA respectively. The area of the single harvester was $1 \times 1 \text{ cm}^2$ (Zhu et al., 2012). The energy generated by palm hitting that stimulated a sciatic nerve of a frog. Twenty times Palm hitting could charge a capacitor of 2 μF to 3 V.

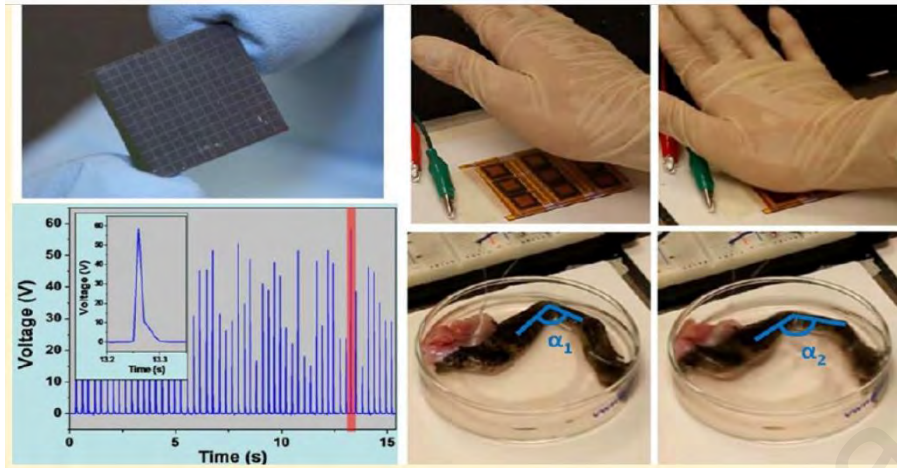


Figure 2.13: High Voltage and Instantaneous Generation of Zinc Oxide Nanowires ZnO Nws for Stimulating a Sciatic Nerve of a Frog (Zhu et al., 2012)

Also, a high compression load was applied by the motion of vehicles that caused of generating voltages up to 10 V (Lin et al., 2013) (see Figure 2.14).

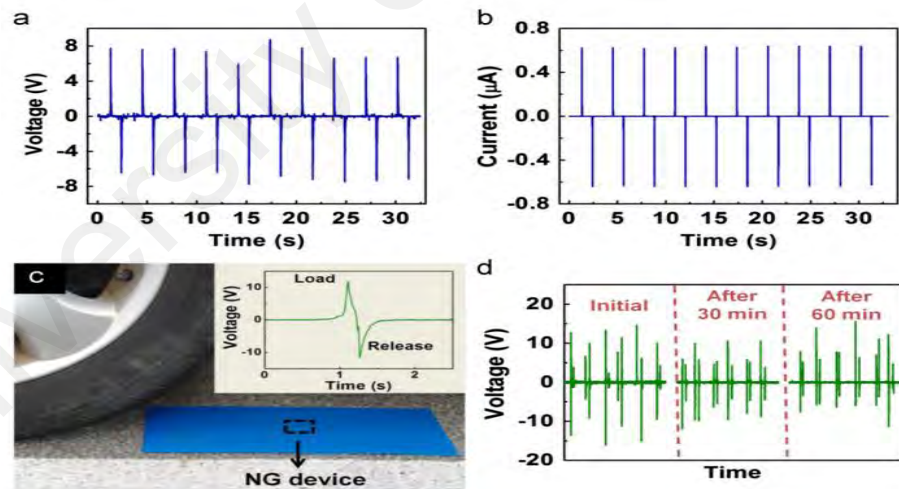


Figure 2.14: Zinc Oxide Nanogenerator Self-power Sensor for Detecting the Vehicle Speed and Vehicle Weigh (Lin et al., 2013)

Lin et al. (2013) fabricated zinc oxide nanogenerator self-power for detecting the speed and weight of vehicles, the output voltage, output current and power density were 8 V, 0.6 mA and 5.3 mW/cm³ respectively. The generated voltage has direct proportion to the

vehicle weight. Piezo-potential depends on the applied compression or bending loads, where researchers recorded voltage peaks on the order of few millivolts. In contrast, other piezoelectric NGs could generate tens of volts under high applied stress (Lin et al., 2013). In most synthesis cases, ZnO-NGs were coated with a polymer such as PMMA. The effect of the coated layer was investigated by Briscoe (2013) in the case of ZnO NWs coated with two coating modes: partial and total immersion. In Figure 2.15, the instantaneous generation of ZnO/PMMA and ZnO/PEDOT: PSS thin films (i.e., the instantaneous peak voltage, short circuit current, and power density) were compared. The current density and power density between ferroelectric materials and ZnO-NGs is compared, and the results are presented in the Tables 2.4 and 2.5. Piezoelectric energy harvesting techniques have been studied by the several scientific disciplines using different approaches. The experimental conditions in most prior studies have not been sufficiently described, where the energy harvesting of piezoelectric materials is achieved only when the material was excited by dynamic stresses. Among these, experimental conditions should be described based on real-time stress evaluations.

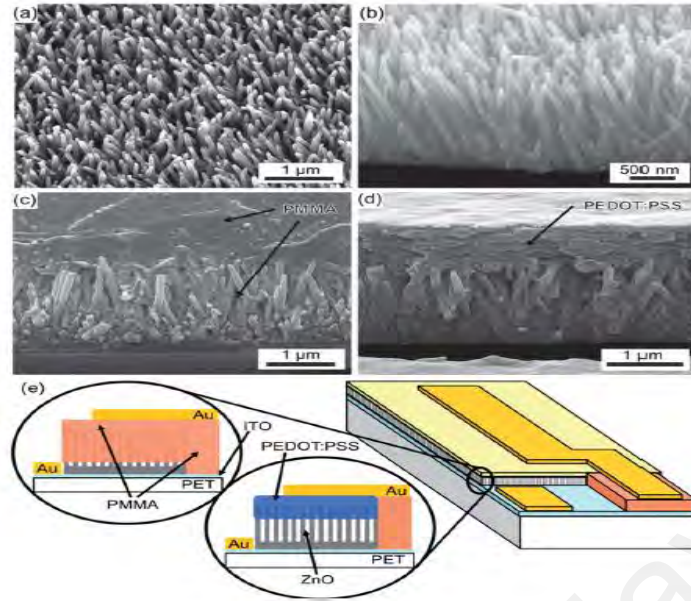


Figure 2.15: The ZnO-Nano Rod/Poly(Methyl Methacrylate) (PMMA) and ZnO/Poly(3,4-Ethylenedioxythiophene) Poly(Styrene Sulfonate) (PEDOT:PSS) Devices (Briscoe et al., 2013)

It's quite difficult to compare the harvested energy based on many prior determinations that inaccurately described (or did not describe at all) the characteristics of dynamic excitations such as the frequency, device area or volume, acceleration, strain rate, and velocity. A mathematical prediction method can overcome this problem using the relationship between acceleration, velocity, and frequency. It was assumed here that the deflection of the harvesters is transferred in a sinusoidal wave, and all the displacement, velocity, and acceleration transfers in a sinusoidal mode. The velocity of the oscillated objects expressed here as function of frequency and displacement is given as follows (sensors, 2016; SpaceAge Control, 2016):

$$V_{Pk} = 2\pi f d \quad (2.11)$$

Some studies provide a description of the strain or strain rate of flexible NG.

$$\epsilon' = \frac{d}{dt} \left(\frac{L(t) - L_o}{L_o} \right) = \frac{v(t)}{L_o} \quad (2.12)$$

where ϵ' is the strain rate, L_o is the original length, and $v(t)$ is the directional velocity or speed of deflection (i.e. bending or releasing). The sinusoidal velocity can be expressed in Eq. (2.13).

$$v(t) = \epsilon' L_o \quad (2.13)$$

The travel displacement of the oscillators or harvesters is determined by the relationship between acceleration and frequency as follows:

$$d_{Pk-Pk} = \frac{g A_{Pk}}{2\pi^2 f^2} \quad (2.14)$$

where d_{Pk-Pk} is the peak to peak sinusoidal displacement, A_{Pk} is the peak acceleration value, f is the frequency, and g is the gravity. Accordingly, the acceleration can be expressed as:

$$A_{Pk} = \frac{2\pi^2 f^2 d}{g} \quad (2.15)$$

A comparison between recent studies on flexible ferroelectric and non-ferroelectric NG harvesters is documented in the Table 2.4 and Table 2.5.

Table 2.4. Power and Current Density of the Flexible Ferroelectric Nanogenerator Material

Materials	Piezoelectric Properties	Test Condition	Application	Kinematic Parameters	Polarisation	Voltage (V _{OC})	Current Density, I _{sc} (μA/cm ²)	Power Density (μW/cm ²)	Ref.
Au/PVDF/Au and triboelectric PTFE/Al (7 × 3) cm ²	N/A	Compressive force; Human hand tapping force was 0.2 N and frequency lower than 7 Hz.	Charged a 10-mF capacitor to 10 V in 25 s; light up 600 LED diodes	N/A	N/A	370	12.00	4440*	(Jung et al., 2015)
PZT carbon nanotubes / PDMS (3 × 3) cm ²	$g_{33} = 28.2 \times 10^{-3}$ V m / N	Bending strain 0.33%	Charging capacitors time is 5 hr and voltage is 16.77 V	$f = 0.3$ Hz $V_{pk} = 4.7$ mm/s $A_{pk} = 8.9$ mm. s ² $d_{pk-pk} = 5$ mm	2 kV/cm for 20 h at 150 °C.	10.0	0.140	1.400*	(Park et al., 2013)
PZT carbon nanotubes (80 cm ²)	$g_{33} = 28.2 \times 10^{-3}$ V m / N	Irregular deformation.	Light up 12 LED directly & without external circuit.	N/A	Electric field of 2kVcm ⁻¹ for 12 h at 140 °C	100	0.125	12.50*	(Park et al., 2013)
NaNbO ₃ -PDMS (4.5cm ² × 0.100μm) Assume the length=3cm	Ferroelectric phase (P21ma symmetry)	Compressive strain of 0.23% strain rate = (12.8%) /s	Power LCD.	$f = 0.33$ Hz $V_{pk} = 3.8$ mm/s $A_{pk} = 7.9$ mm/s ² $d_{pk-pk} \approx 3.6$ mm	60 kV/ cm at RT	3.20	0.016	0.051*	(Jung et al., 2011)
PMN-PT -PDMS (1×0.5×0.015) cm ³	$d_{33} = 371$ pm/V	Compression strain > 0.2% with frequency of 5 Hz.	N/A		50 kV/cm at 150 °C for 24 hrs.	7.80	4.580	35.70*	(Shiyou Xu et al., 2013)
BaTiO ₃ -PDMS (11×11×0.03) cm ³	$d_{33} = 190$ pC/N	Bending stress of 1 MPa.	Maximum voltage = 2.37 V in the four capacitors for 1 hr	N/A	100 kV/cm for 12 hrs.	5.50	0.350	1.930*	(Park et al., 2012)

Table 2.4: Continued

Materials	Piezoelectric Properties	Test Condition	Application	Kinematic Parameters	Polarisation	Voltage (V ^o C)	Current Density, I _{sc} (μA/cm ²)	Power Density (μW/cm ²)	Ref.
LiNbO ₃	D ₃₃ =25 Pm/V	Bending=0.016%, 0.8Hz	N/A	N/A	100Kv/cm	0.46	0.005	0.002*	(Yun et al., 2014)
PZT textile – PDMS (1.5×0.08×0.0005) cm ³	N/A	Bending	Light up LCD, R _{opt} =100 MΩ, P _{opt} =200 μW/cm ³	N/A	4 kV/mm at 130 °C for	6.00	0.380	1.000	(W. Wu et al., 2012)
BaTiO ₃ -PDMS, (82 mm ² × 300 nm)	d ₃₃ = 105 pm/V	Bending strain is 0.55% & finger hits	100 kV/cm, 7 mW/cm ³	N/A	100 kV/cm for 15 h at 150 °C	1.00	0.190	0.190*	(Park et al., 2010)
BaTiO ₃ -PDMS (2×1×0.0001) cm ³	d ₃₃ = 1.5 pm/V	Bending stress	Light up LCD screen, 0.021 μW at R _{opt} =80 MΩ.	N/A	3 kV/mm at RT	2.00	0.025	0.011	(Gao et al., 2015)
ZnSnO ₃ /MWCNTs (3.7×3×0.1) cm ³	Young's modulus of (300–800 kPa)	Finger hit; force 9N; pressure 12 kPa	Light up LED and calculator, P _{opt} =10.8 μW/cm ³ .	N/A	Polarised material.	40.0	0.036	1.440*	(Alam et al., 2015)
SiNW/α-quartz-PET (3×1 × 0.0025) cm ³	N/A	Force = 60 N	Light up LCD screen, P _{opt} =380 nW & R _{opt} =20MΩ.	N/A	Polarised at 2 kV/cm	≈500	0.200	0.126	(Liu et al., 2015)
PMN-PT & MWCNTs (stretchable PEC)(10cm ²)	d ₃₃ ≈690 pC/N ⁻¹ ; k ₃₃ =0.73	Strain Rate 1300 %/s	Three series capacitors charged in 2hr (f=2Hz) to achieve 4.7V, 1.6 V for each capacitor, light up one LED	f=0.5Hz V _{pk} =260mm/s A _{pk} =817 mm/s ² d _{pk-pk} =165.2mm	50 kV/cm at 110 °C	4	0.05	9.200	(Jeong et al., 2015)

(* Peak power (P_{pk})=(I_{sc} × V_{pk})/area (Briscoe et al., 2013; Xie, Mame, Green, Mossi, & Leang, 2010), RT is the room temperature; P_{opt} is the optimal power; R_{opt} is the impedance matching resistance; t is the signal transfer time

Table 2.5: Power and Current Density of the Flexible Non-polarised Nanogenerator Piezoelectric Material

Materials	Test condition	Application	Kinematic Parameters	Voltage, V_{oc} (V)	Current Density, I_{sc} ($\mu\text{A}/\text{cm}^2$)	Power Density ($\mu\text{W}/\text{cm}^2$)	Ref.
ZnSnO ₃ – PDMS (10 × 10 cm)	Pressing by vehicle tire ≈ 21 GPa and strain of	N/A	N/A	20.00	1000	20.00*	(Lee et al., 2014)
ZnO nanowires / PDMS (1.5 × 1 cm)	Compressive stress of 40 MPa.	Energy harvesting from tire rolling, $v_{max}=25$ V $P_{max}=5.3$ mW/cm ³	N/A	8.000	0.600	4.800*	(Lin et al., 2013)
ZnO/PDMA-Schottky contact	Impact speed 0.1 m/s Strain of 0.19%.	N/P	$f=2$ Hz $d_{pk-pk}=0.016$ m $A_{pk}=1.3$ m. $s^2 V_{pk}=0.1$ m/s	1.260	0.018	0.023*	(Xu et al., 2010)
ZnO/PEDOT: PSS (2 × 1 × 0.05cm)	Bending of 10mm.	$R_{op}=475$ kΩ	$A_{pk}=1.8$ m/s ² $V_{pk}=0.094$ m/s $d_{pk-pk}=0.01$ m	0.154	1.580	0.243	(Briscoe et al., 2013)
ZnO-PC100 (0.8 cm ²)	Bending stress	$R_{op}=50$ kΩ.	N/A	1.150	125.0	5.630	(Stassi et al., 2015)
ZnO-Si (0.5 × 0.5cm ²) Thickness 0.8 μm	$d_{33}=49.7$ pm /V pressure of 0.4 kg/cm ² 1000Hz.	$R_{op}=130$ MΩ Light up LED	N/A	0.095	35.00	5100	(Qin et al., 2016)
GaN-Zno-PVDF-Sio2/Si	Bending stress 34 kPa	Lighting up an LED	N/A	3.100	0.124	0.380*	(Li et al., 2016)
ZnO/CuSCN/PEDOT: PSS	N/A	$R_{op}=3.54$ kΩ	N/A	0.389	780.0	303.0	(Jalali et al., 2013)

$$I(*) \text{ peak Power } (P_{pk}) = (V_{oc} \times I_{sc})/\text{area}$$

A comparison of the voltage, current density, power density and kinematic values of NG ferroelectric and NG non-ferroelectric materials has been provided here. Furthermore, all of the flexible harvesters have been compared with brittle PZT as follow. Zinc oxide (non-ferroelectric) harvesters are a strong competitor for piezoelectric ferroelectric films, as recorded in the Tables 2.4 and 2.5. The ferroelectric harvesters exhibit very high voltage (open circuit) whereas the non-ferroelectric harvesters can generate a high current density based on a comparison of the reference voltages in Table 2.4 (Briscoe et al., 2013; Jalali et al., 2013; Qin et al., 2016). The collected data in Table 2.4, Table 2.5, and Table 2.6 show variations in voltage, current density and power density, because the output power depends on material properties and strain. In fact, some studies have provided insufficient details with respect to strain, power density, current density, and internal impedance (short circuit).

Promising high-power-density flexible non-ferroelectric harvesters had been developed (Jalali et al., 2013; Qin et al., 2016). The conductivity of most non-ferroelectric materials is usually increased by adding some conductive filler (Banerjee & Cook-Chennault, 2012; Tian & Wang, 2008) such as carbon nanotubes (CNTs), carbon black (CB) and nano-graphite (Hu et al., 2010; Park et al., 2014). Also, such fillers can enhance the polarisation of ferroelectric materials (Babu, Indu With & Gijsbertus, 2014); however, excessively increasing conductivity above the percolation threshold can quench the ferroelectric phase (Babu, Indu, With & Gijsbertus, 2014).

Power density measurements could calculate from the relationship between voltage (open circuit) and current density ($P_{oc}/A = V_{oc} \times I_{sc}/A$). Therefore, this value does not represent an accurate calculation value. The standard method for computing power density should calculate power across a load resistance. Briscoe (2013) demonstrated the variance between the calculations of power density using ($V_{oc} \times I_{sc}$) method and the power density values when power was computed across a load resistance. The values calculated

from $(V_{oc} \times I_{sc})$ represent overestimated values. Thus, it was recommended to calculate the actual power density across the applied resistance load.

Increasing the kinematics values (i.e. the frequency and acceleration) of ferroelectric films reveal increasing of generated power density due to the fact that ferroelectric materials have significant figures of merit (d_{ij}, g_{ij}) and are therefore characterised by high piezoelectric response. This fact is reflected clearly in Table 2.6, whereas insufficient details are recorded in Table 2.4. It is observed that a few experimental studies of cantilever systems have been carried out to evaluate the performance of flexible ZnO-NGs, where the flexible films were excited at very low frequencies and high deflections rates (Xu et al., 2010; Lin et al., 2013).

In terms of measurement techniques, most researchers have evaluated power density based on voltage and current. It is well known that a short circuit is a complete circuit when current flows in the absence of load resistance (Haffey, 2013). The maximum voltage (open circuit) can be measured in the absence of current flow. The circuit is considered to be an open circuit when the applied resistance is high enough to prevent current flow through the circuit. Other measurements calculate power across an applied load resistance. Some researchers calculated peaks in power density and utilised this parameter to predict overall performance (Xie et al., 2010). Electrical charge can be calculated by integrating the value of current that transfers across a load through a periodic cycle (Jalali et al., 2015).

$$Q = \int_{t_1}^{t_2} I(t) dt \quad (2.16)$$

Accumulated energy is stored in the capacitors and the average delivered energy (E) can be calculated based on the resistance (R) and cycle duration.

$$E = \int_{t_1}^{t_2} \frac{V(t)^2}{R} dt \quad (2.17)$$

The accumulated energy in the capacitor is then delivered to operate LED diodes or LCD screens. Likewise, the operation of 12 blue-series LEDs was achieved when the stored voltage reached to 16.77 V, a full-wave rectifier circuit with five parallel capacitors of 1000 μF was utilised for rectifying and storing the energy. Full charging was realised after five hours (Park et al., 2013). Other harvesters required approximately 50 continuous bending–unbending operations to light up an LED for 1.5 s (Lee et al., 2012). Zhu (2012) generated a voltage of 3V by impacting the ZnO-NG more than 20 times using the palm of a hand palm to charge a capacitor of 2 μF . In this regard, supporting the useful power of such devices could be achieved under higher frequencies and strain. The variations in Young's modulus and the thickness of all the constructed flexible NG layers were a vital technical point, where a large Young's modulus for the electrodes could be the cause of reductions in the strain of NG layer (Jung et al., 2011; Park et al., 2012).

2.6.2 Ferroelectric Brittle Piezoelectric Polycrystalline Harvesters

This section provides a detailed overview of micro-scale grain brittle ferroelectric films. The brittle PZT ferroelectric films were synthesised according to the required configurations of the design. Typically, brittle piezoelectric harvesters have been synthesised by solid-state methods (Islam & Priya, 2006; Nabunmee et al., 2011). The piezoelectric ferroelectric patch is independent of directional electromechanical properties (i.e. d_{33} , d_{31} , d_{15} , g_{33} , g_{31} , etc.) thus, piezoelectric harvesting products have been designed with various architectures according to the type of applied excitation (such as pressing, bending, and extension) (Piezo System, 2013).

A cantilever beam is a commercial design of piezoelectric harvesting field where the harvester is technically integrated into the cantilever and a proof mass is typically attached to the end of the harvester to reduce the natural frequency. This increases the mass value

propagated with the output energy. Cantilever systems could be integrated with electromagnet systems (Steve P Beeby et al., 2007), piezoelectric systems, electrostatic systems, and windmills (Bressers et al., 2011; Çevik, 2011; Myers et al., 2007; Priya, 2005a). Additionally, tide movements have been investigated as a potential source of excitation, which could be harvested using floating piezoelectric cantilevers (Woo et al., 2014). Cymbal transducers have high-energy capabilities on the order of mill-watts (Kim et al., 2004) and it was designed with a bulky configuration that can withstand high compression or tension cycles. Thus, the cymbal has been employed for harvesting the energy from the pavement, the soles of shoes, and automobile engines. Piezo-stacks also employed for energy harvesting purposes.

Sergey (2016) investigated traffic intensity (random excitation) using piezo-stakes and found that optimal performance was achieved when the impedance of the PZT stacks matched the internal impedance of the circuit. The harvested power was in the range of 1-25 mW for frequencies of 10-100 Hz. Such harvesters require high-force excitation reaching up to 2500 N. Likewise, for piezo-cymbal tape harvesting energy from the waste vibration of an automobile engine (2004), harvesting energy requires the application of high-amplitude, high-frequency loads. The generated power output was 39 mW. In fact, the generated irregular signal of piezoelectric harvesters requires rectification and regulation techniques. Therefore, the DC power output could be rectified and amplified using an AC-DC storage circuit (Daniel et al., 2011) and DC-DC converter circuit, where power transfers can be achieved under low-impedance loading. Piezoelectric devices with high figures of merit ($d_{ij}g_{ij}$) are the most preferred for energy harvesting applications, where this value is given by the relationship between the piezoelectric strain constant and piezoelectric voltage constant (Islam & Priya, 2006). In addition, the efficiency of the harvesting oscillator is governed by several influences, such as material properties, device design, structural parameters, and kinematic parameters.

Brittle ferroelectric PZT has superior harvesting for high power density under high excitation, whereas ferroelectric flexible NG has very low performance because of the low kinematic excitation conditions. Recently the comparable performance of non-ferroelectric NG harvesters has been realised (Jalali et al., 2013). In this research field, the main difference between brittle and flexible ferroelectric harvesters was their morphological characteristics (i.e. polycrystalline, NG). It was observed that insufficient estimations and studies have been provided for studying the flexible ferroelectric NG subjected to high excitation and frequency. Thus, this study was interested in generating the energy from nanogenerator excited at high frequency and low deflection rates (distance). Moreover, the predominant harvesting methods that were utilised mostly with the flexible harvesters were compression and releasing, dragging, torsion, bending and releasing. It is well known that the brittle piezoelectric could be subject to crack propagation and fatigue thus the utilising of flexible harvesters can eliminate this problem. Also, it provides solution when the flexibility of cantilever is a critical condition, where the flexible harvesters do not make major effect of the cantilever mechanical properties.

The predicated kinematic parameters and power density are presented in Table 2.6. Brittle PZT requires high frequencies and high acceleration (or the application of high loads) to generate useful power.

Table 2.6: The Power Density of Brittle Piezoelectric Films

Material	Voltage (V)	Area (mm ²)	Frequency (Hz)	Acceleration (g)	Predicated parameters	Current density* ($\mu\text{A}/\text{cm}^2$)	Power (μW)	Power density ($\mu\text{W}/\text{cm}^2$)
PZT (Muralt et al., 2009)	1.6	0.32	870.0	2.00	$d_{pk-pk}=0.006$ mm $V_{pk}=35.87$ mm/s	273.4	1.4	437.50
PZT (Fang et al., 2006)	0.89	1.2	608.0	1.00	$d_{pk-pk}=0.007$ mm $V_{pk}=2.6$ mm/s	202.3	2.2	180.00
PZT (Morimoto et al., 2010)	0.5	92.5	126.0	5.00	$d_{pk-pk}=0.1$ mm $V_{pk}=62.5$ mm/s	526.8	244.0	263.40
PZT (Daniel et al., 2011)	1.6	782	437.0	N/A	N/A	0.84	10.5	1.34
PZT (Sang et al., 2013)	~1.5	900	22.00	6.00 [•]	$d_{pk-pk}=2$ mm $V_{pk}=170.8$ mm/s	2.89	39.0	4.33
PZT (Sodano et al., 2005)	~3	2480	1000	N/A	N/A	2.69	200.0	8.06
PZT (Chih et al., 2006)	3.7*	1200	12.00	N/A	N/A	26.88	1200.0	100.0
PZT (Peigney et al., 2013)	3.6	8800	15.00	0.058	$d_{pk-pk}=1.28$ mm $V_{pk}=60$ mm/s	0.09	30.0	0.340
PZT (Priya, 2005b)	12.4*	14400	12.00	N/A	N/A	4.33	7500.0	52.08
PZT (Al-Ashtari et al., 2013)	N/A	648	215.0	0.300 [•]	$d_{pk-pk}=0.001$ mm $V_{pk}=2.5$ mm/s	N/A	140.0	21.60
PZT (Guan & Liao, 2016)	20*	1425	13.50	N/A	N/A	2.89	825.0	57.89
PZT (Berdy et al., 2012)	N/A	29.4	48.00	19.60	$d_{pk-pk}=2.1$ mm $V_{pk}=637.3$ mm/s	N/A	100.0	3.40

1^(*) Voltage (open circuit) ; ([•]) predicted value

2.7 Piezoelectric Cantilever for Energy Harvesting

Cantilever beam is one of the structures that invested for energy harvesting. Large deformation could be achieved using elastic bodies. The performance of any harvesters depends totally at numerous influences such material properties (i.e. conductivity, polarity, permittivity, impedance), electromechanical properties (Figure of merit (*d.g*)), physical factors (i.e. length, area, thickness, mass, geometry, mechanical influence (i.e. force, young modulus, stiffness, strain rate), dynamic characteristics (natural frequency, damping ratio, mode shape), harvester orientation, position, and degree of freedom. In the last decades, remarkable interesting had been directed toward scavenging the energy from piezoelectric transducers (Danial et al.,2001; Kumar et al.,2014; Nechibvute et al.,2011; Shench et al.,2001). Recently, the piezoelectric harvesters have been significantly developed, which can be fabricated as bulk, thin/thick films, and flexible harvesters. In terms of using cantilever beam system, a feasibly study (Song et al., 2012) as carried out for harvesting the energy from random frequencies that available in the ambient sources, the result affirmed the need for increasing the sensitivity of PZT by increasing the material area, reducing the thickness of the PZT, and finally adding tip mass for reducing the natural frequency where it respects as the most effective methods for enhancing the sensitivity. This technique was developed to utilise of nonlinear system such as piezoelectric cantilevers magnetic system, such system was adopted in the wind turbine generator (Myers et al.,2007; Bressers et al., 2011; Çevik, 2011; Priya, 2005a), high power density had been released due to the high deflection rates of such systems. Also, tides movement had been exploited in energy harvesting field by using floated piezoelectric cantilever. The increasing of current and reducing the internal impedance of multiple parallel PZT-CN layers was achieved by increasing the applied strain (Woo et al.,2014).

Link numerous piezoelectric chips in serial or parallel connecting yield optimisation of the power harvesting. Kang (2016) demonstrated no significant difference between the series and parallel connections. However, parallel connection provided lower impedance than series connection of harvesters.

2.7.1 Theory of Vibration

The vibrated structures refer to the oscillated entities in reciprocating movement where the dynamic characteristics of any oscillator are the modal damping, natural frequency, and mode shape. The motion of a structure occurs in response to external force excitation thus the structural response is the output due to the interaction between the excited force and the dynamic characteristics of the structure.

Basically, the dynamic characteristics expressed by using the Frequency Response Function (FRF). The FRF function is represented as the mathematical representation to the relationship between the input and output of the system. The general solution to the linear forced excitation in frequency domain is shown in Eq. (2.18) as following.

$$\left\{ \underset{n \times 1}{\ddot{\mathbf{X}}(f)} \right\} = \left[\underset{n \times n}{\mathbf{H}(f)} \right] \left[\underset{n \times n}{\mathbf{Q}(f)} \right] \quad (2.18)$$

where $\left[\underset{n \times n}{\mathbf{H}(f)} \right]$ is the FRF square matrix. $\left\{ \underset{n \times 1}{\ddot{\mathbf{X}}(f)} \right\}$ and $\left[\underset{n \times n}{\mathbf{Q}(f)} \right]$ are the output and input of the system in the frequency domain The FRF function is a complex function which can transform from Cartesian coordinate to polar coordinates and vice versa.

Any motion can be recognized by three translation coordinates and three components of rotation. The discrete systems consist of a number of entity masses that move in multi-degrees of freedom (MDOF) as provided by Figure 2.16.

Degree of freedom (DOF) of system represents the motion description on the space. The motion for the large number can be described using a finite number of DOF

(Cornwell et al.,2005). The systems that involve continuous elastic entities can be described by infinite numbers of DOF and the simple cantilever in Figure 2.16 can be used as an example for having an infinite number of tiny particles or discretized points.

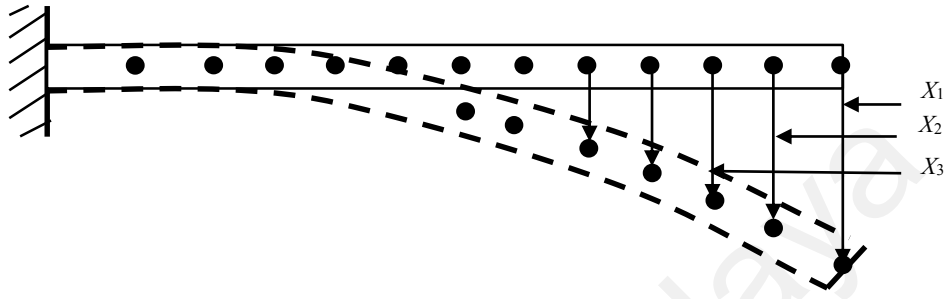


Figure 2.16: Discrete Cantilever Beam System

Since the cantilever has an infinite number of mass points, it is required for the infinite number of coordinates to describe the deflection or mode shape. Such systems are called continuous systems. The system that has a finite number of points or entities is called a discrete system. Mostly, the continuous system deals as a discrete system hence this is necessary for approximating the solutions in a simple manner whereas more accuracy can be reached by increasing the numbers of points or entities (Zauli, 2013). The governing equation of the vibration problem can be described as Eq. (2.19).

$$\mathbf{M}\ddot{\mathbf{X}} + \mathbf{C}\dot{\mathbf{X}} + \mathbf{K}\mathbf{X} = \mathbf{Q} \quad (2.19)$$

where \mathbf{M} , \mathbf{C} and \mathbf{K} are mass, damping and stiffness matrices respectively. $\ddot{\mathbf{X}}$, $\dot{\mathbf{X}}$ and \mathbf{X} are acceleration, velocity and displacement vectors respectively. \mathbf{Q} is the forcing vector. Considering periodic excitation of a shaker, the forcing function can be assumed as $\mathbf{Q} = \mathbf{Q}_0 \cos \omega t$. Then, the spatial coordinate equation of motion above can be uncoupled into the generalized/principal coordinate as follows.

$$\ddot{x}_{p,r} + 2\sigma_r \dot{x}_{p,r} + \omega_0^2 x_{p,r} = q_{p,r} \cos \omega t, \quad i = 1, 2, 3, \dots, m^{th} \text{ DOF} \quad (2.20)$$

where $\ddot{x}_{p,r}$, $\dot{x}_{p,r}$, $x_{p,r}$ are the r^{th} mode steady-state acceleration, velocity and displacement respectively in principal coordinate. The decay rate of r^{th} mode, σ_r is equal to damping ratio, ζ_r multiply with undamped natural frequency, $\omega_{0,r}$. $q_{p,r}$ is the r^{th} mode forcing function in principal coordinate. ω is the excitation frequency of the forcing function in rad/s. By solving Eq. (2.20), the steady-state response in principal coordinate was obtained as follows.

$$x_{p,r} = \frac{q_{p,r}}{\omega_0^2} \beta_r \cos(\omega t - \theta_r), \quad r = 1, 2, 3, \dots, n^{th} \text{ mode} \quad (2.21)$$

In which the magnification factor,

$$\beta_r = \frac{1}{\sqrt{[1 - \omega^2/\omega_0^2]^2 + [2\zeta_r \omega/\omega_0]^2}} \quad (2.22)$$

and the phase angle,

$$\theta_r = \tan^{-1} \left[\frac{2\zeta_r \omega/\omega_0}{1 - \omega^2/\omega_0^2} \right] \quad (2.23)$$

Hence, back transformation is performed to obtain the contribution of the considered mode.

$$X_{i,r} = \phi_{i,r} x_{p,r} \quad (2.24)$$

where $\phi_{i,r}$ is the r^{th} mode normalized mode shape at i^{th} DOF of the structure. The total response of the structure is the combination of response contributed from each mode. It is given by Eq. (2.25).

$$\mathbf{X} = \begin{Bmatrix} X_1 \\ X_2 \\ \vdots \\ X_m \end{Bmatrix} = \begin{Bmatrix} \phi_{1,1}x_{p,1} + \phi_{1,2}x_{p,2} + \dots + \phi_{1,n}x_{p,n} \\ \phi_{2,1}x_{p,1} + \phi_{2,2}x_{p,2} + \dots + \phi_{2,n}x_{p,n} \\ \vdots \\ \phi_{m,1}x_{p,1} + \phi_{m,2}x_{p,2} + \dots + \phi_{m,n}x_{p,n} \end{Bmatrix} \quad (2.25)$$

Theoretically, the piezoelectric harvester should be placed at the location with the highest displacement, $\max(|\mathbf{X}|)$ or the highest acceleration, $\max\left(\left|\ddot{\mathbf{X}} = \frac{d^2\mathbf{X}}{dt^2}\right|\right)$ to harvest maximum power.

2.7.1.1 Factors Affecting the Structural Response

In order to obtain the optimal location for the piezoelectric harvester placement, it is crucial that one has to first evaluate the dynamic characteristics of the given structure, namely natural frequencies, mode shapes and modal damping, as illustrated in Eqs. (2.21) and (2.25). One should be able to analyse the structural response by considering the following factors: (1) Closeness of the natural frequencies to the excitation frequencies; (2) Amount of damping of the resonance modes; (3) Interaction between the distribution of excitation forces and the mode shapes. The detailed description of the factors is given below.

Factor (1) – Structural response increase especially when the excitation frequency close to the natural frequency of the system. For the resonant case, let the excitation frequency matches the 1st mode natural frequency ($\omega = \omega_{0,1}$). The magnification factor of 1st mode is the highest compared to other mode. Hence, the total response of the structure is mainly contributed by Mode 1, i.e. $\mathbf{X} \approx \boldsymbol{\phi}_1 x_{p,1}$. For non-resonant case, let excitation frequency to be somewhere nears the natural frequencies of 1st – 3rd modes. The total response of the structure is mainly contributed by Modes 1-3, i.e. $\mathbf{X} \approx \boldsymbol{\phi}_1 x_{p,1} + \boldsymbol{\phi}_2 x_{p,2} + \boldsymbol{\phi}_3 x_{p,3}$.

Factor (2) – Modal damping plays an important role to reduce the vibration especially when resonance occurs. When $\omega = \omega_0$, the magnification factor, $\beta_r = \frac{1}{2\zeta_r}$. As the damping ratio increases, the magnification factor will be reduced and

hence it reduces the total response of the structure. Note that damping does not cause much change in the response when it away from resonance.

Factor (3) – The generalized force, $q_{p,r}$ is the 3rd factor that affecting the response of the structure, where $q_{p,r} = \phi_{1,r}Q_1 + \phi_{2,r}Q_2 + \dots + \phi_{m,r}Q_m; r = 1, 2, \dots, n^{th}$ mode. The interaction between the distribution of excitation forces and the mode shapes can be separated mainly into two categories: symmetrical or anti-symmetrical. In general, if the force vector is non-symmetrical/symmetrical with the shape vector, zero/ non-zero generalized force will be obtained. Zero generalized force will eventually produce minimal structural response.

2.7.1.2 Frequency Response Function

The FRF is the mathematical representation that describes the complex relationship between the input and the output of a system where it is represented in the frequency domain. This function can transform from Cartesian coordinates to the polar coordinates and vice versa.

$$H_{I:J}(\omega) = \frac{CS_{I:J}(\omega)}{AS_{J:J}(\omega)} = \frac{B_I(\omega)A_J^*(\omega)}{A_I(\omega)A_J^*(\omega)} \quad (2.26)$$

where $H_{I:J}(\omega)$ is the FRF coefficient that represents the ratio between the cross-spectrum to the auto spectrum. $CS_{I:J}(\omega)$ is the cross-spectral density between the output response DOF (I) and input force DOF (J) respectively and $(AS_{J:J}(\omega))$ is the auto-spectrum functions respectively. The variable ω is the angular frequency. Also, it can be represented by the ratio of output response, B to the input force, A , where A is a complex value in the frequency domain. The transfer function is based on H_I estimator, where the numerator part represents the cross-correlated function between output response and the

complex conjugate of input force, while the denominator part represents the auto-correlated function between the input force and the complex conjugate of input force.

2.7.1.3 Coherence (COH)

Coherence (COH) is commonly used to assess the signal spectral for measuring the power transfer between the input and output of a linear system. When the impact force was induced into a linear system by hammer, the responses of the system were recorded simultaneously.

$$\gamma_{I:J}^2(\omega) = \frac{|CS_{I:J}(\omega)|^2}{AS_{I:I}(\omega)AS_{J:J}(\omega)} \quad (2.27)$$

COH, $\gamma_{I:J}^2(\omega)$ is the ratio of square of the cross-spectrum $CS_{I:J}(\omega)$ to the auto-spectrum functions, $AS_{I:I}(\omega)AS_{J:J}(\omega)$. The coefficients I and J represent the output response DOF and input force DOF respectively. The value of COH is ranged between $0 \leq \gamma_{I:J}^2(\omega) \leq 1$ where $|CS_{I:J}(\omega)|^2 \leq AS_{I:I}(\omega)AS_{J:J}(\omega)$.

2.7.1.4 Experimental Modal Analysis (EMA)

EMA is an experimental technique commonly used to identify dynamic characteristics of elastic structures. It often requires the system to be in a complete 'shut down' or 'non-operating' state. This means that no unaccountable excitation force will be induced into the system, except the designed and measurable force such as impact excitation from the tuned hammer (known as impact testing) or random excitation from shaker (known as shaker testing). The responses of the system induced by the designed force will be recorded as well. Transfer functions are also known as Frequency Response Functions (FRFs). For detecting the modal parameters, numerous experimental techniques are employed to excite the structure under testing. As example for such techniques are Single-

Input/Single-Output (SISO), Single-Input/Multi-Output (SIMO) to Multi-Input/Multi-Output (MIMO).

Impact testing with Single Input Multiple Output (SIMO) approach can be used where multiple accelerometer sensors are mounted on the desired discrete set of geometrical positions, which are sufficient to describe the vibration distribution of the structure due to a single input force. In this case, the obtained FRF is called accelerance FRF. The input force location is selected by using driving point FRFs measurement, (i.e. measurement of the $H_{i=j:j}$ where the input response is at the same location as an output force for all the possible force locations). Driving point FRFs with the maximum number of strong (large magnitude) resonance peak is then identified as the potential reference force (Schwarz, Richardson, & Avitabile, 2002). The SIMO approach is selected for its time efficiency. Most importantly, it does not have a problem with a mass loading issue where high measurement accuracy can be achieved. Once FRFs are obtained, various curve fitting algorithms are then used to extract the modal parameters, namely natural frequencies, mode shapes and modal damping shown as follows:

$$H_{i:j}(\omega) = \sum_{r=1}^n \frac{\phi_{i,r} \phi_{j,r}}{(\omega_{0,r}^2 - \omega^2) + (2\zeta_r \omega \omega_{0,r})} \quad (2.28)$$

where $H_{i:j}(\omega)$ = transfer function due to i^{th} DOF and j^{th} DOF of the locations of output response and input force respectively, at the corresponding frequency, ω . $\phi_{i,r}$ & $\phi_{j,r}$ = mode shapes due to i^{th} DOF and j^{th} DOF of the locations of output response and input force respectively, at the corresponding r^{th} mode. $\omega_{0,r}$ & ζ_r = r^{th} mode natural frequency and damping ratio respectively.

2.7.2 The Vibration Technique of Energy Harvesting

An SDOF cantilevers are utilised broadly in piezoelectric energy harvesting field. Piezoelectric harvesters were mounted at the cantilever roots where efficient harvesting will be attained at a high strain region. The optimal position for the small patches was detected at the region that has overall maximum bending moments. Large patches can improve the damping of the system but more increase of piezoelectric size beyond the limitation is the cause of deterioration of the system performance. Increasing the bending moment and the stress yield strongly increases the electromechanical coupling whilst improving the damping factor (Liao & Sodano, 2012a). Selection of the PZT patch location on the MDOF harvester is described here. Cornwell et al. (2005) demonstrated the usage of tuned vibration absorber, (i.e. auxiliary structure) to enhance the power harvesting. Eggborn (2003) conducted a parametric study on the piezoelectric patch location on a beam. Results showed that found that maximum strain energy occurred at the clamped end of the beam, which in turn generated maximum power, compared to zero power generation on the free end of the beam due to zero strain energy occurred. It is well known that vibration energy harvester mechanically resonates at a frequency that coincides with its natural frequency, hence generating maximum electrical power. However, the power output decreases significantly when the excitation frequency slightly shifts from resonant point. One of the strategic methods of realising the optimal power is increasing the resonance bandwidth for meeting the potential frequencies of the environment that varies with time (Liu et al.,2008).

On the other hand, the degree of freedom of harvesting system has also been studied where MDOF revealed double rates of power generation than that of the conventional single degree of freedom system (SDOF). In this concept, Kim (2011) designed a two degrees of freedom (2DOF) system consisting of two cantilevers (pieced together horizontally) and one proof mass, the system produced efficiently higher power

generation than that of the SDOF, (Kim et al.,2011). Cornwell (2005) demonstrated the usage of tuned vibration absorber (i.e. auxiliary structure) to enhance the power harvesting. Placement of a piezoelectric patch on the auxiliary structure can generate more power than when placed on the host structure. It was emphasised that the auxiliary structure should be located at the antinode (i.e. point where maximum displacement occurs at a particular vibration mode). However, the location of auxiliary structure was arbitrarily chosen by considering potential practical location constraints. In addition, these researchers did not investigate the optimal location of the patch on the auxiliary structure. Tang and Yang (2012) had been studying the effect of the location of piezoelectric element on the harvesting performance in a two DOF piezoelectric harvesting system. The results showed a better harvesting performance of the piezoelectric patch that was attached to the primary oscillator mass compared with the patch that was attached to the auxiliary oscillator mass. Xiao et al. (2016) provided a guideline for optimising the harvesting power and bandwidth. A parameter was studied in two DOF patch system, which was operating under various masses and frequency ratios. Thus, by keeping the total mass and the mass ratio of the oscillator constant, an increment in the numbers of DOF will improve the harvested power as well as shift the first vibration mode to a lower frequency region.

On the other hand, several researchers focused on nonlinear technique to improve the broadband characteristic of piezoelectric patch. Mann and Sims (2009) proposed a novel magnetic integrated piezoelectric patch system that engaging the system's nonlinear response, with a much larger range of frequencies as compared to linear energy harvesting, hence improving the energy harvested. Ferrari et al. (2010) implemented a bistable nonlinear oscillator using a magnet, where two equilibrium positions existed. It rapidly switched between these equilibrium positions under proper mechanical excitations in order to increase the velocity as well as the power output.

Furthermore, the implementation of both multiple degrees of freedom (MDOF) and nonlinear techniques in the piezoelectric harvesting system can further improve the performance of the harvester as demonstrated by (Su et al., 2013; Wu et al., 2014).

Strain distribution is another important design parameter to enhance power scavenging. Theoretically, piezoelectric harvesting with uniform strain distribution is preferable due to higher utilisation of its potential energy. In fact, this can be achieved by altering the geometry of the piezoelectric patch. For example, Baker et al. (Baker, Roundy, & Wright, 2005) extended the works from Roundy et al. (2005a) which addressed the uneven strain distribution issue for a conventional cantilever rectangular piezoelectric beam. It was proposed a trapezoidal piezoelectric stack, which had a more uniform strain distribution. The result showed that it was able to increase 30% of the output power per unit volume.

On the other hand, Kim et al. (2004) developed a ‘cymbal’ which was in circular configuration and designed for high force applications. The result showed that the stress applied to the piezoelectric material was more evenly distributed than in a conventional stack configuration. Moreover, Mateu and Moll (2005) found that triangular cantilever generated more power than a rectangular beam. Dutoit et al. (2005) emphasised that there was a need to check the total area under the strain curve. If the mode shape induced by the host structure caused the total area to decrease, the total power would decrease too, and this was known as a strain cancellation phenomenon.

However, if this effect is considered, the power benefit due to strain accumulation is possible. Erturk and Inman (2008) and Erturk et al. (2009) further examined the concept of the effects of strain mode shapes on the harvested energy. The research outcomes verified that the voltage output depends on the area under the strain curve. In the testing, the numbers of nodes of a system undergoing n^{th} mode of vibration are $n-1$, n and $n+1$ for pinned-pinned, clamped-clamped and clamped-pinned boundary conditions respectively.

Strain nodes existing in higher modes would cause the strain to change the sign, (i.e. the resulting voltages in the electrodes to be 180 degrees out of phase), therefore reducing the harvested voltage. It was suggested the use of segmented electrodes instead of continuous electrodes, which avoided the power reduction due to the strain node/ strain cancellation effect. Liao and Sodano (2012b) further examined the effect of patch placement on the damping of vibration modes and the effect of patch size on optimal placement. It was observed that the mass loading effect for all patches, (i.e. 2%, 15% and 30%-70% of area coverage for small-size, mid-size and large-size patches respectively) was significant in the system, shifting the natural frequency and mode shape. Hence, the optimal locations were affected in conjunction with changes in patch size.

Placement of PZT patch on the auxiliary structure can generate more power rather placement on the host structure. The results showed that the harvested voltage was proportional to strain and electrical power was proportional to voltage squared. Tang & Yang (2012) and Xiao et al. (2016) investigated the effect of the location of the piezoelectric element on the harvesting performance in a two DOF. Tang and Yang (2012) showed that the configuration of piezoelectric patch attached to the primary oscillator mass had a better harvesting performance compared to the configuration of piezoelectric patch attached to the auxiliary oscillator mass. Xiao et al. (2016) further improved the configuration by inserting additional piezoelectric elements between every two nearby oscillators to maximize the scavenging power. The examples above show that the optimal placement is crucial for practical implementation in the real system. Previous research showed that location selection of the electrodes/ piezoelectric sensor on a host/ auxiliary structure was a very important factor to maximize the harvesting power. Failure to address it may result in zero harvesting power. Thus, most of the study focused on the implementation of the PZT patch in the high strain region for harvesting the maximum voltage output. For example, Eggborn (2003), Erturk et al. (2009) and Liao & Sodano

(2012b), proposed that PZT patch should be placed at the clamped end (location a) of the cantilever beam for maximum power generation, and this was because the location had the highest strain and power was proportional to this strain (see Figure 2.17). The PZT patch generated poor power at the free end (location z) as it had the lowest strain, (i.e. strain node). The limitation of the PZT patch type d_{31} was mentioned by Eggborn (2003), where it was not possible to place the harvester at the clamped end of beam in some applications, and instead possible for the harvester to be placed at the strain node. Based on the complexity of estimation of the optimal location of stiff and long beams, studying the beam in three orthogonal coordinates x , y and z is necessary.

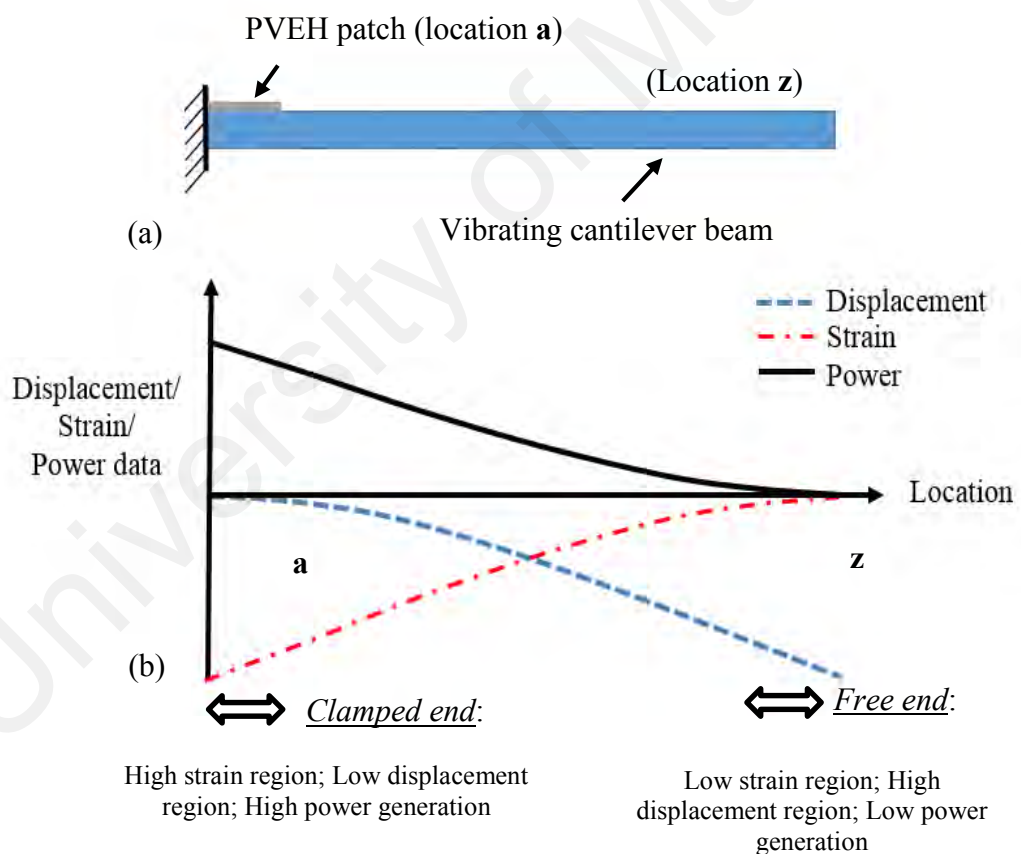


Figure 2.17: (a) Schematic Diagram of a Cantilever Beam and (b) the Effects of PVEH Patch Location on the Displacement, Strain and Power Results as Given by (Eggborn, 2003) and (Alper Erturk et al., 2009)

Khoo et al. (2017) developed a dual cantilever structure. The novel design of dual coupled cantilever consisted of swinging the PZT harvester over a cantilever structure. The results affirmed that the PZT harvester could produce high voltage at the high displacement / acceleration region, which behaves differently compared to conventional PZT patch placement as reported by (Eggborn. 2003; Erturk et al.,2009). This investigation had overcome this limitation by placing the PZT at the high strain region instead of the high acceleration region. This innovative idea gives flexibility to the user to select the desired PZT patch placement method. One should select the suitable placement (i.e. configuration of PZT patch and cantilever PZT) strategically for obtaining the maximum voltage output in the same structure. For example, it is recommended to use the configuration of PZT patch to harvest energy in a low acceleration region while at the same time, the configuration of the cantilever PZT patch can be used to harvest energy in a high acceleration region.

2.8 Piezoelectric Energy Harvesting of Windmills

Piezoelectric energy harvesting has been employed excessively for windmill to harvest the vibrated energy and powering wireless network nodes. These nodes are utilised in numerous sensing applications such as motion detectors, structure health monitoring, and weather stations. Normally, the harvesting processes of windmills are achieved under low frequencies and high strain where the system dynamic characteristic and performance will depend totally on the system design and wind speed. The strain level is an important factor of the piezoelectric windmill system performance (Bressers et al., 2011; Myers et al.,2007). Hence, the generated power is up to 0.6 μ W. Priya (2005a) fabricated a small piezoelectric windmill prototype that operated at low excitation and far from the resonance natural frequency of piezoelectric transducers and the generated power of this system reached to 7.5 mW. High power generation was realised when the transducer was

subject to high deflection or strain rates. On the other hand, severe damages could take place at these transducers due to fatigue and crack propagation. Piezoelectric transducers can be classified into flexible and brittle plates where all these products have different stiffness and natural frequencies, and thus it is important to select the appropriate mechanical and dynamic properties that coincide with the excitation level.

2.8.1 VAWT Exhaust Air System

Extracting the energy from the wind on rapid growth where the researchers sought behind alternative wind sources for overcoming the limitation of the wind speeds and wind stream directions. In the last decades, a new harvesting wind energy technology has been developed to work independently and the VAWT vibration energy recovered system consists of an exhaust air system with dual-rotor windmill this system depends substantially on the air flow rates or airspeed of the exhaust air tower; in other words, there is no need for natural wind resources. Typically, the cooling system is a ventilation device, the waste heat disposal system contributes by transferring the heat and ventilating the building. It consists of driving the fan that transfers the exhaust air to the external environment, and one or two (VAWTs) with its enclosure set up above the outlet of the wind tower for recovering the waste energy (Abdullah, 2016). In this research, the selected exhaust air recovery system was known as the mechanical draft cooling towers. The dynamic characteristics of the VAWT mounted and its enclosures was studied by Yap et al. (2014) where the researcher affirmed that any change of dynamic characteristics such as natural frequency, damping, and mode shape would result in potential damages of the VAWTs structure in addition to the long-term operation of VAWTs (without enclosure) that can be achieved with a vibration lower than 6 mm/s. In fact, when the diffuser integrates with the VAWTs, the vibration would increase to 26

mm/s. Thus, it was recommended to add an extra load (screws) to tighten the VAWTs at its supports that in order to reduce the vibration level. In this case, the natural frequency and amplification factor of the VAWTs were shifted from 7 Hz and 0.2 m N/s² to 9.7 Hz and 0.04 m N/s² respectively.

2.9 Alternative Energy Harvester Circuit

The piezoelectric energy can be harvested from diverse sources in either a stable or an intermittent. The generated energy must be rectified by using AC-DC rectified circuit or using the DC-DC converter circuit (Kim et al,2004). The DC power output can be amplified by using a DC-DC circuit (Daniel et al., 2011) where DC-DC converter circuit will transfer the power under low impedance load.

There are numerous smart electric circuits designed for harvesting the energy using piezoelectric chips. The upgrading of these circuits leads to increase the density of the output energy. The signals can be rectified by using a smart electrical circuit that can store instantaneous current and voltage. Gretarsson (2007) characterised a flexural piezoelectric that connected to the simple rectifier. This circuit consists of two small signal Schottky diodes BYV10-60 and external polyester capacitor (MKT 1813). In fact, the circuit was designed for controlling the current and voltage direction by utilising dual rectifier diodes: diode D₁ prevented the reflection of the current direction and diode D₂ prevented the reflection of voltages as illustrated in Figure 2.18.

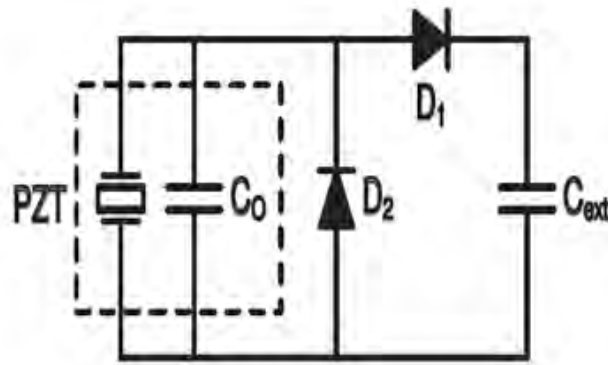


Figure 2.18: Energy Harvesting Circuit (Gretarsson, 2007)

Generally, a full bridge rectifier circuit is integrated with voltage regulation or DC-DC circuit as shown in Figure 2.19. The maximum power is realised when the impedance of piezoelectric chips matches the applied load.

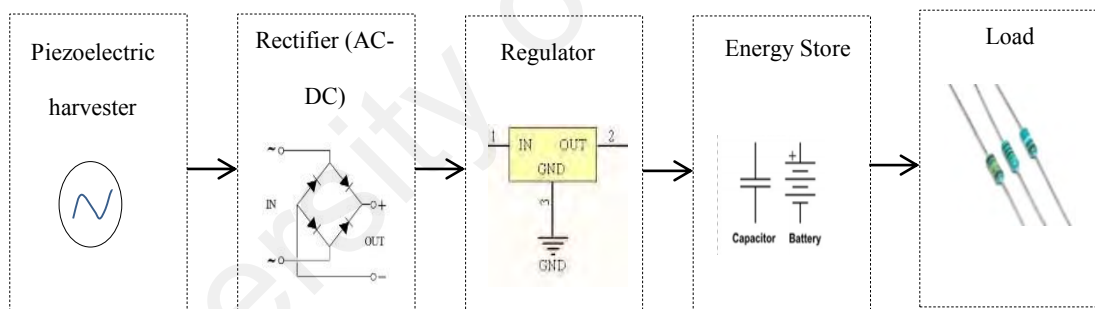


Figure 2.19: Typical Rectifier Bridge Circuit with Voltage Regulator

The researchers have affirmed the possibility of designing low voltage step-up converter circuit, where the harvesting of energy from low vibration sources is one of the major challenges of sustaining the energy. Woias (2013) converted the power efficiently, the increasing of voltage output was above 30% when compared with the voltage start-up source that was below 10 mV and the delivered energy was utilised for powering a potential system. Ongoing of such development of boost converter yield a great possibility to rectify the starting up voltage lower than 6 mV (Woias et al., 2013).

Based on the use of simple rectified circuit with stored capacitor, the accumulated energy will be delivered for operating LED's diodes or LCD screens. Likewise, 12 blue series LEDs were successfully operated under the voltage of 16.77 V, where a full-wave rectifier circuit with five parallel capacitors 1000 μ F was utilised for rectifying and storing the energy. A full charging of capacitors was achieved after five hours (Park et al.,2013). Lee (2012) fabricated a flexible piezoelectric harvester, the required period for changing capacitor was estimated by calculating the number of bending–unbending of the film. The lighting up LED for 1.5s was required about 50 times (bending–unbending operation).

In this regard, the supporting of useful power of such devices could be achieved under higher frequencies and strain. Sodano et al. (2005) had been recharge battery (capacitor 40 mAh), the battery could be recharged in half an hour when the PZT tuned at its natural frequency whereas the required charging time that needs for recharging the battery under random excitation of the PZT (away the natural frequency) was few hours.

2.10 Fabrication Cost of Piezoelectric Harvesters

Piezoelectric material fabrication cost depends totally on the selected fabrication method (e.g. solid state, wet chemical, tape casting, pulsed laser deposition (PLD), sputtering, spinning, screen-printing, etc.). Cost reduction is required for increasing profits. Typically, the reduction of manufacturing cost can be realised by either reducing the raw material prices, labour costs, or reducing the technical processes (i.e. adopting creative design or using alternative products). In other words, the leverage of value engineering can be attained by successfully adopting the ease to manufacture, reducing the material cost, smart design (integration of product parts), optimizing product function, and finally designing a local product (Ajitanath, 2010; Kmwe, 2017). Essentially, a cost analysis aims to investigate the functions of the project, manufacturing process, design, or the means for realising the desirable functions at the lowest life cycle cost consistent with the required aspects of the products (i.e. efficiency, stability, and reliability, availability, and safety matters).

In this section, the manufacturing processes of ferroelectric and non-ferroelectric were studied. Most of the ferroelectric ceramic materials were synthesized by a solid-state method whereas recently the non-ferroelectric materials have been produced attractively due to its low capital cost, high purity and low synthesis temperature (TWI Group, 2018). In terms of the manufacturing processes, a comparison of the power consumed by fabrication of the piezoelectric harvester either ferroelectric or non-ferroelectric is provided in Table 2.7, whereby the table demonstrate a comparison between the fabrication of ferroelectric ceramic based on the solid stated method and the non-ferroelectric method that adopt the wet chemical process. In fact, the fabrication of non-ferroelectric does not impose poling, monitoring, and sintering process which is the cause for reducing the electrical consumption and saving on cost.

For comparing and evaluating purposes, it is logical to size the daily or yearly production of piezoelectric harvesters. The accumulated yearly cost is very large thus reducing the fabrication process is a most practical way. Initially, the daily production of piezoelectric was assumed to be about 100 harvesters per day and using this method the yearly consumption of power could be approximated. In fact, this cost analysis considered the outlay of purchasing the materials and the consumption of power over the fabrication. Based on the provided data, the large benefit is expected from adopting a locally fabricated piezoelectric harvester.

Calculation of the power consumption was adopted based on the use of the following formula:

$$\text{Power (watt)} \times \text{Hours} / 1000 = \text{power (kWh)}$$

The default price of 1kWh= \$0.10 (Calculator, 2018), thus the daily or yearly cost can be estimated. The power consumption cost based the preparation processes of materials was estimated as shown in Table 2.7 where it is assumed that the total daily operated hours is 8 h. In addition, the annual cost was calculated to highlight the accumulation of the cost. It is useful to analysis the cost of the fabrication processes such as the poling and sintering, the polarization is carried out under high voltage and very low current. There is also extra power consumed over monitoring and a thermal treatment process is imposed and must be considered. In general, for poling any harvester, the default and approximate value of consumption power is 0.7 W where the current is equal to 100 μA and the voltage averaged to be 7 kV (MEMS-pie, 2017), as example for cost calculation:

$$\text{Power (W)} = \text{Current (A)} \times \text{Voltage (V)} = 100 \mu\text{A} \times 7000 \text{ (V)} = 0.7 \text{ W}$$

The daily cost for the poling, testing and mentoring can calculate as following:

$$0.7 \times 10^{-3} \text{ kW} \times 8\text{h} \times \$0.10 \text{ (kW}^{-1} \text{ h}^{-1}) \times 100 \text{ (Piece)} = \$0.06 \text{ (100 pieces)}$$

It's obvious that the accumulation of the cost per the year is very large based on the increasing of the amount of harvesters. The consumption of the power for the polarization process is given in Tables 2.9.

Table 2.7: The Cost Analysis of Ferroelectric and Non-ferroelectric Harvesters (GmbH, 2017)

Manufacturing technology	Ferroelectric	Non-Ferroelectric	Approximating Cost per day (8 h)	Approximating Cost per year (8 h daily)
Calcination (furnace with 10kW-18kW) (Mems-pie, 2017b)	√	√	\$8	\$2920.3 - \$5265.6*
Milling process (i.e. Planetary Ball Mill PM 400 1.5 kW)) (Retsch, 2017)	√	√	\$1.2	\$438
Granulation, spray drying, Pressing in the mold, spinning of green fiber, screen printing (1.5kW) (Fufa, 2017)	√	√	\$1.2	\$438
Sintering at elevated temperature (i.e. 1000-1350°C (Mems-pie, 2017b)	√	×	\$8	\$2920.3 - \$5265.6*
Lapping, grinding (i.e. 11.5 kW (Junker, 2017)), surface grinding, diamond cutting	√	×	\$9.2	\$3358
Application of electrodes: Screen printing, PVD processes, e.g. sputtering (i.e. 2 kW (Zhengzhou CY Scientific Instrument Co., 2017))	√	√	\$1.6	\$584
Polarization and testing (Mems-pie, 2017b)	√	×	\$8.06	\$ 2942
Others (i.e. ultrasonic cleaning (300W (sonic, 2017)), Final inspection. etc.)	√	×	\$0.24	\$ 87.6
Total cost (8h)	\$37.5	\$12	\$37.5	\$13687

*The minimum value was considered in calculations

Table 2.8: The Power Consumption for the Polarisation Process (Mems-pie, 2017b)

Number of Samples	Power (kWh)	Cost Per Day (8 h)	Cost Per Year (8 h per day)	Heating at up to 160°C (Furnace 10 kW), monitoring and testing process per year	Total cost per year
1	\$0.0001	\$ 0.0006	\$ 0.200	\$2920 (\$8 daily)	\$2920
100	\$0.0100	\$0.0600	\$ 20.00		\$2940
1000	\$0.1000	\$0.4000	\$200.0		\$3120
1000000	\$10	\$40	\$200000		\$202920

Additionally, the consumption of power for the sintering process was calculated where in some application this process is imposed for long hours (up to 24 h) thus the moderate daily hours assumed to be 8 h. The consumption of power is provided in Table 2.9 based on the furnace size. Assuming the default time is 8 h daily. The fabrication of non-ferroelectric harvester does not require polarisation and sintering processes, compared to ferroelectric harvester as demonstrated in Table 2.7. Due to the cost effectiveness of the non-ferroelectric harvester, it presents a huge competitive advantage compared to the ferroelectric harvester. Therefore, this research will focus on fabricating a low cost non-ferroelectric harvester.

Table 2.9: The Power Consumption for the Sintering Process Using Furnace (Keith, 2017; Sante, 2017)

Furnace Volume	Power	Power Per Hour (kWh)	Cost Per Day (8 h)	Cost Per Year (8 h daily)
300×400×300mm	10 kW	\$1.0	\$8.00	\$ 2920.3
300×500×300mm	12 kW	\$1.2	\$ 9.60	\$ 3504.3
127×457×381mm	18 kW	\$1.8	\$14.4	\$ 5256.0

2.11 Summary

Over the past decades, researchers have aimed to develop sustainable self-powered piezoelectric harvesters, as part of efforts to reduce carbon emissions and fabricate long lasting self-generating devices. Piezoelectric devices have been employed in mechanical, electronic, medical, and wireless applications and the piezoelectric products have numerous forms and morphological configurations. In a recent advance in piezoelectric nanogenerator (NG) materials, both ferroelectric and non-ferroelectric harvesters have been employed to harvest waste mechanical energy. It was found that the overall performance of both types of the harvesters is comparable in term of their power-generation performance. However, the current research started shifting from ferroelectric harvester to non-ferroelectric harvester due to the lower manufacturing cost. In fact, most of the non-ferroelectric harvesters were constructed from zinc oxide generator (i.e. non-ferroelectric in nature). Based on the literature review outcome, there was no attempt on eliminating the ferroelectricity property of the piezoelectric material based on the p-n junction technique. Thus, there is a room for improvement in this area. Thus, this study will demonstrate the quenching of ferroelectricity by increasing the material conductivity using p-type carrier material and fabricate a new non-ferroelectric harvester by using PZnT-NT. On the other hand, there was lacking experimental technique to determine the optimal location of the harvester location. This issue is critical as misplace the piezoelectric harvester on a node point of a structure may obtain a poor power harvesting result. In addition, theoretical calculation or finite element analysis were not suitable to determine the optimal location in a real operating structure due to the difficulty in modelling the actual boundary condition and real excitation force such as complicated wind turbine system. Therefore, this study will demonstrate the harvester location selection scheme by using the experimental EMA and ODS techniques.

CHAPTER 3: RESEARCH METHODOLOGY

3.1 Introduction

This chapter presents the experimental procedure and the methodology in three sections:

(1) Fabricating and characterising the $0.7\text{PbZn}_{0.3}\text{Ti}_{0.7}\text{O}_3$ - $0.3\text{Na}_2\text{TiO}_3$ (PZnT-NT) material before the harvesting of energy is evaluated.

(2) The location selection scheme will be carried out based on a voltage measurement, EMA and ODS analysis. The location selection scheme will be based on a measurement procedure on both the harvester and its host structure to identify the optimal location.

(3) The PZnT-NT harvester will be implemented over the VAWT and the optimal location will be detected by the EMA, ODS analysis and voltage measurement. Finally, the performance of the harvester will be evaluated and compared with the performance of other commercial piezoelectric harvesters.

In terms of the fabrication of the PZnT-NT harvester, a non-ferroelectric generator will be fabricated from $0.7\text{PbZn}_{0.3}\text{Ti}_{0.7}\text{O}_3$ - $0.3\text{Na}_2\text{TiO}_3$ (PZnT-NT). The PZnT-NT material consists of $\text{PbZn}_{0.7}\text{Ti}_{0.3}\text{O}_3$ (i.e. ferroelectric material) and Na_2TiO_3 (i.e. conductive filler). In this regard, the study will investigate the morphological structure of the PZnT-NT and characterise its physical properties (i.e. the conductivity, permittivity, and loss tangent). Specifically, the *p-n* junction was constructed where *n*-type and *p*-type structures was grown hydrothermally (low temperature). The main differences between wet chemistry (i.e. hydrothermal method) products and similar products of solid-phase synthesis are much smaller crystallites and, usually, lower temperature and shorter duration of phase formation.

Finally, the PZnT-NT properties will be compared with the properties of pure PbZnTiO_3 . The harvesting performance of the device will be studied experimentally over a cantilever test rig. The cantilever is excited by a motor operating at a frequency and acceleration of 30 Hz and 0.4 m/s^2 respectively, and then the generated voltage will be rectified using a full wave rectifier circuit. Based on the importance of recognizing the optimal location, the research perspective aims to avoid the poor location that has low vibration excitations and cause of low harvesting energy. To achieve this, EMA and ODS will be performed to obtain the dynamic behaviour and its actual deflection. The modal parameters will be utilised in selecting a good location that optimise the performance of the piezoelectric harvester by increasing the available amount of vibration energy. The voltage, force, and acceleration are measured through the module channels designed in DASyLab[®] (an icon-based, data acquisition, control and analysis software package).

Finally, the PZnT-NT will be implemented over the VAWT and the harvested volume power density and surface power density of PZnT-NT generator will be measured. The performance of the proposed device (with a size of $20 \times 15 \times 1 \text{ mm}^3$) will be compared with commercial microfiber composite ($80 \times 57 \times 0.335 \text{ mm}^3$), piezoelectric bimorph device ($70 \times 50 \times 0.7 \text{ mm}^3$) and PZT ($63.5 \times 31.8 \times 0.38 \text{ mm}^3$). In terms of the fabrication of material, the generator (i.e. non-ferroelectric) material is one of the more attractive applications for its desired manufacturing processes and also has the cost-competitive advantage. The new PZnT-NT generator will be fabricated from PbZnTiO_3 (PZnT) ferroelectric material and Na_2TiO_3 (NT). To the best of our knowledge, there are inadequate studies available based on the use of PbZnTiO_3 as an energy harvester, although it has been utilised prior as a microwave resonator (Kim et al., 1999), gas sensor (Obayashi et al., 1976) and as a memory storage device (Limited; & Kanagawa, 2008a). It is important to investigate the ferroelectricity property of the material to ensure that the proper preparation method is selected to meet the expected performance of the vibration energy harvester.

3.2 Preparation of $0.7\text{PbZn}_{0.3}\text{Ti}_{0.7}\text{O}_3$ - $0.3\text{Na}_2\text{TiO}_3$ Harvester

Piezoelectric generator was fabricated from a $0.7\text{PbZn}_{0.3}\text{Ti}_{0.7}\text{O}_3$ - $0.3\text{Na}_2\text{TiO}_3$ (PZnT-NT) system via wet chemical method. The detail standard and procedure of the wet chemical method can be found in the references (Byrappa, 2013; Darinee Phromyothin, 2017). The $\text{PbZn}_{0.3}\text{Ti}_{0.7}\text{O}_3$ powder was fabricated from lead oxide (99.5% purity R&M Marketing. Essex U.K.), titanium dioxide (99.5% purity R&M Marketing. Essex U.K.) and zinc oxide (>99.0-100.5% purity R&M Marketing. Essex U.K.). The $\text{PZn}_{0.3}\text{Ti}_{0.7}\text{O}_3$ was prepared with a [1:1] stoichiometry, where the powder was calcined at 850 °C for three hours with a heating/cooling rate of 5 °C/min. The powder was mixed by ball milling for one hour. Sodium titanate were synthesised with a molar stoichiometry of [NaOH: TiO_2 , 2:1] and mixed with $0.7\text{PbZn}_{0.3}\text{Ti}_{0.7}\text{O}_3$ powder where the $0.7\text{PbZn}_{0.3}\text{Ti}_{0.7}\text{O}_3$ was sprayed by the distilled water for increasing the solubility. Furthermore, the particles binding was increased through the pressing process, where the sample was pressed in rectangular stainless steel mold at three tons with deposited the electrodes in both sides, where the electrodes consist of a copper (80 μm) anode and zinc (420 μm) cathode, and then treated at 250 °C for 30 min. Finally, the electrodes were covered by high adhesive plastic tape for a hermetic covering to provide protection against environmental damage. In addition, the standardized measurement was followed the IEEE Standard (The Institute of Electrical and Electronics Engineers, 1988) that presented the measurement of dielectric properties and the using of rectified circuit was presented in (Daniel et al.,2012).

All the preparation process and the utilised equipment were illustrated in appendix B.1. Field emission scanning electron microscope (FESEM) image analysis was carried out to explore the surface characteristics of sample after removing the copper electrode. Particles size distribution steps were given in appendix C1 and C2. The fabrication process of the PZnT-NT harvester is illustrated in Figure 3.1.

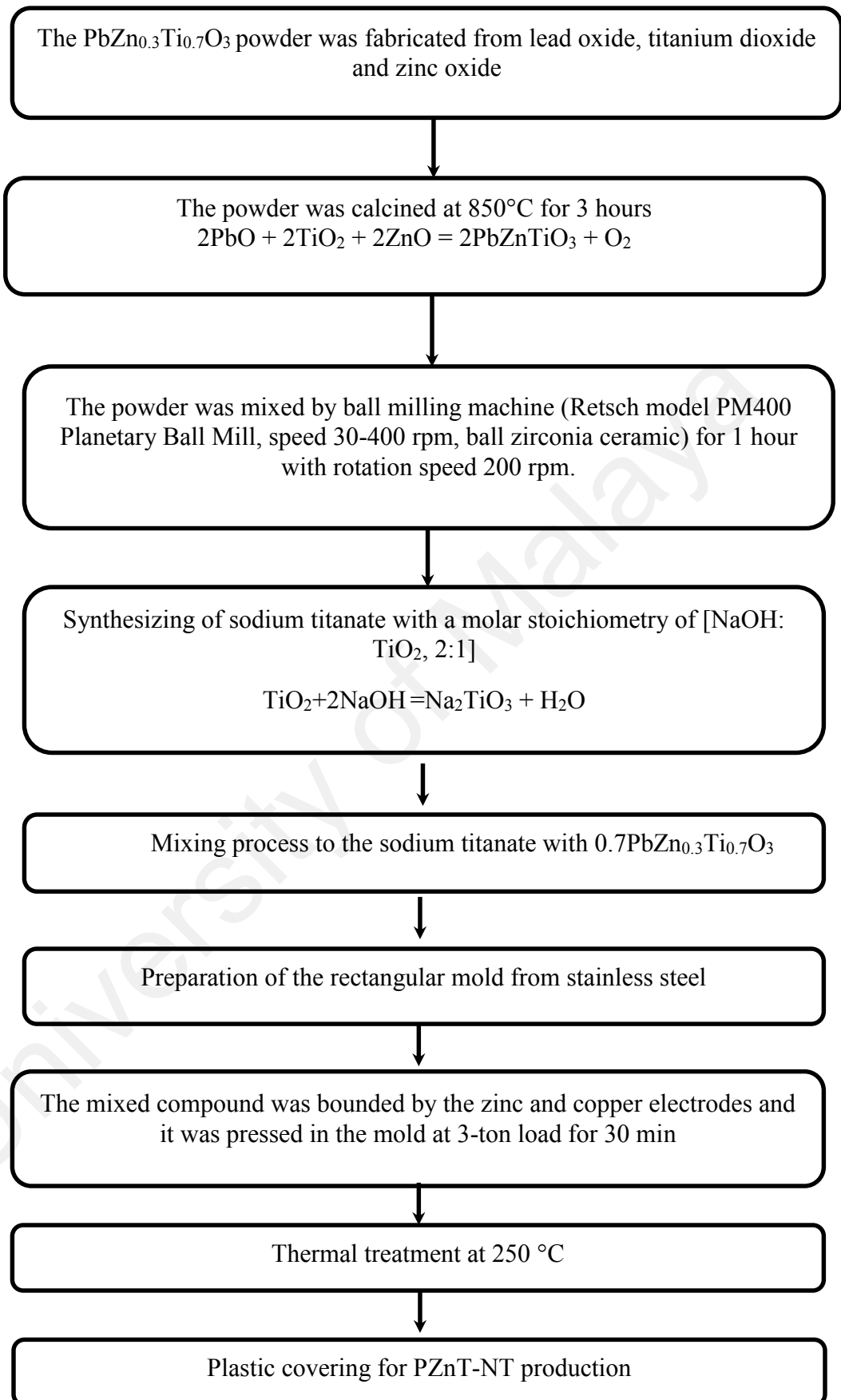


Figure 3.1: The Fabrication Process Flow Chart of the PZnT-NT

The physical properties of the harvester were measured by using a precision impedance analyser (model 4294A) where the capacitance, dielectric constant, loss tangent, and conductivity were recorded and studied based the polarised phase of the material. The powder was examined by X-ray diffraction system (PANalytical X'Pert3 X-ray diffractometer) using anode material copper (Cu) 40 mA, 40 kV, and the microstructure of the propertied PZnT-NT system was observed by FESEM image analysis. The fabricated harvester is illustrated in Figure 3.2.

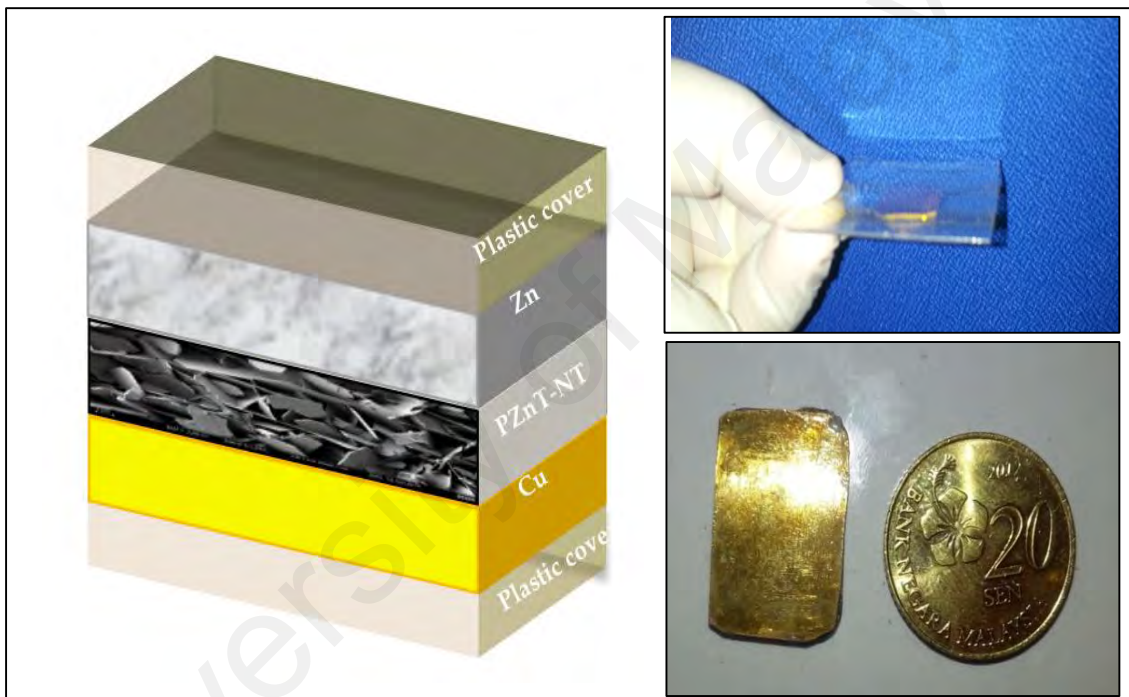


Figure 3.2: The Piezoelectric Harvester Made of $0.7\text{PbZn}_{0.3}\text{Ti}_{0.7}\text{O}_3-0.3\text{Na}_2\text{TiO}_3$

3.2.1 Dielectric Measurement and Conductivity of PZnT-NT

The electrical characteristics of PZnT-NT material were evaluated by measuring the dielectric properties which consist of the relative permittivity, loss tangent, and conductivity. The PZnT-NT sample was connected to the input terminals of the Agilent 4294A analyser (frequency range from 4 Hz to 110 MHz) where the input terminal was supplied by the AC signal and the output was measured at various frequencies. The impedance analyser was equipped with data acquisition software. The measured parameters are the relative dielectric (i.e. real part and imaginary part) that vary with frequencies. The relative permittivity was calculated from the relation between the dielectric real part and the imaginary part $k^T = \epsilon' - j\epsilon''$ (see Eq.2.6) and subsequently, the loss tangent was determined from $\tan(\delta) = \frac{\epsilon''}{\epsilon'}$ (see Eq.2.7). Finally, the conductivity was calculated from $\sigma = \omega \epsilon' \epsilon_0 \tan(\delta)$ (see Eq.2.8). Figure 3.3 illustrates the impedance analyser and the PZnT-NT under test.

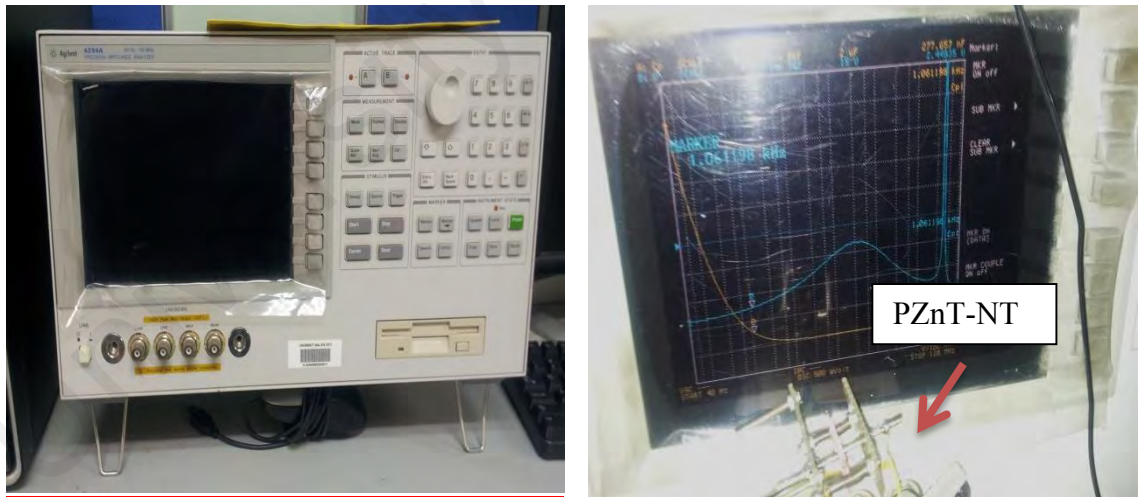


Figure 3.3: (a) Agilent 4294A Analyser, (b) PZnT-NT Coupled to the Input Terminal

For diagnosing the ferroelectricity of the material, the PZnT-NT was polarised under a high electric field where the sample was immersed in the silicon oil bath to prevent the current leakage. The hysteresis loop was recorded to the pure PZnT and the PZnT-NT,

where the maximum applied voltages were 7500 V and 700 V respectively. In fact, after applying the voltages, the polarisation was detected from the electric field and permittivity value. The data acquired was sent to computer software that would provide information about the electric field, polarisation, coercive field and remnant polarisation. The remnant polarisation and coercive field were then detected and compared. Description of the unit cell geometric and measuring the crystal lattice dimension was carried out using the X-ray diffraction system (PANalytical X'Pert3 X-ray diffractometer) to the calcined powder. After the preparation of the PZnT-NT sample, a field emission scanning electron microscope (FESEM) was utilised for detecting the crystallography nature of the PZnT-NT. The FESEM images with high purity were captured in the nano scale resolution. The X-ray diffraction system and FESEM are shown in Figure 3.4.



Figure 3.4: (a) X-ray Diffraction System (PANalytical X'Pert3 X-ray Diffractometer), (b) Field Emission Scanning Electron Microscope (ZEISS Sdn. Bhd)

3.2.2 Energy Harvesting of PZnT-NT over the Test Rig

The energy harvesting test was carried out by fixing the piezoelectric harvesters directly above the host cantilever test rig which was excited to produce a cyclic excitation at a low excitation frequency (i.e. 30 Hz) and at a low acceleration (i.e. 0.4 m/s^2). The generated power was compared with other commercial piezoelectric harvesters, such as PZT, MFC and PZT bimorphs. All the vibration data were measured by an accelerometer (model: SNAP S100C) and send through a data acquisition unit (model: NI USB-9162). The data were then analysed by using virtual instrument software (i.e. DASyLab) in order to obtain the frequency, acceleration and generated voltage. The experimental setups are shown in Figure 3.5.

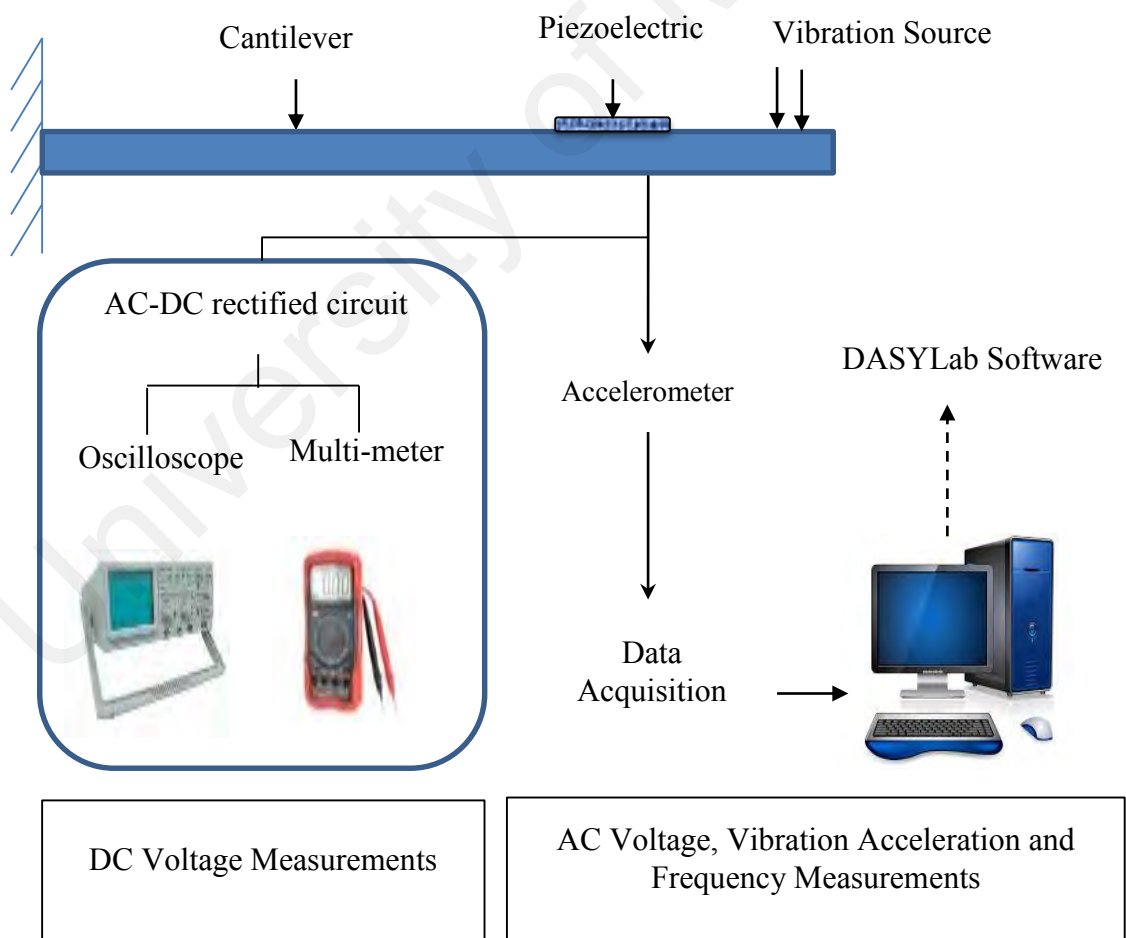


Figure 3.5 : Energy Harvesting Experimental Setup

To achieve full-wave rectification, the AC voltage generated by the vibration harvester was rectified by using a voltage regulator circuit. The AC-DC converter consists of four Schottky diode bridges (1N5817). An oscilloscope (SS5702) and multi-meter (model ZELM05 ATEX 0274) were employed for measuring the DC voltage across the capacitor and the load resistance as is illustrated in Figure 3.6. Maximum harvesting energy was verified when the internal impedance of the piezoelectric matched the applied load resistance. The installations of numerous piezoelectric harvesters are illustrated in Appendix A.2, A.3 and A.4.

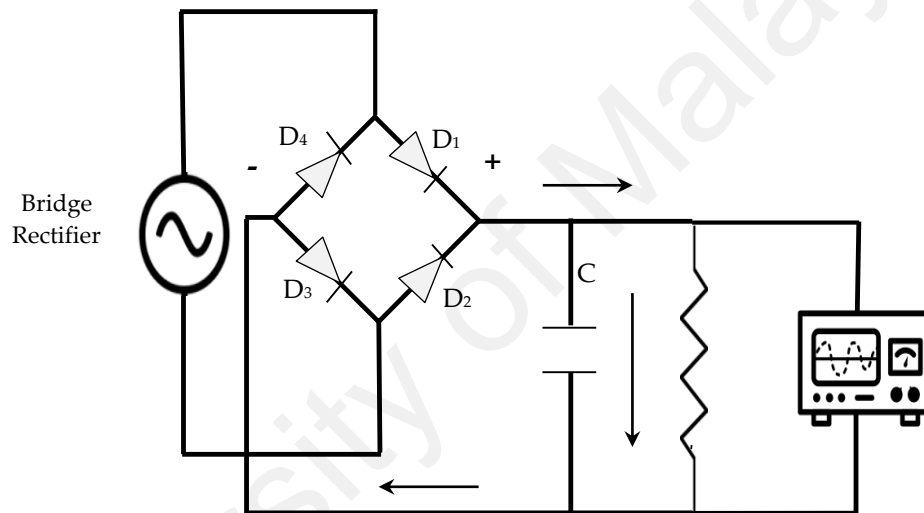


Figure 3.6: Schematic Diagram for the Full Wave Rectification Circuit and the Load Resistance

In this study, the PZT, PZT-5H bimorph and MFC patch were employed for comparing and evaluating the power outputs. PZT (T215-H4-503) have very high electromechanical properties and moderate stiffness.

MFC was characterised by high piezoelectric coefficients (d_{33}), high permittivity (ϵ), high dielectric losses and low mechanical quality factors (Daniels et al.,2013; Jan Tichý et al., 2010a; Thomas, 2008), beside that, MFC have high flexibility (low stiffness)

whereas the PZT-5H bimorph was very rigid (high stiffness). The typical properties of PZT, MFC and PZT-5H are provided in Table 3.1.

Table 3.1: The Microfiber and Piezoelectric Bimorph Properties

Material	PZT (T215-H4-503)	Micro-Fiber Composite (MFC- PZT5A1, M8557P2) (material, 2017)	Piezoelectric Bimorph (PZT-5H)
Typical capacitance (nF)	450	325	184
Piezoelectric strain constant, d_{33} (pC/N)	650	470	600
Piezoelectric voltage constant, g_{33} (10^{-3} Vm/N)	24	25	19.4
Permittivity, $\frac{\epsilon_{33}^T}{\epsilon_0}$ (at 1 kHz)	3800	1300	3500
Electrode material and configuration	Silver electrodes	Flexible MFC with gold electrodes	Rigid Bimorph with copper- silver electrodes
Dimension (mm³)	63.5×31.8×0.51	80×57×0.335	70×50×0.7

3.2.3 Recharging Lithium Ion Battery using the Piezoelectric Harvesters

The energy was harvested from piezoelectric according to the IEC 62830-1 Ed. 1.0 b:2017 standard. The experimental setup is similar to the procedure that carried out to investigate the power density and voltage where the difference was of using an ion battery (i.e capacitance of 40 mAh) instead the resistance load the connected to the rectified circuit. This battery can be recharged to illuminate three serial LEDs diodes. In more detail, the energy harvesting test was carried out over the cantilever host structure where the piezoelectric harvester was attached directly above the test rig. The cantilever was excited at a frequency of 30 Hz and acceleration of 0.4 m/s^2 . The acceleration at the harvested point was measured by using an accelerometer (model: SNAP S100C), the acquired data was sent through a data acquisition unit (model: NI USB-9162) and analysis was done by the designed DASYLAB worksheet. Additionally, the frequency of the cantilever was measured by a Tachometer instrument (Monarch Pocket Laser Tach 200). The cantilever was excited by DC motor (24V, 30 W, 3000 rpm), the experimental set up is shown in Figure 3.7 (a). Full-wave rectification was achieved by using a voltage regulator circuit. The DC voltage across the capacitor and the load was measured by the oscilloscope (SS5702) and multi-meter (model ZELM05 ATEX 0274), and an ion battery – three diodes circuit was connected to the anode and cathode ends of the capacitor as illustrate in Figure 3.7 (b). The generated power was compared with other commercial piezoelectric harvesters, such as PZT, MFC, and PZT bimorphs.

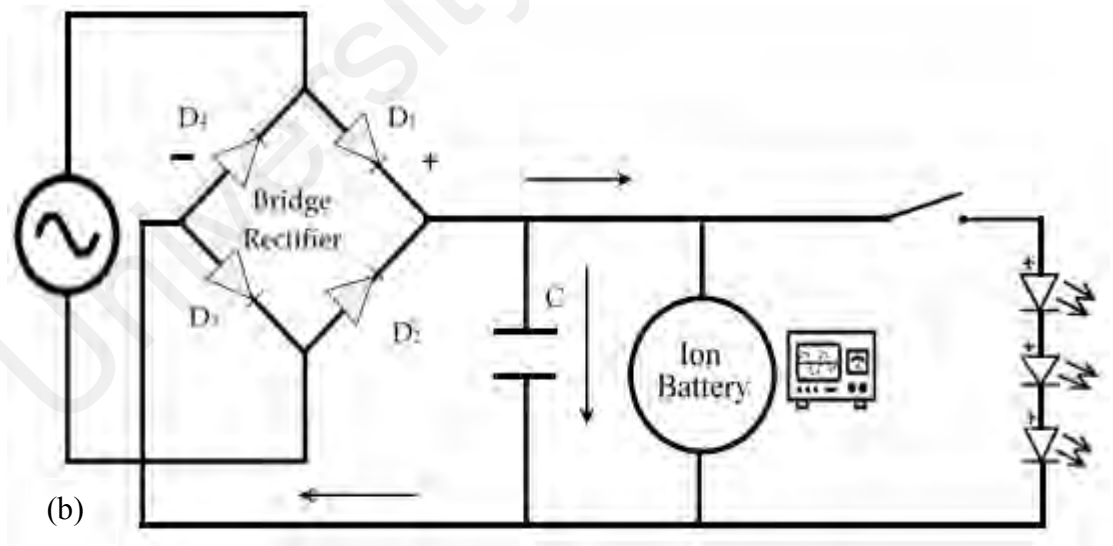
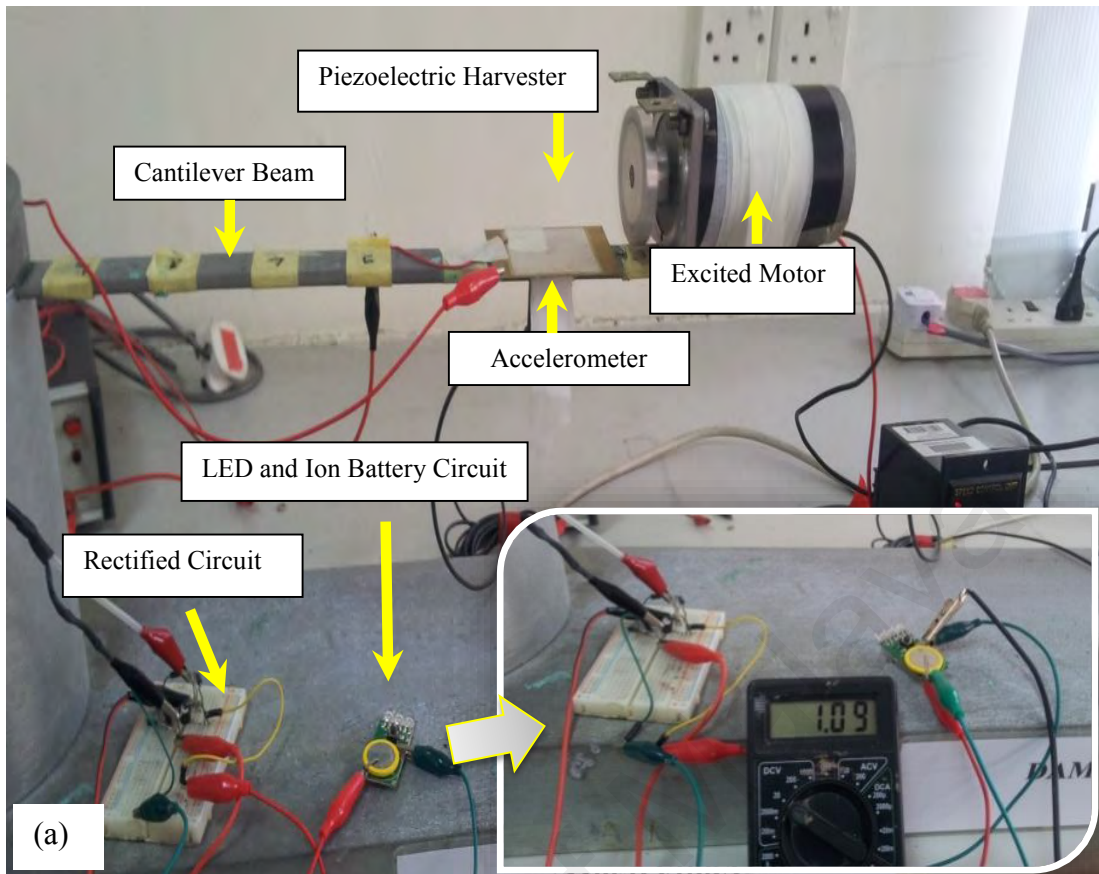


Figure 3.7: Experimental Set up (a) Cantilever Beam Excited by DC Motor (b) Rectified Circuit with Ion Battery and three LEDs Diodes

3.3 Shaker Test to Evaluate the Resonance of the PZnT-NT

Accordingly, the AC voltage was generated by the harvester where it varied with the excitation frequency. The highest amplitude of harvester deformation was realised when the harvester was tuned at its natural frequency. The PZnT-NT was mounted directly over the shaker and was excited where the force sensor. The vibration signal was acquired by NI USB-9162 with a sampling rate of 2048 samples per seconds, block size of 8192 samples, and block average of 30 blocks. The shaker was excited in frequencies ranging from 10–300 Hz and the shaker's force was assumed to be constant throughout the study by using a power amplifier. The baseline test or shaker test was conducted where the voltage was generated purely by the harvester (that was excited directly by the shaker) as illustrated in Figure 3.8.



Figure 3.8: Baseline Test

3.4 Location Selection Scheme for Piezoelectric Energy Harvesting

This section presents the selection scheme of optimal locations of the piezoelectric plate on a cantilever beam structure based on the vibration mode shape and its ODS. The PZnT-NT is placed on the cantilever beam structure subjected to excitation by impact hammer or excited shaker (i.e. excitation at the natural frequencies of the cantilever and

/ or the natural frequency of the harvester). The voltage magnitude was recorded when the PZnT-NT was roved from one point to another over the cantilever beam.

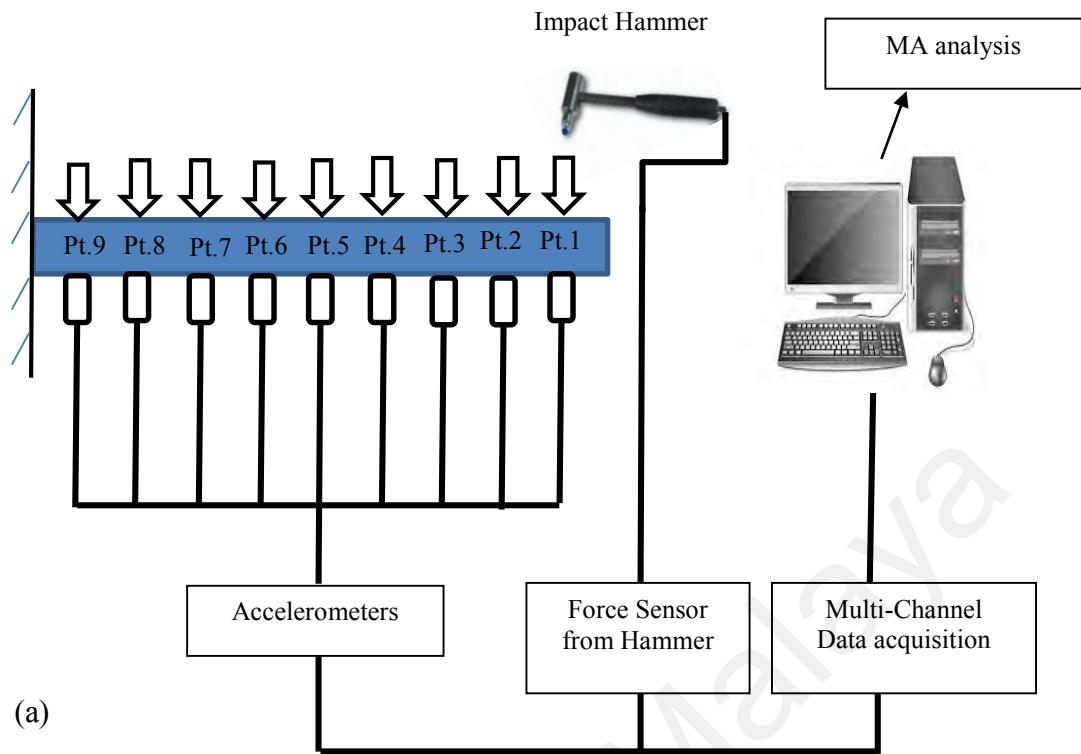
3.4.1 Experimental Modal Analysis of Cantilever Test Rig

Modal analysis was conducted to measure the dynamic characteristics of the cantilever test rig. A modally tuned PCB[®] ICP impact hammer model 086C03 was used to excite the cantilever host structure. The selection of the optimal location was carried out using a Single-Input/Single-Output (SISO) approach where the impacts force was excited the point at the free end and the resultant simultaneously respond was recorded by stationary accelerometers. The excitation force was measured by a force sensor embedded at the tip of the impact hammer and it was sent to the multi-channel data acquisition (DAQ) system through four-channel DAQ hardware (i.e. model NI USB 9234) that integrated with a compact DAQ chassis (i.e. model NI CDAQ-9172). All induced acceleration responses at the 9 measurement points were captured by the DAQ as well. The DAQ system was connected to a signal analyser which was equipped with data acquisition software (i.e. DASyLab[®]). The number of data acquired per second (i.e. sampling rate is 2048 Hz) and the block size is 8192 samples. The FRF obtained was then post-processed by using ME'scopeVES[®] software to obtain the modal parameters. The installation of the test is illustrated in Figure 3.9 (a). Details of equipment properties are given in Appendix A.1.

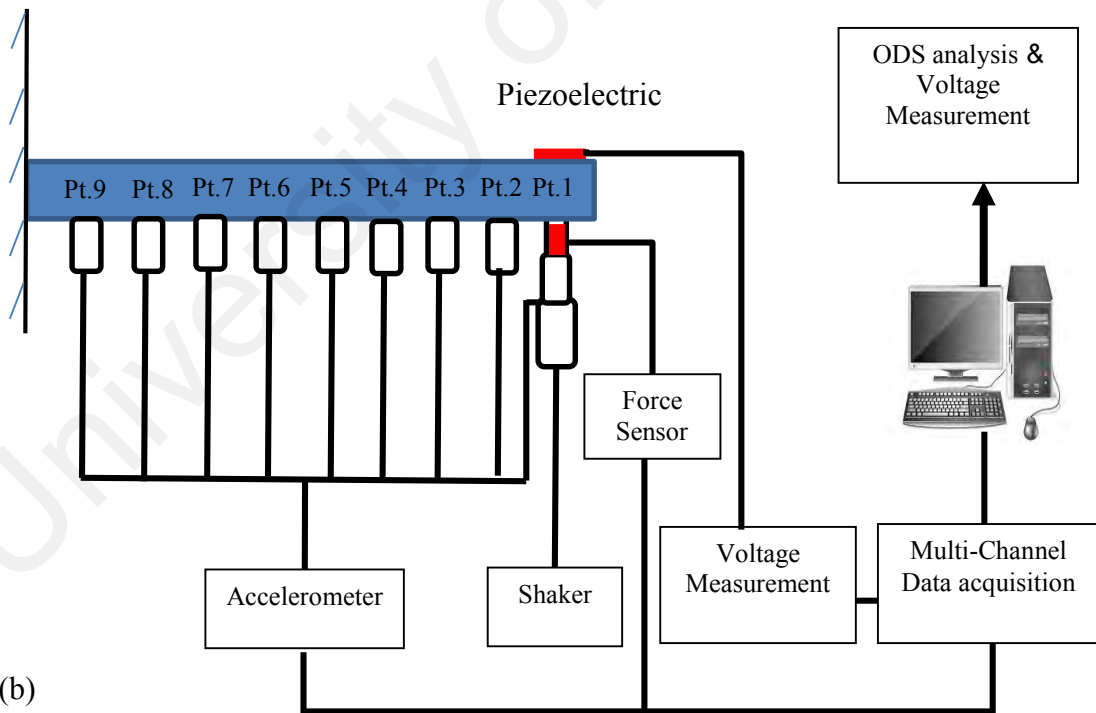
3.4.2 ODS Analysis

The experimental setup for both the ODS analysis and voltage measurement are the same as shown in Figure 3.9 (b), and therefore, their data can be acquired simultaneously. An electromagnetic shaker (B&K LDS[®] model V101) and its power amplifier (B&K LDS[®] model PA25E) were used to vibrate the cantilever host structure at the desired excitation frequency. A PCB[®] force sensor model 208C01 was used to monitor the force (1 N) induced by the shaker. The shaker's force was assumed constant throughout the study. Time history of acceleration responses and harvested voltage were captured by the DAQ (NI USB 9232) and the response was detected by DAQ (NI USB 9234).

Generally, the experimental procedure is the same as EMA and the only difference is the excitation type. The ODS analysis was performed when the operated force excites the free end of the cantilever. The acquired data with sampling rate and block size of 2048 samples per seconds and 8192 samples was processed through the designed worksheet of the DASyLab, after which, the ODS sets were transferred to the visual engineering post-process software, (i.e. ME'scopeVES[®]). The obtained ODS set (i.e. time domain or frequency domain) was used to visualise the vibration pattern for detecting the optimal harvesting location.



(a)

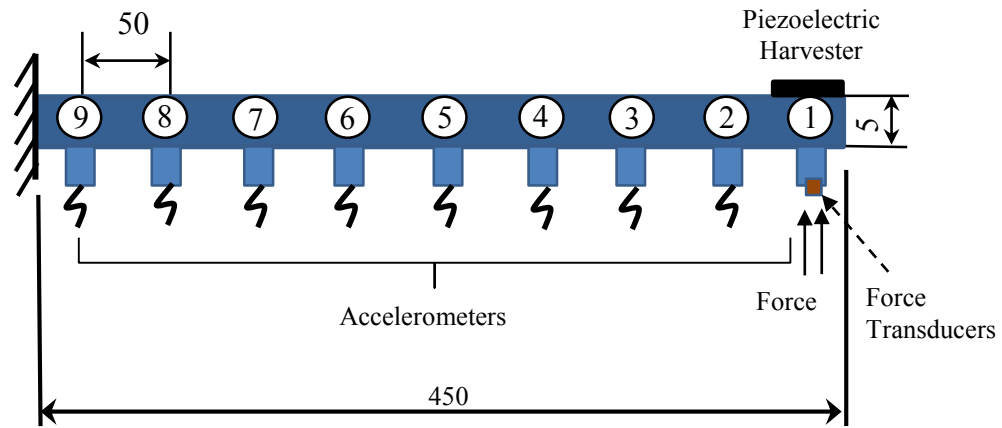


(b)

Figure 3.9: Experimental Set-up (a) EMA, (b) ODS Analysis and Voltage Measurement

3.4.3 Voltage Measurement Verification Test

The piezoelectric harvester was mounted directly over the cantilever ($450 \times 25 \times 0.5$ mm³). The excited force was applied in the free end of the cantilever using the shaker. The PZnT-NT was attached to the cantilever using a removable adhesive polymer, and then the PZnT-NT was moved over the discrete point over the cantilever during the measurement process. The force sensor (model 208C01) was mounted over the shaker for monitoring and capturing the shaker excitation at the free end. The shaker was tuned on frequency of 95.2 Hz and the A PCB sensor model 208c01 was used to measure the force induced by the shaker. A DASyLab worksheet was designed to record the force, frequency, and AC voltage. The voltage was then captured by DAQ (NI USB 9232). The maximum peak and minimum peak were indicated based on the voltage amplitudes (V_{pk-pk}). The test rig has 9 discrete locations as shown in Figure 3.10.



(a)



(b)



(c)

Figure 3.10: Voltage Measurement Test (a) Cantilever Test Rig, (b) Multi-Channel Data Acquisition (DAQ) Devices Integrated with the Compact DAQ Chassis, (c) Signal Generate and Power Amplifier

3.5 Vertical Axis Wind Turbine VAWT Exhaust Air System

The VAWTs are illustrated in Figure 3.11(a). The VAWT consists rotor, cylindrical cantilever beam and generator. The generator is fixed to the vertical beam structure supported by the 4 screws (fixed boundary condition). The vertical beam structure has

adjustable height capability and the end of the beam is supported by a “X” shape stand. The stand has 4 hemisphere supports at its end, and they were attached to the ground by the means of simply frictionless support. The VAWT structure and the exhaust tower are separated apart from each other without connection, as illustrated in Figure 3.11(b).

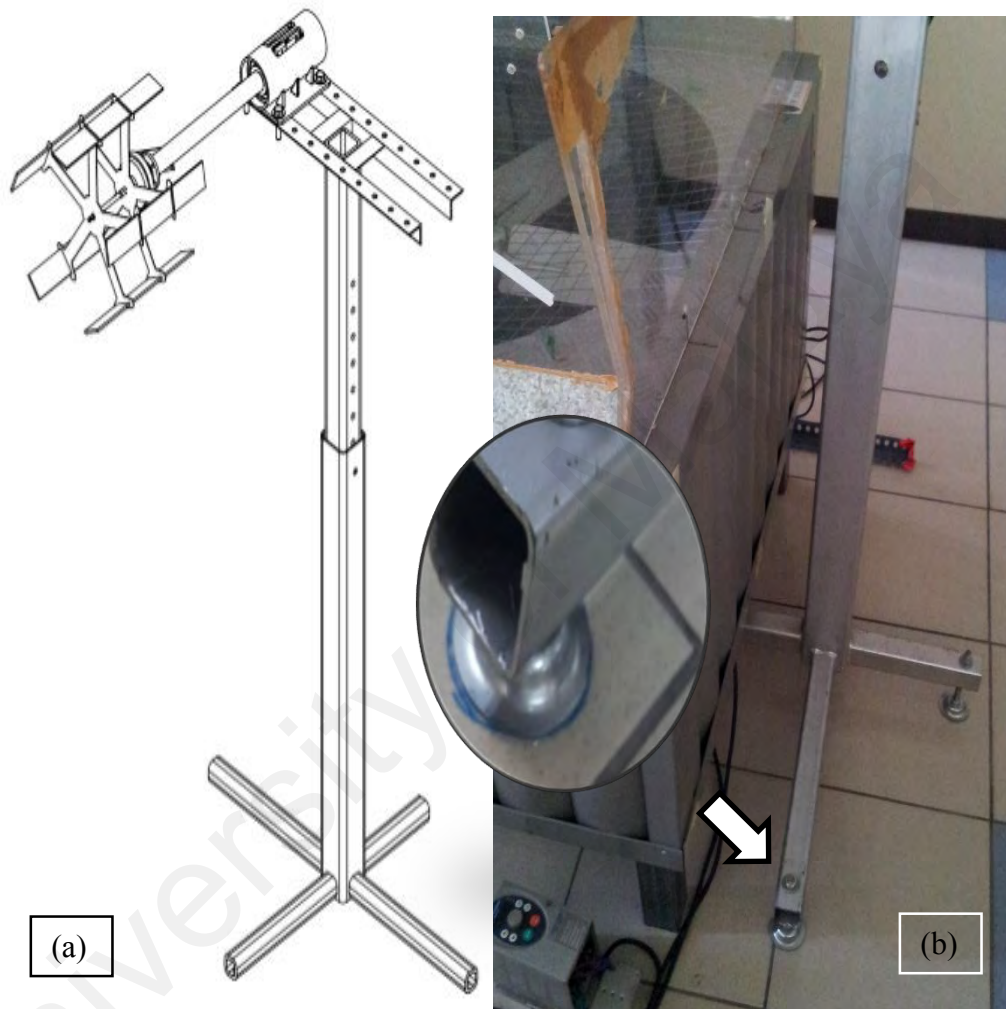


Figure 3.11: Assembly of VAWTs System (Tong et al., 2011) (a) Schematic Drawing of VAWT (b) The Boundary Condition of the VAWT and Tower

The exhaust tower is illustrated in Figure 3.12. The wind turbine characteristics such as the performance and the physical parameters are presented in Table 3.2. The exhaust air fan tower consists an exhaust fan shielded by metallic square box structure. The exhaust tower has 4 square supports and they were attached to the ground by the means of simply frictionless support.



Figure 3.12 : Exhaust Air Cooling Tower (Tong et al., 2011)

Table 3.2: Wind Turbine Characteristics (a)Performance (b)Physical Parameter (Tong et al., 2011; Abdullah, 2016)

(a) Performance		(b) Physical Parameter	
Rated power	10 W	Rotor power	0.3 m
Rated wind speed	10 m/s	Blade length	0.3 m
Cut-in wind speed	2 m/s	Rotor weight	2 kg
Cut-out wind speed	40 m/s	Number of aerofoil blade	5
Survival wind speed	40 m/s	Aerofoil type	MH 114 (Refers to (“UIUC Airfoil coordinate Database”))
		Aerofoil chord length	0.045 m
		Pitch angle	10° (nose outward, uniform along blade length)

In this study, the VAWT was located above the exhaust fan at the vertical distance of 400 mm to the outlet plane and horizontal distance of 250 mm. This location was measured from the centre of the exhaust tower and it was assumed that this location has the highest wind speed and optimum power generation, while the fan speed was set at 910 rpm, as reported in the previous study (Abdullah, 2016).

3.5.1 Experimental Set-up of Wind Turbine VAWT Exhaust Air Recovery System

This section aims to harvest the waste vibration energy of the (10W H VAWT from Shanghai Aeolus Wind Power Technology Co. Ltd). The VAWT diameter and length were 30 cm with a chord length of 4.5 cm. The performance (rotation speed) of the VAWT has variances at various VAWT positions and various fan speeds. The optimal setting of the VAWT was investigated through experimental and simulation techniques previously carried out by Abdullah (2016). The optimal position of the VAWT was located at the third band region of the outlet (i.e. radius of 250 mm) for the exhaust fan speed of 910 rpm. The VAWT was installed at horizontal and vertical distances of 250 mm and 400 mm respectively away from the centre of the outlet (Ahmad Fazlizan, 2016). The schematic diagram for the optimal position is shown in Figure 3.13.

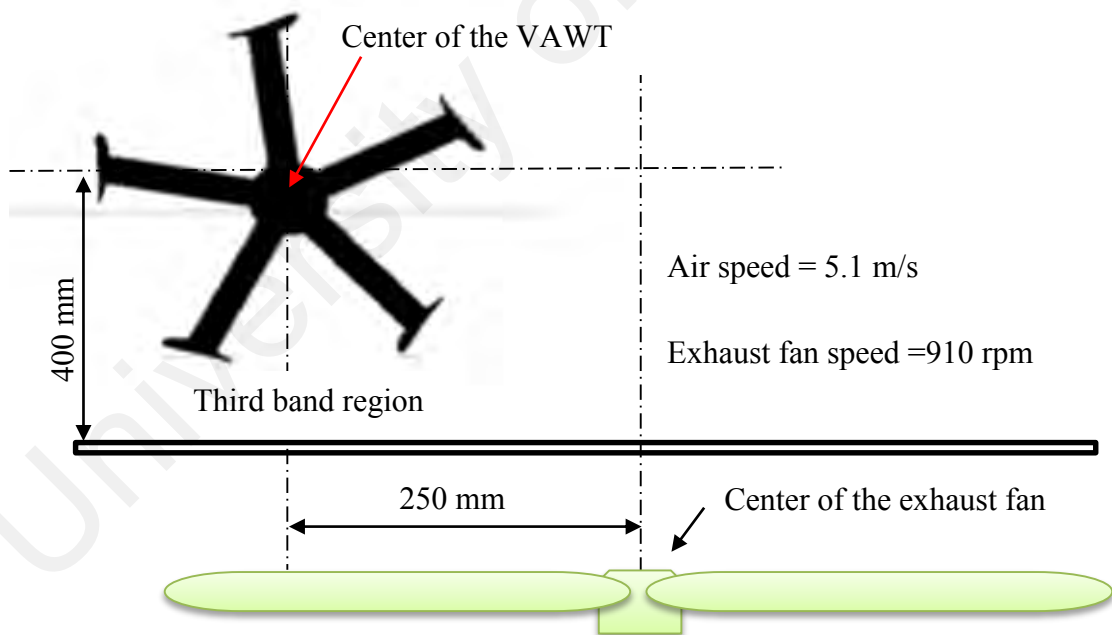


Figure 3.13: The Optimal Position of the VAWT Over the Exhaust Tower

In fact, the exhaust air recover wind turbine system was enclosed by the diffuser plates. The diffuser had provided a particular controlling of the air stream flow where it was employed as a power augmentation device.

This design was implemented to increase the recovered energy by the VAWT that was mounted above the cooling tower. Thus, it was very necessary to detect the optimal location for the piezoelectric harvester over the VAWT beam, the experimental setup of the VAWT is shown in Figure 3.14.

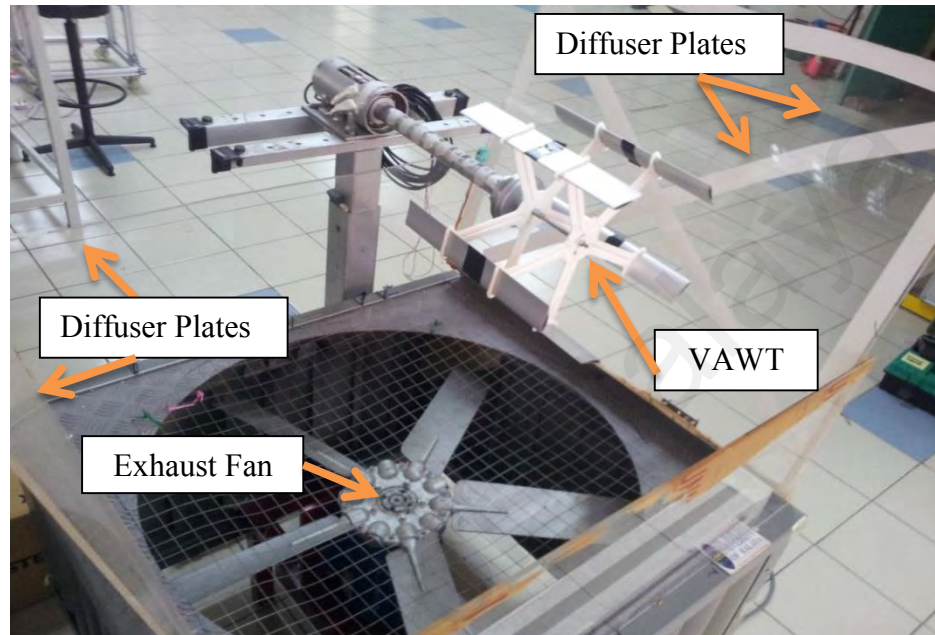


Figure 3.14: Experimental Set-up of Exhaust Wind Turbine Recovery System Integrated with Diffuser Plates

The waste dynamic energy of the VAWT's beam-exhaust air system was harvested and converted to useful electric energy. It is important to visualise the vibration pattern of the VAWT's beam and detect its dynamic characteristics. Accordingly, the VAWT beam was divided into 10 segments and 9 measurement points where the harvester was mounted over the point (i.e. point 1) of the VAWT to measure the AC voltage and this should be compared with voltage at point 9.

3.5.2 Experimental Modal Analysis and Operation Deflection Shape of VAWT

The selection of the optimal harvesting location was carried out over the VAWT beam. The test was conducted using tri-axial accelerometer at fixed stationary point, based on the hammer test, the impact force will excite 9 points in one direction and the tri-axial accelerometer will simultaneously provide response in three directions as shown in Figure 3.15(a). Thus, the obtained FRF's for the structure is 27. To further explain this, when the point 9 was excited in the direction Z, the response will be captured at 1x, 1y, and 1z, and so the measured FRF's will be 1x:9z, 1y:9z, and 1z:9z. The same detected information was measured at the other points (Avitabile, 1998). Vibration shapes were obtained from EMA or ODS analysis where it was utilised in selecting an optimal location for the piezoelectric plate to harvest the maximum voltage. When the piezoelectric plate was placed on a structure under vibration/resonance, the optimal location, (i.e. maximum vibration points / anti-nodal points) was determined by the location selection scheme. The ODS was used to visualise the vibration pattern in real excitation ambience where the applied forces by the wind are unknown. Note that both EMA and ODS analysis used the same sampling rate of 2048 Hz and block size of 8192.

3.5.1.2 Voltage Measurement of VAWT based on PZnT-NT

The experimental setup for the ODS analysis was carried out based on the FRF measurement in three orthogonal directions as shown in Figure 3.15(b). The ODS analysis was performed where the data were acquired simultaneously after operating the tower fan and exciting the VAWT.

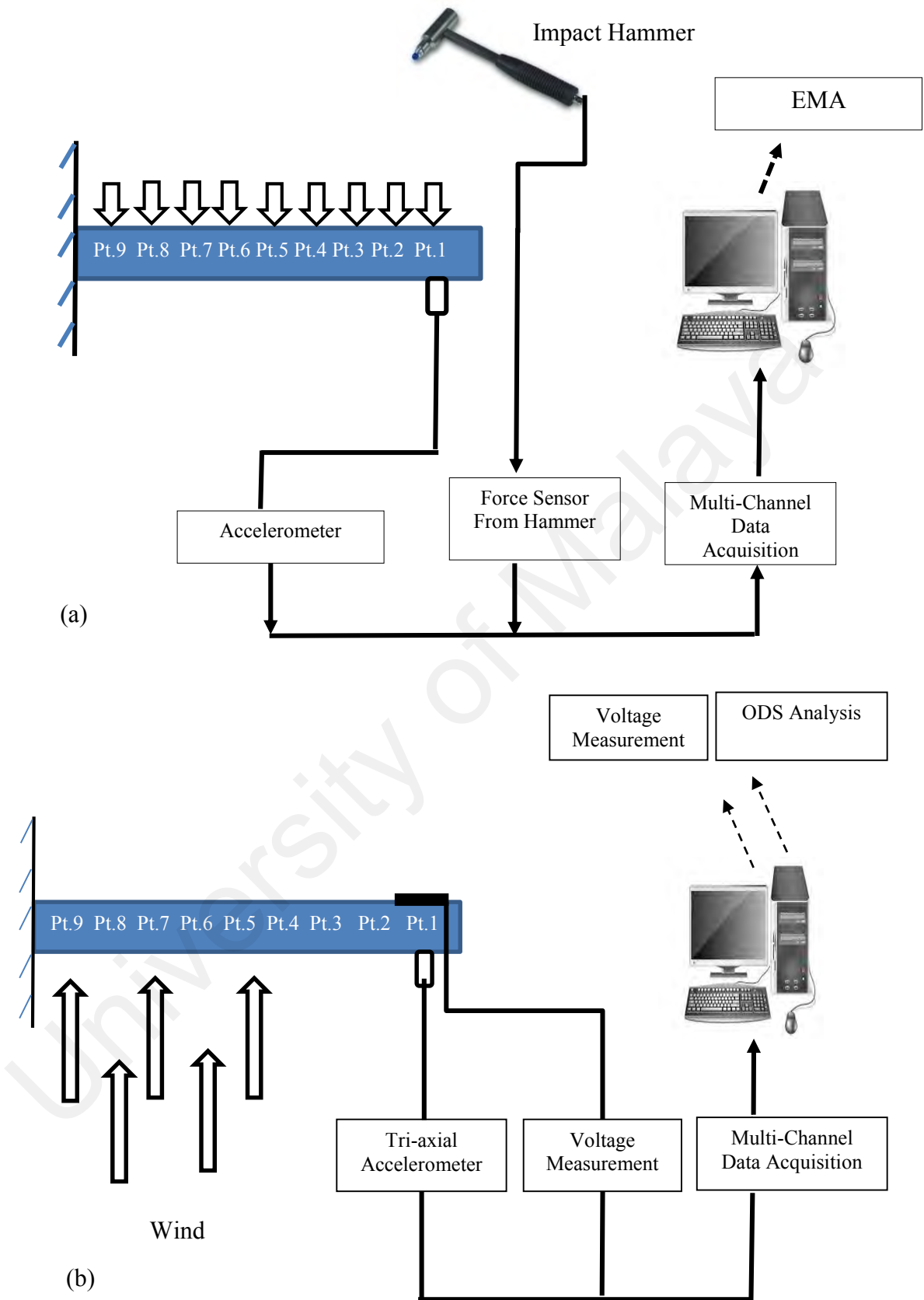


Figure 3.15: (a) EMA, and (b) ODS Analyses of the VAWT

The exhaust air cooling tower would apply unknown forces at the VAWT, thus utilisation of the tri-axial accelerometer would be the most practical technique to visualise the vibration pattern. The induced acceleration responses at point 1 were measured by the tri-axial accelerometer and the acquisition data were captured by the DAQ hardware (NI USB 9234). The DASyLab was used to acquire the data with a sampling rate and block size of 2048 Hz and 8192 samples having a block average of 30. Then, the ODS sets would be transferred to the post-processing software (i.e. ME'scopeVES[®]). The obtained ODS set in the frequency domain was visualised for the vibration pattern.

3.5.1.2 Voltage Measurement of VAWT based on PZnT-NT

The VAWT beam was divided into 10 segments with 9 measurement points, where at point 1 (i.e. free end of beam), it was equipped with tri-axial accelerometers that recorded the responses in three DOF (i.e. x, y, and z direction). The PZnT-NT was mounted over the VAWT based on the obtained results of both EMA and ODS analysis. The highest and lowest AC voltage amplitudes were recorded to validate the EMA and ODS results. The AC voltage was measured at two points (i.e. point 1 and point 9) where it utilised data acquisition hardware NI 9232, whilst the sampling rate and the block size were 2048 Hz and 8192 samples respectively.

3.5.1.3 EMA of the VAWT

EMA analysis was implemented over the discrete VAWT using a modally tuned PCB® ICP impact hammer (Model 5800B4 with sensitivity 10.91 mV/g) to excite the cantilever host structure. The force sensor inside the tip of the impact hammer was used to record the force signal and send it to the multi-channel data acquisition (DAQ) system through NI USB 9234 which was connected in a compact DAQ chassis (i.e. model NI CDAQ-9172). The induced acceleration responses at point 1 (i.e. response of three orthogonal directions x, y, and z directions) was captured by the NI USB 9234 as well. The measured FRF set is shown in Figure 3.16 (a). The DAQ system was connected to a signal analyser which was equipped with data acquisition software (i.e. DASyLab®). The function was transferred to the post-processing software (i.e. ME'scopeVES®). The dynamic characteristics were evaluated (i.e. natural frequency, damping ratio, and mode shape). Conducting EMA requires extra caution through conducting the experiment due to any change of boundary conditions that will cause alterations in dynamic characteristics of the structure. The installation of the experiment is shown in Figure 3.16 (b).

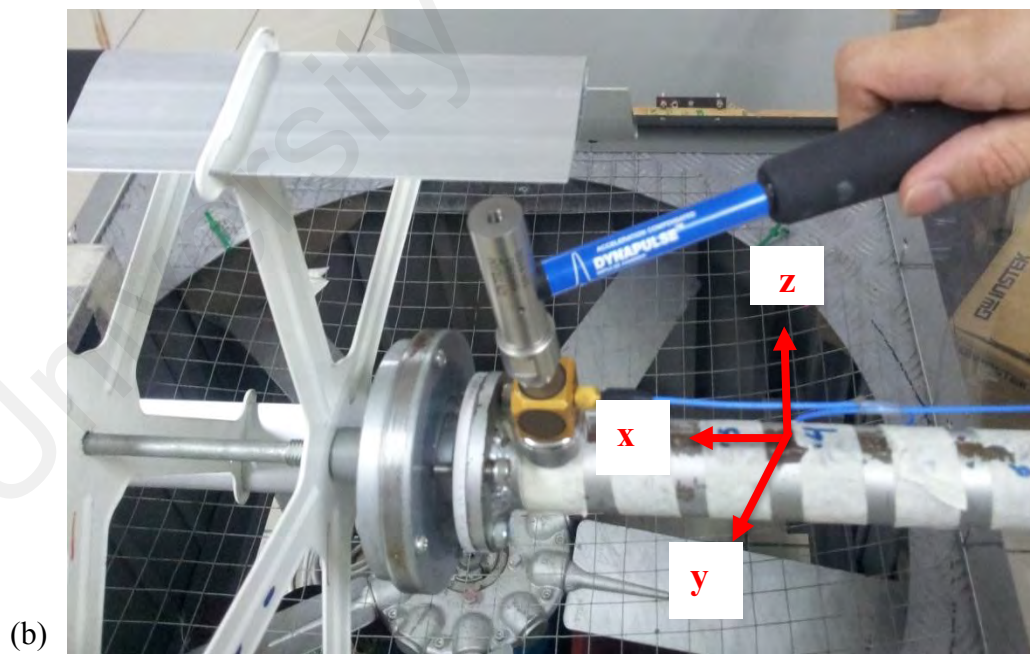
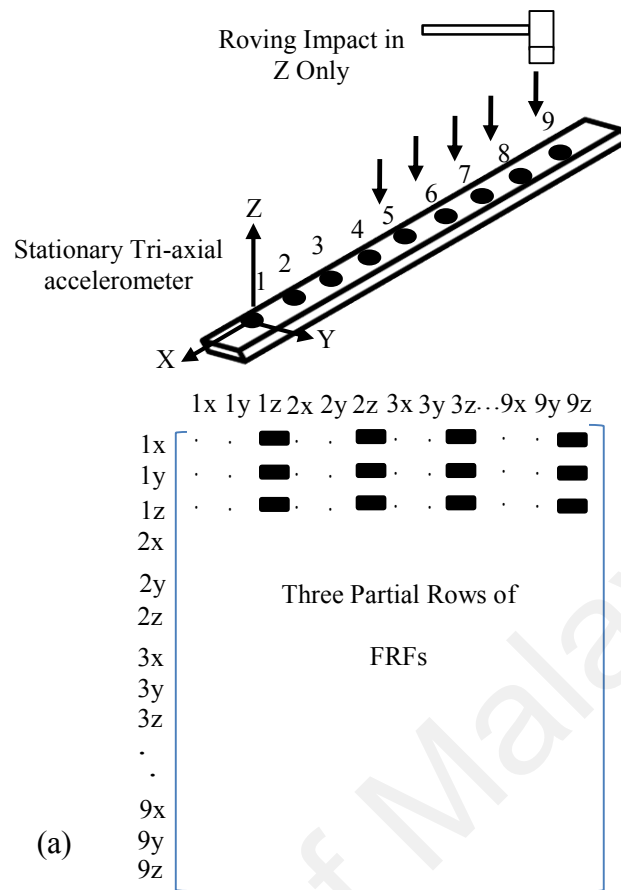


Figure 3.16: EMA Analysis of VAWT: (a) The FRFs Matrix, (b) Hammer Test

3.5.3 Implementing the PZnT-NT and DC Energy Harvesting over the VAWT

The PZnT-NT was implemented over the VAWT beam, where the harvesters were mounted over the detected location. The generated AC voltage was acquired by the NI 9232 hardware and send to the DASyLab worksheet. For harvesting the DC signal, it should be rectified the AC signal. After the rectification of the signal, the signal was stored in the capacitor (i.e. 100 μ F), and then the power was calculated after applying resistive loads in the range of (1.99-5200) k Ω . Figure 3.17 depicts the harvesting of numerous piezoelectric harvesters over the VAWT.

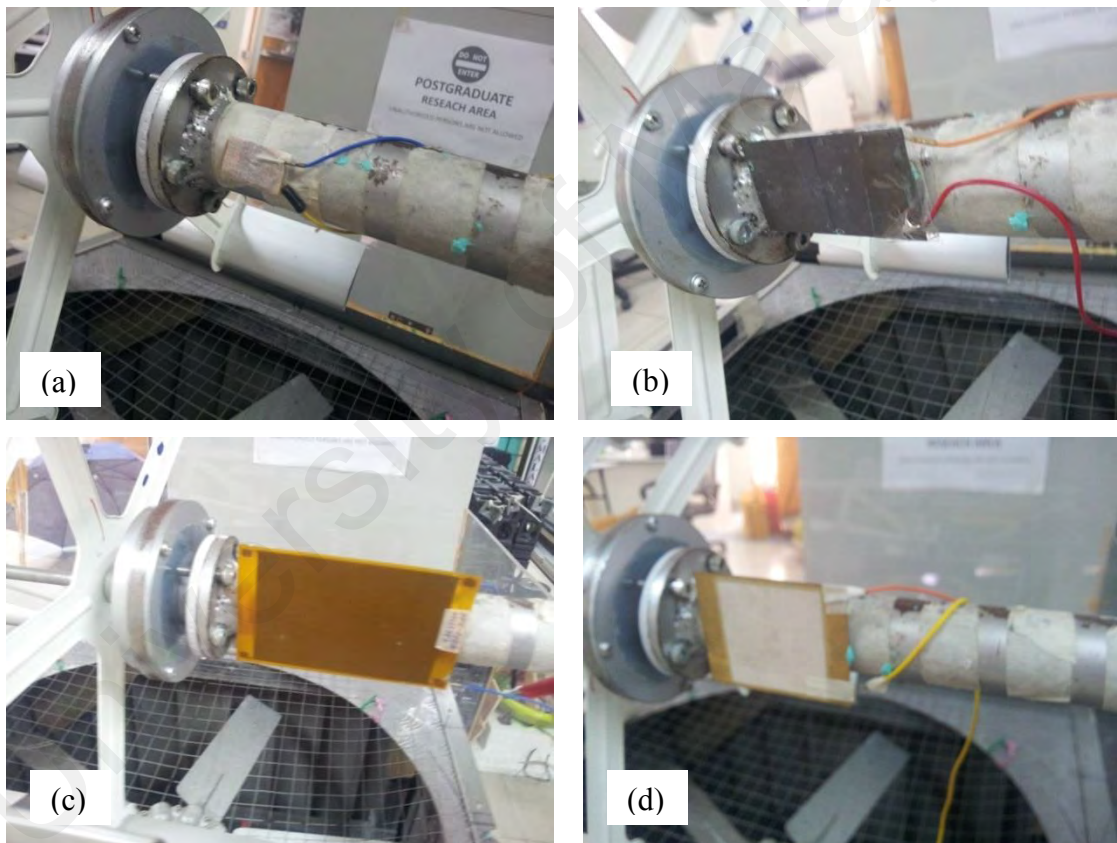


Figure 3.17 : Energy Harvesting of the VAWT: (a) PZnT-NT, (b) PZT, (c) MFC, (d) PZT Bimorph

The performance was compared based on the generated power and power density of numerous commercial harvesters such as PZT, PZT bimorph and MFC.

3.6 Cost Analysis

This research aimed to fabricate a new harvester, with ease of fabrication and also being cost effective to be fabricated locally. First of all, cost benefit will be calculated based on the provided cost by the supplied companies. Accordingly, the details of the purchased raw materials and its electrodes materials strip that are required to fabricate the PZnT-NT are given in Appendix F.1 and F.2. Additionally, the details of the purchased commercial harvesters are given in Appendix F.3 and F.4, represented by the supplied piezoelectric harvester' bills. The commercial piezoelectric harvesters PZT types, sizes, and costs are given in Table 3.3. From Table 3.3, it shows that the PZnT-NT has the lowest prices followed by the PZT Bimorph, PZT and MFC. Later, the power generation performance of the harvester will be investigated throughout this study and the cost effectiveness of each harvester will be compared by considering the power harvesting performance and its price. The result will be reported in section 4.10.

Table 3.3: Piezoelectric Harvesters' Prices Excluding the Tax and Shipping

Harvester Name	Part Number	Size (mm ³)	Price (1 piece)
PZT (Systems, 2015)	Quick-Mount, -503 (T215-H4-503)	1029.8 (63.5 × 31.8 × 0.51)	\$217
MFC (Smart Material,2015)	M 8557 P2	1527.6 (80 × 57 × 0.33)	\$ 280
PZT harvester transducer (PZT Electronic Ceramic Co., 2018)	PZT Bimorph	2450 (70 × 50 × 0.7)	\$20
Current Work	PZnT-NT	300 (20 × 15 × 1)	\$1.5

CHAPTER 4: RESULTS AND DISCUSSIONS

4.1 Introduction

In the first portion of this research, the $\text{PbZnTiO}_3\text{-Na}_2\text{TiO}_3$ generator was characterised based on the study of the material permittivity and the conductivity effect was studied and provided in a comparison frame with pure PbZnTiO_3 . Following this, the performance of the fabricated harvester was tested over a cantilever test rig; and thus, the voltage, power, current, and power density were determined via rectifying the generated AC signal. A full wave rectifier circuit was designed for converting the AC to DC signal, and the rectifier circuit has been provided by the capacitor for storing the energy. The power density was measured after connecting a resistive load across the storage capacitor where the capacitor assists in reducing the DC voltage variant or reducing the DC voltage ripple. Furthermore, the performance of the PZnT-NT harvester was examined by comparing the power density of PZnT-NT with other commercial harvesters.

The second portion of this research has focused on estimating the optimal location over the test rig. The dynamic characteristics (i.e. the natural frequency, damping ratio and mode shape) of the test rig were obtained. A Single-Input/Multi-Output (SIMO) approach was implemented on the test rig. In fact, when the piezoelectric harvester was placed on the cantilever, the harvested voltage varied at distinct locations where this variation could be explained by the vibration mode shape and ODS. Finally, the location selection scheme was implemented in a real environment, the vibration mode shape and vibration pattern were detected in the VAWT, and the overall deflection was measured in three orthogonal directions.

For optimising the acquired data and reducing measurement time, the multi-reference testing (response reference DOF) was implemented with simultaneous measurement tool (triaxial accelerometer). The SIMO approach was performed on the VAWT beam hence, different modes deflect in different orthogonal directions (three reference DOFs)

(Herlufsen, 2004). Roving impact hammer test was conducted where the obtained mode shapes were determined for 27 FRFs measurements.

The third portion of the research has focused on the fabricated harvester on its optimal location on the VAWT. The PZnT-NT harvester was coupled with an AC-DC rectifier circuit, and the signal was stored in the capacitor then the resistance load was connected in parallel to the capacitor for measuring the power consumption of the circuit. Also, the generated AC voltage was measured when the harvester placed on the free and the clamped end of the VAWT. Furthermore, the generated AC signal of the PZnT-NT was presented under different excitation sources type (i.e. shaker, VAWT and finger pressing).

4.2 Characterisation of PZnT-NT Harvester

Herein the crystallographic detail of the PZnT-NT raw material was presented, the $\text{PbZn}_{0.3}\text{Ti}_{0.7}\text{O}_3$ comprises two crystalline phase, i.e. Tetragonal and Hexagonal with space group P4mm and P63mc respectively. The Tetragonal crystal lattice is a (Å) 3.9, b (Å) 3.9, and c (Å) 4.0, and the lattice angles (Alpha= Beta=Gamma) are 90° . Hexagonal crystal lattice is a (Å) 3.2, b (Å) 3.2, and c (Å) 5.2 and the lattice angles (Alpha = Beta \neq Gamma) are 90° , 90° and 120° respectively. In fact, the Hexagonal crystal lattice comes from the presence of zinc oxide. The crystal system of Na_2TiO_3 is Tetragonal and the space group is I41/mad. The crystal lattice is a (Å) 3.7, b (Å) 3.7, and c (Å) 9.5, and the lattice angles (Alpha= Beta=Gamma) are 90° , as shown in Figure 4.1.

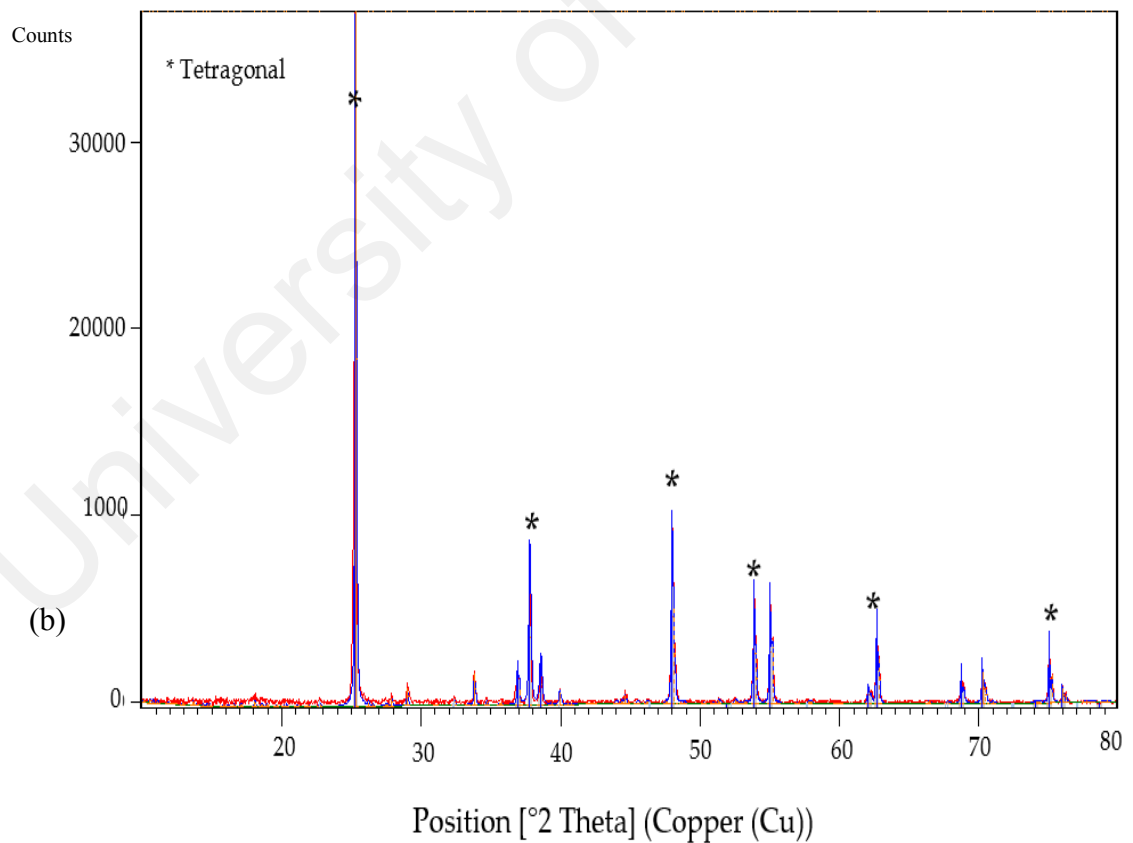
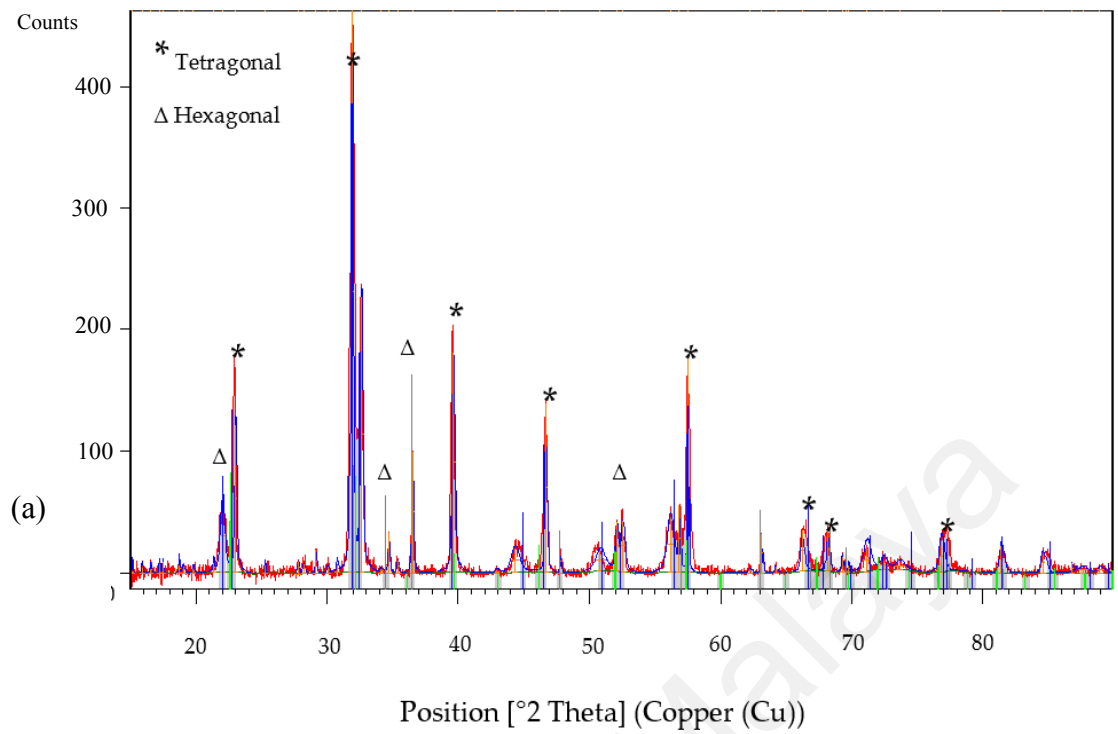


Figure 4.1: XRD Patterns of $0.7\text{PbZn}_{0.3}\text{Ti}_{0.7}\text{O}_3 - 0.3\text{Na}_2\text{TiO}_3$: (a) $\text{PbZn}_{0.3}\text{Ti}_{0.7}\text{O}_3$, (b) Na_2TiO_3 .

The FESEM microscope image demonstrates the fabricated $0.7\text{PbZn}_{0.3}\text{Ti}_{0.7}\text{O}_3-0.3\text{Na}_2\text{TiO}_3$ where the system consists of $\text{PbZn}_{0.3}\text{Ti}_{0.7}\text{O}_3$ and sodium titanate nano-sheets, as illustrated in Figure 4.2. The particles size-measurement evidence is given in Appendix C. Particles size was estimated by using Image J software.

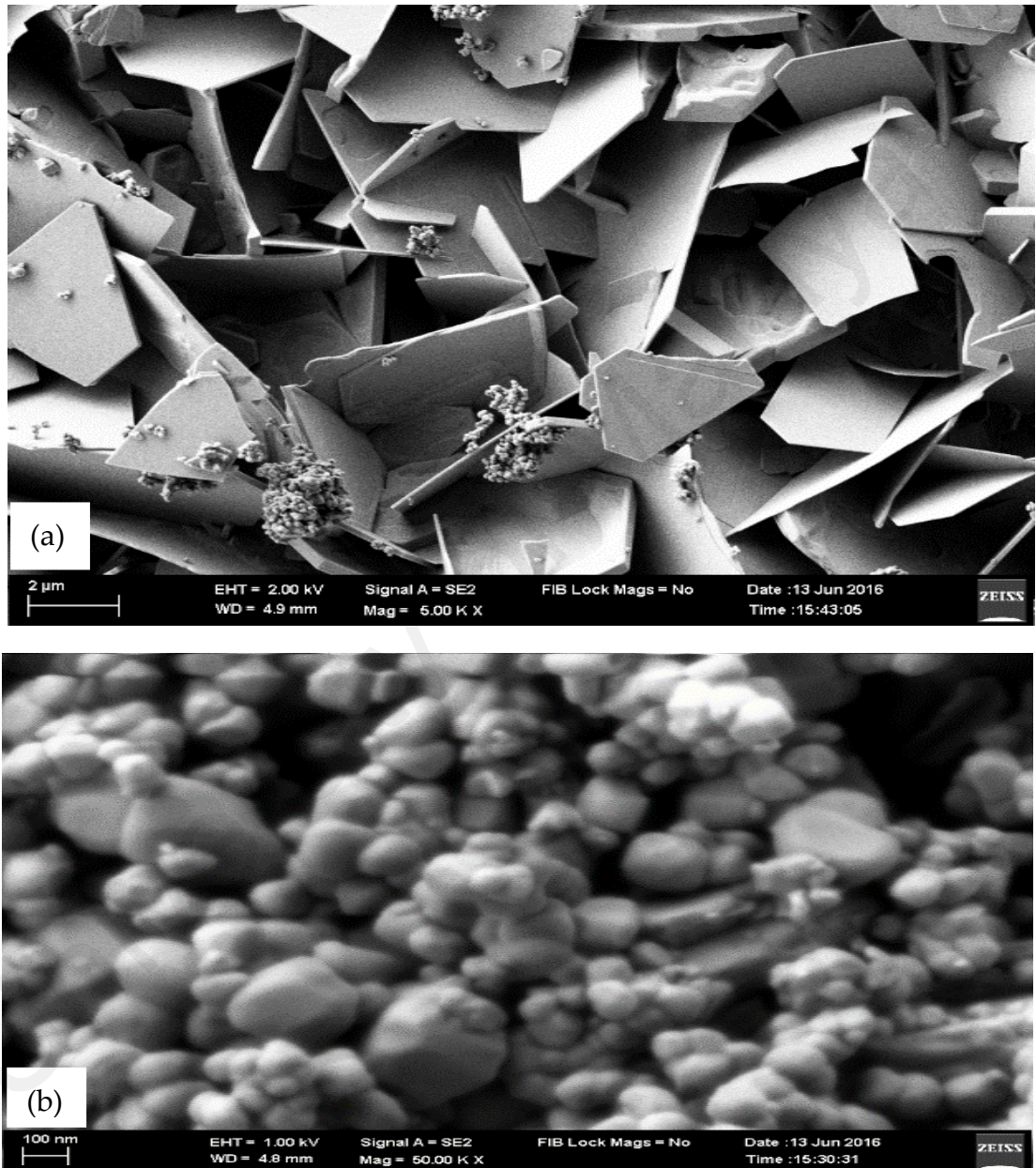


Figure 4.2: Surface Characteristics of: (a) Sodium Titanate (Na_2TiO_3) Sheets, (b) $\text{PbZn}_{0.3}\text{Ti}_{0.7}\text{O}_3$ Particles

The PZnT-NT was compacted between two electrodes where the electric dipoles will be induced by Zn electrode (Cathode) and the Cu electrode (Anode). The arrangement of the harvester layout is illustrated in Figure 4.3.

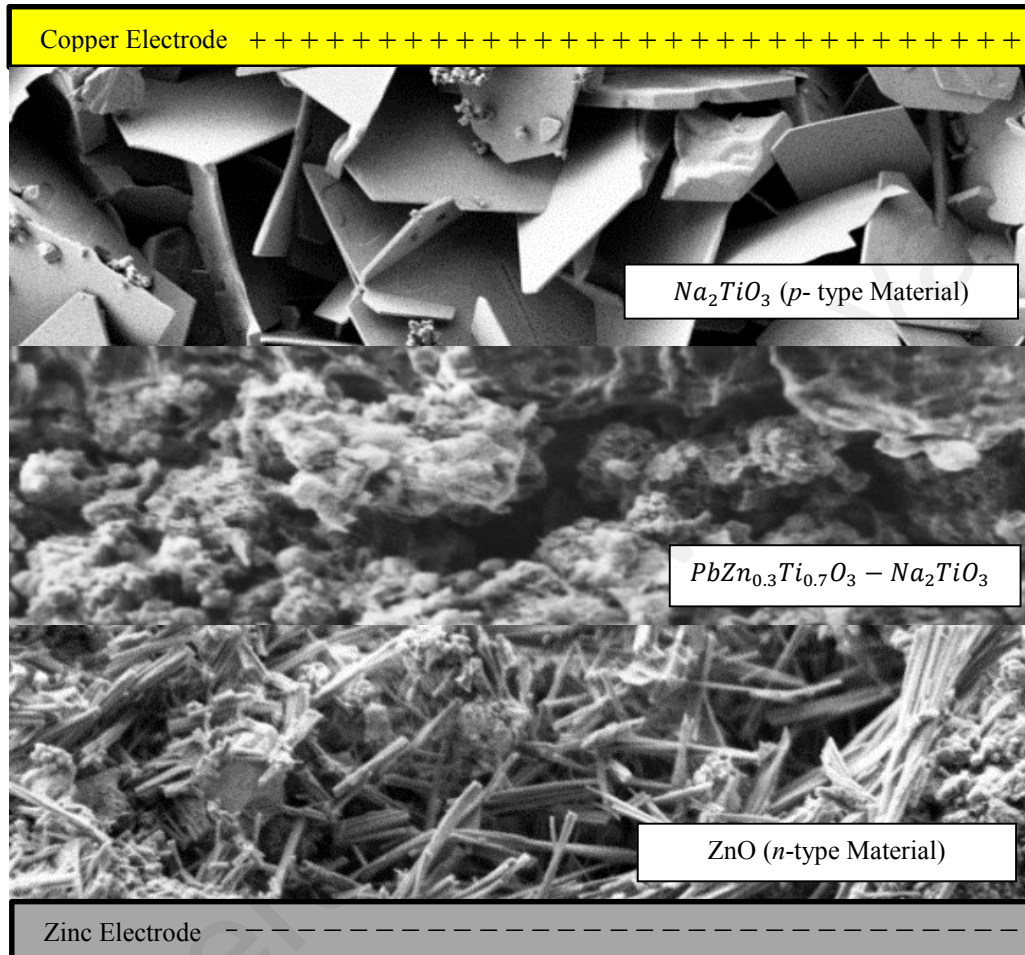


Figure 4.3: FESEM PZnT-NT Layouts

Zinc oxide nanofiber (i.e. *n*- type layer) was grown over the zinc electrode where the Na_2TiO_3 was constructed in the copper to construct a *p*-type layer. Applying vertically and periodic compressive load (i.e. pressing) will be result of obtaining an AC signal where the dipoles of the PZnT-NT will be oriented and accumulated nearby the zinc and copper electrodes. Accordingly, a positive AC- signal will be derived as illustrated in the Figures 4.4 (a) and (c). If a continuous compressive load is given, it will result in a step function (i.e. DC voltage) as shown in Figure 4.4 (c), due to the continuous orientation

and flow of the dipoles. Upon the releasing of the applied force, inverse signal will be constructed due to the reorientation of the dipoles, which results in a negative peak voltage as illustrated in Figures 4.4 (b) and (d). For a continuous pressing and releasing movement, the orientation and reorientation of the dipoles will cause collision between electrons and atoms, therefore causing energy dissipation in term of heat and friction. This dissipated energy is known as loss tangent (which indicates the mobility of dipoles).

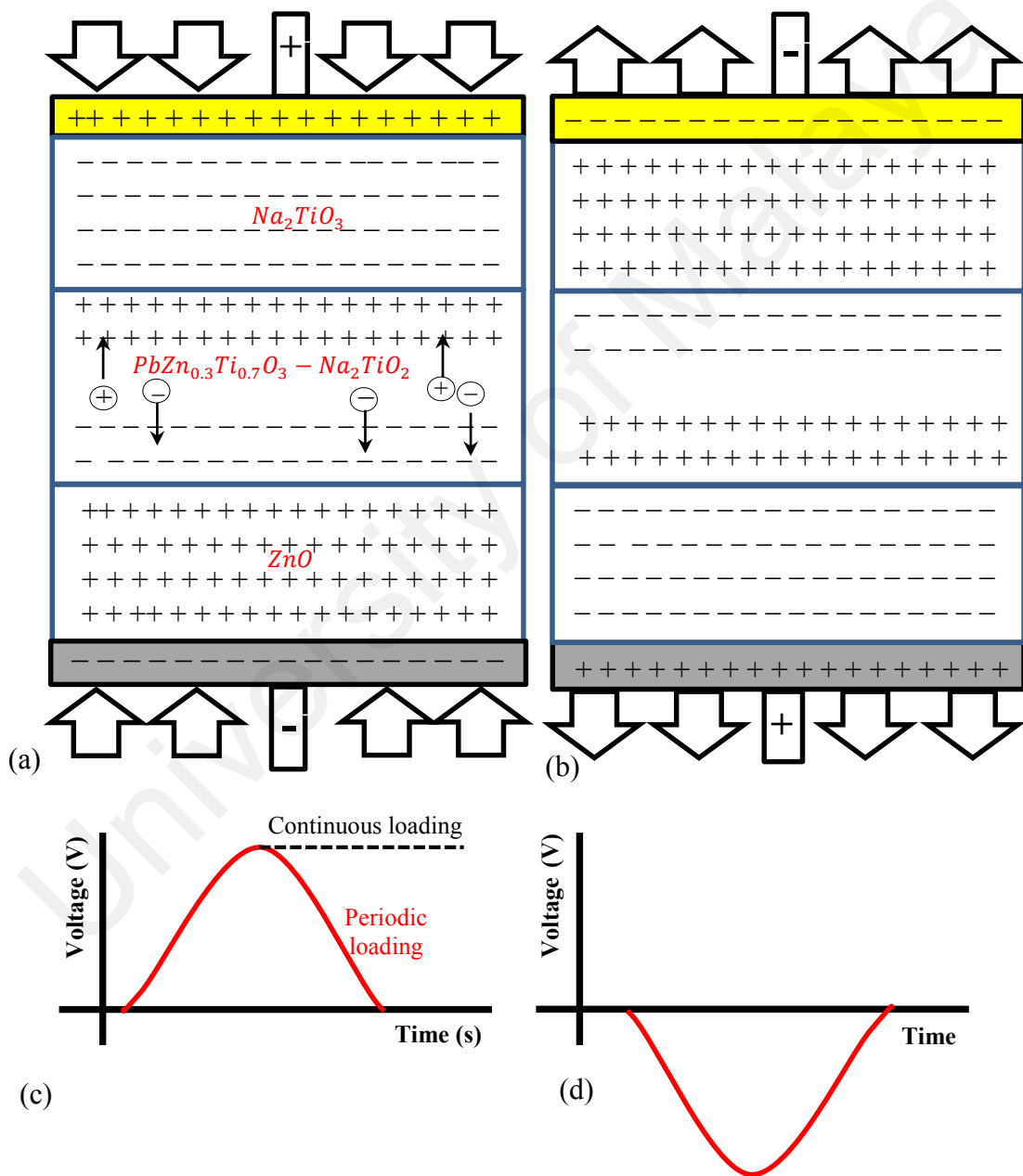


Figure 4.4: PZnT-NT Layouts during (a) Pressing & (b) Releasing Movements, and Its (c) Generated Voltage under Pressing & (d) Generated Voltage after Releasing

Permittivity of material is an important property of the dielectric materials where the permittivity represents the ratio between the charge density of material to the charge in the vacuum. In other words, if the material has a large number of dipoles (charges) that move freely, and then accumulate at the positive and negative terminals (i.e. electrodes), the material in this case has a high permittivity (i.e. high storage charge under an electric field). Thus, it is important to measure the permittivity of PZnT-NT to measure the ability of the PZnT-NT to polarise under electric field. In order to increase the permittivity, the conductivity of material should be increased to facilitate the dipoles motion (Callister & Rethwisch, 2000).

The piezoelectric dielectric constant was characterised by using an impedance analyser from 4 Hz to 110 MHz, where PZnT-NT demonstrated a high dielectric constant. Figure 4.5 (a) presents the variation between PZnT-NT and the pure $\text{PbZn}_{0.3}\text{Ti}_{0.7}\text{O}_3$. Indeed, sodium titanate has the essential role of increasing the conductivity between composite particles. High variation in relative permittivity between the PZnT-NT and the pure $\text{PbZn}_{0.3}\text{Ti}_{0.7}\text{O}_3$ was observed below the frequency of 5 kHz, where the permittivity of PZnT-NT decreases intensely with the increasing of the frequency.

The PZnT-NT yielded a high loss tangent of 3.84 at frequency of 1 kHz, while the pure $\text{PbZn}_{0.3}\text{Ti}_{0.7}\text{O}_3$ produced very low loss tangent (i.e. 0.122) due to both stored energy and dissipated energy were low. The maximum loss tangent was 4.89 at frequency of 5.5 kHz, where below this level the storage energy was higher than the dissipated energy. This fact is illustrated in Figure 4.5(b). By increasing the conductivity through doping the *n*-type or *p*-type material to a pure piezoelectric material, it is expected that the loss tangent can be improved as illustrated in Eq. (2.8), and hence *p-n* junction technology can improve the power generation ability of the enhanced piezoelectric harvesters (Yin et al., 2015), compared with other pure piezoelectric materials.

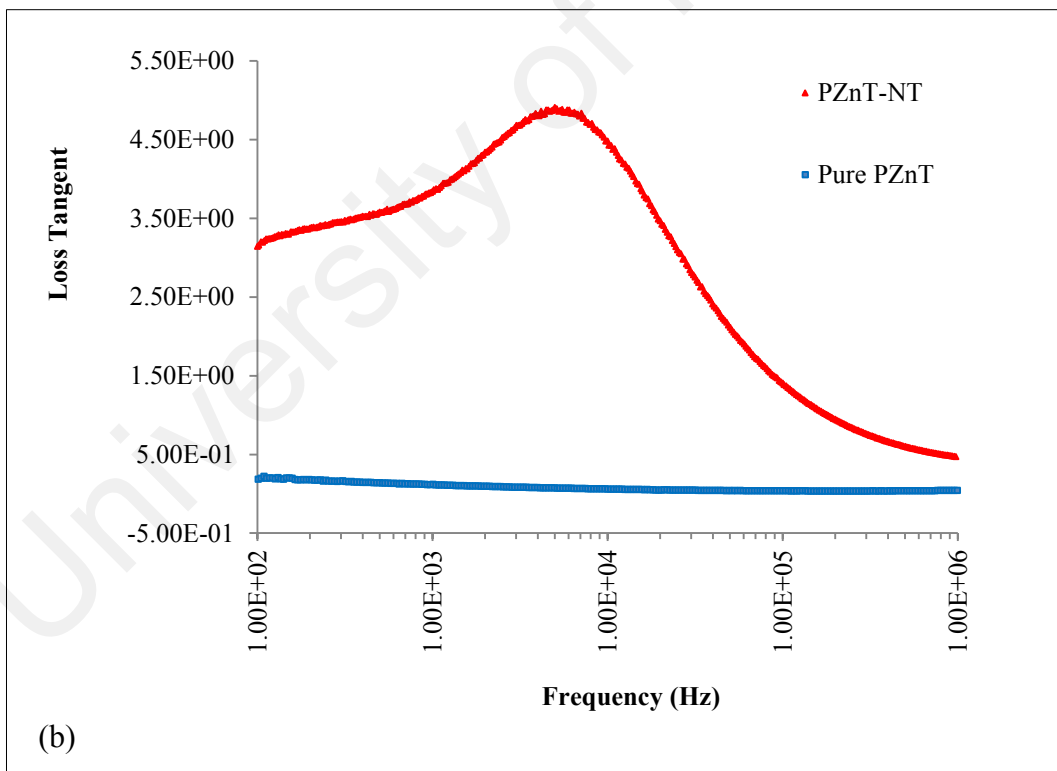
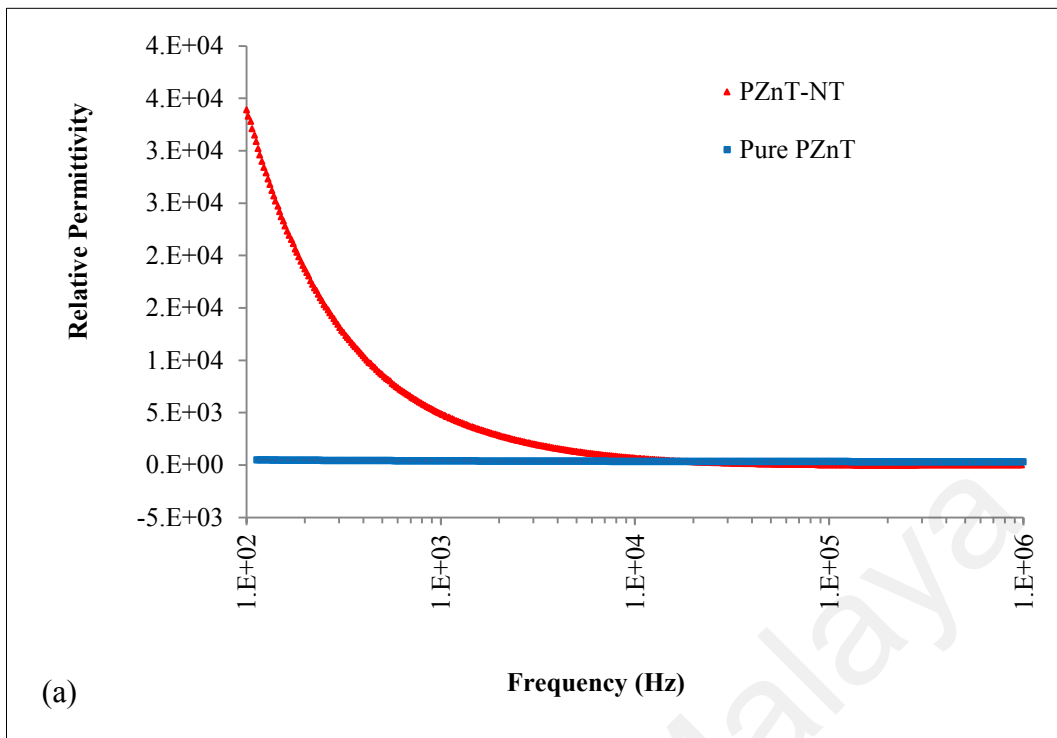


Figure 4.5: (a) The Dielectric Properties, (b) Loss Tangent of PZnT-NT

Conductivity of PZnT-NT and pure $\text{PbZn}_{0.3}\text{Ti}_{0.7}\text{O}_3$ are provided in Figure 4.6. It was observed that the conductivity increased by adding the Na_2TiO_3 material. The material had high dissipation of energy, due to the damping of the dipole moment and the influence of the conductive filler. The electrical conductivity (σ_e) of the PZnT-NT, the pure $\text{PbZn}_{0.3}\text{Ti}_{0.7}\text{O}_3$ and the raw Na_2TiO_3 (Zero% PZnT) are 3.76×10^{-4} S/m, 2.88×10^{-6} S/m and 1.15×10^{-3} S/m respectively, under room temperature and frequency of 1 kHz.

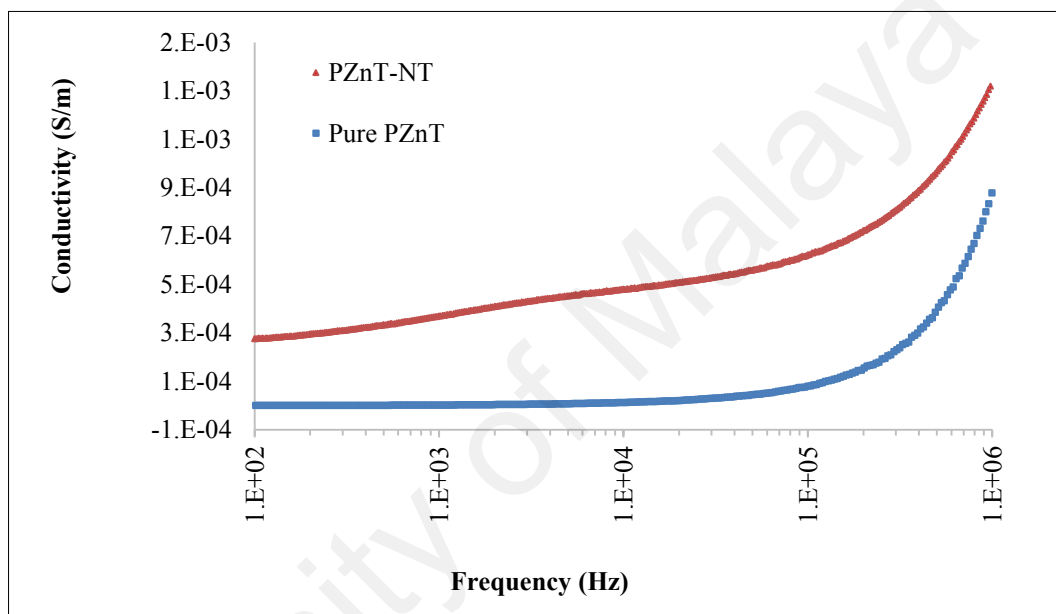


Figure 4.6: Conductivity of the PZnT-NT & Pure PZnT at Room Temperature

Figure 4.7 illustrated the hysteresis loops of the $\text{PbZn}_{0.3}\text{Ti}_{0.7}\text{O}_3$ that was sintered at 850°C . It was observed that the material exhibited a ferroelectric behaviour. The $\text{PbZn}_{0.3}\text{Ti}_{0.7}\text{O}_3$ produced a low remnant polarisation (P_r) of $1.09 \mu\text{C}/\text{cm}^2$ and maximum electric field of $47.09 \text{ kV}/\text{cm}$, the coercive was $8.4 \text{ kV}/\text{cm}$. It is worthwhile to mention that in recent advance, the remnant polarisation of ferroelectric materials could be reached up to $62 \mu\text{C}/\text{cm}^2$ of the piezoelectric ferroelectric (Amorin et al., 2012). As a consequence, the low remnant polarisation is an indicator of the low response of the $\text{PbZn}_{0.3}\text{Ti}_{0.7}\text{O}_3$ and the shifting forward quenches the polarity can lead to enhance the performance.

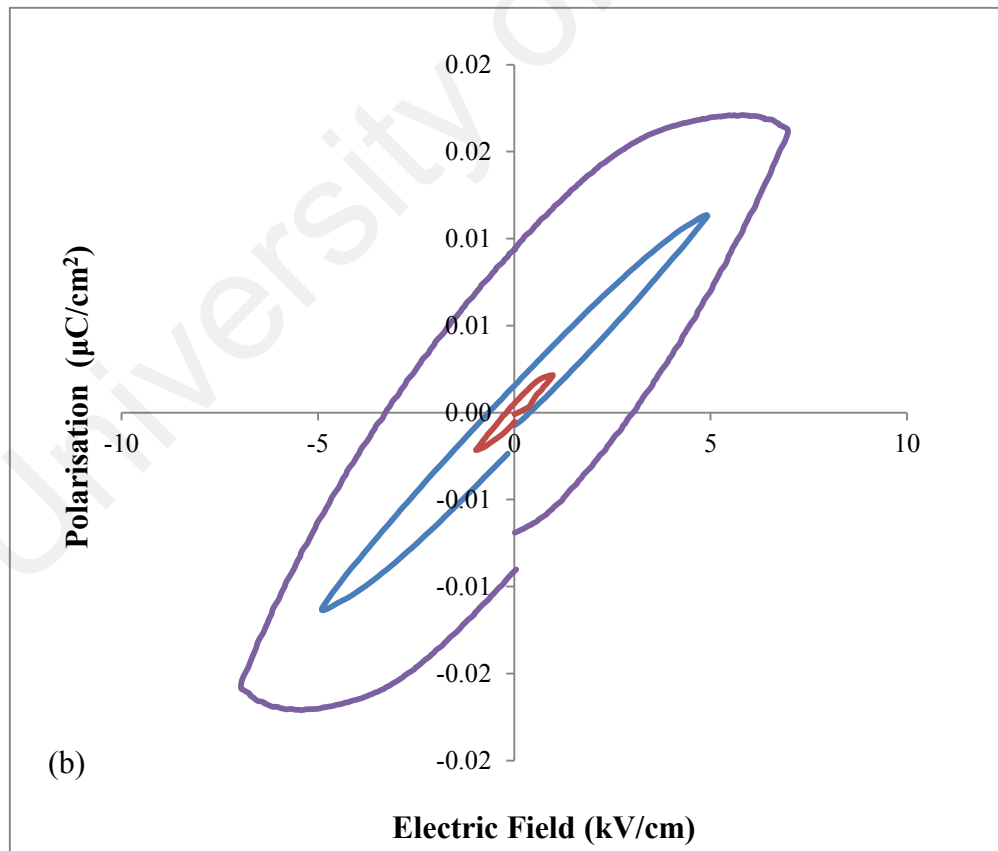
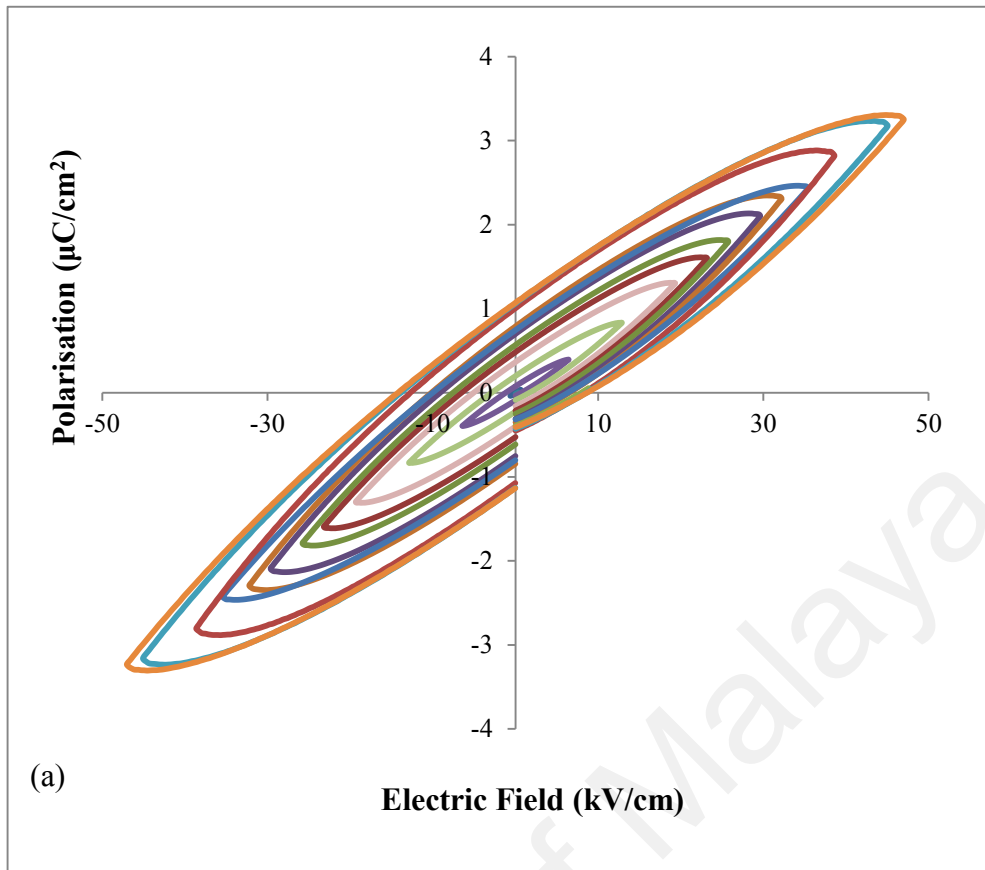


Figure 4.7: Hysteresis Loop of: (a) Pure $\text{PbZn}_{0.3}\text{Ti}_{0.7}\text{O}_3$, (b) $0.9\text{PbZn}_{0.3}\text{Ti}_{0.7}\text{O}_3-0.1\text{Na}_2\text{TiO}_3$ Versus Various Applied Electric Fields

In this study, the hysteresis loop of $0.7\text{PbZn}_{0.3}\text{Ti}_{0.7}\text{O}_3-0.3\text{Na}_2\text{TiO}_3$ was unable to obtain under high voltage up to 1 kV/cm due to the conductivity. Thus, the reduction of the percentage of the conductive filler (i.e. performs hysteresis loop test for $0.9\text{PbZn}_{0.3}\text{Ti}_{0.7}\text{O}_3-0.1\text{Na}_2\text{TiO}_3$ material instead of $0.7\text{PbZn}_{0.3}\text{Ti}_{0.7}\text{O}_3-0.3\text{Na}_2\text{TiO}_3$ material) was implemented.

The recorded results of the poled $0.9\text{PbZn}_{0.3}\text{Ti}_{0.7}\text{O}_3-0.1\text{Na}_2\text{TiO}_3$ showed reduction of the ferroelectric property, the remnant polarisation, the maximum electric field and the coercive field were $0.009 \mu\text{C}/\text{cm}^2$, 7 kV/cm and 3.065 kV/cm respectively. In overall, results showed that dielectric property (relative permittivity) of the proposed PZnT-NT generator can be enhanced by adding conductive filler material. This will eventually enhance the generated power density.

4.3 The Performance of PZnT-NT Device

In the initial investigation, the ability of the proposed harvester to power LEDs (5 mm) at frequencies up to 10 Hz was an indicator of the optimised performance that was realised under such low frequency and acceleration rates. The illuminated LEDs is illustrated in Figure 4.8. In this study, all the harvesters (PZnT-NT, PZT bimorph and MFC) were examined under the excitation frequency of 30 Hz and acceleration response of 0.4 m/s^2 .

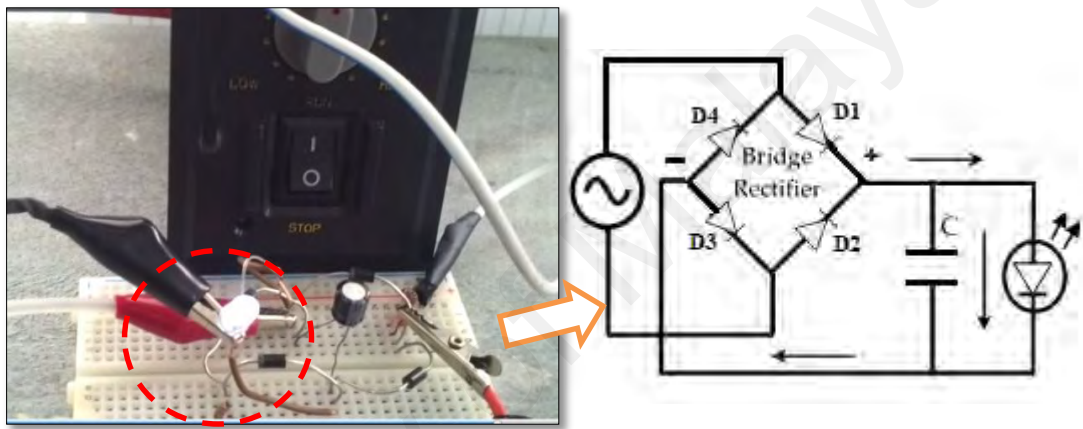


Figure 4.8: Flashing up LED (5mm)

The comparison of the harvesters' performances such as voltage generation, current and power density was reported. The voltage was recorded across a range of resistances between $1.9 \text{ k}\Omega$ and $5.2 \text{ M}\Omega$.

To analysis the measurement errors and detect the deviation ranges that caused by the fluctuation of device measurements, the voltage averages were calculated for four experimental results and the standard deviation as well as the relative uncertainty were determined. The relative uncertainty is the percentage ratio between the absolute error of measurement and the measured value, where it represents the size of measurement error. In practice, a measurement error with less than 15% relative error indicates a reliable and good measurement. The performance of the PZnT-NT was compared with PZT, MFC

and PZT bimorphs, and the results show an outstanding performance of the PZnT-NT despite its insignificant size. There were increased in the voltage (V) with the increasing of resistance (R_L). Furthermore, it was found that the PZnT-NT and PZT generated the highest voltage of 4.623 ± 0.164 V and 4.993 ± 0.251 V at load resistance of 2900 k Ω and 5200 k Ω respectively. Also, the highest voltage of MFC and PZT bimorph were 3.023 ± 0.167 V and 3.182 ± 0.169 V respectively, at load resistance of 2900 k Ω . This fact is illustrated in Figure 4.9.

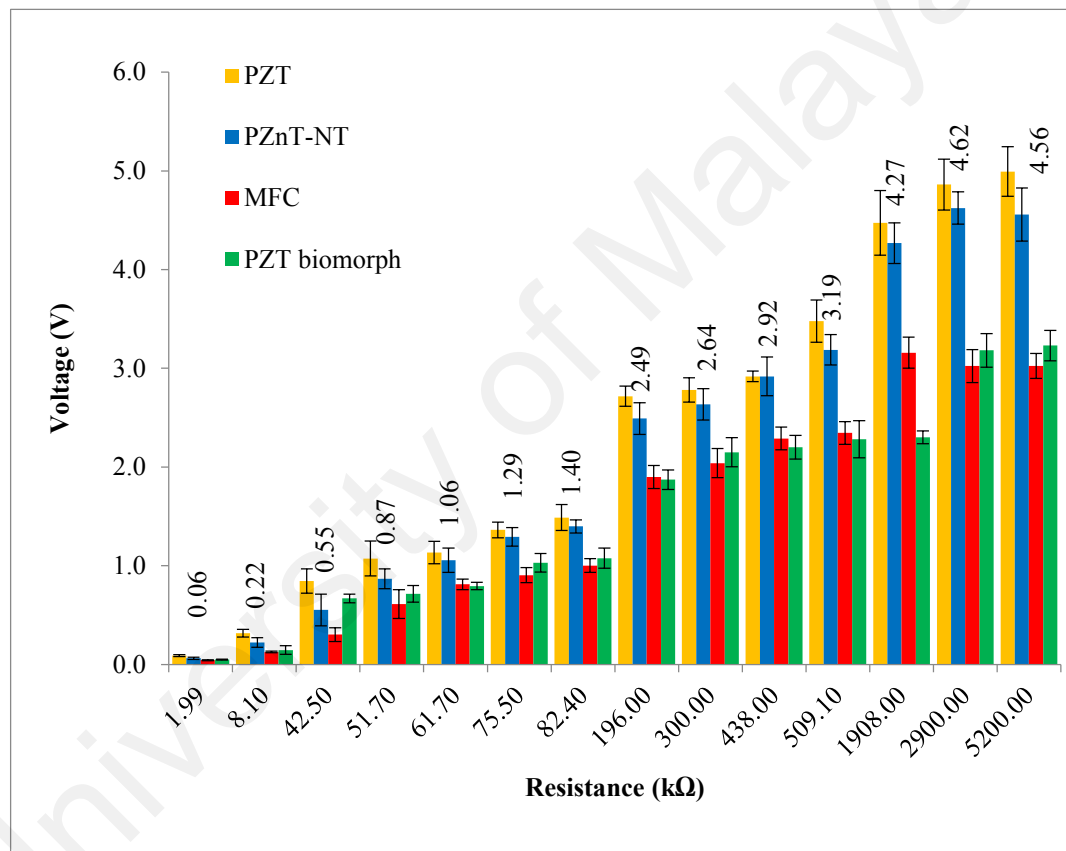


Figure 4.9: The Generated Voltage at Frequency 30 Hz of Various Harvesters

The measured relative uncertainty of PZnT-NT, PZT, MFC, and PZT bimorph were 4%, 6 %, 5 %, and 5% respectively. The sizes of errors were within 15% comparing with the measured voltages, thus the comparison of their results is valid and reliable. The voltage generation of the PZT is the highest because it is a ceramic with ferroelectric property that has superior electromechanical properties. This means it could generate high

voltage by small deflection or acceleration. The MFC and PZT bimorph have comparable electromechanical property, but lower performance than PZT as reported in Table 3.1, therefore they provide lower voltage than PZT. It is worthwhile to mention that MFC has very low stiffness (i.e. high flexibility) and PZT bimorph has high stiffness, while PZT has moderate stiffness. In this study, PZnT-NT shows great and comparable DC voltage generation, compared to the PZT. This is due to the enhancement of the electromechanical property of its non-ferroelectric property through the material conductivity improvement as demonstrated in section 4.2.

The increasing of conductivity assists of improving the electromechanical properties of PZnT-NT where the energy gap of the material will be reduced, and the electrons will have sufficient energy to jump from the valance band to the conduction band. Basically, the conductivity has direct proportion with the current density (i.e. $J = \sigma E$) where σ is the conductivity and E is the electric field (Callister, 2001). It was observed that the zinc-oxide nanofiber was grown above the zinc electrode which caused of constructing *n*-type layer (i.e. the electrons is the majority carriers). Furthermore, the formatted sheets layer that connected to the Cu electrode was the Na₂TiO₃ sheets layer. The Na₂TiO₃ represent the *p*-type layer (i.e. the holes are the majority carriers). The PZnT-NT would induce electrons flow from Zn electrode to the Cu electrode. Applying vertical compressive force would result of obtaining direct current (DC) output signal.

Consequently, the dissipated power was recorded across the full wave of the rectifying circuit; the maximum power was verified when a circuit load matched the impedance of the transducer. At the optimal load and steady state conditions, the stored energy of the capacitor that was supplied by PZnT-NT, PZT, MFC and PZT bimorphs was 0.34 mJ, 0.378mJ, 0.139 mJ, and 0.065 mJ respectively. The optimal power of the PZnT-NT was verified at the load resistance of 196.2 k Ω , where the maximum power was obtained at 0.032 ± 0.003 mW. The optimal power of the PZT, MFC and PZT bimorphs were 0.0353

± 0.003 mW, 0.018 ± 0.002 mW and 0.018 ± 0.002 mW respectively, corresponding to the load resistance of 196.2 k Ω . The relative uncertainties of power measurement values were 10%, 12%, 11%, and & 8% respectively. The comparison of power generation is illustrated in Figure 4.10 and the calculated power based on Eq. 2.10 are given in Appendix D.1. The variations between the current density for PZnT-NT, PZT, MFC and PZT bimorphs are illustrated in Figure 4.11 (a) where the calculated current density based on $I=V/AR$ is given in Appendix D.3.

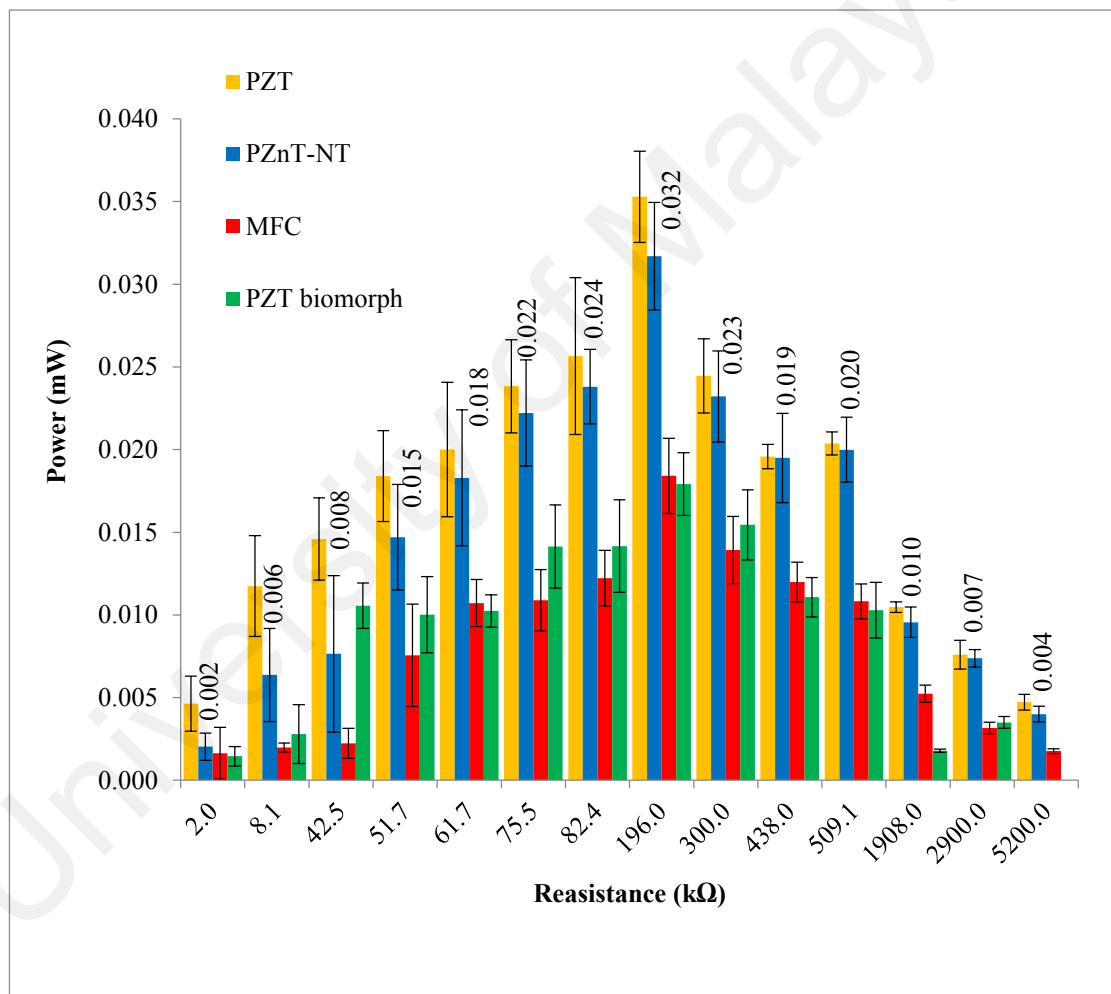


Figure 4.10: The Optimal Power Output of Various Harvesters

The maximum currents density of the PZnT-NT, PZT, MFC and PZT bimorphs were recorded at 10.499 ± 1.034 $\mu\text{A}/\text{cm}^2$, 4.559 ± 0.442 $\mu\text{A}/\text{cm}^2$, 1.423 ± 0.176 $\mu\text{A}/\text{cm}^2$ and 1.018 ± 0.080 $\mu\text{A}/\text{cm}^2$, respectively. The relative uncertainties were 10%, 10%, 12%, and

8% respectively. By considering the harvester's size, the power densities of various types of harvesters as shown in Figure 4.11(b). The results affirmed that the PZnT-NT harvester produced the highest power density (i.e. $0.106 \pm 0.011 \mu\text{W}/\text{mm}^3$), whereas the power density of the PZT was $0.039 \pm 0.003 \mu\text{W}/\text{mm}^3$. For the MFC and PZT bimorph the power densities were $0.012 \pm 0.001 \mu\text{W}/\text{mm}^3$ and $0.007 \pm 0.001 \mu\text{W}/\text{mm}^3$ respectively. Their relative uncertainties were 10%, 12%, 11%, and 6% respectively and the detail can be found in Appendix D1 and D.2.

University of Malaya

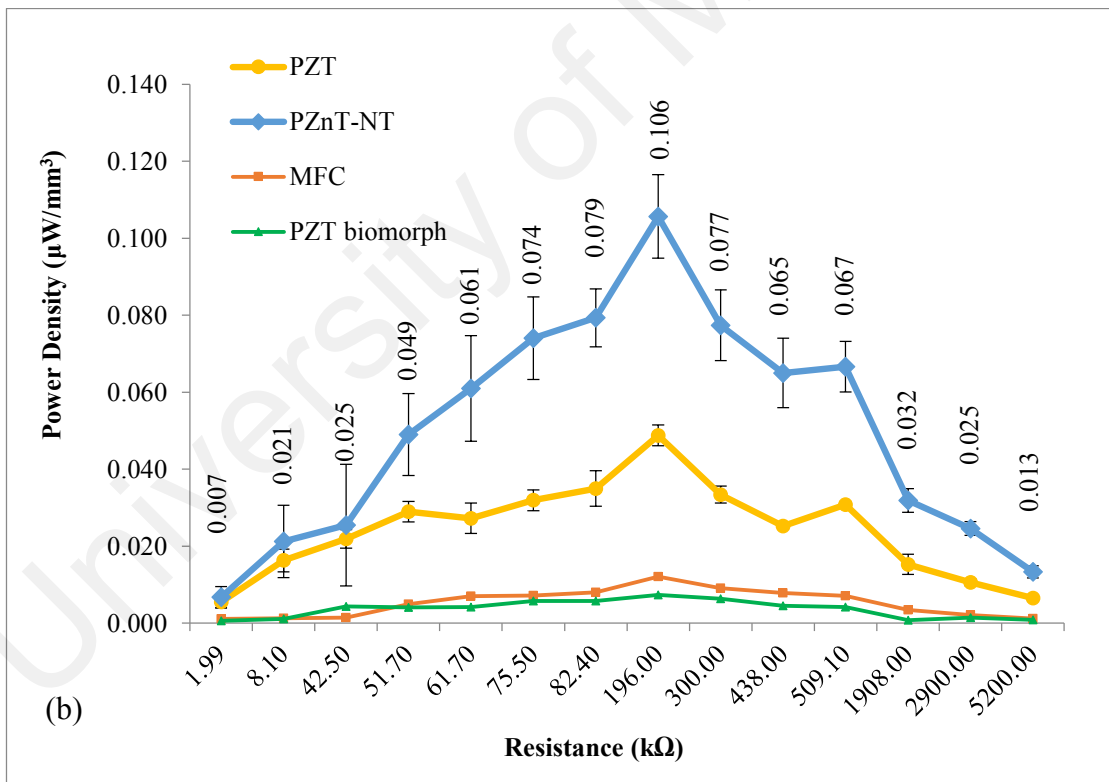
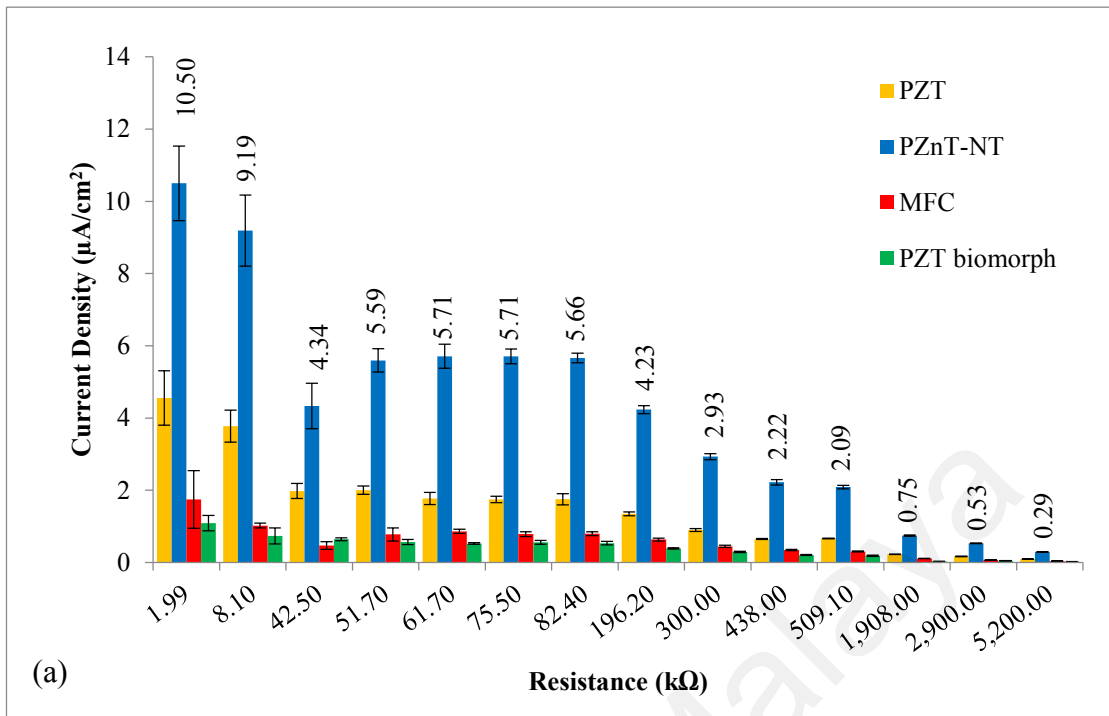


Figure 4.11: (a) Current Density and, (b) Power Density of Piezoelectric Devices versus Resistance

In general, the harvested energy level varies excessively from microwatts (μW) to milliwatts (mW); this is depending upon several factors, such as piezoelectric type, design of piezoelectric elements, mechanical properties, dynamic properties, electrical circuit, mechanical force, excitation frequency, vibration response, etc. This study focused on the design of piezoelectric element, which was attached to a cantilever system under low excitation frequency and low acceleration environments. The performance of the proposed harvester was compared to the results of existing research works which implemented their harvesters in a cantilever system under similar range of excitation frequency and acceleration. The existing research works (Berdy et al., 2012; P. Cornwell et al., 2005; Do, Jung, Kang, Kang, & Yoon, 2013; Leland, Lai, & Wright, 2004; H. Liu, Tay, Quan, Kobayashi, & Lee, 2011; Peigney & Siegert, 2013; Roundy, Wright, & Rabaey, 2003; S. Zhang, Yan, Luo, Miao, & Xu, 2015) produced volume power density of $[0.9\text{E-}2, 20\text{E-}2] \mu\text{W}/\text{mm}^3$ under the excitation frequency of $[1.4, 100]$ Hz and the acceleration of $[0.2, 10] \text{m}/\text{s}^2$.

The current work produced a power density of $0.106 \pm 0.011 \mu\text{W}/\text{mm}^3$ at frequency and acceleration of 30 Hz and $0.4 \text{m}/\text{s}^2$ respectively, compared with other studies as recorded in Table 4.1, the PZnT-NT showed high power density under low excitations. It is worthwhile to mention that various figures of merit such as AC voltage (open circuit without resistance), DC voltage (open circuit with resistance), current (short circuit without resistance), volume power density or surface power density were reported in the previous literature. So far there is no standard in selecting the figures of merit in the best knowledge of the authors. This makes the comparison difficult as most prior studies may not describe the kinematic parameters or use various figures of merit to present the harvester performance efficiency. To give a general overview of the harvester performance, the comparison with other existing generators using the surface power density is made in Table 4.2. The existing research works produced surface power density

of [0.0006, 303] $\mu\text{W}/\text{mm}^2$ under the excitation frequency of [0.5, 30] Hz and the acceleration of [0.4, 1.8] m/s^2 .

Moreover, the maximum open circuit DC voltage across the resistance as shown in Appendix D.1 of the PZnT-NT was measured 5.27 V, whereas the DC current density (short circuit) was calculated as 256.4 $\mu\text{A}/\text{cm}^2$. The current and the standard deviation was calculated in Appendix D.3

The current work produced a surface power density of 10.6 $\mu\text{W}/\text{cm}^2$ at frequency and acceleration of 30 Hz and 0.4 m/s^2 respectively, which showed good progress toward building self-powered generators.

University of Malaya

Table 4.1: Comparison of Volume Power Density Based on Low Acceleration and Frequency

Ref.	Active Material	Harvesting Technique	Active Volume (mm ³)	Acceleration (m/s ²)	Frequency (Hz)	Volume Power Density ($\mu\text{W}/\text{mm}^3$)
(Peigney & Siegert, 2013)	PZT bimorph	Cantilever	7040	0.2	15.0	2.69E-02
(Do et al., 2013)	PbZr _{0.52} Ti _{0.48} O ₃ (PZT) Flexible films	Bending and releasing	0.100	N/A	1.40	8.40E-02
(Leland et al., 2004)	PZT ceramic	Cantilever*	3106	0.5	27.0	9.00E-03
(Zhang et al., 2015)	MFC Flexible film	Cantilever	117.6	N/A	51.9	1.70E-02
(Cornwell et al., 2005)	PZT ceramic	Cantilever*	≈248.0	0.4	38.2	1.80E-01
(Roundy et al., 2003)	PZT ceramic	Cantilever*	N/A	0.5 - 5.0	100	7.00E-02
(Berdy et al., 2012)	PZT ceramic	Cantilever*	588.0	2.0	49.7	2.00E-01
(Liu et al., 2011)	PZT ceramic	Cantilever*	10.10	10.0	47.0	8.55E-02
Current work	PZnT-NT	Cantilever	300.0	0.4	30.0	1.06E-01

I(*) The PZT without cantilever as auxiliary beam

Table 4.2: Comparison of Surface Power Density for Numerous Nanogenerators

Ref.	Materials	Polarisation	Harvesting Technique	Area (cm ²)	Frequency (Hz); Acceleration (m/s ²)	Voltage (open circuit) (V)	Current Density, (short circuit) (μ A/cm ²)	Surface Power density (μ W/cm ²)
(Park et al., 2012)	BaTiO ₃ -PDMS	Ferroelectric	Bending & release	121	N/A	5.50	0.350	1.925
(Park et al., 2010)	BaTiO ₃ -PDMS		Bending & release	0.82	N/A	1.00	0.190	0.190
(Jeong et al., 2015)	PMN-PT & MWCNTs		Stretchable	10	0.5 Hz; 0.817 m/s ²	4.00	0.050	0.200
(Alam et al., 2015)	ZnSnO ₃ /MWCNTs		Pressing by finger	11.1	N/A	40.0*	0.036*	1.080*
(Wu et al., 2012)	PZT-PDMS		Bending	0.12	N/A	6.00*	0.380*	200.000*
(Lee et al., 2016)	PbTiO ₃ nanotubes		Random movement	80×10 ⁻⁶	N/A	0.620	0.001	0.001
(Stassi et al., 2015)	ZnO-PC100		Bending	0.8	N/A	1.15*	125.0*	5.630*
(Lin et al., 2013)	ZnO/PEDOT: PSS		Pressing & release	1.5	N/A	8.00	0.600	4.800
(Lee et al., 2012)	ZnO-PCBM-P3HT		Bending	N/A	N/A	1.45*	3.030*	22.900*
(Briscoe et al., 2013)	ZnO/PEDOT: PSS		Bending	2	1.8 m/s ²	0.154	1.580	0.243
(Sheng Xu et al., 2010)	ZnO / PMMA	Impact	N/A	2 Hz; 1.3 m/s ²	1.26	0.018	0.023	
(Jalali et al., 2013)	ZnO/CuSCN/PEDOT: PSS	N/A	N/A	N/A	0.389	780.0	202.420	
(Current Work)	PZnT-NT	Non-ferroelectric	Cantilever	3	30 Hz; 0.4 m/s ²	5.27*	256.4*	10.000*

*The power density was computed by using DC voltage with optimum resistance as implemented in this study; the value without * indicates that the study computed the power density by multiplying the voltage (open circuit) and current density directly. This approach is not encouraging as reported by Jalali et al. (2013).

4.4 Recharging Battery from PZnT-NT Device

Power harvesting from PZnT-NT was investigated over the cantilever test rig at the excitation of 30 Hz and when the acceleration was in range of 0.4 m/s^2 . The generated power was stored after rectifying the signal using the diodes bridge rectifier circuit and capacitor ($100 \mu\text{F}$). The circuit was connected to the storage system that consisted of a rechargeable ion battery (i.e. capacitance of 40 mAh) equipped with three LED diodes, as illustrated in Figure 4.12. The battery was charged until it reached 2.46 V, where the required charging period was approximately 7 hours. The accumulated voltage over charging time for PZnT-NT, PZT, PZT bimorph and MFC is plotted in the Figure 4.13. Figure 4.13 shows that the accumulated voltage of PZT was the highest followed by PZnT-NT, MFC and PZT bimorph. This is because the PZT produced the highest power output compared to the other harvesters as illustrated in Figure 4.10. The PZnT-NT has better power density than PZT as shown in Figure 4.11, if a greater size of the PZnT-NT was used, the accumulated voltage of the PZnT-NT will be improved.



Figure 4.12: The Storage Battery Circuit with Three LEDs

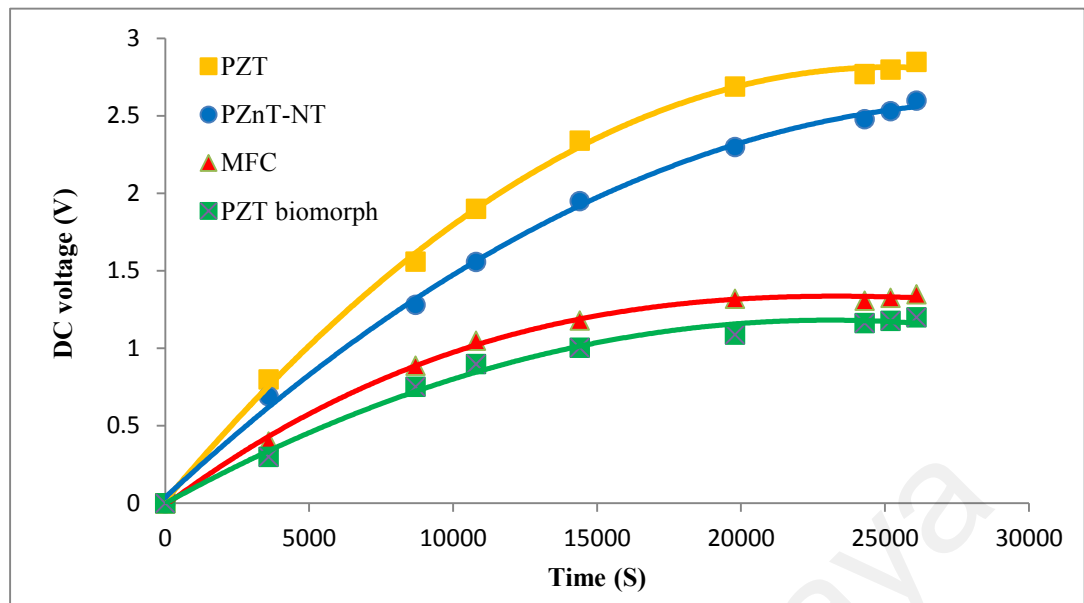


Figure 4.13: Energy Harvesting based on PZnT-NT and Charging Time of Rechargeable Ion-Battery

4.5 The Alternating Generated Voltage of PZnT-NT

The PZnT-NT demonstrates the ability to generate AC voltage when it is subjected to quasi-static (i.e. finger pressing) or excitation of dynamic loads. The recorded AC voltage average at a frequency of 90 Hz was up to $0.22 V_{pk-pk}$. The generated AC voltage signal is illustrated in Figure 4.14 when the PZnT-NT was hosted on the cantilever. It's obvious that the generated voltage increases with the increasing of the applied force and the deflection rate. The piezoelectric generate higher AC voltage when it mounted over the shaker directly, where the voltage was lower when the harvested was compacted to the cantilever beam (very high stiffness), what caused of reducing the deflection rate of the harvester.

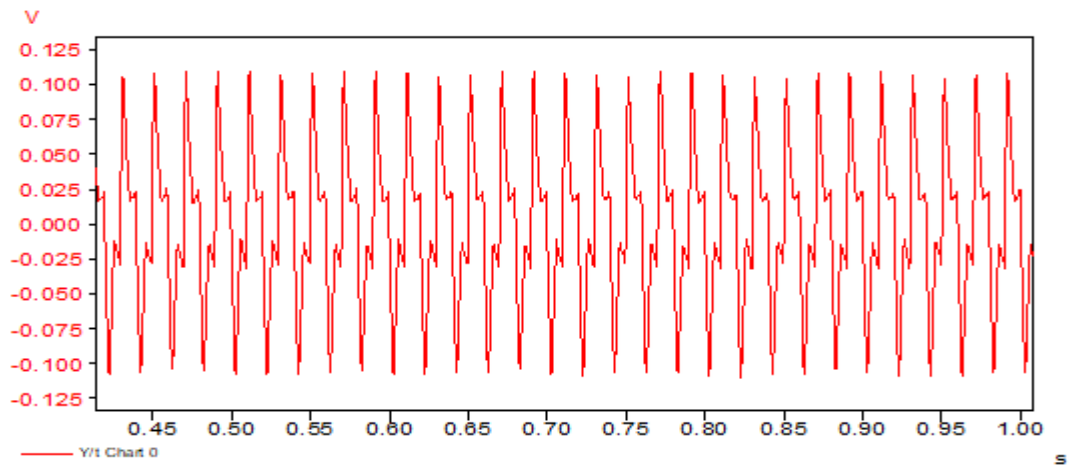


Figure 4.14: Voltage Generated Signal of PZnT-NT Mounted over Cantilever and Excited at Frequency of 90 Hz

Apart from that, the voltage average is provided in Figure 4.15 for the PZnT-NT, where the PZnT-NT was mounted directly above the shaker, and the maximum V_{pk-pk} could reach 0.5 V when the force was 3 N.

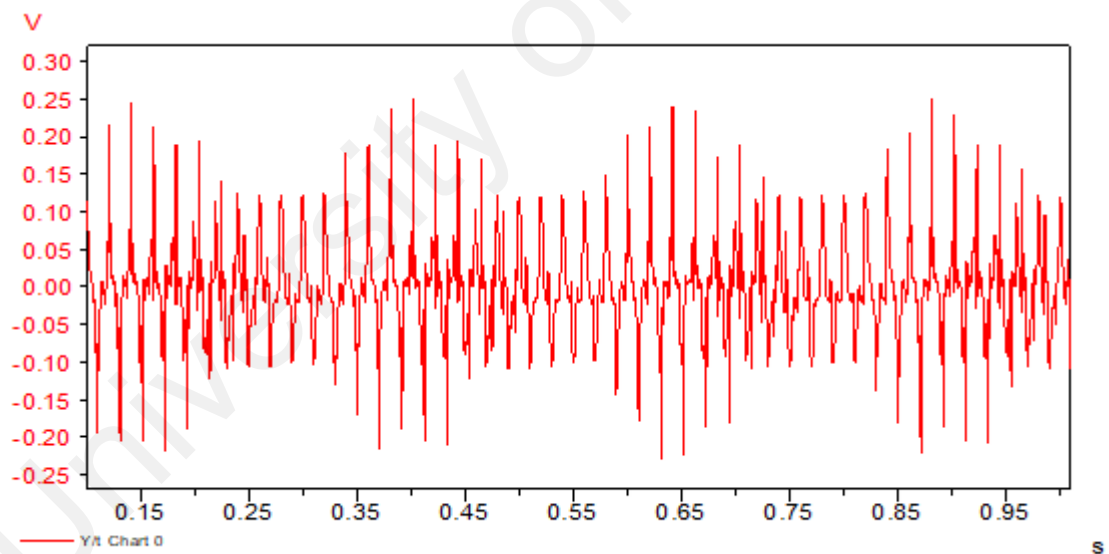


Figure 4.15: AC Voltage using Shaker Excitation at 90 Hz

The PZnT-NT was tested by pressing the harvester using only the finger. The maximum AC voltage was up to 0.9 V_{pk-pk} as shown in Figure 4.16.

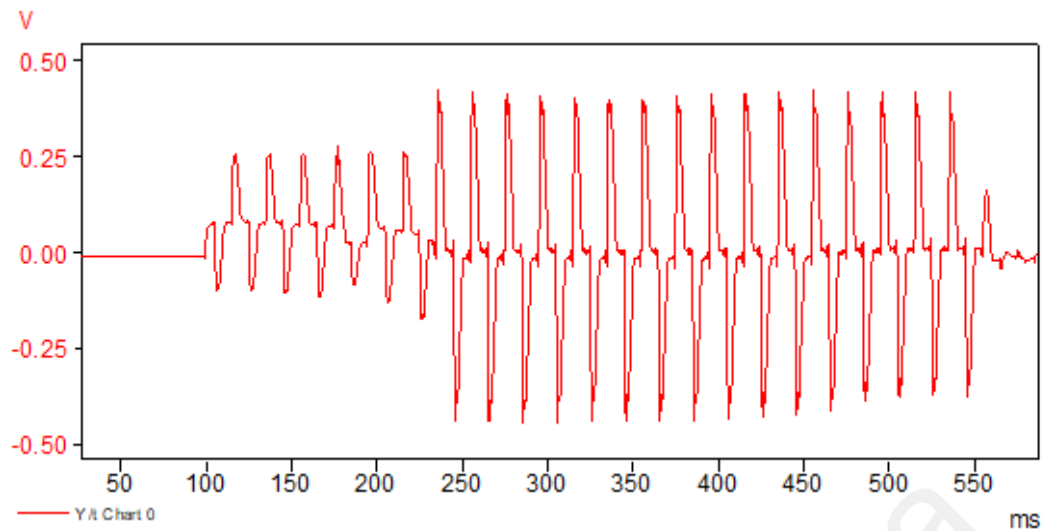


Figure 4.16: The AC Voltage of PZnT-NT under Finger Pressing

4.6 Voltage Measurement Baseline Test

Non-invasive measurements were tested and compared based on two conditions: (1) exciting frequency matched the natural frequency of PZnT-NT; and (2) exciting frequency matched the natural frequency of the host structure. These conditions were considered for evaluating the structural dynamic effects of the overall harvesting performance for PZnT-NT. The performance of PZnT-NT without the structural dynamic effect (i.e. PZnT-NT was directly attached to shaker) was also examined. The voltage outputs of the PZnT-NT in two different excitation frequencies were recorded separately and used as a reference baseline for further analysis.

The shaker was excited in frequencies ranging from 10–300 Hz. The maximum voltage peak was fulfilled at a frequency of 90 Hz as provided in Figure 4.17.

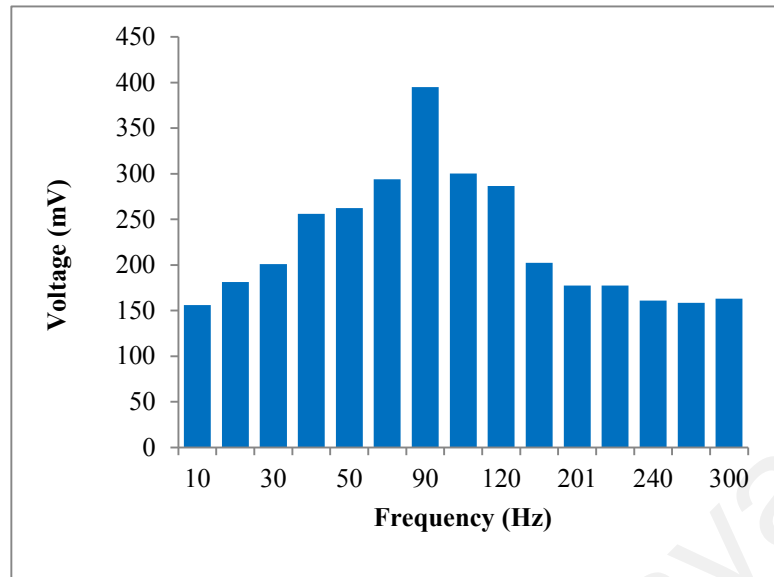


Figure 4.17: The Maximum Voltage Generation of PZnT-NT based on Frequencies in Range of (10-300 Hz)

4.6.1 Experimental Modal Analysis of Cantilever

As a part of the location selection scheme procedure the EMA results were presented in this section. The dynamic characteristics of the test rig were obtained by EMA, and the impact testing based on SIMO approach was performed on the cantilever beam (i.e. host vibrating structure). From the measured FRF set, there were three resonant mode shapes located in the frequency range of 0 –300 Hz as shown in Figure 4.18. It was observed that point 1 has a high displacement in all the resonance modes whereas point 9 was the nodal point. The first three natural frequencies are 23.1 Hz, 95.2 Hz, and 254 Hz, their corresponding mode shapes are shown in Table 4.3 respectively.

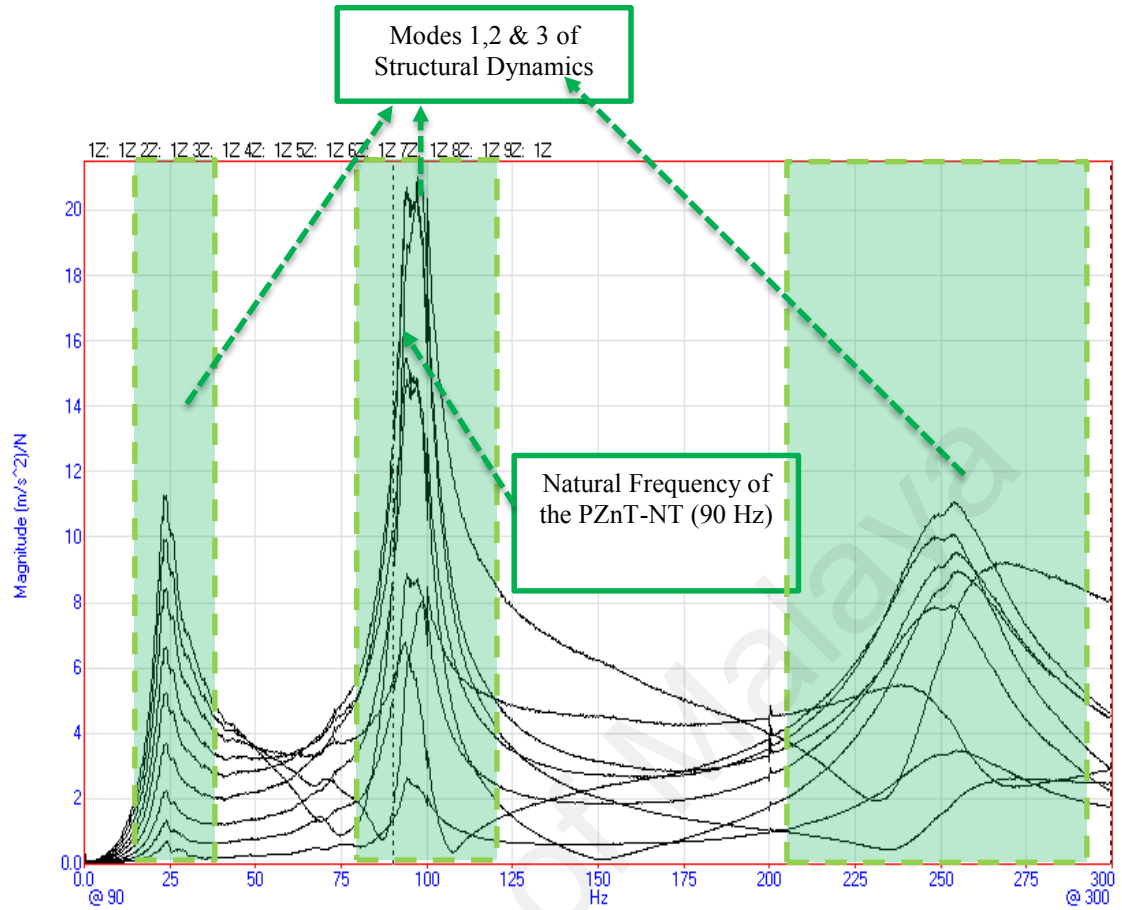


Figure 4.18: FRF of Cantilever Beam using Impact Testing

Table 4.3: Natural Frequencies, Damping and Mode Shapes of Cantilever Beam

Mode	Natural Frequency (Hz)	Damping (%)	Mode Shape
1	23.1	11.9	
2	95.2	5.21	
3	254	1.76	

4.7 Location Selection Scheme of Cantilever

The selection location scheme on the cantilever beam was studied systematically, where the cantilever was subjected to an excitation frequency of 95.2 Hz. The voltage was recorded when the PZnT-NT was roving from one point to another, and the average of the AC voltage (i.e. V_{pk-pk}) is given in Figure 4.19.

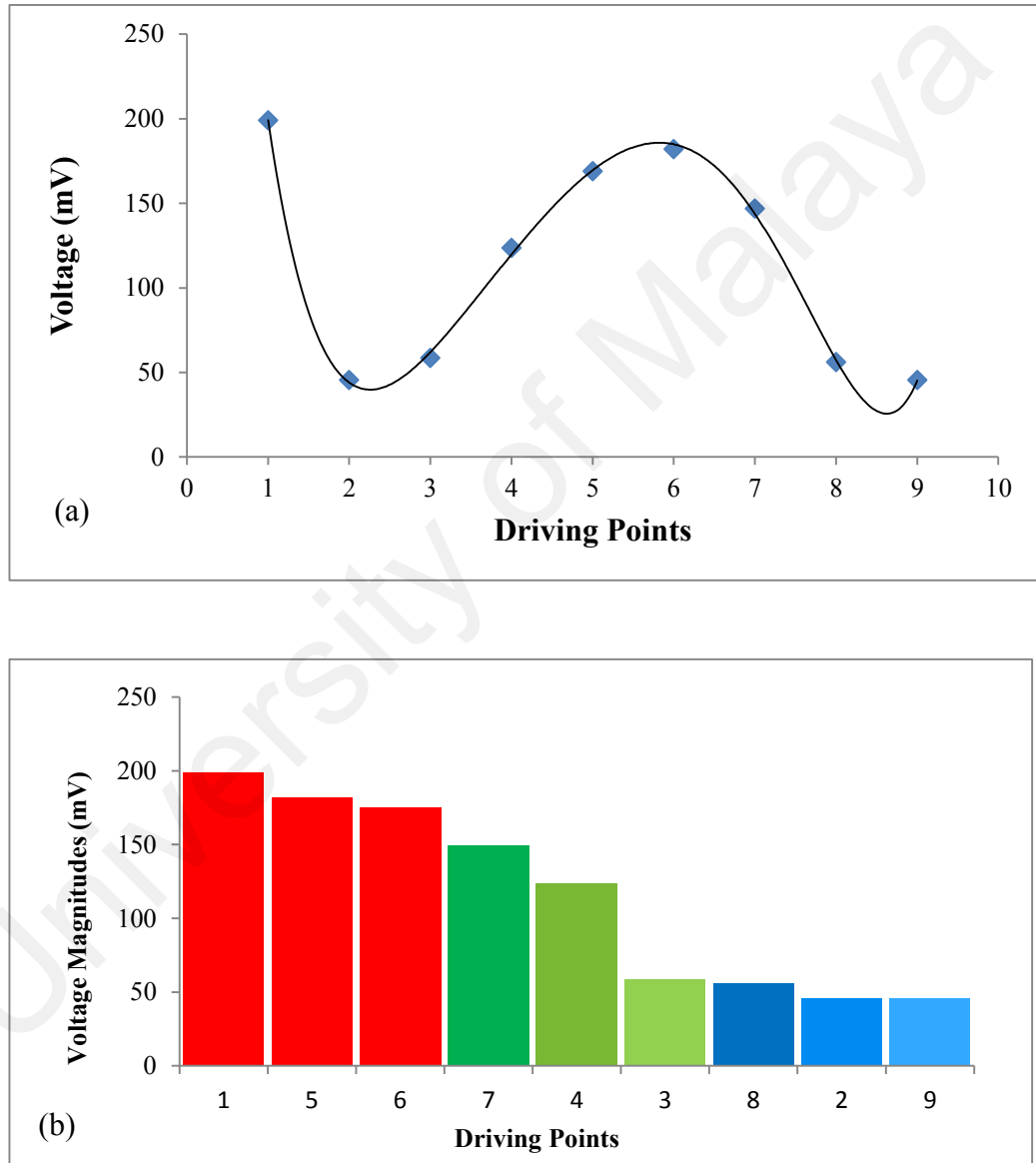


Figure 4.19: (a) Harvested Voltage, (b) Magnitude Ranking at 95.2 Hz

It was observed that the harvested voltages at points 2 and 9 were minimal when compared to the other points. The maximum voltage amplitudes were at points 1 and 5, and this means that voltage amplitudes (V_{pk-pk}) were recorded in the range of (199 – 46 mV). The PZnT-NT placed at the highest displacement point (i.e. point 1) this could yield a reduction of voltage at nodal point up to 77 %.

According to EMA results, a mode shape at 95.2 Hz was the second bending mode of the cantilever beam, where the nodal points (points with minimal response) fall on points 2, 3, and 9 as shown in Figure 4.20. This explains that when the PZnT-NT was placed at points 2, 3, and 9, the structural vibration was minimal.

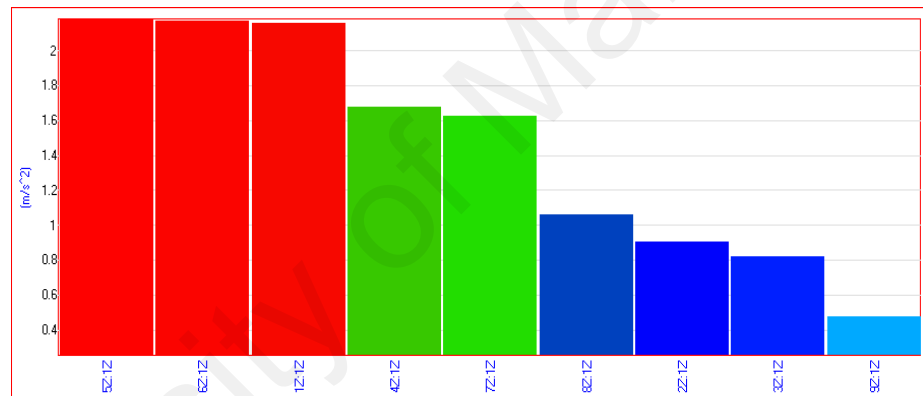


Figure 4.20: EMA Magnitude Ranking at 95.2Hz

From ODS analysis, Figure 4.21(a) shows the vibration pattern of the cantilever. The displacement versus time is provided in Figure 4.21(b).

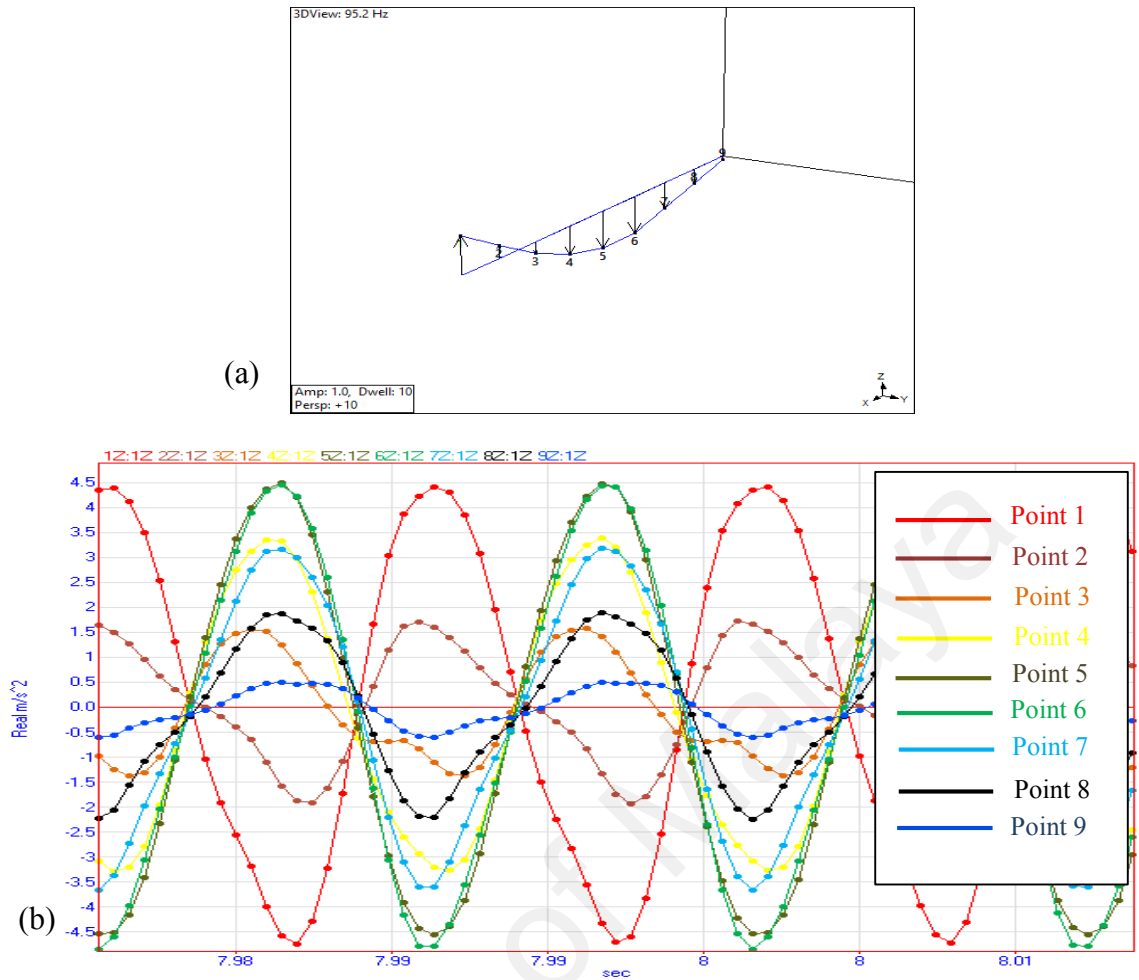


Figure 4.21: ODS Analysis at Frequency 95.2 Hz (a) Vibration Pattern (b) The Displacement versus Time

For the nodal points located at point 2, 3, and 9, the maximum displacements appeared at points 1, 5, and 6 where the magnitude ranking is specified in Figure 4.22 (a). These results coincide with the mode shape that was varied by voltage measurement of the PZnT-NT. The ODS spectrum at 95.2 Hz is shown in Figure 4.22(b).

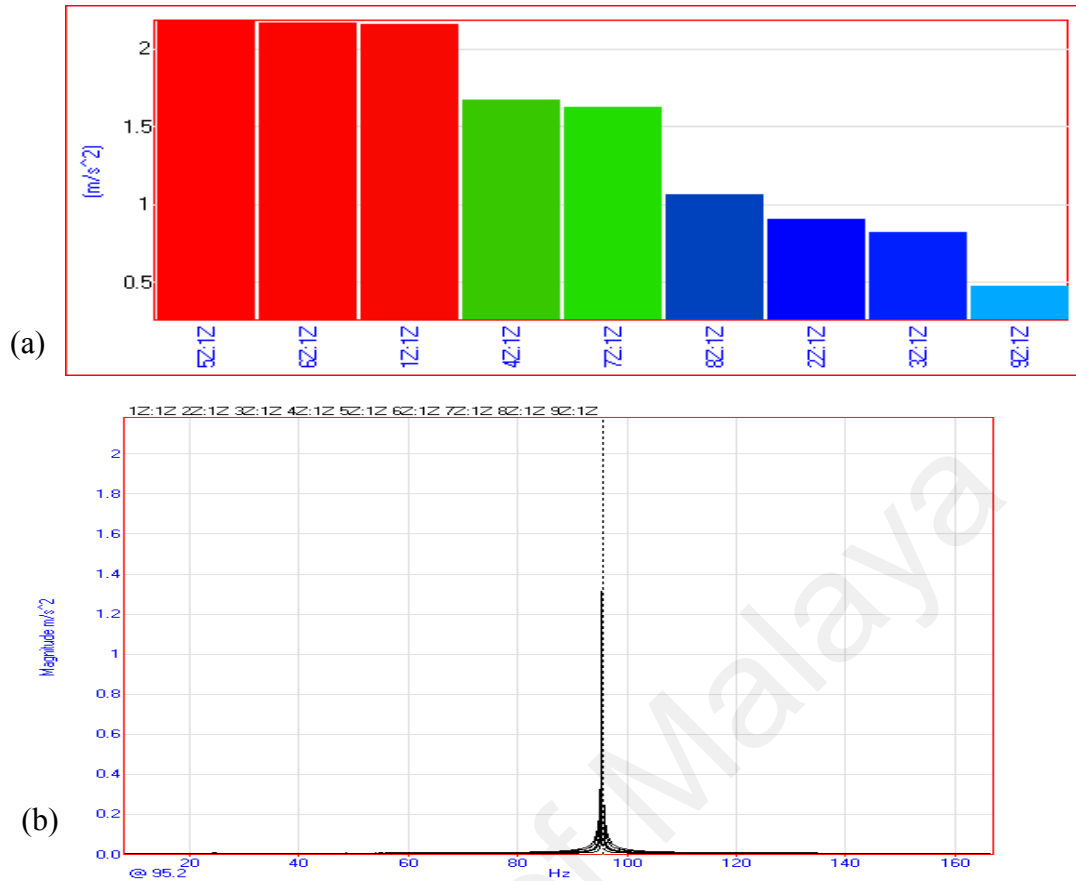
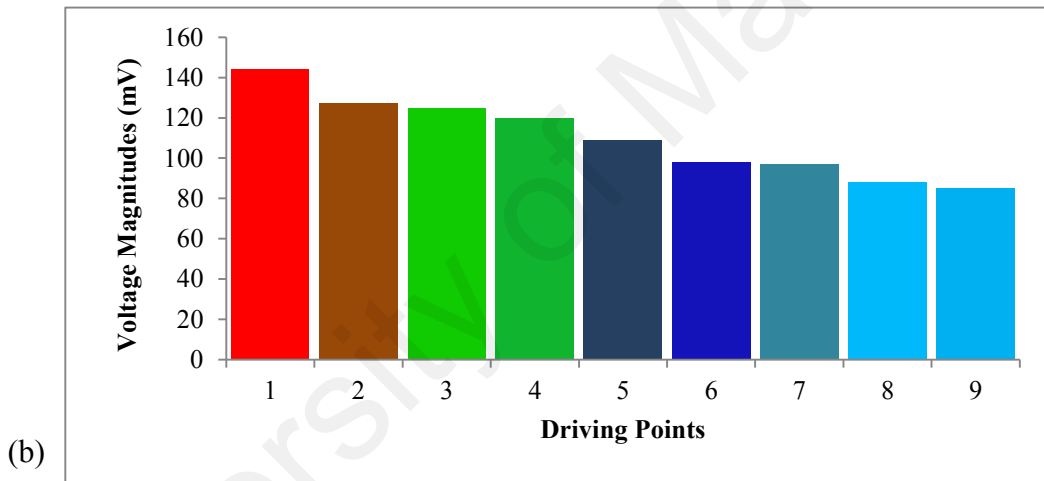
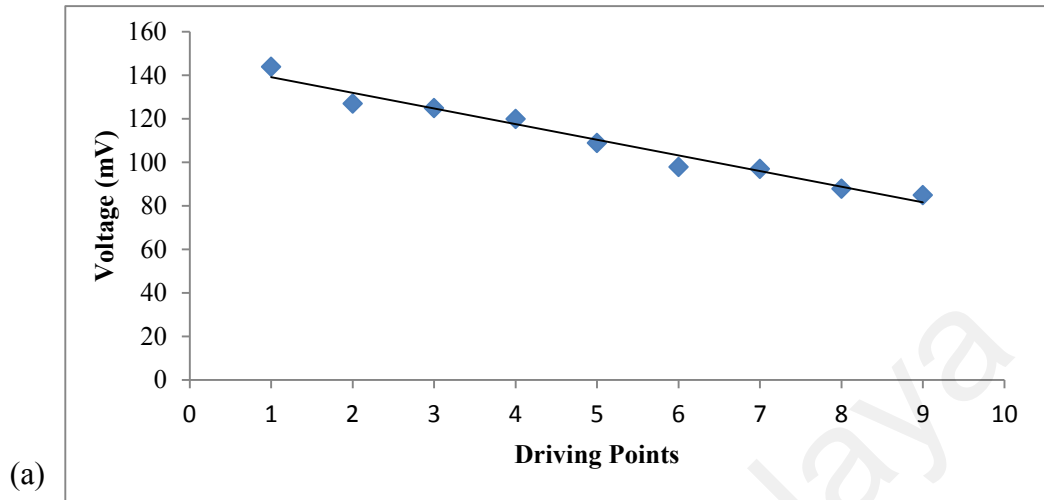


Figure 4.22: (a) Magnitude Ranking, (b) ODS Spectrum at 95.2 Hz

Similar trends were observed using ODS of the cantilever beam at 95.2 Hz. The dynamic response at 95.2 Hz was mainly contributed by the second vibration mode of the cantilever beam. It vibrated at the deflection shape which was dominated by the second mode, where point 2 and point 9 had the minimal vibrations. The proposed cantilever based PZnT-NT system was able to produce voltage from micro-vibration, i.e. to produce $[0.45 \ 0.220] V_{ac}$ (pk-pk) from maximum and minimum displacements of $[0.6 \ 4.5] \mu m$ at 9 examined locations. Harvesting energy from minimum mechanical energy at micro movements indicates a good progress towards building a self-powered system (Amor et al., 2008).

Similarly, the cantilever was subjected to an excitation frequency of 23.1 Hz that was equivalent to the first natural frequency. The voltage was recorded when the PZnT-NT

was roved from one point to another, with the average of the AC voltage (i.e. V_{pk-pk}) are given in the Figure 4.23.



It was observed that the harvested voltage at 9 was minimal when compared to other points. The maximum voltage amplitudes were at point 1 hence, the voltage amplitudes (V_{pk-pk}) were recorded in the range of (144 – 85 mV). The first natural frequency was 23.1 Hz, and the EMA results such as the mode shape and the magnitude ranking are provided in Figure 4.24, where the nodal point (points with minimal response) was at point 9.

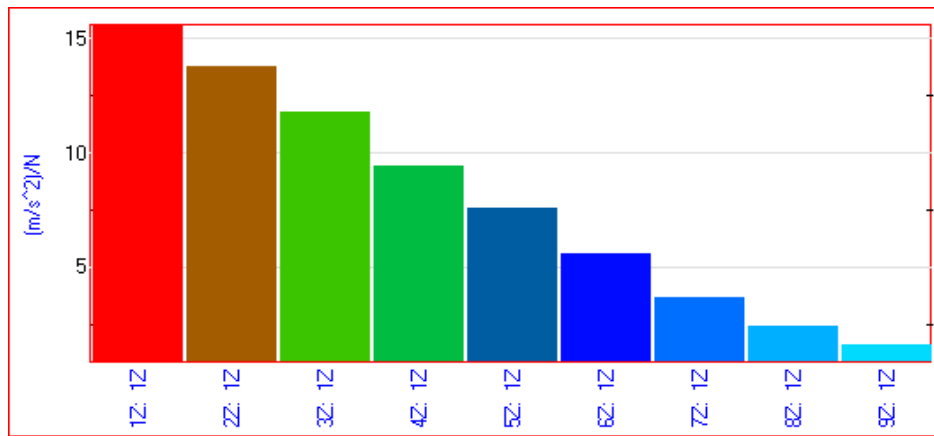


Figure 4.24: EMA Magnitude Ranking 23.1 Hz

The vibration pattern and magnitude range were demonstrated based on the obtained ODS at frequency of 23.1 Hz as illustrated in Figure 4.25. The obtained results coincide logically and practically with the detected findings based on the EMA and ODS at the second natural frequency.

In summary, the mode shape and vibration pattern that were obtained from the EMA and ODS analysis could assist users in determining the optimal location for harvesting the maximum voltage for the cantilever system under motor excitation. The measurement time of conducting EMA is more time consuming than ODS analysis, while ODS analysis provides a more efficient and straightforward method to identify the optimum harvesting location. However, ODS result is only applicable for a particular operating condition. If the working environment such as the operating frequency changes, then another set of ODS analysis should be carried out to determine the new optimum location of the harvester. In this case, EMA method poses a huge advantage over the ODS analysis, as it provides a comprehensive dynamic characteristic information of the structure in all frequency ranges of interest. Thus, there is a trade-off between the ODS and EMA methods in selecting the optimum harvesting location of a structure. User should select the best method to identify the optimum location based on their needs.

For example, it is recommended to use the ODS method on a structure with fixed operating frequency; to use EMA method for structure with dynamic changes of the operating frequency.

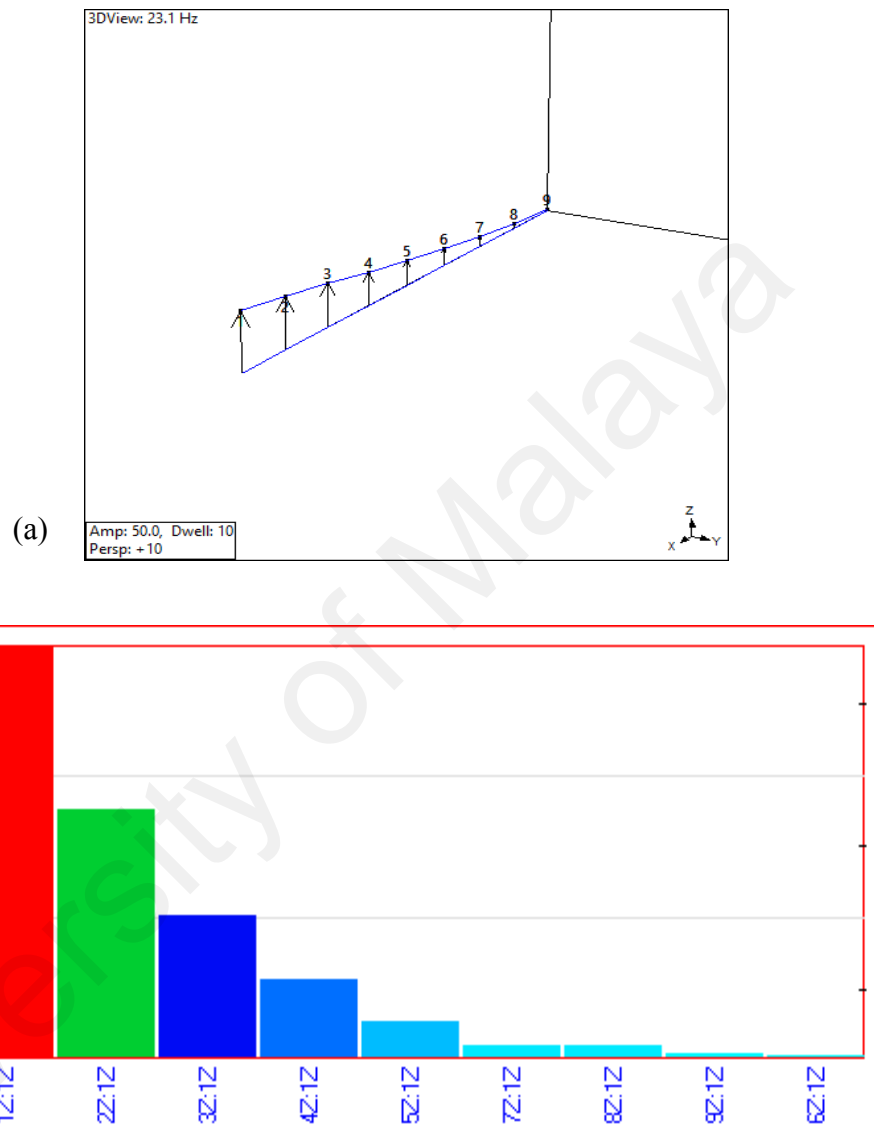


Figure 4.25: (a) ODS Vibration Pattern, (b) ODS Magnitude Ranking at 23.1 Hz

4.7.1 Structural Dynamics Effects on the Harvesting Performance

This study investigates the structural dynamics of the cantilever beam in the effort to optimise the voltage harvested by the piezoelectric plate which was placed on the cantilever beam. It was noted that the piezoelectric plate could harvest maximum voltage when it was being excited at 90 Hz.

The maximum harvested peak voltage was recorded at $0.395 V_{pk-pk}$ and it was treated as the baseline voltage. The piezoelectric plate was placed directly on the top of the shaker without any interference from structural vibration and the excitation force from the shaker was maintained. When this piezoelectric plate was placed on the operating cantilever beam and excited at 90 Hz, there was a 28 % reduction in harvested voltage and it was recorded at $0.286 V_{pk-pk}$. The reduction could be explained based on the structural dynamics aspect of the cantilever beam. The baseline voltage at 90 Hz of PZnT-NT was located close to the second resonance mode of the cantilever. The harvested voltage was mainly contributed by the shaker excitation. A comparison between voltage baseline and voltage measurement based the location selection scheme are shown in Figure 4.26, where the voltage was measured at excitations of 90 Hz. It was observed that the difference between the voltage amplitude (at point 1) and the baseline measurement was 27.5%.

In a real-life application where the structure could not be excited at the piezoelectric plate's natural frequency, the selection scheme of optimal location should be utilised in order to find the optimal harvested voltage by the piezoelectric plate. When the cantilever beam was excited at 95.2 Hz which was close to the piezoelectric plate's natural frequency, the maximum harvested peak voltage was $0.198 V_{pk-pk}$ at one of the anti-nodal points of the second mode shape (point 1).

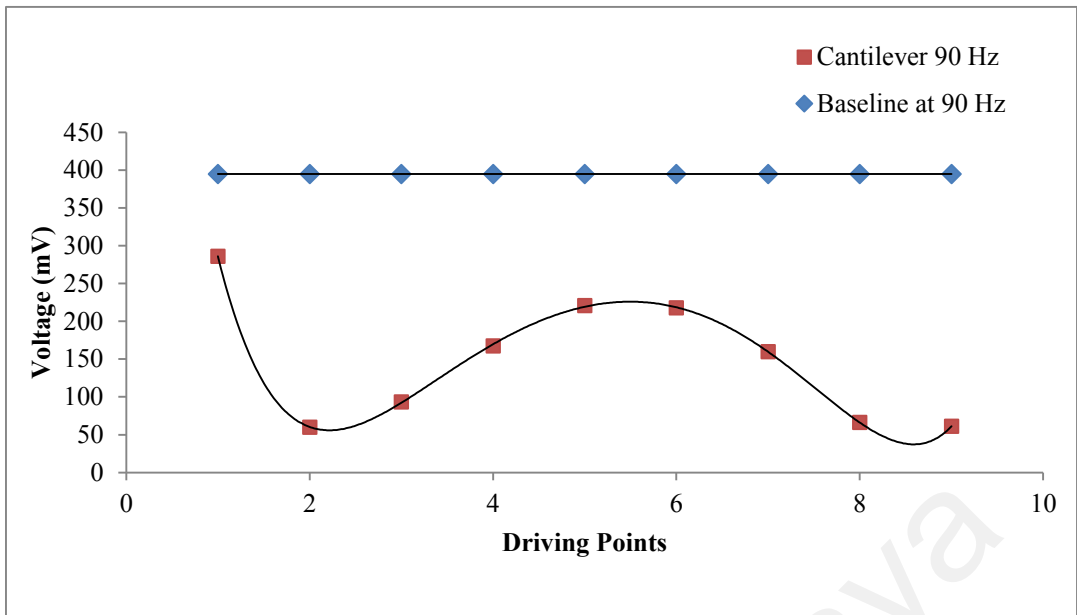


Figure 4.26: Harvested Voltage at 90 Hz Excitation for Various Measurement Points in Comparison to Baseline Voltage

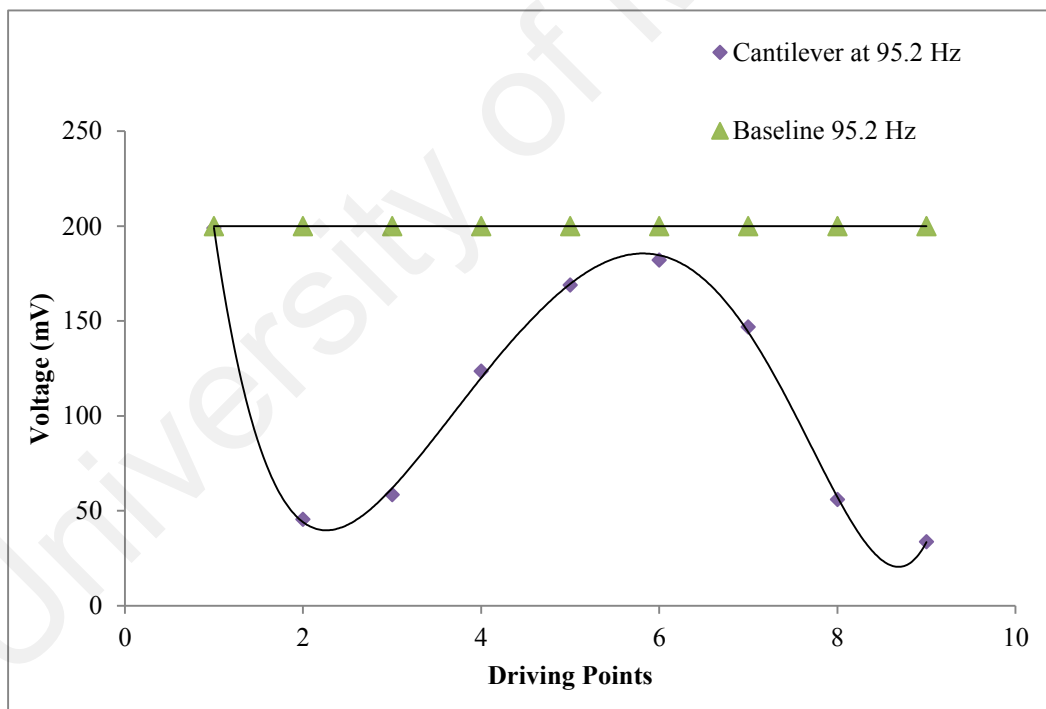


Figure 4.27: Harvested Voltage at 95.2 Hz Excitation for Various Measurement Points in Comparison to Baseline Voltage

As compared to the baseline voltage at 95.2 Hz, the maximum peak voltage harvested was only recorded at 0.200 V_{pk-pk} , and it showed a very low voltage amplitude difference

of 1%. Hence, the piezoelectric plate was placed at the optimal location (i.e. the anti-nodal point that is detected based the EMA and ODS measurement). Based on the location scheme, placing the piezoelectric plate at the nodal point of the mode shape or minimum vibration point, i.e. point 2 ($0.046 V_{ac}$) and point 9 ($0.033 V_{ac}$) should be avoided. This could yield a more than 77% reduction in voltage harvested by the piezoelectric plate.

4.8 Selection of an Optimal Location of VAWT Beam

Based on the integrated EMA and ODS analyses in selecting an optimal location of cantilever, the result showed the vibration mode of the beam where the piezoelectric was able to harvest high voltage in the high displacement region and that the nodal points should be avoided. Thus, this section presents the selection scheme of the optimal harvesting location on the VAWT beam structure based on vibration mode shape and its ODS. The piezoelectric plate was placed on the VAWT beam structure and subjected to wind flow excitations. The harvested voltage varied at different locations of the VAWT beam. The voltage harvested by the piezoelectric plate and its voltage magnitude ranking was recorded. The dynamic characteristics of the VAWT were detected by the EMA analysis technique. The measured FRF was processed in ME'scopeVES and the modal parameters were obtained by using the curve fitting method. Based on the curve fitting results, the natural frequency, damping ratio, and the residue mode shapes were obtained. To know how much dose the beam moves during the VAWT operation and visualise the dynamic deformation of the beam, the ODS spectrum was obtained in three orthogonal directions (i.e. x, y, and z coordinates).

4.8.1 ODS Spectrum of VAWT

Operational deflection shape was carried out over the VAWT beam. The VAWT beam was divided into 10 segments with 9 measurement points, where Point 1 (i.e. the free end of beam) was equipped with tri-axial accelerometers that recorded the responses in three DOF (i.e. x, y, and z directions). The ODS spectrum is illustrated in Figure 4.28. It was obvious that the interested frequencies range were located in the range between (0.5–300 Hz) and thus the overall deflection shape was animated to visualise the vibration pattern that caused by the wind flow excitations.

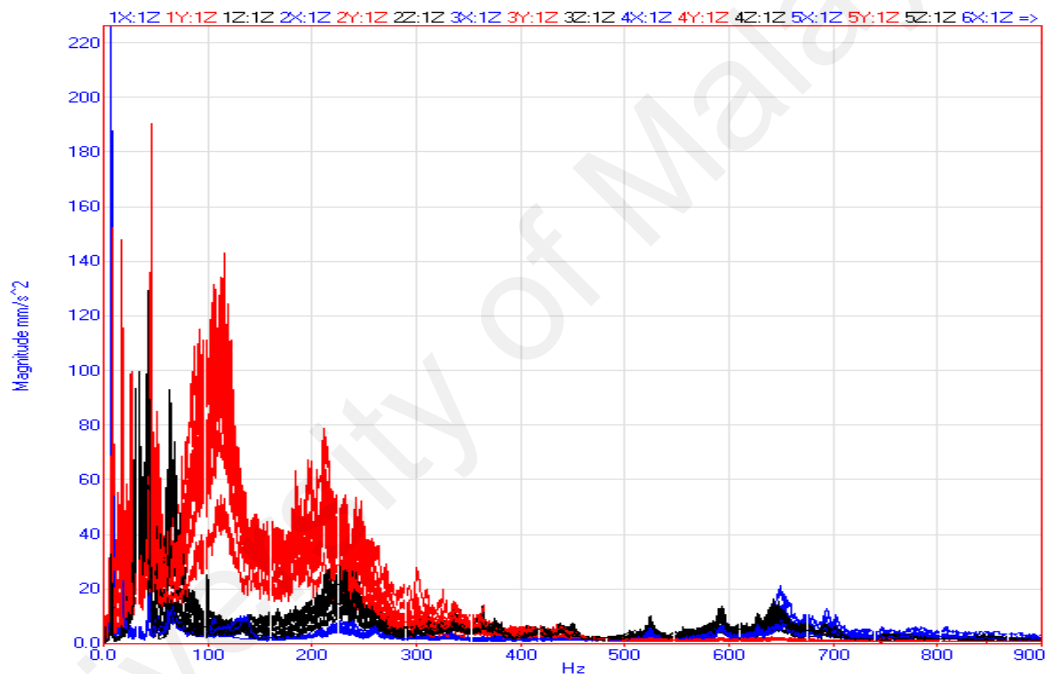


Figure 4.28: ODS Spectrum of VAWT Beam at Three Directions

Based on that, the selected frequencies range of EMA would be in the range of 0.5–300 Hz. The responses on three directional axes were determined of the free end (i.e. point 1) and the clamped end (i.e. point 9) as shown in Figure 4.30, whereby the highest displacement was realised at the free end. The overall vibration pattern was animated, and the deflection movement was similar to the elliptical motion path as shown in Figure 4.29.

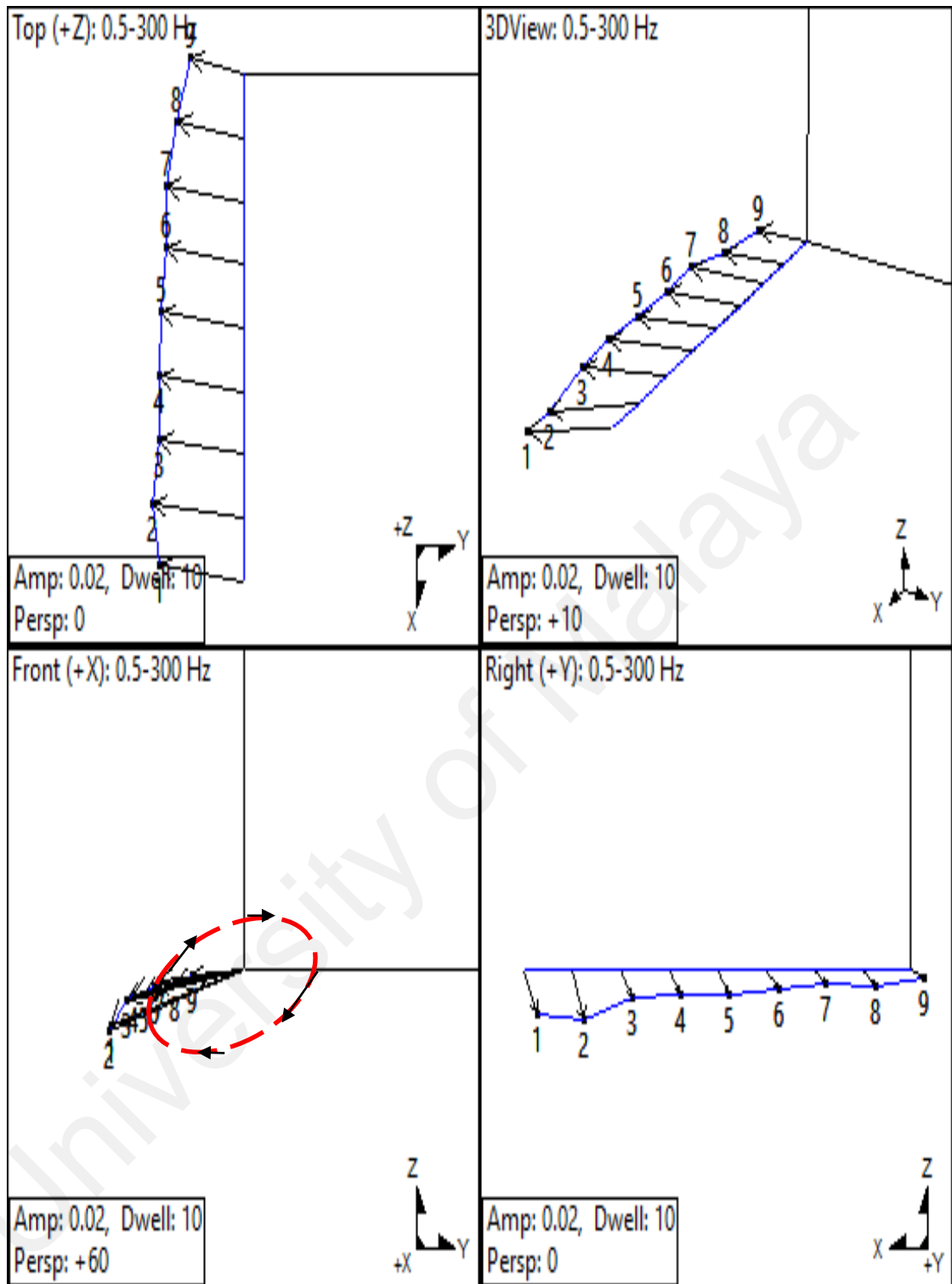


Figure 4.29: The Overall Deflection Shape based on ODS Analysis at Frequency in the Range of (0.5–300 Hz)

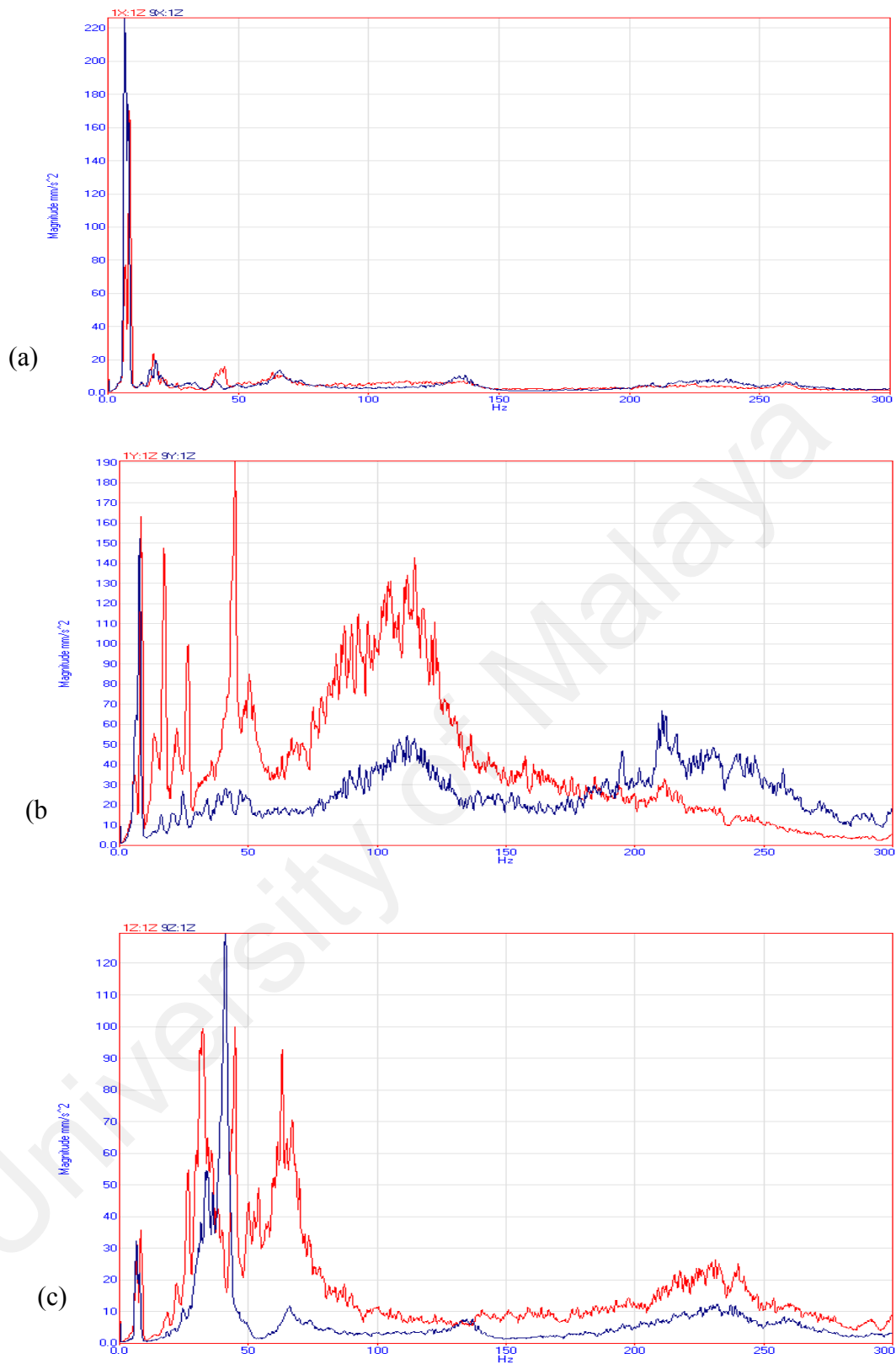


Figure 4.30: ODS Spectrum of the Free End (Point 1) (Label is Red) and the Clamped End (point 9) of VAWT Beam (Label is Blue): (a) Response Compared in x-axis (b) Response Compared in y-axis, (c) Response Compared in z-axis)

The vibration pattern demonstrated extensive excitations towards the y-axis (i.e. the horizontal direction of the VAWT). In fact, the diffuser plates of the VAWT had caused the increased in lateral force against the VAWT beam. Figure 4.31 illustrates the diffuser effect against the VAWT beam.

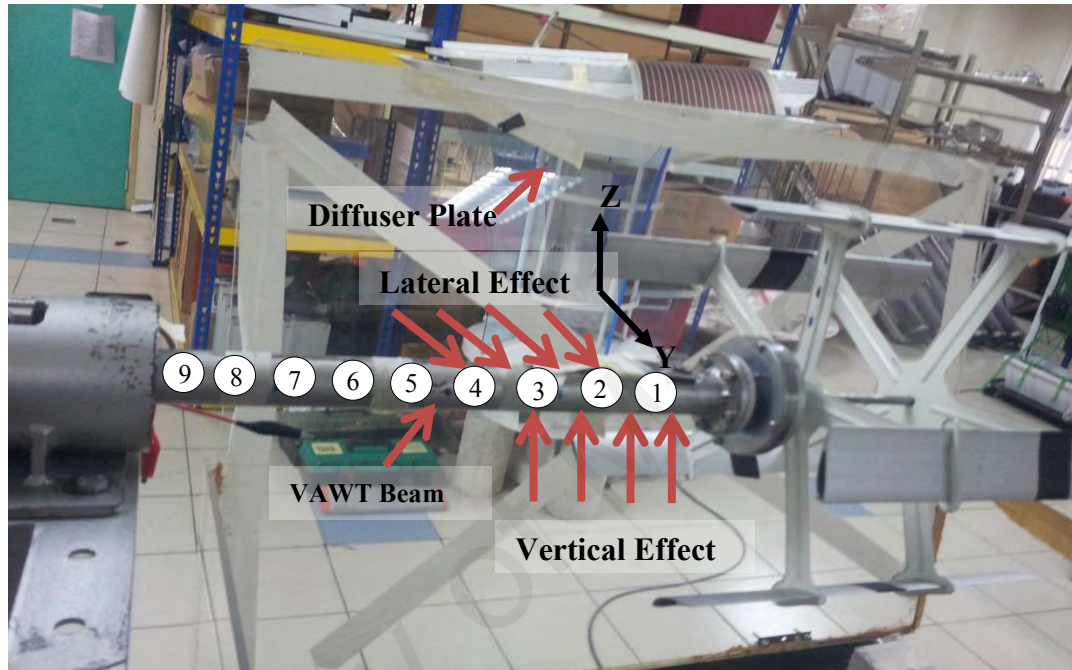


Figure 4.31: Diffuser and the Wind Effect of the VAWT

The highest displacement was displayed towards the y-axis. The overall deflection shape that selected at frequencies in the range of (0.5–300 Hz) as illustrates in Figure 4.29. It was obvious that the lowest displacement was at point 9 and all the points of the beam moved in semi-elliptical paths.

4.8.2 EMA Analysis of the VAWT

The EMA was carried out on the VAWT beam. The impact hammer excited the beam toward the y-axis and z-axis separately, and the corresponding responses were recorded in three orthogonal directions. On the x-axis, it is impossible to obtain the mode shape across the VAWT due to there being no discrete points on this section and there no large force effect (wind flow) could occur. The dynamic characteristics of the beam were determined using the curve fitting for the sets of FRF. Accordingly, the natural frequencies, damping ratios and mode shape were determined. Finally, these FRF sets are bonded (i.e. y-axis & z-axis) in the ME'scopeVES window, and the mode shape was visualised where the obtained mode shape and vibration pattern were compared. The acquired FRF in three orthogonal directions is shown in Figure 4.32. For indicating the quality of FRF, the coherence is illustrated in Figure 4.33.

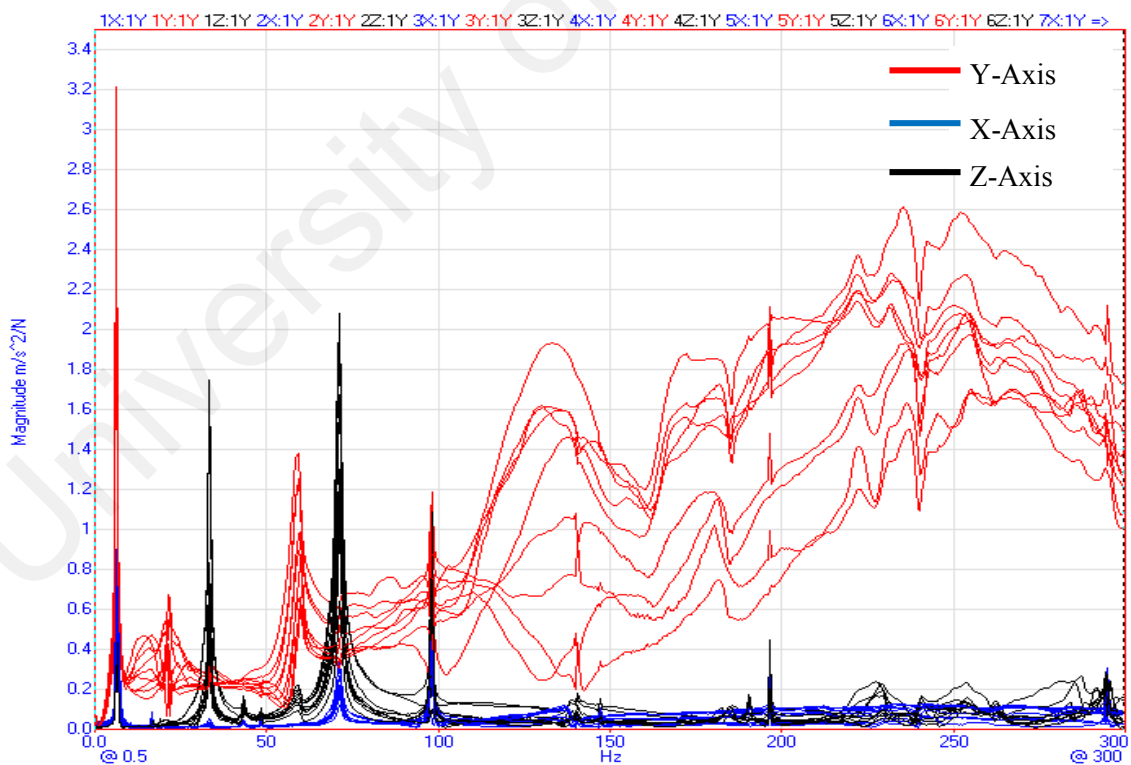


Figure 4.32: The Set of FRFs based on the EMA Analysis of VAWT in Three Orthogonal Directions when the Excited Force Acts in Y- direction

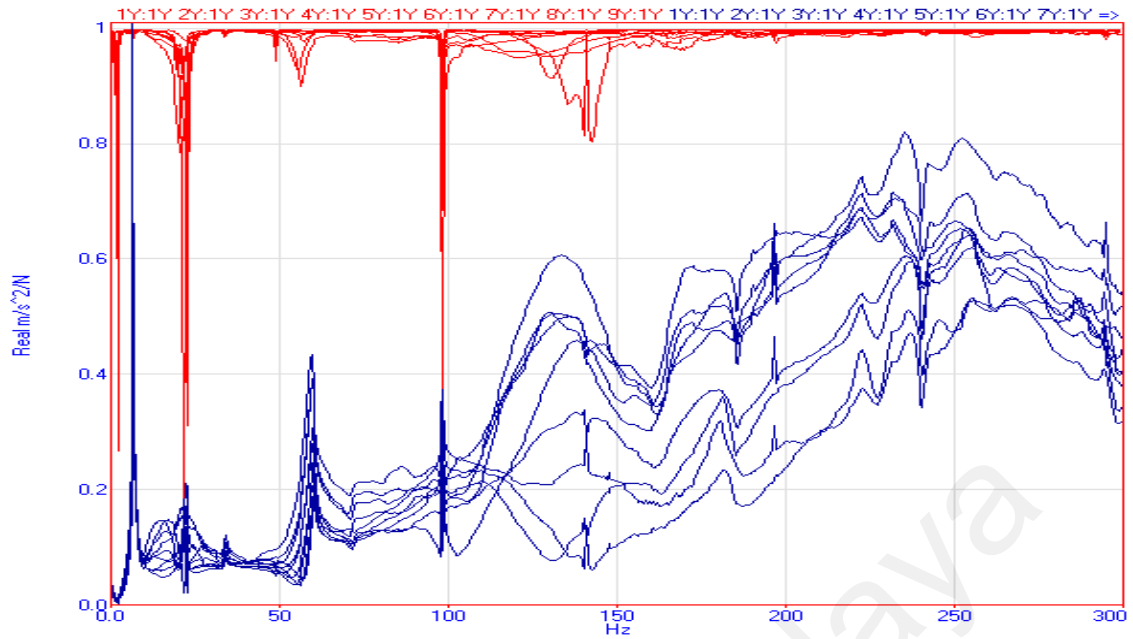


Figure 4.33: The FRF Raw Data and Coherence Set based on the EMA Analysis of VAWT when the Force Excitation Act in Y-direction

The dynamic characteristics of the VAWT beam were presented in Table 4.4, and the overall mode shape based on EMA analysis was at frequencies in range of (0.5–300 Hz). The deflection results of the beam due to EMA in the Y-axis coincided with the ODS results where the frequency response function of the free end (point 1) was higher in magnitude compared with the clamped end (point 9) as illustrated in Figure 4.34.

Table 4.4: The Dynamic Characteristics of the VAWT Beam when the Force Act in y-direction

Mode shape	Frequency (Hz)	Damping ratio (%)
1	6.62	1.170
2	58.7	1.950
3	98.5	0.187

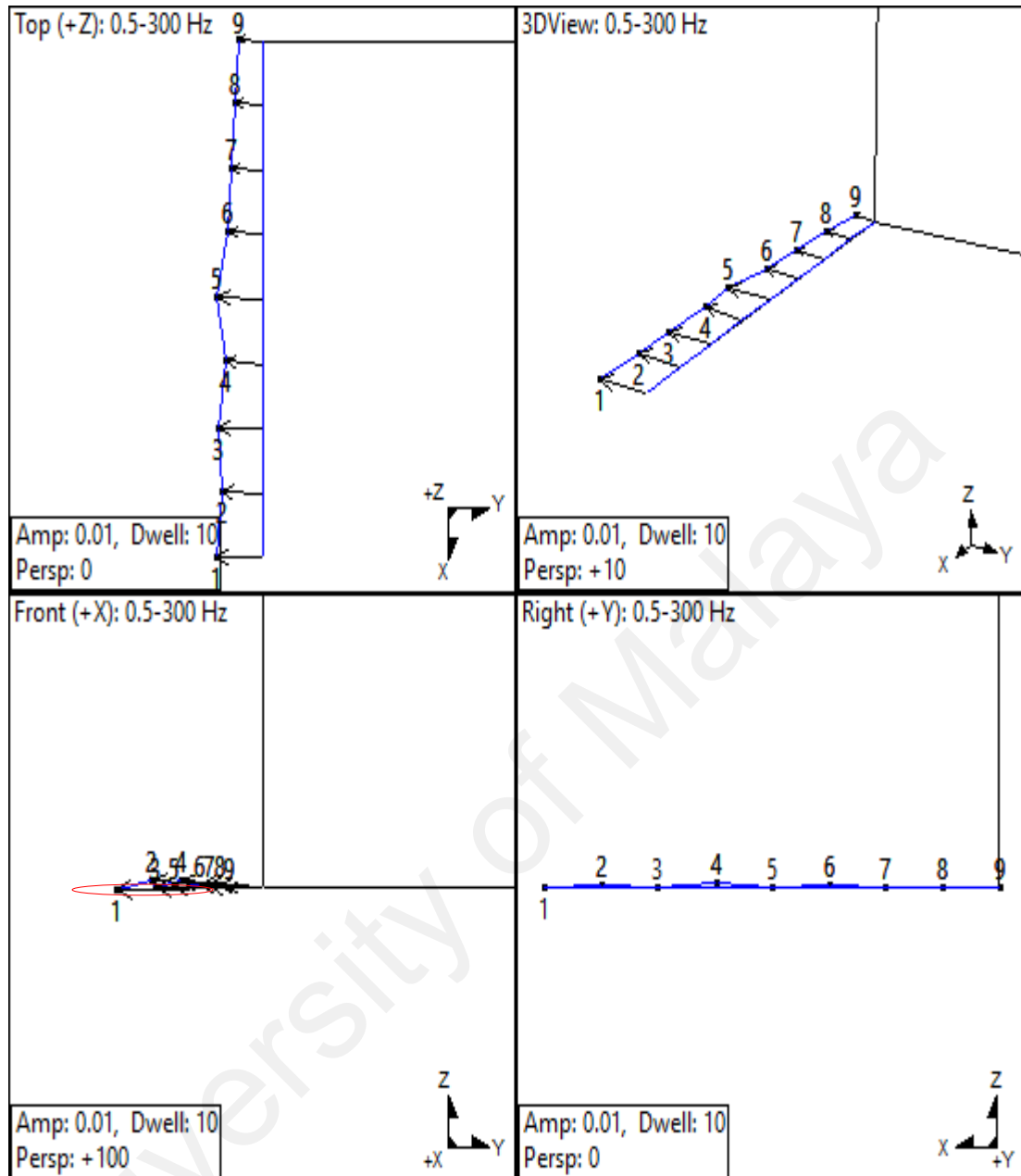


Figure 4.34: The Overall Dynamic Respond of the VAWT based on EMA Analysis at Frequency in Range of (0.5-300 Hz) when the Force Act in Y-axis

The EMA was carried out at the VAWT beam when the hammer excited the beam towards the z-direction, the FRF sets were acquired in the three orthogonal directions as provided in Figure 4.35. The quality of the FRF represented was measured by the coherence (COH) function, if COH is greater than 0.9, the FRF measurement is considered to be good especially at the natural frequency region.

Therefore, the determined COH analysis was greater than 0.9 at the natural frequencies regions and thus the FRF measurement was obtained accurately as it is illustrated in Figure 4.36. The overall mode shape was animated where the motion was dominant in the z-direction shape. The deflection result of the beam due to EMA in z-axis coincided with the ODS results where the frequency response function of the free end (point 1) was higher in magnitude compared with the clamped end (point 9) as illustrated in Figure 4.37.

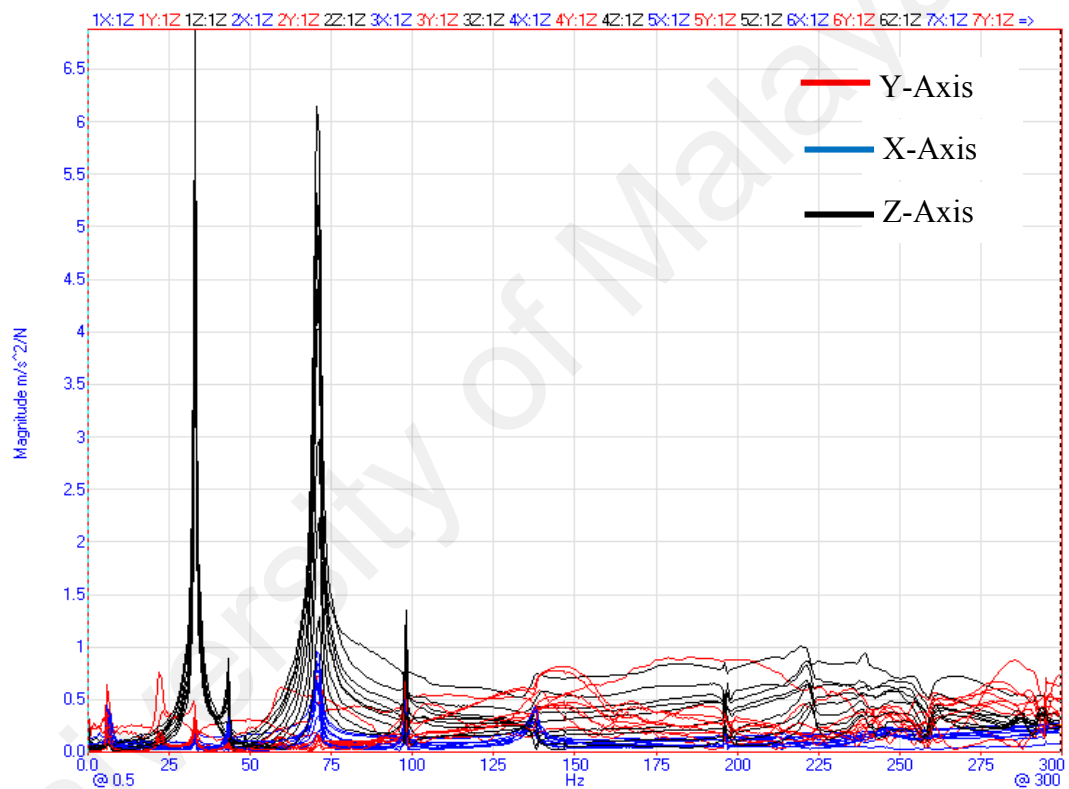


Figure 4.35: The FRF Set on the EMA Analysis of VAWT in Three Orthogonal Directions when the Impact Forces Act in Z-direction

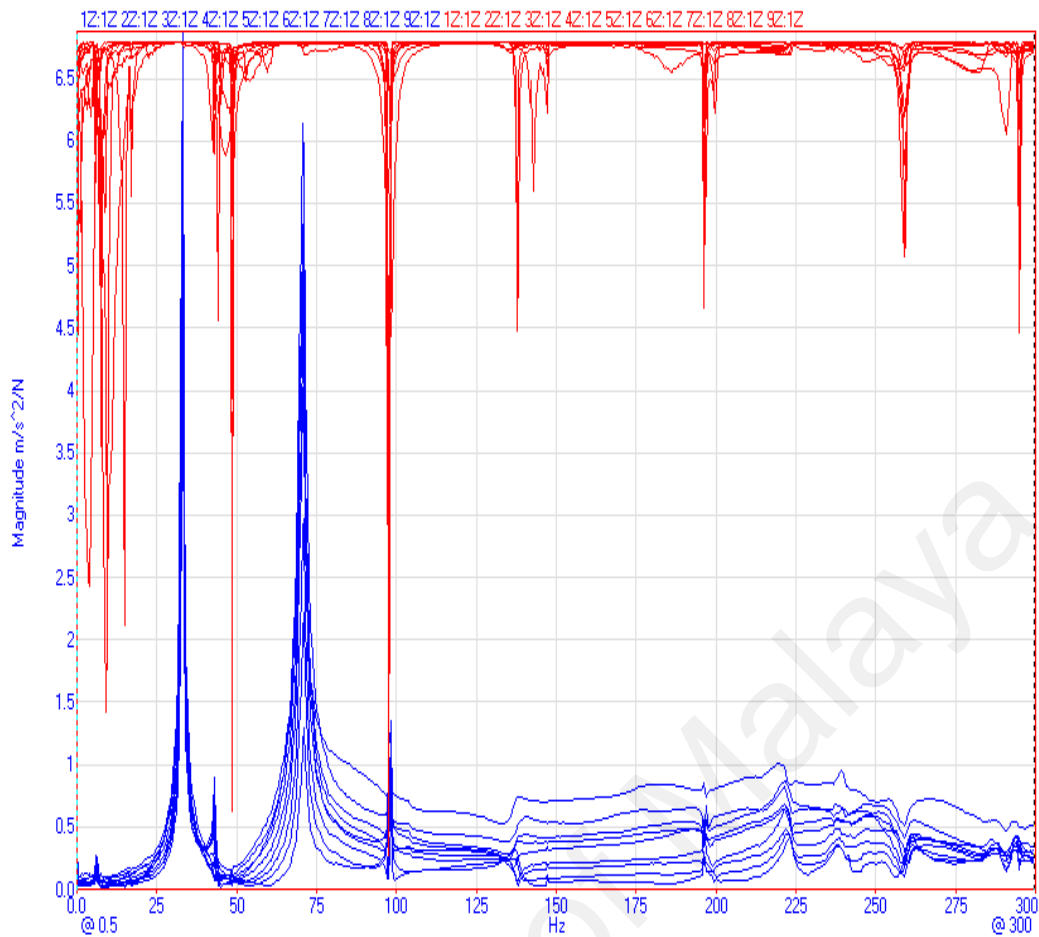


Figure 4.36: The FRF Raw Data and Coherence Set based on the EMA Analysis of VAWT when the Force Excitation Act in Z-direction

Dynamic characteristics of beam when the force act in z-direction test present two modes shapes with natural frequencies of 33.6 Hz ,71.21 Hz and damping ratios of 0.89% ,1.24% respectively. The Overall Mode Shape based on EMA Analysis at Frequency in Range of (0.5-300 Hz) Z-axis Direction is illustrated in Figure 4.37.

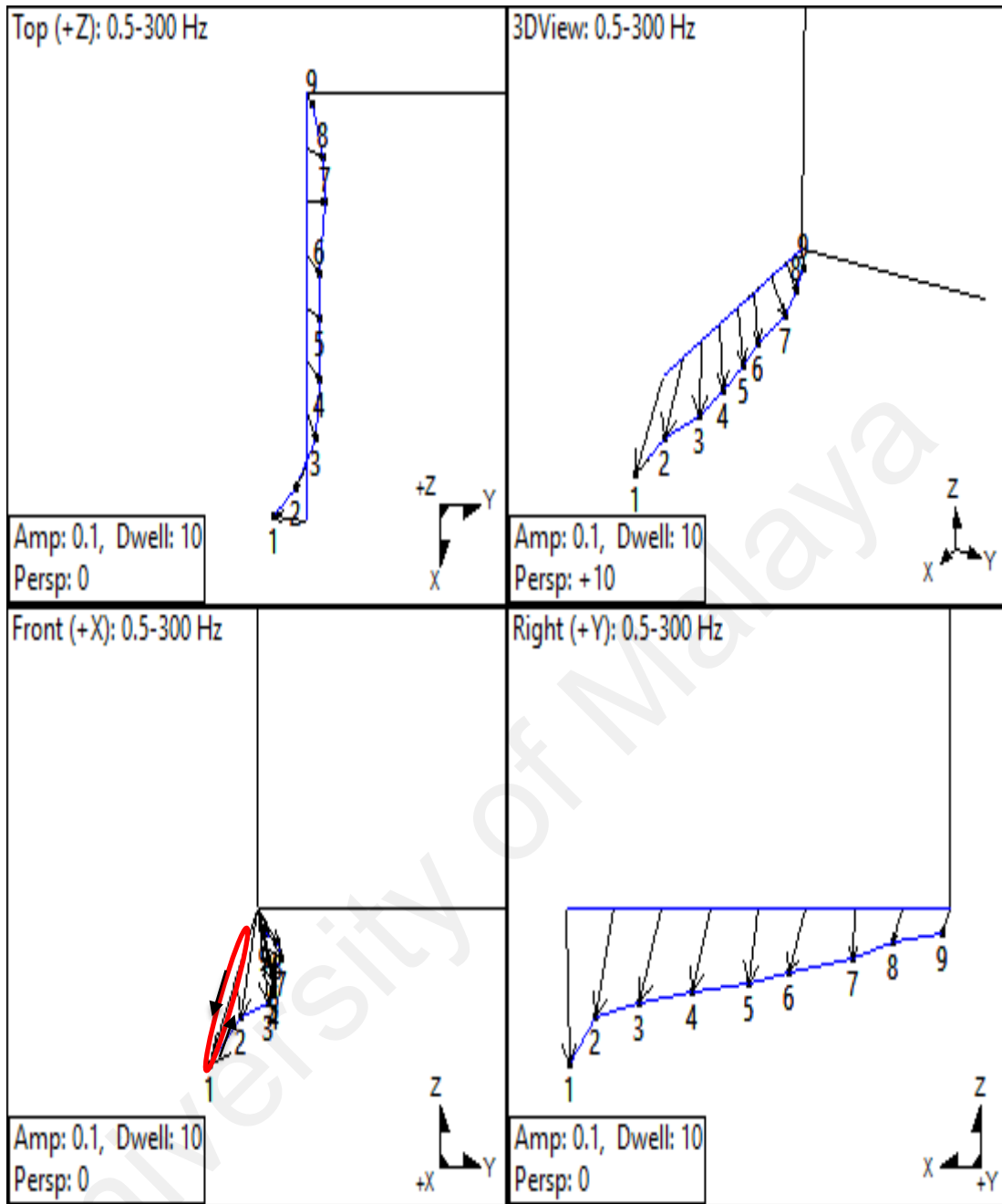


Figure 4.37: The Overall Mode Shape based on EMA Analysis at Frequency in Range of (0.5-300 Hz) Z-axis Direction

In the real excitation environment, the VAWT beam was subjected to rotor excitation as well as the wind flow (i.e. which consist of lateral and vertical effects). Considering these force components were acting on the VAWT beam simultaneously, the deflection result of the beam due to EMA in y-axis and z-axis are shown in Figure 4.38. The result

coincided with the ODS result where point 1 had the highest displacement in both the x-axis and y-axis directions, which were moving in elliptical path. From the results, the y-axis component contributed more to the overall deflection compared to the z-axis component. Therefore, the optimal harvesting location was found to be located at the point 1 and toward Y-axis.

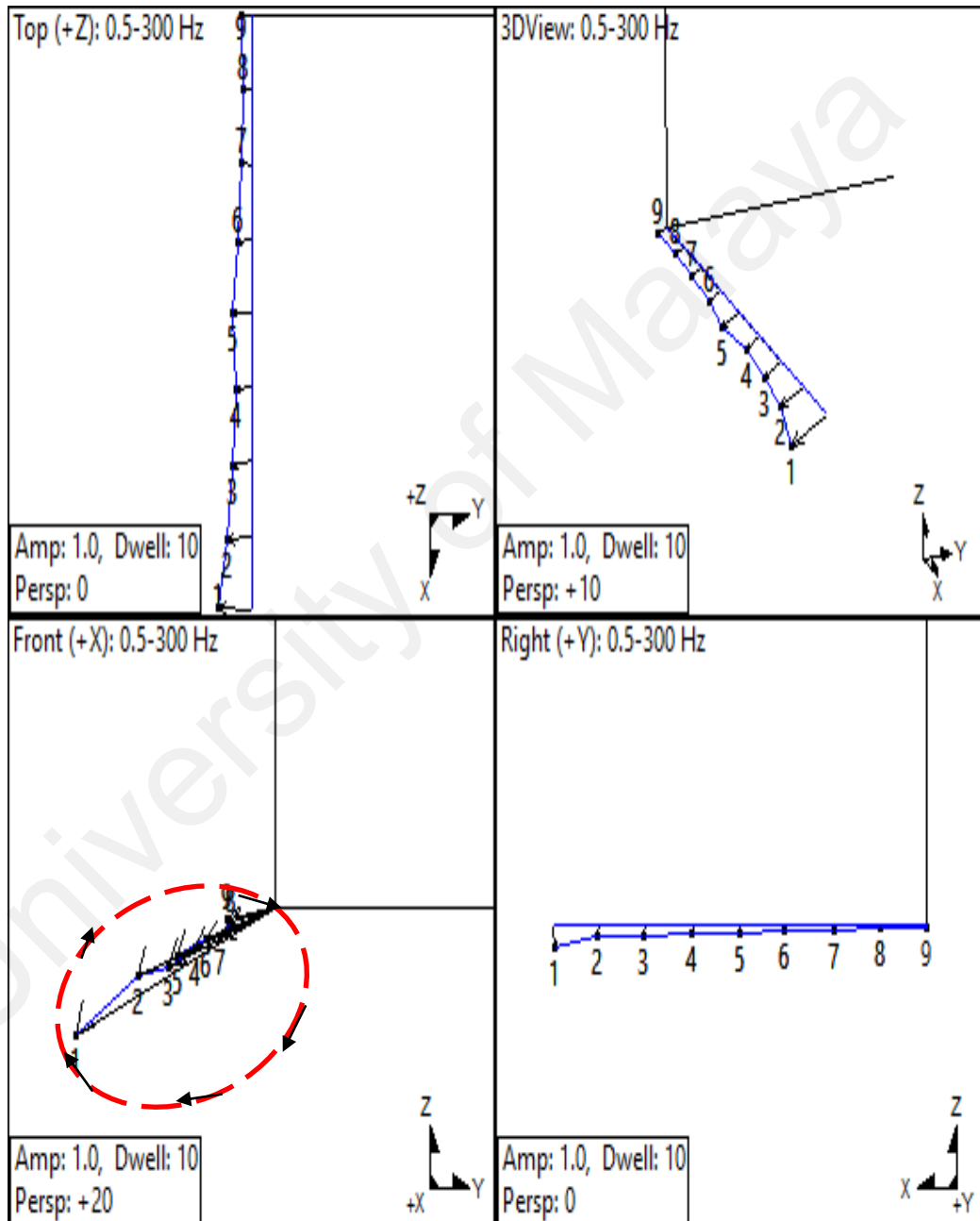


Figure 4.38: The Overall Mode Shape based on EMA Analysis at Frequency in Range of (0.5-300 Hz) Y-axis and Z-axis Direction

4.8.3 The AC Voltage of the PZnT-NT in the VAWT

The acquired AC voltage from the PZnT-NT that mounted at point 1 and point 9 were recorded for the instantaneous acceleration data (i.e. three orthogonal directions). The highest voltage was recorded at point 1 whilst it was found low at point 9. Apart from that, the acceleration in x, y, and z are also recorded in Appendix E.1.

The maximum generated AC voltage was at point 1 and the average value was reached to $0.405 V_{pk-pk}$. At point 9, the average voltage value was $0.105 V_{pk-pk}$, where the reduction of voltage at point 9 was 74%. Also, the instantaneous accelerations in 3DOF (x, y, and z-direction) were recorded where the highest acceleration data was observed towards the y-axis. In fact, the excitation toward y-axis was caused by the diffuser plate influences. This fact is illustrated in Figure 4.39 (see Appendix E.1 & Appendix E.2) and Figure 4.40 (see Appendix E.3 & Appendix E.4).

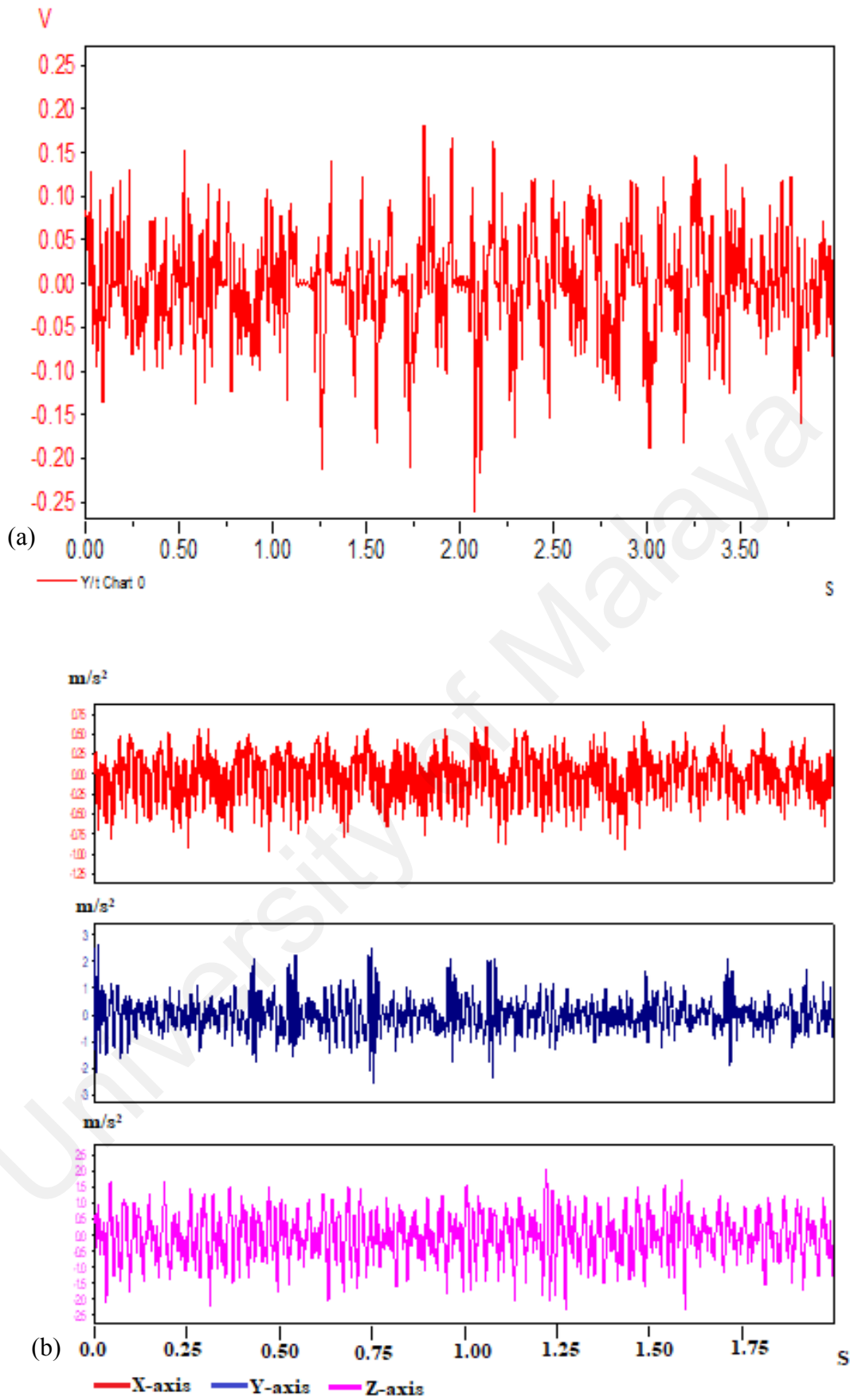


Figure 4.39: (a) Recorded AC Voltage, (b) The Instantaneous Acceleration (i.e. x,y, and z) at Point 1 of VAWT Beam

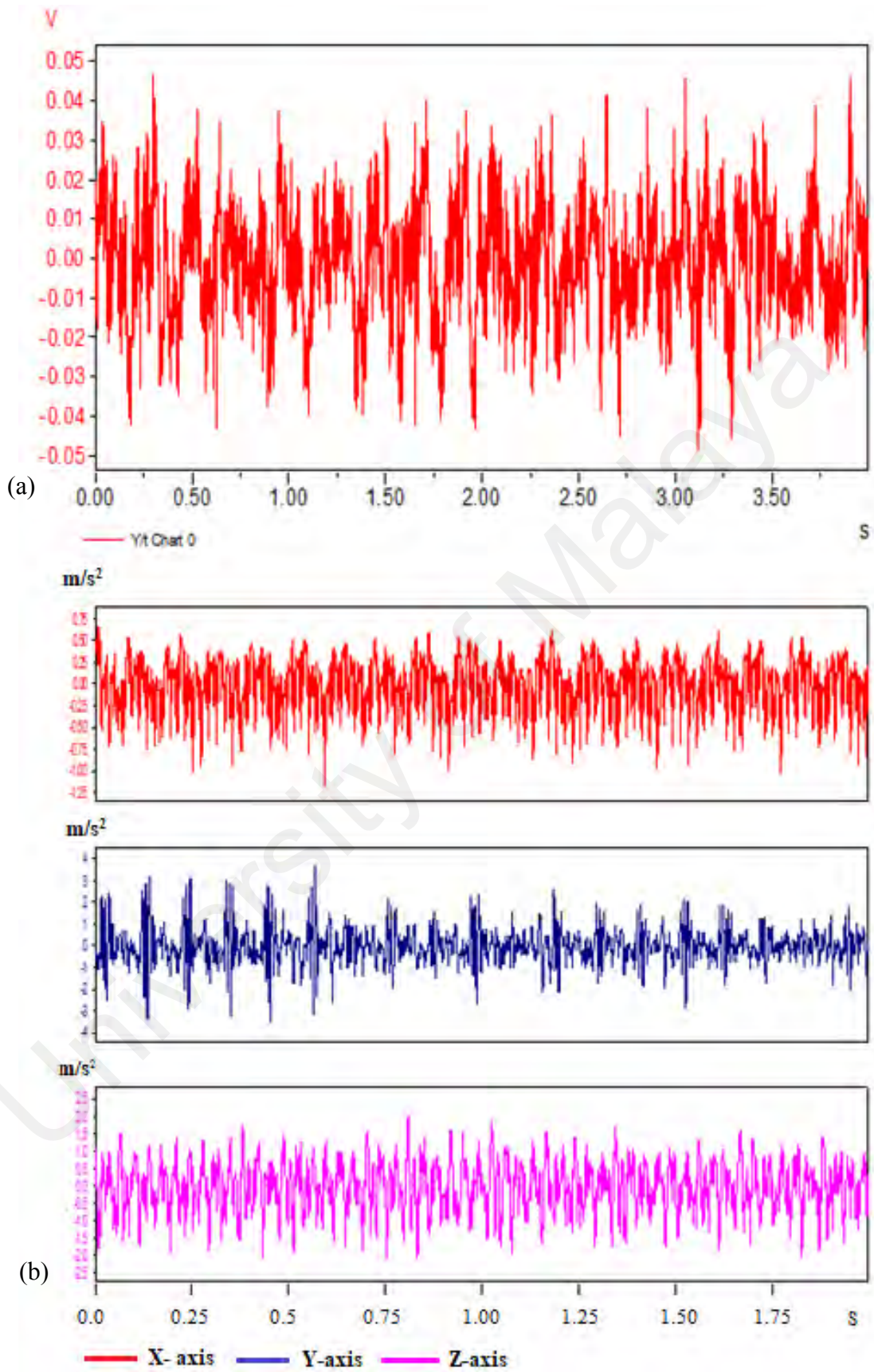


Figure 4.40: (a) The AC Voltage, (b) The Instantaneous Acceleration (i.e. x,y, and z) at Point 9 of VAWT Beam

4.9 The DC Energy Harvesting of VAWT

The PZnT-NT was attached to the point 1 where this point had higher displacement and the recorded voltage was compared with other commercial harvesters as presented in Figure 4.41. PZnT-NT produced higher power density than other harvesters. Accordingly, the harvested power values are illustrated in Figure 4.42 and the power densities are shown in Figure 4.43. All the recorded values are provided in Appendix D.1. The recorded data are available in D.4. The power density of the PZnT-NT was higher than that of PZT, MFC and the PZT bimorph. The power density was improved by 66%, 93.8% and 94% using the proposed PZnT-NT over the PZT, MFC and the PZT bimorph respectively. Beside to the prior explanations regarding the superiority of PZnT-NT power density comparing with PZT (i.e. cantilever test), the flat surface of the PZT and PZT bimorph weren't fitted totally (i.e. high stiffness) at the cylindrical surface of the axis VAWT whereas the PZnT-NT was mounted to capture the VAWT axis totally.

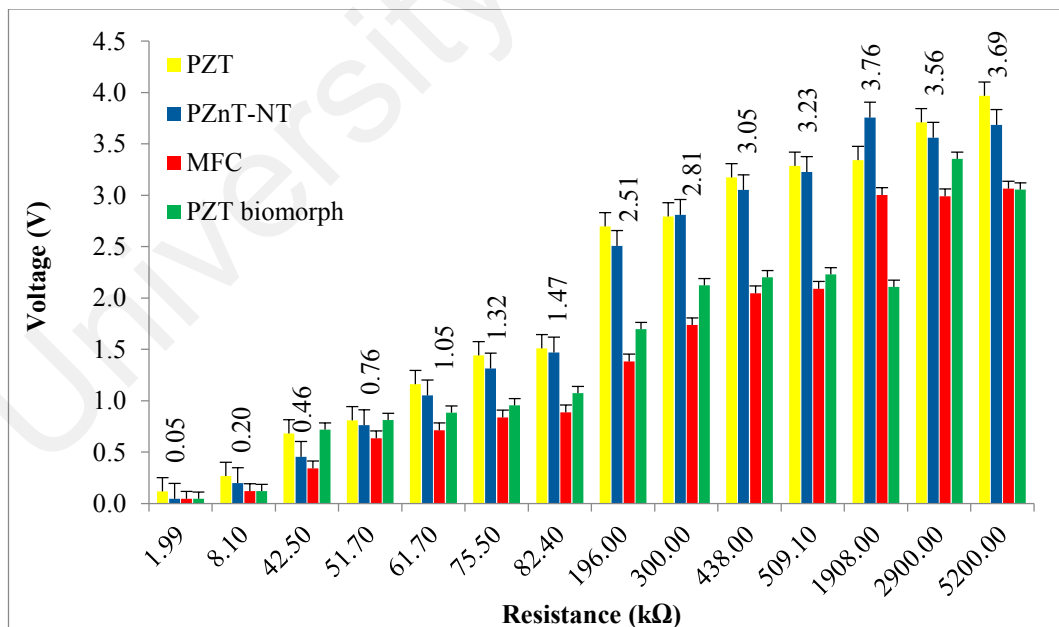


Figure 4.41: DC Voltage of PZnT-NT across Different Loads

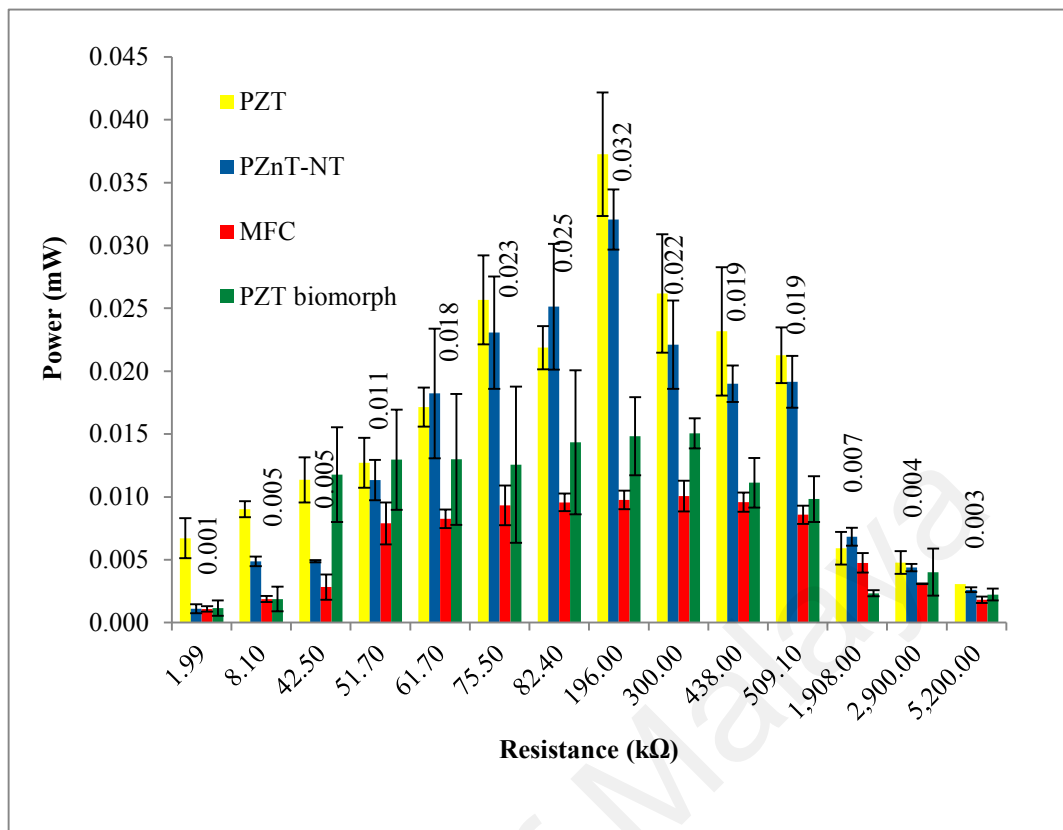


Figure 4.42: The Generated Power of the Piezoelectric Harvesters Compact to VAWT Structure

The generated power of the PZT is higher than that of PZnT-NT. The obtained results based the using the VAWT structure have semi-equal or close to the values that recorded by using the cantilever host structure. The large differences of voltage generation could take the place at the harvester only at its natural frequencies (e.g. 90 Hz). Similarly, for the case of power density, the power densities of PZT, PZnT-NT, MFC and PZT biomorph where PZnT-NT generated a power density of $0.107 \pm 0.008 \mu\text{W}/\text{mm}^3$ and for PZT it was $0.036 \pm 0.005 \mu\text{W}/\text{mm}^3$. MFC and PZT biomorph showed a comparable performance to each other. The standard deviation was calculated, and the size of the relative uncertainty was determined, the relative of error percentages that obtained were within 15%, thus the measurement is valid and reliable.

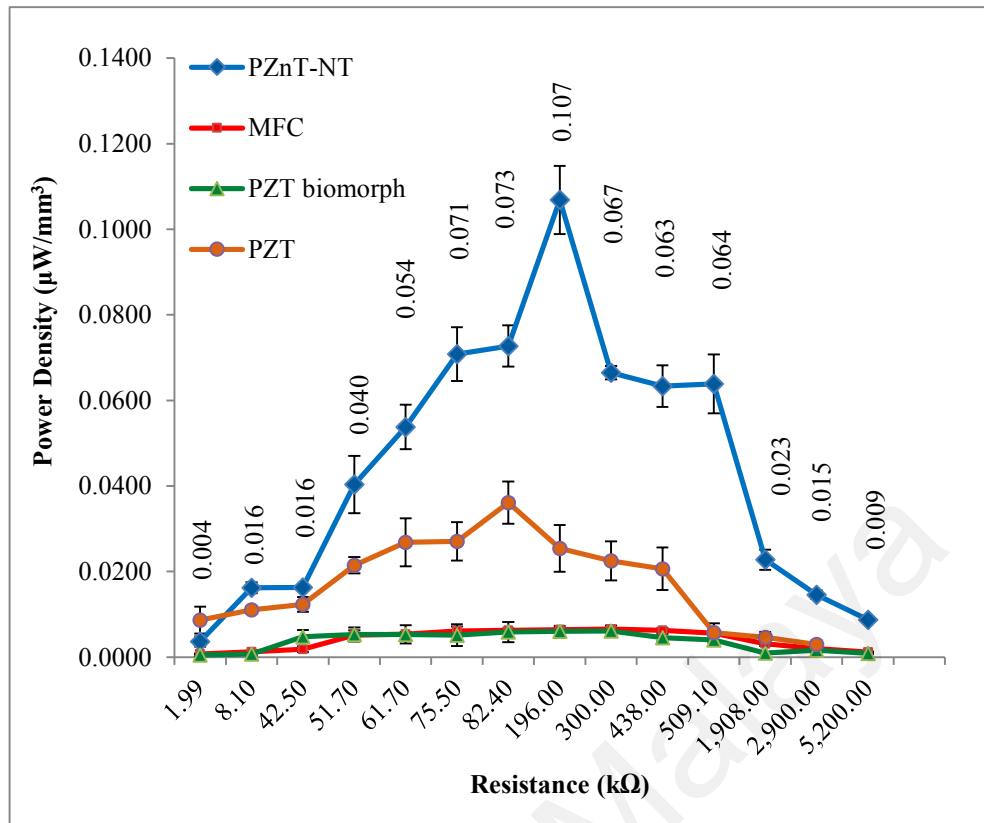


Figure 4.43: Optimal Power Density of PZnT-NT Comparing with Others Commercial Harvesters

4.10 Cost Analysis of the Piezoelectric Harvesters

In this section, the cost of piezoelectric harvesters and its harvesting performance is presented in the Table 4.5. Power generated per dollar of each harvester is calculated as well to compare the cost effectiveness of each piezoelectric harvester. It shows that the fabricated PZnT-NT harvester has the highest power generated per dollar, $(\frac{\mu\text{W}/\text{mm}^3}{\$}) \times 10^5$ (i.e. 7066.7 ± 733.3), compared to other harvesters such as PZT (i.e. 22.1 ± 1.4), MFC (i.e. 4.3 ± 0.4) and PZT bimorph (i.e. 35.0 ± 5.0). PZnT-NT harvester improved the cost effectiveness by approximately 320%, 1643%, 201% in the case of using PZT, MFC and PZT bimorph respectively. It is worthwhile to mention that the PZnT-NT was fabricated locally while others commercial harvesters such as PZT, MFC and PZT bimorph were bought from commercial foreign company in oversea. This is the main reason that causes a huge difference in the cost effectiveness of using PZnT-NT compared to other harvester in Malaysia. In future, if more piezoelectric manufacturer and companies presents in the local market in Malaysia, the price difference can be shortened due to tax exemption and cheaper transportation price. In short, this study shows that the usage of non-ferroelectric PZnT-NT presents a huge competitive advantage compared to the commercial ferroelectric harvester.

Table 4.5: List of the Utilized Harvesters and Performance and Prices

Harvester name	Part Number	Size (mm ³)	Price (1 piece)	Power Density ($\mu\text{W}/\text{mm}^3$)	Power Generated per Dollar $(\frac{\mu\text{W}/\text{mm}^3}{\$}) \times 10^5$
PZT	Quick-Mount, (T215-H4-503)	1029.8	\$217.00	0.048 \pm 0.003	(22.1 \pm 1.4)
MFC	M 8557 P2	1527.6	\$ 280.00	0.012 \pm 0.001	(4.3 \pm 0.4)
PZT Bimorph	N/A	1527.6	\$20.00	0.007 \pm 0.001	(35.0 \pm 5.0)
Current Work	PZnT-NT	2450.0	\$1.50	0.106 \pm 0.011	(7066.7 \pm 733.3)

CHAPTER 5: CONCLUSIONS AND RECOMMENDATIONS

5.1 Conclusion

This work introduces a novel harvester with high potentiality to harvest the vibration energy. A new material consisting of PbZnTiO_3 and Na_2TiO_3 is fabricated and tested. Furthermore, the research provides a strategy for selecting the optimal harvesting location over the vibrating structure such as the cantilever beam under shaker excitation or a VAWT beam under wind excitation. Specifically, this study is interested in harvesting the waste vibration energy of the VAWT. The optimal location has been detected using two non-destructive tests, namely the modal analysis and ODS analysis. In short, the research outcomes were recorded as follows.

- 1- A low cost non-ferroelectric $0.7\text{PbZn}_{0.3}\text{Ti}_{0.7}\text{O}_3$ - $0.3\text{Na}_2\text{TiO}_3$ generator is successfully fabricated via a wet chemical method for the vibration energy harvester. The fabricated PZnT-NT harvester consists of a ferroelectric material ($\text{PbZn}_{0.3}\text{Ti}_{0.7}\text{O}_3$) and an ion exchange material (Na_2TiO_3). The $\text{PbZn}_{0.3}\text{Ti}_{0.7}\text{O}_3$ has low ferroelectric properties and low conductivity. The enhancement of the $\text{PbZn}_{0.3}\text{Ti}_{0.7}\text{O}_3$ performance is achieved by increasing its conductivity (i.e., reducing the remnant polarisation) via increasing the Na_2TiO_3 weight percentage. Using this method, the permittivity can be increased, leading to power density enhancement.
- 2- The novel non-ferroelectric PZnT-NT generator demonstrates its ability to harvest the unwanted vibration energy from a vibrating cantilever beam, which is excited at a frequency and acceleration of 30 Hz and 0.4 m/s^2 respectively. The proposed harvester provides enough power to power an LED, indicating the practical application of the self-powered system. Furthermore, the results show that the PZnT-NT harvester has

produced the highest volume power density (i.e., $0.106 \pm 0.011 \mu\text{W}/\text{mm}^3$), when compared to the PZT (i.e. $0.048 \pm 0.003 \mu\text{W}/\text{mm}^3$), MFC (i.e. $0.012 \pm 0.001 \mu\text{W}/\text{mm}^3$) and PZT bimorphs (i.e. $0.007 \pm 0.001 \mu\text{W}/\text{mm}^3$). It is also, compared to other existing generators using the surface power density. The current work produces a surface power density of $10.6 \pm 1.1 \mu\text{W}/\text{cm}^2$ which is verified a great potentiality of PZnT-NT materials in harvesting a useful energy from low acceleration and low frequency environments.

3- Vibration data obtained from the EMA or ODS analyses are utilised in selecting an optimal harvesting location on a vibrating structure, i.e. cantilever test rig. The optimal location, (i.e. ideal point with highest vibration energy / anti-nodal points) that determined by the location selection scheme can yield high power output. Meanwhile, if the piezoelectric plate is placed at any minimal vibration points or nodal point on the structure as determined by the location selection scheme, a low power output will be obtained. At the second resonance mode (95.2 Hz), implemented the harvesters at the nodal points such as at point 9 can yield reductive of harvesting voltage by up to 77%. The proposed cantilever based PZnT-NT system can be produced voltages from micro-vibration, where the maximum and minimum recorded displacements at a frequency of 90 Hz were $[0.6 \text{ } 4.5] \mu\text{m}$ at 9 examined locations. When this piezoelectric plate is placed on the operating cantilever beam and excited at 90 Hz, it is observed there is a 28% reduction in harvested voltage based on the baseline voltage.

4- The modal analysis and ODS analysis are carried out to identify the optimal location of the VAWT beam. It is observed that the diffuser affects the air flow of the exhaust air system and is the cause of significant vibration pattern towards the y-axis. The overall animated movement is an elliptical path and the optimal location is located at the free end. The PZnT-NT is implemented on the VAWT at its optimal location (i.e.

point 1) whereas implementing the harvester at point 9 has yielded a reduction of voltage at a percentage of 73%. Finally, the PZnT-NT is implemented over the VAWT beam and it created a successful harvesting (DC-voltage) of the waste vibration energy. The power density of the PZnT-NT is higher than that of PZT, MFC and the PZT bimorph whereby the improvement of power density are 66%, 93.8%, and 94% respectively.

- 5- The fabrication of PZnT-NT has high cost effective comparing with other commercial harvesters.

5.2 Recommendations

For future works, it is recommended to further the enhancement of manufacturing the PZnT-NT harvester. This can be done by synthesising it with high accuracy using sophisticated industrial processes (e.g. thin/ thick film manufacturing processes, tape casting, pulsed laser deposition (PLD), sputtering, spinning, screen-printing and to numerous others manufacturing methods). Increasing the area of the harvester, studying the potentiality of connecting many harvesters in serial and parallel manners, developing smart electronic rectifier circuits such as AC-DC and DC-DC, as well as, selecting the harvester of optimal stiffness.

The PZnT-NT can be fabricated as a flexible and wearable address, but it can also be designed based on the Schottky contact theory; or advocate the $p-n$ junction technique where the pure PZnT-NT with additive (n -type) layer that integrate with Na_2TiO_3 (p -type layer) to format $p-n$ junction contact where the generated signal can be rectified instantaneously upon continuous pressing.

This study demonstrated that the mode shape and vibration pattern that were obtained from the EMA and ODS analysis could assist users in determining the optimal location for harvesting the maximum voltage for the cantilever system under motor excitation, as well as the VAWT structure under complex wind excitation (i.e. dynamically change over

time). It is recommended to utilise the location selection scheme for detecting the optimal location over any vibrated beam, where the EMA and ODS are useful tools that can provide the ability to visualise the mode shape and vibration pattern of beam. In real life, the structures excite in several directions instantaneously and thus, the utilising of the tri-axial accelerometers will provide FRF sets in numerous DOF directions. It is recommended to utilise the location selection scheme for detecting the optimal location over other parts of exhaust air-cooling tower, where the EMA and ODS are useful tools that provide the ability to visualise the mode shape and vibration pattern of the beam. In real life, the structures excite in several directions (DOF) instantaneously and thus, the utilisation of the tri-axial accelerometers will assist in recording the response and visualising the mode shape in numerous DOF directions. Precaution: User should not assume that the optimum location obtained from this study will be the same as other similar structure. This is because different system might have different dynamic characteristics and different operating frequencies. Thus, we must conduct the EMA and ODS to understand the complex relationship between the wind excitation force and the structure's dynamic behaviour every time before we implement the piezoelectric harvester to a new structure/ system.

The pyroelectric property of material can be assisted of increasing the generated voltage. Thus, the material can be utilised for convert the heat energy to useful electrical energy.

Finally, it recommended to fabricate such harvester locally due to it have high cost effective

REFERENCES

- Abdullah, A. F. (2016). *Design and testing of a novel exhaust air energy recovery wind turbine generator* (Doctoral thesis, University of Malaya, Kuala Lumpur, Malaysia). Retrieved from <http://studentsrepo.um.edu.my/6405/>
- Ajitanath, P. (2014). Cost reduction of a product through value analysis & value engineering. *International Journal of Industrial*, 4 (6), 2278-9456.
- Al-Ashtari, W., Hunstig, M., Hemsel, T., & Sextro, W. (2013). Increasing the power of piezoelectric energy harvesters by magnetic stiffening. *Journal of Intelligent Material Systems and Structures*, 24(11): 1332-1342.
- Alam, M. M., Ghosh, S. K., Sultana, A., & Mandal, D. (2015). Lead-free ZnSnO₃/MWCNTs-based self-poled flexible hybrid nanogenerator for piezoelectric power generation. *Nanotechnology*, 26(16), 165403.
- Amor, N. B., Kanoun, O., Lay-Ekuakille, A., Specchia, G., Vendramin, G., & Trotta, A. (2008). Energy harvesting from human body for biomedical autonomous systems. *Proceedings of the Sensors, Lecce, Italy* (pp. 678-680). New Jersey, USA: IEEE.
- Amorín, H., Correas, C., Ramos, P., Hungría, T., Castro, A., & Algueró, M. (2012). Very high remnant polarisation and phase-change electromechanical response of BiFeO₃-PbTiO₃ at the multiferroic morphotropic phase boundary. *Applied Physics Letters*, 101(17), 172908.
- Anton, S. R., & Sodano, H. A. (2007). A review of power harvesting using piezoelectric materials (2003–2006). *Smart materials and Structures*, 36(3), 197-205.
- APC International, L. (2013). Piezo igniters. Retrieved from <https://www.americanpiezo.com/standard-products/piezo-igniters.html>
- APC International, L. (2014). Soft vs. Hard ceramics. Retrieved from <https://www.americanpiezo.com/piezo-theory/ceramics.html>
- Audigier, D., Eyraud, L., Eyraud, P., Eyraud, F., Glissa, N., Gonnard, P., ... & Sprumont, M. (1991, August). Typical characteristics of a piezoelectric ceramic material for squeeze igniters. *Proceedings of the Ninth IEEE International Symposium on* (pp. 383-386). University Park, PA, USA: IEEE. Retrieved from <https://ieeexplore.ieee.org/document/522382/>

- Avitabile, P. (1998). Is there a difference between a roving hammer and roving accelerometer test. Retrieved from https://www.uml.edu/docs/aug98_tcm18-189812.pdf
- Avvari, P. V., Yang, Y., & Soh, C. K. (2016). Long-term fatigue behaviour of a cantilever piezoelectric energy harvester. *Journal of Intelligent Material Systems and Structures*, 28(9), 1188-1210.
- Ayed, S. B., Najjar, F., & Abdelkefi, A. (2009). Shape improvement for piezoelectric energy harvesting applications, *Proceedings of the 3rd International Conference on Signals, Circuits and Systems, Medenine, Tunisia* (pp. 1-6). USA: IEEE.
- Babu, I., & de With, G. (2014). Enhanced electromechanical properties of piezoelectric thin flexible films. *Composites Science and Technology*, 104, 74-80.
- Baker, J., Roundy, S., & Wright, P. (2005). Alternative geometries for increasing power density in vibration energy scavenging for wireless sensor networks. *Proceedings of the Third International Energy Conversion Engineering, San Francisco, CA.* (pp.5617). USA : AIAA.
- Banerjee, S., & Cook-Chennault, K. (2012). An investigation into the influence of electrically conductive particle size on electromechanical coupling and effective dielectric strain coefficients in three phase composite piezoelectric polymers. *Composites Part A: Applied Science and Manufacturing*, 43(9), 1612-1619.
- Baudry, H. (1987). Screen printing piezoelectric devices. *Microelectronics International*, 4(3), 71-74.
- Beeby, S. P., Torah, R., Tudor, M., Glynne-Jones, P., O'Donnell, T., Saha, C., & Roy, S. (2007). A micro electromagnetic generator for vibration energy harvesting. *Journal of Micromechanics and Microengineering*, 17(7), 1257.
- Beeby, S. P., Tudor, M. J., & White, N. M. (2006). Energy harvesting vibration sources for microsystems applications. *Measurement science and technology*, 17(12), 175-195.
- Berdy, D. F., Srisungsitthisunti, P., Jung, B., Xu, X., Rhoads, J. F., & Peroulis, D. (2012). Low-frequency meandering piezoelectric vibration energy harvester. *IEEE transactions on ultrasonics, ferroelectrics, and frequency control*, 59(5), 846-858.

- Bhavanasi, V., Kumar, V., Parida, K., Wang, J., & Lee, P. S. (2015). Enhanced piezoelectric energy harvesting performance of flexible pvdF-trfe bilayer films with graphene oxide. *ACS Applied Materials & Interfaces*, 8(1), 521-529.
- Bosotti, A., Paparella, R., Puricelli, F. (2004). *PI Piezo lifetime test report*. Retrieved from <http://irfu.cea.fr/Phocea/file.php?class=std&file=Doc/Care/note-2005-020-SRF.pdf>.
- Bowen, C., Kim, H., Weaver, P., & Dunn, S. (2014). Piezoelectric and ferroelectric materials and structures for energy harvesting applications. *Energy & Environmental Science*, 7(1), 25-44.
- Bressers, S., Avirovik, D., Lallart, M., Inman, D. J., & Priya, S. (2011). Contact-less wind turbine utilising piezoelectric bimorphs with magnetic actuation. *Proceedings of the Society for Experimental Mechanics Series*, Bethel, CT (pp. 233-243). USA: Springer New York, NY.
- Briscoe, J., Jalali, N., Woolliams, P., Stewart, M., Weaver, P. M., Cain, M., & Dunn, S. (2013). Measurement techniques for piezoelectric nanogenerators. *Energy & Environmental Science*, 6(10), 3035-3045.
- Byrappa, K., & Yoshimura, M. (2012). *Handbook of hydrothermal technology*, Norwich, NY.: William Andrew.
- Callister, W. D., & Rethwisch, D. G. (2000). *Fundamentals of materials science and engineering*, London, UK: Wiley.
- Calculator, E. u. (2018). Electricity usage of an an Electric furnace. Retrieved from http://energyusecalculator.com/electricity_furnace.htm
- Cao, W. (2005). Ferroelectrics: The strain limits on switching. *Nat Mater*, 4(10), 727-728.
- Celina, M. C., Elliott, J. M., Chaplya, P. M., Jones, G. D., Mowery, D. M., Assink, R. A., & ... Martin, J. W. (2005). Characterisation, performance and optimisation of PVDF as a piezoelectric film for advanced space mirror concepts. *Sandia National Laboratories reports*, SAND2005-6846. Retrieved from <https://prod.sandia.gov/techlib-noauth/access-control.cgi/2005/056846.pdf>
- Ceramic, P. M.-P. (2013). Retrieved from www.piceramic.com/pdf/piezo_material.pdf

- Çevik, G., Akşit, M. F. Asif Şabanoviç. (2011). *Piezoelectric wind power harnessing – an overview. Proceedings of the International nce on Sustainable Energy Technologies, İstanbul* (pp. 1-9). Türkiye: Sabanci University Research Database. Retrieved from <http://research.sabanciuniv.edu/18850/>
- Chih-Ta Chen, R. A. I., and Shashank Priya. (2006). Electric energy generator. *IEEE transactions on ultrasonics, ferroelectrics, and frequency control*, 53(3).
- Cornwell, P., Goethal, J., Kowko, J., & Damianakis, M. (2005). Enhancing power harvesting using a tuned auxiliary structure. *Journal of Intelligent Material Systems and Structures*, 16(10), 825-834.
- Cornwell, P. J., Goethal, J., Kowko, J., & Damianakis, M. (2005). Enhancing power harvesting using a tuned auxiliary structure. *Journal of Intelligent Material Systems and Structures*, 16(10), 825-834.
- Craciun, F., Verardi, P., Dinescu, M., & Guidarelli, G. (1999). Reactive pulsed laser deposition of piezoelectric and ferroelectric thin films. *Thin Solid Films*, 343, 90-93.
- Dakua, I., & Afzulpurkar, N. (2013). Piezoelectric energy generation and harvesting at the nano-scale: materials and devices. *Nanomaterials and Nanotechnology*, 3, 21.
- Daniel, M., Lavarda, Jairo Vinicius, Dias, Felipe Aguiar, & Silva, Samuel da. (2012). Vibration energy harvesting using piezoelectric transducer and non-controlled rectifiers circuits. *Journal of the Brazilian Society of Mechanical Sciences and Engineering*, 34(spe), 378-385.
- Daniels, A., Meiling, Z., & Tiwari, A. (2013). Evaluation of piezoelectric material properties for a higher power output from energy harvesters with insight into material selection using a coupled piezoelectric-circuit-finite element method. *IEEE Transactions on Ultrasonics, Ferroelectrics and Frequency Control*, 60(12), 2626-2633.
- Davidson, J., & Mo, C. (2014). Recent advances in energy harvesting technologies for structural health monitoring applications. *Smart Materials Research*, 2014(410316), 1-14.
- Defay, E. (Ed.) (2013). *Integration of ferroelectric and piezoelectric thin films: concepts and applications for microsystems*, USA: John Wiley & Sons.

- Do, Y. H., Jung, W. S., Kang, M. G., Kang, C. Y., & Yoon, S. J. (2013). Preparation on transparent flexible piezoelectric energy harvester based on PZT films by laser lift-off process. *Sensors and Actuators A: Physical*, 200, 51-55.
- Du, X.-h., Wang, Q.-M., Belegundu, U., Bhalla, A., & Uchino, K. (1999). Crystal orientation dependence of piezoelectric properties of single crystal barium titanate. *Materials Letters*, 40(3), 109-113.
- Dutoit, N. E., Wardle, B. L., & Kim, S. G. (2005). Design considerations for MEMS-scale piezoelectric mechanical vibration energy harvesters. *Integrated Ferroelectrics*, 71(1), 121-160.
- Eggborn, T. (2003). *Analytical models to predict power harvesting with piezoelectric materials* (Doctoral thesis ,Virginia Tech, Blacksburg, VA 24061, USA). Retrieved from <http://scholar.lib.vt.edu/theses/available/etd-05192003-150202/unrestricted/EggbornThesis1.pdf>
- Erturk, A., & Inman, D. J. (2008). On mechanical modeling of cantilevered piezoelectric vibration energy harvesters. *Journal of Intelligent Material Systems and Structures*, 19(11), 1311-1325.
- Erturk, A., Tarazaga, P. A., Farmer, J. R., & Inman, D. J. (2009). Effect of strain nodes and electrode configuration on piezoelectric energy harvesting from cantilevered beams. *Journal of Vibration and Acoustics*, 131(1), 011010.
- Esterly, D. M. (2002). *Manufacturing of poly (vinylidene fluoride) and evaluation of its mechanical properties* (Doctoral dissertation, Virginia Tech, Blacksburg, USA), Retrieved from <https://vtechworks.lib.vt.edu/bitstream/handle/10919/34677/Desterly.pdf>
- Eyraud, L., Guiffard, B., Audigier, D., Lebrun, L., & Guyomar, D. (2008). Electron transfer mechanism in PZT ceramics application to squeeze ignition. *Ferroelectrics*, 366(1), 37-44.
- Fan, F.-R., Tian, Z.-Q., & Lin Wang, Z. (2012). Flexible triboelectric generator. *Nano Energy*, 1(2), 328-334.
- Fang, H.-B., Liu, J.-Q., Xu, Z.-Y., Dong, L., Wang, L., Chen, D., . . . Liu, Y. (2006). Fabrication and performance of MEMS-based piezoelectric power generator for vibration energy harvesting. *Microelectronics Journal*, 37(11), 1280-1284.

- Ferrari, M., Ferrari, V., Guizzetti, M., Andò, B., Baglio, S., & Trigona, C. (2010). Improved energy harvesting from wideband vibrations by nonlinear piezoelectric converters. *Sensors and Actuators A: Physical*, 162(2), 425-431.
- Fufa. (2017). Thin film Silk screen printing machine. Retrieved from http://www.chinascreenprintingmachine.com/products.html?gclid=EAIaIQobChMIl-fzsqW93AIVwxOPCh1JDQGREAAAYASAAEgJ-__D_BwE
- Gao, T., Liao, J., Wang, J., Qiu, Y., Yang, Q., Zhang, M., . . . Wang, Q.-m. (2015). Highly oriented BaTiO₃ film self-assembled using an interfacial strategy and its application as a flexible piezoelectric generator for wind energy harvesting. *Journal of Materials Chemistry A*, 3(18), 9965-9971.
- GmbH, P. C. (2017a). Piezo Elements Made by Pressing Technology. Retrieved from (<https://www.piceramic.com/en/piezo-technology/manufacturing-technology/pressing/>)
- Gretarsson, D. (2007). *Energy harvesting using piezoelectric generators* (Bachelor's thesis, Technical University of Denmark, DTU, DK-2800 Kgs. Lyngby, Denmark). Retrieved from <https://docplayer.net/21753299-Energy-harvesting-using-piezoelectric-generators-dagur-gretarsson-s021235.html>
- Guan, M., & Liao, W.-H. (2016). Design and analysis of a piezoelectric energy harvester for rotational motion system. *Energy Conversion and Management*, 111, 239-244.
- Gupta, M. K., Kim, S.-W., & Kumar, B. (2016). Flexible high performance lead-free Na_{0.47}K_{0.47}Li_{0.06}NbO₃ microcubes-structures based piezoelectric energy harvester. *ACS Applied Materials & Interfaces*, 8(3), 1766-1773
- Gusarov, B. (2015). *PVDF piezoelectric polymers: characterisation and application to thermal energy harvesting* (Doctoral dissertation, Université Grenoble Alpes, venue Centrale, France). Retrieved from <https://tel.archives-ouvertes.fr/tel-01241414/document>
- Haccart, T., Cattan, E., & Remiens, D. (2002). Dielectric, ferroelectric and piezoelectric properties of sputtered PZT thin films on Si substrates: influence of film thickness and orientation. *Semiconductor Physics, Quantum Electronics & Optoelectronics*, 5(1), 78-88.
- Haffey, C. (2013). Short circuits. Retrieved from <https://www.youtube.com/watch?v=GGVlaQbeJHo>

- Hau, S. K., Wong, K. H., Chan, P. W., & Choy, C. L. (1995). Intrinsic resputtering in pulsed- laser deposition of lead- zirconate- titanate thin films. *Applied Physics Letters*, 66(2), 245-247.
- He, X., Shang, Z., Cheng, Y., & Zhu, Y. (2013). A micromachined low-frequency piezoelectric harvester for vibration and wind energy scavenging. *Journal of Micromechanics and Microengineering*, 23(12), 125009.
- Herlufsen, H. (2004). Modal analysis using multi-reference and multiple-input multiple-output techniques. Retrieved from <https://www.semanticscholar.org/paper/Modal-Analysis-using-Multi-reference-and-Techniques-Herlufsen/1ffbaf1a3b592ae49907db476a7848cd7f9bab3e>
- Hu, S., Shen, S. Y., & Han, H. C. (2010). Preparation and properties of PZN-PZT/PVDF piezoelectric composites modified by graphite, *Advances in Liquid Crystals*, 428, 552-555
- Iijima, T., Ito, S., Matsuda, H., Dugnani, R., & Chang, F.-K. (2004). Ferroelectric and piezoelectric properties of disk shape lead zirconate titanate thick films. *Materials Transactions*, 45(2), 233-235.
- Institute, T. P. (2016). Energy. Retrieved from <http://www.piezoinstitute.com/applications/energy/>
- Islam, R. A., & Priya, S. (2006). High-energy density ceramic composition in the system $\text{Pb}(\text{Zr},\text{Ti})\text{O}_3\text{-Pb}[(\text{Zn},\text{Ni})_{1/3}\text{Nb}_{2/3}]\text{O}_3$. *Journal of the American Ceramic Society*, 89(10), 3147-3156.
- Islam, R. A., & Priyaa, S. (2006). Realisation of high-energy density polycrystalline piezoelectric ceramics. *Applied Physics Letters*, 88(032903).
- Jalali, N., Briscoe, J., Tan, Y. Z., Woolliams, P., Stewart, M., Weaver, P. M., . . . Dunn, S. (2015). ZnO nanorod surface modification with PDDA/PSS Bi-layer assembly for performance improvement of ZnO piezoelectric energy harvesting devices. *Journal of Sol-Gel Science and Technology*, 73(3), 544-549.
- Jalali, N., Briscoe, J., Woolliams, P., Stewart, M., Weaver, P. M., Cain, M., & Dunn, S. (2013). Passivation of zinc oxide nanowires for improved piezoelectric energy harvesting devices. *Proceedings of the 13th International Conference on Micro and Nanotechnology for Power Generation and Energy Conversion Application* (pp. 012131), London: IOP Publishing.

- Jan Tichý, Jiří Erhart, Kittinger, E., and, & Přivratská, J. (2010a). *Fundamentals of piezoelectric sensorics*, Berlin: Springer Heidelberg Dordrecht London New York.
- Jan Tichý, Jiří Erhart, Kittinger, E., and, & Přivratská, J. (2010b). *Fundamentals of piezoelectric sensorics*, Berlin: Springer Heidelberg Dordrecht London New York.
- Jantunen, H., Hu, T., Uusimäki, A., & Leppävuori, S. (2004). Tape casting of ferroelectric, dielectric, piezoelectric and ferromagnetic materials. *Journal of the European Ceramic Society*, 24(6), 1077-1081.
- Jeong, C. K., Lee, J., Han, S., Ryu, J., Hwang, G. T., Park, D. Y., . . . Ko, S. H. (2015). A Hyper- stretchable elastic- composite energy harvester. *Advanced Materials*, 27(18), 2866-2875.
- Johnson, M. (1997). Sensor arrangement for ice bank control, Retrieved from <https://www.google.com/patents/US5627310>
- Joo, J., Chow, B. Y., Prakash, M., Boyden, E. S., & Jacobson, J. M. (2011). Face-selective electrostatic control of hydrothermal zinc oxide nanowire synthesis. *Nature materials*, 10(8), 596.
- Jung, J. H., Lee, M., Hong, J.-I., Ding, Y., Chen, C.-Y., Chou, L.-J., & Wang, Z. L. (2011). Lead-free NaNbO₃ nanowires for a high output piezoelectric nanogenerator. *ACS Nano*, 5(12), 10041-10046.
- Jung, W.-S., Kang, M.-G., Moon, H. G., Baek, S.-H., Yoon, S.-J., Wang, Z.-L., . . . Kang, C.-Y. (2015). High output piezo/triboelectric hybrid generator. *Scientific reports*, 5, 9309.
- Junker. (2017). Centerless cylindrical grinding. Retrieved from <http://pdf.directindustry.com/pdf/erwin-junker-maschinenfabrik-gmbh/titan/9216-743136.html>
- Kakegawa, K., Matsunaga, O., Kato, T., & Sasaki, Y. (1995). Compositional change and compositional fluctuation in Pb (Zr, Ti) O₃ containing excess PbO. *Journal of the American Ceramic Society*, 78(4), 1071-1075.
- Kang, M.-G., Jung, W.-S., Kang, C.-Y., & Yoon, S.-J. (2016). Recent progress on PZT based piezoelectric energy harvesting technologies. *Actuators*, 5(1), 5.

- Karan, S. K., Mandal, D., & Khatua, B. B. (2015). Self-powered flexible Fe-doped RGO/PVDF nanocomposite: An excellent material for a piezoelectric energy harvester. *Nanoscale*, 7(24), 10655-10666.
- Keppens, V. (2016). Piezoelectric materials' Ferroelectricity' in a metal. Retrieved from http://www.nature.com/nmat/journal/v12/n11/fig_tab/nmat3774_F1.html
- Keith. (2017). 1700°C Front or bottom loading furnaces. Retrieved from <https://www.keithcompany.com/1700c-box-furnace-front-loading-furnace.html>
- Physik Instrumente, PI, GmbH & Co. KG. (2013). Piezo materials based on lead zirconate Titanate (PZT). Retrieved from <https://www.physikinstrumente.com/en/technology/piezo-technology/piezoelectric-materials/>
- Khoo, S. Y., Radeef, Z. S., Ong, Z. C., Huang, Y.-H., Chong, W. T., & Ismail, Z. (2017). Structural dynamics effect on voltage generation from dual coupled cantilever based piezoelectric vibration energy harvester system. *Measurement*, 107, 41-52.
- Kim, H.-U., Lee, W.-H., Dias, H. R., & Priya, S. (2009). Piezoelectric microgenerators-current status and challenges. *IEEE transactions on ultrasonics, ferroelectrics, and frequency control*, 56(8), 1555-1568.
- Kim, H., Priya, S., Stephanou, H., & Uchino, K. (2007). Consideration of impedance matching techniques for efficient piezoelectric energy harvesting. *IEEE transactions on ultrasonics, ferroelectrics, and frequency control*, 54(9).
- Kim, H. T., Nahm, S., Byun, J. D., & Kim, Y. (1999). Low- fired (Zn, Mg) TiO₃ microwave dielectrics. *Journal of the American Ceramic Society*, 82(12), 3476-3480.
- Kim, H. W., Batra, A., Priya, S., Uchino, K., Markley, D., Newnham, R. E., & Hofmann, H. F. (2004). Energy harvesting using a piezoelectric "Cymbal" transducer in dynamic environment. *Japanese Journal of Applied Physics*, 43(9R), 6178.
- Kim, I.-H., Jung, H.-J., Lee, B. M., & Jang, S.-J. (2011). Broadband energy-harvesting using a two degree-of-freedom vibrating body. *Applied Physics Letters*, 98(21), 214102.
- Kittel, C. (1951). Theory of antiferroelectric crystals. *Physical Review*, 82(5), 729.

- Kmwe. (2017). Concept & value engineering. Retrieved from https://www.kmwe.com/Capabilities/Engineering/concept_value.htm
- Kok, S. L. (2011). Energy harvesting technologies: Thick-film piezoelectric microgenerator, *Sustainable Energy Harvesting Technologies-Past, Present and Future* (pp.192-214). London, Unit Kindum: InTech.
- Kong, L. B., Ma, J., Zhang, R. F., Zhu, W., & Tan, O. K. (2002). Lead zirconate titanate ceramics achieved by reaction sintering of PbO and high-energy ball milled (ZrTi)O₂ nanosized powders. *Materials Letters*, 55(6), 370-377.
- Kumar, B., Lee, K. Y., Park, H.-K., Chae, S. J., Lee, Y. H., & Kim, S.-W. (2011). Controlled growth of ZnO nanowire, nanowall, and hybrid nanostructures on graphene for piezoelectric nanogenerators, *Acs Nano*, 5(5), 4197-4204.
- Kumar Singh, D., Srivastava, R., & Srivastava, R. (2014). Analysis of energy harvesting from vibrating structure. *MIT International Journal of Mechanical Engineering*, 4(2), 100-103.
- Kumari, N., Singh, A., & Mandal, J. (2013). Lead zirconate titanate piezoelectric ceramics with nickel oxide additions. *International Refereed Journal of Engineering and Science*, 2, 51-55.
- Lebrun, L., Sebald, G., Guiffard, B., Richard, C., Guyomar, D., & Pleska, E. (2004). Investigations on ferroelectric PMN-PT and PZN-PT single crystals ability for power or resonant actuators. *Ultrasonics*, 42(1), 501-505.
- Lee, K. Y., Kim, D., Lee, J. H., Kim, T. Y., Gupta, M. K., & Kim, S. W. (2014). Unidirectional high- power generation via stress- induced dipole alignment from ZnSnO₃ nanocubes/polymer hybrid piezoelectric nanogenerator. *Advanced Functional Materials*, 24(1), 37-43.
- Lee, K. Y., Kumar, B., Seo, J.-S., Kim, K.-H., Sohn, J. I., Cha, S. N., . . . Kim, S.-W. (2012). P-type polymer-hybridized high-performance piezoelectric nanogenerators. *Nano Letters*, 12(4), 1959-1964.
- Lee, S. G., & Kim, S. D. (2006). Piezoelectric vibrator with multi acting vibrator: Google Patents. Retrieved from <https://patents.google.com/patent/WO2006059856A1/en17>
- Lee, Y. B., Han, J. K., Noothongkaew, S., Kim, S. K., Song, W., Myung, S., . . . An, K. S. (2016). Toward arbitrary- direction energy harvesting through flexible

piezoelectric nanogenerators using perovskite PbTiO_3 nanotube arrays. *Advanced Materials*, 29(6), 1604500.

Leland, E. S., Lai, E. M., & Wright, P. K. (2004). A self-powered wireless sensor for indoor environmental monitoring. *Proceedings of the Wireless Networking Symposium, University of Texas at Austin Department of Electrical & Computer Engineering* (pp 1-5). TX.: WNCG.

Li, S., Yuan, J., & Lipson, H. (2011). Ambient wind energy harvesting using cross-flow fluttering, *Journal of Applied Physics*, 109(2), 026104.

Li, X., Song, J., Feng, S., Xie, X., Li, Z., Wang, L., . . . Lu, W. (2016). High-efficiency piezoelectric micro harvester for collecting low-frequency mechanical energy. *Nanotechnology*, 27(48), 485402.

Liao, Y., & Sodano, H. A. (2012a). Optimal placement of piezoelectric material on a cantilever beam for maximum piezoelectric damping and power harvesting efficiency. *Smart Materials and Structures*, 21(10), 105014.

Liao, Y., & Sodano, H. A. (2012b). Optimal placement of piezoelectric material on a cantilever beam for maximum piezoelectric damping and power harvesting efficiency. *Smart materials and Structures*, 21(10), 105014: 105011-105019.

Limited;, T. S. F., & Kanagawa, K.-s. (2008a). Ferroelectric memory device Retrieved from <https://www.google.com/patents/EP0923135B1?cl=en>

Limited, S., F., L.(2008). Ferroelectric memory device, *European Patent Office*. Retrieved from <https://www.google.com/patents/EP0923135B1?cl=en>

Ltd, T. (2018). Sol-gel processing. Retrieved from <https://www.twi-global.com/technical-knowledge/faqs/faq-what-is-sol-gel-processing/>

Lin, L., Hu, Y., Xu, C., Zhang, Y., Zhang, R., Wen, X., & Lin Wang, Z. (2013). Transparent flexible nanogenerator as self-powered sensor for transportation monitoring. *Nano Energy*, 2(1), 75-81.

Lin, Z.-H., Yang, Y., Wu, J. M., Liu, Y., Zhang, F., & Wang, Z. L. (2012). BaTiO_3 nanotubes-based flexible and transparent nanogenerators. *The Journal of Physical Chemistry Letters*, 3(23), 3599-3604.

Liu, H., Tay, C. J., Quan, C., Kobayashi, T., & Lee, C. (2011). Piezoelectric MEMS energy harvester for low-frequency vibrations with wideband operation range and

steadily increased output power. *Journal of Microelectromechanical Systems*, 20(5), 1131-1142.

Liu, H., Zhang, S., Kobayashi, T., Chen, T., & Lee, C. (2014). Flow sensing and energy harvesting characteristics of a wind-driven piezoelectric Pb (Zr_{0.52}, Ti_{0.48}) O₃ microcantilever. *Micro & Nano Letters*, 9(4), 286-289.

Liu, J.-Q., Fang, H.-B., Xu, Z.-Y., Mao, X.-H., Shen, X.-C., Chen, D., . . . Cai, B.-C. (2008). A MEMS-based piezoelectric power generator array for vibration energy harvesting. *Microelectronics Journal*, 39(5), 802-806.

Liu, L., Lu, K., Wang, T., Liao, F., Peng, M., & Shao, M. (2015). Flexible piezoelectric nanogenerators based on silicon nanowire/ α -quartz composites for mechanical energy harvesting. *Materials Letters*, 160, 222-226.

Liu, W., & Ren, X. (2009). Large piezoelectric effect in Pb-free ceramics. *Physical Review Letters*, 103(25), 257602.

Lu, B., Chen, Y., Ou, D., Chen, H., Diao, L., Zhang, W., . . . Feng, X. (2015). Ultra-flexible piezoelectric devices integrated with heart to harvest the biomechanical energy. *Scientific Reports*, 5, 16065.

Lumentut, M. F., & Howard, I. M. (2014). Intrinsic geometries and properties of piezo-MEMS power harvesters with tip mass offset using new electromechanical finite element vibration analysis. *Proceedings of the Advanced Intelligent Mechatronics IEEE/ASME International Conference* (pp. 760-765). France: IEEE

Lund, A., Jonasson, C., Johansson, C., Haagensen, D., & Hagström, B. (2012). Piezoelectric polymeric bicomponent fibers produced by melt spinning. *Journal of Applied Polymer Science*, 126(2), 490-500.

Mann, B., & Sims, N. (2009). Energy harvesting from the nonlinear oscillations of magnetic levitation. *Journal of Sound and Vibration*, 319(1), 515-530.

Material, S. (2015). Macro fiber composite (MFC). Retrieved from <http://www.smart-material.com/MFC-product-main.html>

Material, S. (2016). Energy harvesting overview. Retrieved from <http://www.smart-material.com/EH-product-main.html>

Materials, E. S. (2016). Material developments. Retrieved from <http://esm.fisica.uminho.pt/index.php/areas/materialdevelopments>

- Materials, M. A. (2016). Piezoelectric ceramics. Retrieved from https://www.morganadvancedmaterials.com/sites/default/files/documents/r6001_piezo_brochureweb.pdf
- Mateu, L., & Moll, F. (2005). Optimum piezoelectric bending beam structures for energy harvesting using shoe inserts. *Journal of Intelligent Material Systems and Structures*, 16(10), 835-845.
- Mems-pie. (2017a). The MEMS-pie project. Retrieved from <https://www.sintef.no/projectweb/mems-pie/performance>
- Mems-pie. (2017b). Testing and characterisation. Retrieved from <https://www.sintef.no/projectweb/mems-pie/testing-and-characterisation/>
- Michael, F., (1953). Recent estimates of the abundance of the elements in the earth's crust. Retrieved July 14, from <https://pubs.usgs.gov/circ/1953/0285/report.pdf>
- Mindtouch. (2018). Tetragonal distortion of the perovskite unit cell in the ferroelectric oxide PZT, $\text{PbTi}_x\text{Zr}_{1-x}\text{O}_3$. Retrieved from [https://chem.libretexts.org/LibreTexts/Douglas_College/DC%3A_Chem_2330_\(O'Connor\)/6%3A_Solids/6.3%3A_Crystal_Structure](https://chem.libretexts.org/LibreTexts/Douglas_College/DC%3A_Chem_2330_(O'Connor)/6%3A_Solids/6.3%3A_Crystal_Structure).
- Morimoto, K., Kanno, I., Wasa, K., & Kotera, H. (2010). High-efficiency piezoelectric energy harvesters of c-axis-oriented epitaxial PZT films transferred onto stainless steel cantilevers. *Sensors and Actuators A: Physical*, 163(1), 428-432.
- Muralt, P., Marzencki, M., Belgacem, B., Calame, F., & Basrour, S. (2009). Vibration energy harvesting with PZT micro device. *Procedia Chemistry*, 1(1), 1191-1194.
- Myers, R., Vickers, M., Kim, H., & Priya, S. (2007). Small scale windmill. *Applied Physics Letters*, 90(5), 054106-054106-054103.
- Nabunmee, S., Taweetunkasiri, Jarupoom, P., & Rujijanagul, G. (2011). Synthesis and properties of 0.8PZT-0.10PZN-0.10PNN ceramics. *Ferroelectrics*, 416(1), 22-28.
- Naifar, S., Bradai, S., Viehweger, C., & Kanoun, O. (2016). Survey of electromagnetic and magnetoelectric vibration energy harvesters for low frequency Excitation. *Measurement*, [In Press].
- Nechibvute, A., Akande, A., & Luhanga, P. (2011). Modelling of a PZT beam for voltage generation (2011). *Pertanika J. Sci. & Technol*, 19 (2): 259 – 271.

- Nesbitt W.H., David C.R., Laxminarayana S., Yu-Hsuan Su. (2000). Microhydraulic transducer technology for actuation and power generation. *Proceeding of SPIE's 7th Annual International Symposium on Smart Structures and Materials, Newport Beach, CA* (pp 1-9). United States: SPIE.
- Nogas-Ćwikiel, E. (2011). Fabrication of Mn doped PZT for ceramic-polymer composites. *Archives of Metallurgy and Materials*, 56(4), 1065-1069.
- Noliac. (2013). Actuators, bending. Retrieved from <http://www.noliac.com/Default.aspx?ID=52>
- Nolica. (2015). Materials. Retrieved from <http://www.noliac.com/products/materials/>
- Obayashi, H., Sakurai, Y., & Gejo, T. (1976). Perovskite-type oxides as ethanol sensors. *Journal of Solid State Chemistry*, 17(3), 299-303.
- Retsch. (2017). Planetary ball mill PM 400. Retrieved from http://lab-mills.com/planetary/?gclid=EAIaIQobChMIIsIKkg6S93AIVF4WPCh22IQNnEAAYASAAEgKYcPD_BwE
- Park, K.-I., Xu, S., Liu, Y., Hwang, G.-T., Kang, S.-J. L., Wang, Z. L., & Lee, K. J. (2010). Piezoelectric BaTiO₃ thin film nanogenerator on plastic substrates. *Nano Letters*, 10(12), 4939-4943.
- Park, K. I., Jeong, C. K., Ryu, J., Hwang, G. T., & Lee, K. J. (2013). Flexible and large-area nanocomposite generators based on lead zirconate titanate particles and carbon nanotubes. *Advanced Energy Materials*, 3(12), 1539-1544.
- Park, K. I., Lee, M., Liu, Y., Moon, S., Hwang, G. T., Zhu, G., . . . Wang, Z. L. (2012). Flexible nanocomposite generator made of BaTiO₃ nanoparticles and graphitic carbons. *Advanced Materials*, 24(22), 2999-3004.
- Patel, S., Chauhan, A., & Vaish, R. (2014). A technique for giant mechanical energy harvesting using ferroelectric/antiferroelectric materials. *Journal of Applied Physics*, 115(8), 084908.
- Patel, S., Moghal, A. A. B., Madhar, N. A., Chauhan, A., & Vaish, R. (2015). Cyclic piezoelectric energy harvesting in PMN-PT single crystals. *Ferroelectrics*, 481(1), 138-145.

- Pazde-Araujo, C., Ramesh, R., & Taylor, G. W. (2001). Science and technology of integrated ferroelectrics: *Selected Papers from Eleven Years of the Proceedings of the International Symposium of Integrated Ferroelectronics* (Vol. 11), London: CRC Press.
- Peigney, M., & Siegert, D. (2013). Piezoelectric energy harvesting from traffic-induced bridge vibrations. *Smart Materials and Structures*, 22(9), 095019.
- Physikinstrumente. (2013). Piezo actuators extreme lifetime, for industrial reliability requirements. Retrieved from http://www.physikinstrumente.com/en/products/piezo/picma_lifetime.php
- Piezo System, I. (2013). Energy harvesting. Retrieved from <http://www.piezo.com/prodeh0nav.html>
- Piezo systems, i. (2016). Piezoelectric bending sensors (generators). Retrieved from <http://www.piezo.com/prodbg1brass.html>
- Sabar D. Hutagalung . (2016). Piezoelectric effect. Retrieved from <http://slideplayer.com/slide/4630957/>
- Sante. (2017). Muffle furnace. Retrieved from <http://www.santefurnace.com/home-productinfo-id-3.html>
- Phromyothin, D., Phatban, P., Jessadaluk, S., Khemasiri, N., Kowong, R., Vuttivong, S., ... & Horphathum, M. (2017). Growth of ZnO nanorods via low temperature hydrothermal method and their application for Hydrogen production. *Materials Today*, 4(5), 6326-6330.
- Porex. (2015). Polyvinylidene fluoride (PVDF). Retrieved from <http://www.porex.com/technologies/materials/porous-plastics/polyvinylidene-fluoride/>
- Priya, S. (2005a). Modeling of electric energy harvesting using piezoelectric windmill. *Applied Physics Letters*, 87(18).
- Priya, S. (2005b). Modeling of electric energy harvesting using piezoelectric windmill. *Applied Physics Letters*, 87(18), 184101.

- PZT Electronic Ceramic Co., L. (2018). Piezoelectric energy harvesting transducers. Retrieved from <http://www.piezoelements.com/piezo-ceramic/piezo-plate/piezoelectric-energy-harvesting-transducers.html>
- Qin, W., Li, T., Li, Y., Qiu, J., Ma, X., Chen, X., . . . Zhang, W. (2016). A high power ZnO thin film piezoelectric generator. *Applied Surface Science*, 364, 670-675.
- Rezaei-Hosseiniabadi, N., Tabesh, A., Dehghani, R., & Aghili, A. (2015). An efficient piezoelectric windmill topology for energy harvesting from low-speed air flows. *Industrial Electronics, IEEE Transactions on*, 62(6), 3576-3583.
- Roth, R. S. (1957). Classification of perovskite and other ABO_3 -type compounds. *J. Res. Nat. Bur. Stand*, 58(2), 75-88.
- Roundy, S., Leland, E. S., Baker, J., Carleton, E., Reilly, E., Lai, E., . . . Sundararajan, V. (2005a). Improving power output for vibration-based energy scavengers. *IEEE Pervasive computing*, 4(1), 28-36.
- Roundy, S., Leland, E. S., Baker, J., Carleton, E., Reilly, E., Lai, E., . . . Sundararajan, V. (2005b). Improving power output for vibration-based energy scavengers. *Pervasive Computing, IEEE*, 4(1), 28-36.
- Roundy, S., Wright, P. K., & Rabaey, J. (2003). A study of low level vibrations as a power source for wireless sensor nodes. *Computer communications*, 26(11), 1131-1144.
- Sang, C., Dayou, J., & Liew, W. H. (2013). Increasing the output from piezoelectric energy harvester using width-split method with verification. *International Journal of Precision Engineering and Manufacturing*, 14(12), 2149-2155.
- Schwarz, B., Richardson, M., & Avitabile, P. (2002). Locating optimal references for modal testing. *Proceedings of the 20th international modal analysis conference, Los Angeles, CA* (pp.1-7). USA: SPIE
- Sensors, H. (2016). Vibration monitoring for industrial applications. Retrieved from <http://www.hansfordsensors.com/resources/vibration-calculator/>
- Shen, D. (2009). *Piezoelectric energy harvesting devices for low frequency vibration application*. (Doctor dissertation, University in Partial, Alabama, U.S.). Retrieved from <https://etd.auburn.edu/handle/10415/1603>
- Shenck, N. S., Paradiso, J. A. (2001). Energy scavenging with shoe-mounted piezoelectrics. *Micro IEEE*, 21(3), 30-42.

- Shevtsov, S., & Chang, S.-H. (2016). Modeling of vibration energy harvesting system with power PZT stack loaded on Li-Ion battery. *International Journal of Hydrogen Energy* 41(29), 12618-12625.
- Shibata, K., Oka, F., Ohishi, A., Mishima, T., & Kanno, I. (2008). Piezoelectric properties of (K, Na) NbO₃ films deposited by RF magnetron sputtering. *Applied Physics Express*, 1(1), 011501.
- Sodano, H., A., Inman, D., J., & Park, G. (2005). Comparison of piezoelectric energy harvesting devices for recharging batteries. *Journal of Intelligent Material Systems and Structures*, 16(10), 799-807.
- sonic, G. (2017). Clerance 6L heated ultrasonic cleaner ultrasonic jewelry cleaner ultrasonic cleaning machine GT sonic-P6. Retrieved from <https://www.aliexpress.com/item/6L-Ultrasonic-Cleaner-Heating-Timer-Power-Adjustable-Stainless-Tank-EU/32630297977.html>
- Song, D., Chan Ho, Y., Seong K.H., Se Bin, K., Min Sik, W., & Tae-Hyun, S. (2012). Feasibility study on application of piezoelectricity to convert vibrations of Korea Train eXpress. *Proceedings of the European Conference on the Applications of Polar Dielectrics and 2012 International Symp Piezoresponse Force Microscopy and Nanoscale Phenomena in Polar Materials (ISAF/ECAPD/PFM), Intl Symp Aveiro, Portugal(pp.1-4)*. USA: IEEE.
- Song, G., Li, H., Gajic, B., Zhou, W., Chen, P., & Gu, H. (2013). Wind turbine blade health monitoring with piezoceramic-based wireless sensor network. *International Journal of Smart and Nano Materials*, 4(3), 150-166.
- Rebecca P. , N. (2016). NASA space suit could harness astronaut's energy to power electro. Retrieved from <http://www.ecouterre.com/nasa-spacesuit-could-harness-astronauts-energy-to-power-electronics/nasa-piezo-electric-spacesuit-1/>
- SpaceAge Control, I. (2016). Sinusoidal motion calculator. Retrieved from <http://www.spaceagecontrol.com/calcsinm.htm?col=col1&what=D&V11=0.2&F11=0.3&A21=&F21=&V31=&A31=&F12=&D12=&A22=&F22=&A32=&D32=&F13=&D13=&F23=&V23=&V33=&D33=&A14=&D14=&V24=200&D24=12&A34=&V34=&units=Metric&submit=Calculate>
- Starner, T. (1996). Human-powered wearable computing. *IBM System Journal*, 35.
- Stassi, S., Cauda, V., Ottone, C., Chiodoni, A., Pirri, C. F., & Canavese, G. (2015). Flexible piezoelectric energy nanogenerator based on ZnO nanotubes hosted in a polycarbonate membrane. *Nano Energy*, 13, 474-481.

- Su, W.-J., Zu, J., & Zhu, Y. (2013). Design and development of a broadband magnet-induced dual-cantilever piezoelectric energy harvester. *Journal of Intelligent Material Systems and Structures*, 25(4), 430-442.
- Suyitno, S., Purwanto, A., Hidayat, R. L. L. G., Sholahudin, I., Yusuf, M., Huda, S., & Arifin, Z. (2014). Fabrication and characterisation of zinc oxide-based electrospun nanofibers for mechanical energy harvesting. *Journal of Nanotechnology in Engineering and Medicine*, 5(1), 011002.
- Tan, Y., Hoe, K., & Panda, S. (2006). Energy harvesting using piezoelectric igniter for self-powered radio frequency (RF) wireless sensors. *Proceedings of the IEEE International Conference on Industrial Technology, New Jersey* (pp. 1711-1716). USA: IEEE
- Tan, Y., & Panda, S. (2007). A novel piezoelectric based wind energy harvester for low-power autonomous wind speed sensor. *Proceedings of the 33rd Annual Conference of the IEEE Industrial Electronics Society (IECON), Taipei, Taiwan* (pp. 2175-2180). USA: IEEE.
- Tan, Y., Zhang, J., Wu, Y., Wang, C., Koval, V., Shi, B., . . . Yan, H. (2015). Unfolding grain size effects in barium titanate ferroelectric ceramics. *Scientific reports*, 5.
- Tang, L., & Yang, Y. (2012). A multiple-degree-of-freedom piezoelectric energy harvesting model. *Journal of Intelligent Material Systems and Structures*, 23(14), 1631-1647.
- Thomas, P. D., Kunzmann, J., Schönecker, A. (2008). Energy harvesting systems using piezo-electric macro fiber composites. Retrieved from https://www.researchgate.net/publication/241156016_Energy_harvesting_systems_using_piezo-electric_MFCs
- Tian, S., & Wang, X. (2008). Fabrication and performances of epoxy/multi-walled carbon nanotubes/piezoelectric ceramic composites as rigid piezo-damping materials. *Journal of Materials Science*, 43(14), 4979-4987.
- Tong, C. W., Chew, P. S., Abdullah, A. F., Sean, O. C., & Ching, T. C. (2011). Exhaust air and wind energy recovery system for clean energy generation. *Proceedings of the International Conference on Environment and Industrial Innovation*, Kuala Lumpur, Malaysia.
- Uršič, H., Santo Zarnik, M., & Kosec, M. (2011). Pb (Mg_{1/3}Nb_{2/3}) O₃-PbTiO₃ (PMN-PT) material for actuator applications. *Smart Materials Research*, 2011(452901), 1-6.

- Vasudevan, R. K., Balke, N., Maksymovych, P., Jesse, S., & Kalinin, S. V. (2017). Ferroelectric or non-ferroelectric: Why so many materials exhibit “ferroelectricity” on the nanoscale. *Applied Physics Reviews*, 4(2), 021302.
- Wang, X., Yang, B., Liu, J., Zhu, Y., Yang, C., & He, Q. (2016). A flexible triboelectric-piezoelectric hybrid nanogenerator based on P (VDF-TrFE) nanofibers and PDMS/MWCNT for wearable devices. *Scientific reports*, 6, 36409.
- Woiyas, P., Islam, M., Heller, S., & Roth, R. (2013). A low-voltage boost converter using a forward converter with integrated Meissner oscillator. *Journal of Physics*, 476(1), 012081.
- Woo M. S., B. K. H., Kim J. H., Kim S. B. , Song D.& Sung T. H. . (2014). Relationship between current and impedance in piezoelectric energy harvesting system for water waves. *J Electroceram* ,34(2-3), 180-184.
- Wu, H., Tang, L., Yang, Y., & Soh, C. K. (2014). Development of a broadband nonlinear two-degree-of-freedom piezoelectric energy harvester. *Journal of Intelligent Material Systems and Structures*, 25(14), 1875-1889.
- Wu, W., Bai, S., Yuan, M., Qin, Y., Wang, Z. L., & Jing, T. (2012). Lead zirconate titanate nanowire textile nanogenerator for wearable energy-harvesting and self-powered devices. *ACS Nano*, 6(7), 6231-6235.
- Xiao, H., Wang, X., & John, S. (2016). A multi-degree of freedom piezoelectric vibration energy harvester with piezoelectric elements inserted between two nearby oscillators. *Mechanical Systems and Signal Processing*, 68-69, 138-154.
- Xie, J., Mane, X., Green, C., Mossi, K., & Leang, K. K. (2010). Performance of thin piezoelectric materials for pyroelectric energy harvesting. *Journal of Intelligent Material Systems and Structures*, 21(3), 243-249.
- Xu, S., Qin, Y., Xu, C., Wei, Y., Yang, R., & Wang, Z. L. (2010). Self-powered nanowire devices. *Nature Nanotechnology*, 5(5), 366-373.
- Xu, S., Yeh, Y.-w., Poirier, G., McAlpine, M. C., Register, R. A., & Yao, N. (2013). Flexible piezoelectric PMN–PT nanowire-based nanocomposite and device. *Nano Letters*, 13(6), 2393-2398.
- Xue, D., Zhou, Y., Bao, H., Gao, J., Zhou, C., & Ren, X. (2011). Large piezoelectric effect in Pb-free Ba (Ti, Sn) O_{3-x} (Ba, Ca) TiO₃ ceramics. *Applied Physics Letters*, 99(12), 122901.

- Yang, Y., Guo, W., Pradel, K. C., Zhu, G., Zhou, Y., Zhang, Y., . . . Wang, Z. L. (2012). Pyroelectric nanogenerators for harvesting thermoelectric energy. *Nano Letters*, *12*(6), 2833-2838.
- Yap, H., Ong, Z., Chong, W., Kong, K., Khoo, S., Ismail, Z., & Rahman, A. (2014). Design optimisation of shroud-augmented dual-rotor exhaust air energy recovery wind turbine generator using hybrid non-destructive evaluation approach. *Energy Procedia*, *61*, 1266-1269.
- Yin, B., Qiu, Y., Zhang, H., Lei, J., Chang, Y., Ji, J., . . . Hu, L. (2015). Piezoelectric performance enhancement of ZnO flexible nanogenerator by a NiO–ZnO p–n junction formation. *Nano Energy*, *14*, 95-101.
- Yun, B. K., Park, Y. K., Lee, M., Lee, N., Jo, W., Lee, S., & Jung, J. H. (2014). Lead-free LiNbO₃ nanowire-based nanocomposite for piezoelectric power generation. *Nanoscale research letters*, *9*(1), 1-7.
- Zauli, G. (2013). Fundamentals of vibration. Retrieved from http://www.unife.it/ing/lm.meccanica/insegnamenti/meccanica-delle-vibrazioni/materiale-didattico/copy_of_a-a-2016-17-dispense-e-programma/03-rao_cap1-fundamentals-of-vibration.pdf
- Zhang, C., He, X.-F., Li, S.-Y., Cheng, Y.-Q., & Rao, Y. (2015). A wind energy powered wireless temperature sensor node. *Sensors*, *15*(3), 5020-5031.
- Zhang, R., Jiang, B., & Cao, W. (2001). Elastic, piezoelectric, and dielectric properties of multidomain 0.67 Pb (Mg_{1/3}Nb_{2/3}) O₃-0.33 PbTiO₃ single crystals. *Journal of Applied Physics*, *90*(7), 3471-3475.
- Zhang, S., Yan, B., Luo, Y., Miao, W., & Xu, M. (2015). An enhanced piezoelectric vibration energy harvesting system with macro fiber composite. *Shock and Vibration*, *2015*(916870), 1-7.
- Zhengzhou CY Scientific Instrument Co., L. (2017). Magnetron plasma sputtering coater/magnetron sputtering machine/magnetron sputtering system. Retrieved from https://www.alibaba.com/product-detail/Magnetron-Plasma-Sputtering-Coater-magnetron-sputtering_60279037910.html
- Zhou, Q., Lam, K. H., Zheng, H., Qiu, W., & Shung, K. K. (2014). Piezoelectric single crystal ultrasonic transducers for biomedical applications. *Progress in materials science*, *66*, 87-111.

Zhou, Y. (2006). *Effect of electric conductivity in ferroelectric structures* (Doctoral dissertation, The Hong Kong Polytechnic University, Hung Hom, Hong Kong). Retrieved from <http://ira.lib.polyu.edu.hk/handle/10397/3715>

Zhu, G., Wang, A. C., Liu, Y., Zhou, Y., & Wang, Z. L. (2012). Functional electrical stimulation by nanogenerator with 58 V output voltage. *Nano Letters*, *12*(6), 3086-3090.

Zhu, G., Yang, R., Wang, S., & Wang, Z. L. (2010). Flexible high-output nanogenerator based on lateral ZnO nanowire array. *Nano Letters*, *10*(8), 3151-3155.

University of Malaya

LIST OF PUBLICATIONS AND PAPERS PRESENTED

ISI Journal Articles:

- 1- Zainab, S.R., Chong, W.T., Ong, Z.C., & Khoo, S.Y. (2017). Energy harvesting based on a novel piezoelectric $0.7\text{PbZn}_{0.3}\text{Ti}_{0.7}\text{O}_3$ $0.3\text{Na}_2\text{TiO}_3$ nanogenerator. *Energies*, 10(5), 646.
- 2- Khoo, S.Y., Zainab, S.R., Ong, Z.C., Huang, Y.H., Chong, W.T., & Ismail, Z. (2017). Structural dynamics effect on voltage generation from dual coupled cantilever based piezoelectric vibration energy harvester system. *Measurement*, 107, 41- 52.
- 3- Zainab, S.R., Chong, W.T., Khoo, S.Y., Ong, Z.C. (2017) Piezoelectric material Categories and Applications in terms of their properties. Submission to sensors journal.

International Conference

- 1- Zainab, S.R., Chong, W.T., Khoo, S.Y., Ong, Z.C. (2016). PbZnTiO_3 - Na_2TiO_3 PZT-NT soft piezoelectric transducers for energy harvesting applications, *Proceedings of the Kuala Lumpur 4th International Conference on "Engineering & Technology, Computer, Basic & Applied Sciences"* (ECBA- 2016), Kuala Lumpur, Malaysia.